Journal of Oncology

Targeted Molecular Therapy in Glioblastoma

Lead Guest Editor: Claudio Festuccia

Guest Editors: Assunta L. Biordi, Vincenzo Tombolini, Akira Hara, and David S. Bailey

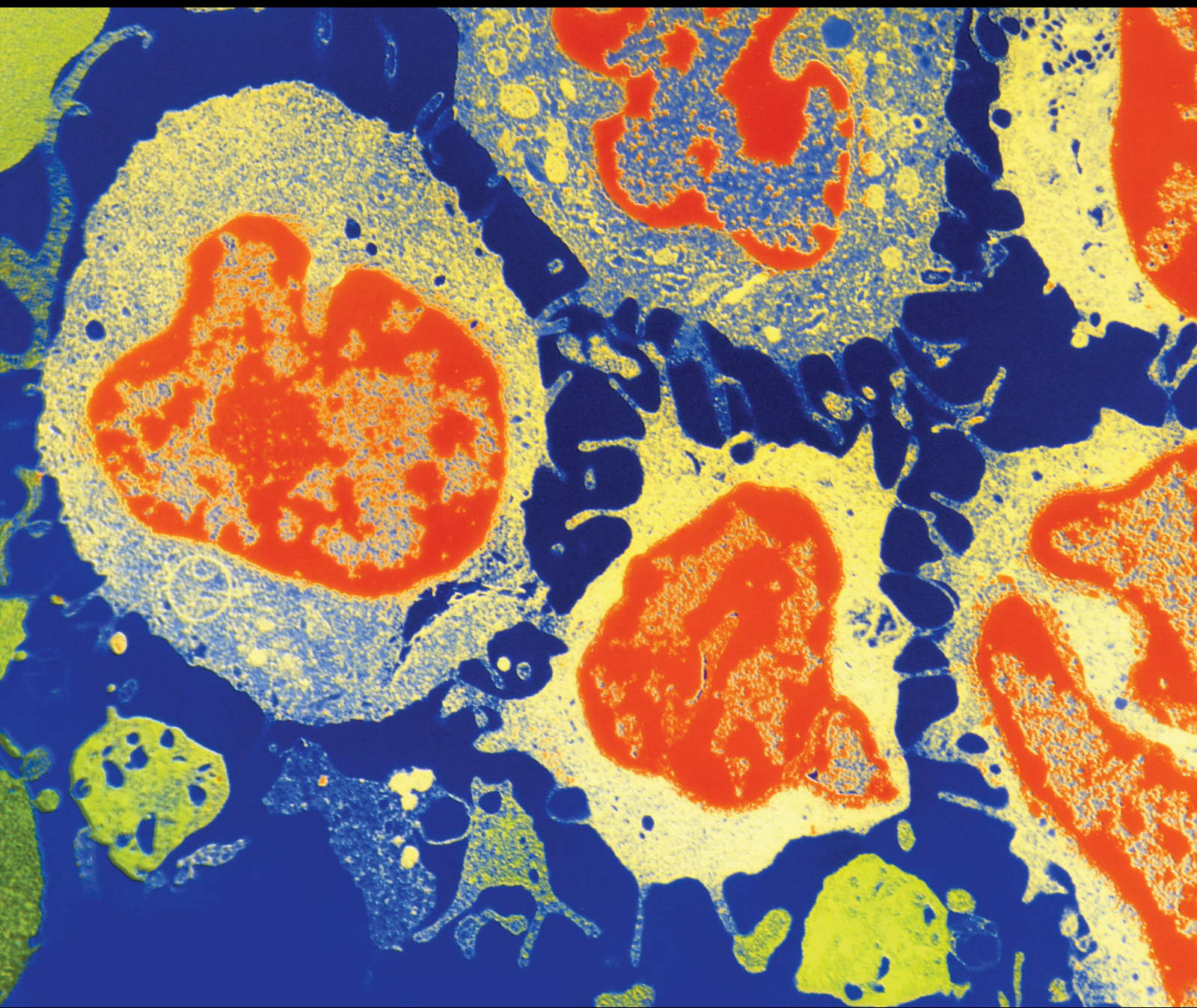

Targeted Molecular Therapy in Glioblastoma

Journal of Oncology

Targeted Molecular Therapy in Glioblastoma

Lead Guest Editor: Claudio Festuccia
Guest Editors: Assunta L. Biordi, Vincenzo Tombolini, Akira Hara, and David S. Bailey

Editorial Board

Contents

Hindawi
Journal of Oncology
Volume 2020, Article ID 5104876, 3 pages
https://doi.org/10.1155/2020/5104876

Editorial

Targeted Molecular Therapy in Glioblastoma

Claudio Festuccia,[1] **Assunta Leda Biordi**,[1] **Vincenzo Tombolini**,[2] **Akira Hara**,[3] **and David Bailey**[4]

[1]*Department of Applied Clinical Sciences and Biotechnologies, University of L'Aquila, L'Aquila, Italy*
[2]*Department of Experimental Medicine, University La Sapienza, Rome, Italy*
[3]*Gifu University Graduate School of Medicine, Gifu, Japan*
[4]*IOTA Pharmaceuticals Ltd., Cambridge University Biomedical Innovation Hub, Cambridge, UK*

Correspondence should be addressed to Claudio Festuccia; claudio.festuccia@univaq.it

Received 21 December 2019; Accepted 23 December 2019; Published 14 January 2020

Glioblastoma multiforme (GBM) is the most common and malignant type of primary brain tumor, exhibiting poor response to therapy and seemingly inevitable recurrence. The current standard of care for treating newly diagnosed GBM is maximal safe resection followed by radiation with concurrent and adjuvant temozolomide, a regimen which has been shown to improve median overall survival (12.1 months vs. 14.6 months) and 2-year (27.2% vs. 10.9%) and 5-year (10.9% vs. 1.9%) survival rates when compared with radiation alone.

This special issue was aimed at updating researchers on current topics and progress made in basic, preclinical, and clinical glioblastoma research. It also provided a platform for pharmaceutical and translational scientists to submit original research articles, review articles, and clinical studies, focusing on the evaluation of new molecular pathways as pharmacological targets for treatment strategies which may improve the management of aggressive, drug-resistant GBM, in the hope that a deeper knowledge of GBM biology may eventually lead to effective targeted therapeutic approaches based on the inhibition of tumor-specific proteins or molecular pathways.

Unfortunately, this neoplasia contains an elevated percentage of transformed, self-maintaining, multipotent, tumour-initiating cancer stem cells, mainly present in highly hypoxic areas of the tumor in conjunction with palisading necrosis. Despite multimodal therapies, prognosis for GBM is still dismal. Many features contribute to this therapeutic challenge, including high intratumoral and intertumoral heterogeneity, resistance to therapy, migration and invasion, and immunosuppression. Nevertheless, with the advent of novel high-throughput drug screening technologies, together with a growing body of genetic and transcriptomic information, significant progress has been made to understand the molecular and immunological signatures underlying the pathology of glioblastoma.

We received 11 reports for publication, accepting 7 after peer review. A brief summary of all accepted papers is provided below.

Elevated invasive capacity is one of the key tumoral features associated with treatment resistance, recurrence, and poor overall survival in GBM. The research group of Akira Ara at the Gifu University Graduate School of Medicine (Gifu, Japan) reviewed treatment strategies based on histological targets against invasive and resistant GBM using the classification of the "secondary structures of Scherer." One of the main reasons that gliomas are not cured by surgery is the topographically diffuse nature of the disease. In addition to the high degree of intratumor variability mentioned previously, the extensive spreading of malignant tumor cells within the brain parenchyma results in an inability to completely resect this tumor. Hans-Joachim Scherer was a pioneer in the study of glioma growth patterns. In 1940, Scherer described the appearance and behavior of glioma cells migrating away from the main tumor mass through the brain parenchyma. The patterns of glioma cell infiltration have since been referred to as the "secondary structures of Scherer." Infiltrating glioma cells migrate

through the normal parenchyma, collect just below the pial margin (subpial spread), surround neurons and vessels (perineuronal and perivascular satellitosis), and migrate through the white matter tracts (intrafascicular spread). Examples of observed secondary structures include perineuronal growth (perineuronal satellitosis), surface/subpial growth, perivascular growth, and intrafascicular growth. In order to develop therapeutic interventions to mitigate glioma cell migration, it is important to understand the biological mechanisms underlying the formation of these secondary structures. The review examined new molecular pathways based on the histopathological evidence of GBM invasion as a major prognostic factor in the high recurrence rate for GBMs. Specific molecular parameters, in addition to traditional histopathological analysis, have been used to define tumor classification in the revised 4th edition of the WHO Classification of CNS tumors, published in 2016. Detailed histopathological analysis based on the combination of molecular parameters with traditional analytical methods can now be used to evaluate efficacy of targeted therapies against cellular and genetic heterogeneity within both invasive and drug-resistant glioblastoma.

The molecular machinery underlying GBM invasiveness involves an intricate network of signaling pathways and interactions with the extracellular matrix and neighboring host cells. In this special issue, a collaboration amongst researchers from the Department of Neurological Surgery and Spine Unit and Genetics Unit (Hospital Universitario and Instituto de Investigación Marqués de Valdecilla in Santander, Spain), the Division of Neurosurgery (University of Toronto, Canada), and the MacFeeters-Hamilton Center for Neuro-Oncology Research (Princess Margaret Cancer Center in Toronto, Canada) is reported, reviewing and highlighting the molecular and clinical hallmarks of invasion in GBM. In this paper, C. Velásquez et al. review data on adhesion molecules, extracellular matrix (ECM) components, epithelial-to-mesenchymal transition (EMT), cytoskeleton-remodeling proteins, cross-talk with host cells and immune modulation, as well as the signaling pathways associated with GBM invasion (including those involving receptor tyrosine kinases, Wnt (both canonical and β-catenin-independent pathways), hedgehog-GLI1, and nuclear factor-κB. The authors analyze the clinical implications of GBM invasiveness and assess GBM invasion in the clinical setting, by imaging GBM invasion intraoperatively to guide surgical resection and radiation therapy of the infiltrative tumor.

G. Steponaitis et al., Laboratory of Molecular Neuro-Oncology, Lithuanian University of Health Sciences (Kaunas, Lithuania), elucidated the oncosuppressive role of runt-related transcription factor 3 (RUNX3) in human astrocytomas. RUNX3 is a tumor suppressor gene whose inactivation was shown to be related to carcinogenesis in several cancers. Methylation status and protein expression levels of RUNX3 were measured by methylation-specific PCR and Western blotting in tissues harvested from normal tissues and glioma of different grades. These researchers demonstrate that RUNX3 gene methylation and protein expression downregulation are glioma malignancy-dependent and contribute to tumor progression. Importantly, these authors also demonstrated that re-expression of RUNX3 in the glioblastoma U87-MG cell line decreased cell viability *in vitro*. However, it remains to be demonstrated whether transfection of RUNX3 can reduce tumor progression and increase survival *in vivo* after injection of cells in nude mice.

E. Berney et al., Departments of Physiology/Anatomy and Pediatrics, University of North Texas Health Science Center (Fort Worth, Texas, USA), reported data on the scavenger receptor class B type 1 (SR-B1) as a potential target for treating glioblastoma. These studies involved the evaluation of reconstituted high-density lipoprotein (rHDL) nanoparticles (NPs) as delivery agents for the drug mammalian target of rapamycin (mTOR) inhibitor everolimus (EVR) to GBM cells. Cytotoxicity studies and assessment of downstream effects, including apoptosis, migration, and cell cycle events, were probed, in relation to the expression of SR-B1 by GBM cells. The authors revealed that rHDL/EVR formulation was 185 times more potent than free EVR against the high SR-B1 expressing GBM cell line LN 229. In addition, cell cycle analysis revealed that rHDL/EVR-treated LN229 cells had a 5.8 times higher apoptotic cell population than those treated with EVR. The sensitivity of GBM cells to EVR treatment was also strongly correlated with SR-B1 expression. So, delivering EVR and likely other agents, via a biocompatible transport system targeted to the SR-B1 receptor, could lead to effective personalized therapy of GBM.

C. Cilibrasi et al., School of Medicine and Surgery (University of Milano-Bicocca), in collaboration with the NeuroMI, Milan Center of Neuroscience, the Departments of Neurology and Neuroscience, San Gerardo Hospital, the Department of Neurology and Neurosurgery, Montreal Neurological Institute and Hospital (McGill University, Montreal, Quebec, Canada), the International Center for Digestive Health (ICDH), University of Milano-Bicocca, and the Genome Damage and Stability Center, School of Life Sciences, University of Sussex, UK, showed that a ploidy increase promotes sensitivity of glioma stem cells to Aurora kinase inhibition, investigating the effect of Aurora kinase inhibition in five glioma stem cell lines isolated from glioblastoma patients. As expected, cell lines responded to the loss of Aurora kinase with cytokinesis failure and mitotic exit without cell division. Surprisingly, this resulted in a proliferative arrest in only two of the five cell lines. Sensitive cell lines entered a senescent/autophagic state following aberrant mitotic exit, while the nonsensitive cell lines continued to proliferate. This senescence response did not correlate with TP53 mutation status but only occurred in the cell lines with the highest chromosome content. Repeated rounds of Aurora kinase inhibition caused a gradual increase in chromosome content in the resistant cell lines, eventually leading to a similar senescence response and proliferative arrest. The results suggest that a ploidy threshold is the main determinant of Aurora kinase sensitivity in TP53 mutant glioma stem cells. Thus, ploidy could be used as a biomarker for treating glioma patients with Aurora kinase inhibitors in TP53 mutant glioma stem cells. Further research will be necessary to explore the mechanism of ploidy-induced senescence and the precise reason why a particular ploidy threshold appears to trigger this response.

A. Menezes et al. investigated the impact of HDAC activity on GBM cell behavior and plasticity by live cell imaging. These researchers knocked down HDAC activity pharmacologically using two different inhibitors (TSA and SAHA) in two different tumor cell types: a commercial GBM cell line (U87-MG) and a primary tumor (GBM011). Upon 72 hours of *in vitro* HDAC inhibitor treatment, GBM cells presented a very unusual elongated cell shape due to the formation of tunneling tubes which appeared independent of TGFβ-induced EMT. Live cell imaging revealed that voltage-sensitive Ca++ signaling was disrupted upon HDAC activity blockade. This behavior was coupled to down-regulation of vimentin and connexin gene expression, suggesting that HDAC activity blockade downgrades GBM aggressiveness due to tumor cell competence and plasticity modulation *in vitro*. To investigate these effects, GBM oncospheres were xenografted into the chick developing neural tube. Remarkably, when placed within the developing neural tube, HDAC inhibitor-treated GBM cells ectopically expressed HNK-1, a tumor suppressor marker tightly correlated to increased survival of patients. These results describe, for the first time in the literature, the relevance of HDAC inhibition to *in vivo* tumor cell morphology and competence in an appropriate response to environmental cues. Ultimately, the results highlight the relevance of chromatin remodeling for tumor cell plasticity and shed light on the clinical targeting of the epigenome in GBM therapy.

The blood-brain barrier (BBB) is an anatomical functional unit created by characteristic endothelial cells forming blood vessels within the central nervous system. The main function of the BBB is protecting brain tissue from harmful elements present in the blood while still allowing the passage of substances necessary for metabolic functions. BBB endothelial cells form a continuous and nonfenestrated endothelium, sealed by occluding cellular junctions (tight junctions), whose compactness prevents the passage of hydrophilic and high-molecular weight substances from the blood to the brain parenchyma, performing filtration which is much more selective than that of endothelial cells in the capillaries of other parts of the body. Further structural features of the BBB include projections of astrocytic cells, called astrocytic peduncles (also known as the "glial limiting" membrane), which surround the endothelial cells of the BBB, providing an additional "barrier." Although the structure of the BBB is often impaired in GBM, it is thought that BBB penetrance still represents a serious barrier to drug delivery to the tumor. Different methods have been exploited to bypass the BBB and increase the tumor uptake of therapeutic agents. In this issue, M. Shi and L. Sanche of the Department of Radiation Oncology, School of Medicine, Hangzhou, China and the Department of Nuclear Medicine and Radiobiology, Université de Sherbrooke, Canada, evaluated the efficacy of convection-enhanced delivery (CED), using multiple drugs with different antitumor mechanisms, concomitant with radiation and chemotherapy. Importantly, the simultaneous use of these procedures demonstrated supra-additive effects over standard drug treatments, representing a promising modality for brain tumor therapy. The authors also evaluated the efficacy of different CED-based strategies as part of Phase II and III clinical trials. CED bypasses the BBB, increases drug uptake by the tumor, and reduces systemic toxicity.

Conflicts of Interest

The editors declare that they have no conflicts of interest.

Acknowledgments

The editors would like to express their gratitude to all authors who made this special issue possible. They hope this collection of articles will be useful to the scientific community.

Claudio Festuccia
Assunta Leda Biordi
Vincenzo Tombolini
Akira Hara
David Bailey

Hindawi
Journal of Oncology
Volume 2019, Article ID 9014045, 15 pages
https://doi.org/10.1155/2019/9014045

Research Article

A Ploidy Increase Promotes Sensitivity of Glioma Stem Cells to Aurora Kinases Inhibition

Chiara Cilibrasi,[1,2,3] Andrèe Guzzi,[1] Riccardo Bazzoni,[1,3] Gabriele Riva,[1,3,4] Massimiliano Cadamuro,[1,5] Helfrid Hochegger,[6] and Angela Bentivegna[1,3]

[1]*School of Medicine and Surgery, University of Milano-Bicocca, 20900 Monza, Italy*
[2]*Ph.D. Program in Neuroscience, University of Milano-Bicocca, 20900 Monza, Italy*
[3]*NeuroMI, Milan Center of Neuroscience, University of Milano-Bicocca, Dept. of Neurology and Neuroscience, San Gerardo Hospital, 20900 Monza, Italy*
[4]*Department of Neurology and Neurosurgery, Montreal Neurological Institute and Hospital, McGill University, Montreal, QC, Canada*
[5]*International Center for Digestive Health (ICDH), University of Milano-Bicocca, 20900 Monza, Italy*
[6]*Genome Damage and Stability Center, School of Life Sciences, University of Sussex, Falmer, Brighton, UK*

Correspondence should be addressed to Angela Bentivegna; angela.bentivegna@unimib.it

Received 15 March 2019; Revised 9 June 2019; Accepted 24 June 2019; Published 19 August 2019

Academic Editor: Claudio Festuccia

Glioma stem cells account for glioblastoma relapse and resistance to conventional therapies, and protein kinases, involved in the regulation of the mitotic machinery (i.e., Aurora kinases), have recently emerged as attractive therapeutic targets. In this study, we investigated the effect of Aurora kinases inhibition in five glioma stem cell lines isolated from glioblastoma patients. As expected, cell lines responded to the loss of Aurora kinases with cytokinesis failure and mitotic exit without cell division. Surprisingly, this resulted in a proliferative arrest in only two of the five cell lines. These sensitive cell lines entered a senescent/autophagic state following aberrant mitotic exit, while the non-sensitive cell lines continued to proliferate. This senescence response did not correlate with TP53 mutation status but only occurred in the cell lines with the highest chromosome content. Repeated rounds of Aurora kinases inhibition caused a gradual increase in chromosome content in the resistant cell lines and eventually caused a similar senescence response and proliferative arrest. Our results suggest that a ploidy threshold is the main determinant of Aurora kinases sensitivity in TP53 mutant glioma stem cells. Thus, ploidy could be used as a biomarker for treating glioma patients with Aurora kinases inhibitors.

1. Introduction

Glioblastoma (GBM) is the most common primary malignant brain tumor in adults [1]. Despite multimodality treatments, including surgery, radio- and chemotherapy, outcomes are very poor, with less than 15% of patients alive after two years [2]. A likely cause for recurrence is the presence of a subpopulation of cancer cells with stem-like properties, called glioma stem cells (GSCs) that are resistant to therapies and rapidly repopulate the tumor following the initial treatment [3–5].

GSCs are characterized by their ability to give rise to a differentiated progeny, by their potential to induce glioma-like tumors in mouse xenografts, and by the expression of stem cell markers, such as CD133 and Nestin [6]. A common yet poorly understood feature of GSCs is the elevated chromosomal instability (CIN) [7]. Increases in CIN elicit a p53 dependent response in nontransformed cells [8] but is a common feature of cancer [9].

A variety of mechanisms have been proposed as responsible for CIN, including defects in genes involved in the regulation of the mitotic machinery, such as the Aurora kinases (AurKs) [9]. AurKs are a family of three serine/threonine kinases (AurKs A, B, and C), which play an essential role in controlling mitotic spindle regulation and sister chromatid segregation [10]. AurKs deregulation has been found in a wide range of cancers, including GBM, and is associated with genetic instability and poor prognosis [11–14]. Therefore,

they have emerged as attractive therapeutic targets for cancer treatment [15] and several AurKs inhibitors with clinical efficacy in phases I and II of clinical trials have been developed [16].

One of the most clinically advanced compounds is Danusertib (formerly PHA-739358) [17–21], a potent small-molecule 3-aminopyrazole inhibiting the ATP binding site of Aurora kinases. Danusertib has shown considerable therapeutic potential in a wide range of cancers, including advanced solid tumors and leukemias [22–24]. However, to our knowledge, to date there are no reports on the use of Danusertib for the treatment of GBM and its effect on GSCs.

In the present study, we investigated the efficacy of Danusertib on five established GSC lines isolated from GBM patients [7]. The immediate response to Danusertib exposure was uniform among GSC lines and resulted in cytokinesis failure and mitotic exit without division. Surprisingly, only three cell lines responded to this aberrant mitosis by proliferative arrest due to a senescence/autophagy response, while the other cell lines continued to proliferate. Our results suggest that sensitivity to Danusertib in GSCs is determined by a ploidy threshold, beyond which resistant cells enter a p53 independent senescence program.

2. Materials and Methods

2.1. Cell Lines and Cell Culture Conditions. All the GSC lines (GBM2, G144, G179, G166, GliNS2) were isolated from patients affected by GBM and previously characterized for their stemness properties [25, 26]. GSCs and human foetal neural stem cells (NSCs) (CB660) expansion was carried out as described in [7].

2.2. Drug and Treatments. Danusertib (PHA-739358, Selleckem, Houston, Texas, USA) was dissolved in dimethyl sulfoxide (DMSO) to a stock concentration of 10 mM and stored at -80°C. Dilutions to the required concentrations were made using complete medium. Single or two rounds of treatments were performed as reported in Figure 7.

EgV inhibitor STLC (S-Trityl-L-Cysteine, Tocris, Bristol, UK) was dissolved in DMSO at a stock concentration of 50 mM and stored at -20°C. It was used at a final concentration of 5 μM.

DMSO had no effect on the cell survival.

2.3. TaqMan Gene Expression Assay. RNA was extracted from GSCs and NSCs using the Direct-zol RNA MiniPrep (Zymo Research, Irvine, California, USA) according to the manufacturer's protocol. RNA quantity and quality were analyzed using a Nanodrop ND-1000 spectrophotometer (Thermo Scientific, Waltham, Massachusetts, USA).

RNA samples were converted into first-strand cDNA using the M-MLV reverse transcriptase (Invitrogen). cDNA was quantified using a Nanodrop ND-1000 spectrophotometer (Thermo Scientific).

TaqMan gene expression assays (Applied Biosystems, Foster City, California, USA) were performed in order to evaluate the expression levels of AurKs A, B, and C in GSCs. GAPDH was used as a housekeeping gene, while CB660 cells were used as normal controls. All the probes used were purchased from Applied Biosystems. Quantitative PCR was carried out using the ABI StepOne (Applied Biosystems), according to the manufacturer's instructions. The cycle conditions were as follows: 2 min 50°C; 10 min 95°C; 40 cycles: 15 s 95°C, 1 min 60°C. Relative gene expression was determined using data from the real-time cycler and the $\Delta\Delta C_t$ method. The cut-off values for gene expression fold changes were established at +/- 1,5. The gene expression data were obtained as mean values derived from two independent experiments.

2.4. Western Blotting. AurKs protein levels were investigated in cells synchronized by treatment with 5 μM STLC for 24 h and collected by mitotic shake off. Western blotting was performed as already described in [27]. Primary rabbit anti-AurKA (1:500, Abcam, Cambridge, UK) and anti-AurKB (1:500, Abcam) antibodies were used. Mouse anti-α-tubulin (1:10000, Abcam) was used as a loading control. Anti-rabbit (1:5000, DAKO by Agilent technologies, Santa Clara, California, USA) or anti-mouse (1:5000, DAKO) HRP-conjugated antibodies were used as secondary antibodies for 1 hour at room temperature. Chemiluminescent detection was performed using an ECL Solution. Emission was captured with radiograph films (Amersham Hyperfilm, GE Healthcare) using an automatic Ecomax X-ray Film Processor.

Beclin and LC3 were detected in GBM2 and G166 cells after one or two rounds of 500 nM Danusertib exposure. Western blotting was performed as already described in [28]. Primary rabbit anti-Beclin (1:1000, Cell signaling technology, Danvers, Massachusetts, USA) and anti-LC3-I and II (1:1000, Cell signaling technology) were used. Mouse anti-GAPDH (1:10000, Santa Cruz Biotechnologies, Dallas, Texas, USA) was used as a loading control. Secondary anti-rabbit (1:2000, Bio-Rad) or anti-mouse (1:2000, Merck, Billerica, Massachusetts, USA) antibodies were used. Proteins were visualized using SuperSignal West Pico or Dura chemiluminescent substrate (Thermo Scientific) with a G-BOX station (Syngene, Bommsandra Bangalore, India).

AurKs, Beclin, and LC3-I and LC3-II bands were quantified with ImageJ (https://imagej.nih.gov/ij/). The experiments were performed at least in triplicate.

2.5. MTT Assay. Cell viability was assessed in all the GSC lines by MTT (3-[4,5dimethylthiazol-2-yl]-2,5-diphenyl tetrazolium bromide, Sigma, Saint Louis, Missouri, USA) assay, as already described in [29], after 24, 48, and 72 h exposure to increasing doses of Danusertib (5-50-200-500-1000-5000 nM). MTT was also performed on GBM2 and G166 cell lines after two rounds of treatment with 500 nM Danusertib. The percentage of inhibition was determined as follows: [(treated-cell absorbance/untreated cell absorbance) × 100]. The results reported are the mean values of three different experiments performed at least in triplicate.

2.6. Conventional Cytogenetics. Conventional cytogenetics techniques were performed as described in [7] in order to determine the effect of 48 h of treatment with 500 nM Danusertib on the mitotic index and cell ploidy. Briefly, cells were treated with 0,2 μg/ml of Colcemid (Roche) and then

harvested and incubated with a hypotonic solution of 0,56% w/v of KCl for 15 minutes at room temperature. Subsequently, cells were fixed with a fixative solution composed of 3:1 methanol:acetic acid. Chromosomes were QFQ banded using quinacrine mustard (Roche) and slides were mounted in McIlvaine buffer. Slides were analysed using Nikon Eclipse 80i fluorescence microscope (Nikon) equipped with a COHU High Performance CCD camera. The mitotic index was evaluated counting the percentage of mitosis scoring at least 1000 nuclei, while ploidy was investigated by evaluating the number of chromosomes/metaphase on 30/50 metaphases. Chromosomes spreads were analysed using the Genikon software. Data were obtained as mean values derived from two independent experiments.

2.7. Neurosphere Formation Assay. Cells treated with Danusertib 50 nM and 500 nM for 48 h were retrieved from flasks to obtain a single cell suspension and counted by trypan blue assay. $4x10^3$ cells for each condition were plated in a well of a six-well plate and let to grow for a week. Spheres were counted through the observation at a phase contrast microscopy. Data were obtained as mean values derived from two independent experiments.

2.8. Morphological Analysis. Morphological analysis was assessed as already described in [29]. Cells were treated with Danusertib (5-50-200-500-1000 nM) for different times of exposure (24-48-72 h).

2.9. Giemsa Staining. Cells grown on coverslips and treated with Danusertib 500 nM for 48 h were fixed with 70% methanol, stained with 10% Giemsa solution (Gibco by Thermo Scientific) in distilled water for 15 minutes, and rinsed off in tap water. Coverslips were let to dry and mounted using Polyvinyl alcohol mounting medium (Merck). Nuclei morphology was evaluated through the observation at phase contrast microscopy. Based on nuclei morphology, cells were divided into four classes: normal nuclei, polymorphic nuclei, multinucleated cells, and micronucleated cells. Representative images were taken for each cell line using 100x oil lens.

2.10. DNA Integrity Evaluation. Genomic DNA was extracted from untreated and 48 hs 500 nM Danusertib treated GSCs using the DNeasy Blood & Tissue Kit (Qiagen, Hilden, Germany) according to the manufacturer's protocol.

DNA integrity analysis was performed using an automated tape-based electrophoresis (2200 TapeStation, Agilent technologies) according to the manufacturer's instructions. It automatically calculated the DNA concentration and provided the DNA integrity number (DIN). This numerical assessment of the genomic DNA integrity can range from 1 to 10. DIN>7 indicates highly intact genomic DNA, while DIN<7 indicates a degraded genomic DNA.

2.11. Immunofluorescence. Phosphorylated Aurora kinases levels were evaluated after Danusertib 500 nM exposure for 48 h.

Cells were grown on coverslips, synchronized using STLC 5 μM, and fixed with 3.7% paraformaldehyde (Merck) and 70% methanol, for 10 minutes and 1 minute, respectively.

Cells were permeabilized in PBS 0.1% NP40 for 15 minutes, blocked in 3% BSA (Sigma) for 30 minutes, and incubated with mouse anti-γtubulin (1:100, Abcam), rabbit anti-phospho-Aurora A/B/C (1:100, Cell signalling technology), and human anti-Crest (1:100, Antibodies incorporated) primary antibodies for one hour at 37°C. Slides were washed and probed with 488-donkey-anti-mouse (1:2000, Life technologies by Thermo Scientific), 594-goat-anti-rabbit (1:2000, Life technologies by Thermo Scientific), or 670-goat-anti-human (1:2000, Abcam) secondary antibodies for one hour at room temperature. Coverslips were incubated with DAPI for 10 minutes and mounted using the ProLong Diamond mounting solution (Life technologies by Thermo Scientific).

Images were acquired through a 60x oil immersion lens on a Delta Vision Olympus IX70 microscope equipped with a CCD camera using Micromanager software. Images deconvolution was performed using SVI Huygens Professional Deconvolution Software (version 3.5) (Scientific Volume Imaging). For quantitative analysis of phosphorylated Aurora kinases levels, images were imported into Omero software and analyzed with ImageJ software (https://imagej.nih.gov/ij/). Data were obtained as mean values derived from two independent experiments.

2.12. Live Cell Imaging. Live cell imaging analysis was performed on GBM2 and G166 cell lines in order to evaluate cell fate when Danusertib 500 nM was added into cell culture.

GSCs were plated in 4 wells chambered slides (Ibidi, Martinsried, Germany) coated with Matrigel and incubated on the Olympus IX71 or IX73 microscopes, equipped with a CCD camera, temperature controller (37°C), and CO_2 (5%) incubation chamber, soon after the addiction of Danusertib 500 nM.

Images of multiple fields per well were collected every 5 min overnight using a dry 20x objective lens. Images were acquired using the MicroManager software and analyzed by means of ImageJ software.

2.13. TP53 Sanger Sequencing. Genomic DNA was extracted from GSCs using the DNeasy Blood & Tissue Kit (Qiagen) according to the manufacturer's protocol. DNA quantity and quality were analyzed using a Nanodrop ND-1000 spectrophotometer (Thermo Scientific).

TP53 exons 5, 6, 7, and 8, representing the mutational hot spot region, were sequenced. The set of primers used to amplify the target DNA and to sequence the DNA was purchased from Life technologies (Supplementary Table S5).

An end-point PCR was performed to amplify the TP53 target loci. DNA quality was examined using an agarose gel electrophoresis. PCR products were purified by means of the EuroSap enzymatic Kit (Euroclone, Pero, Italy). Next, the sequencing reaction was performed using the BigDye terminator v.3.1 kit (Applied Biosystem) according to the manufacturer's protocol. The following thermal cycling conditions were used: 96°C for 40 seconds; 25 cycles composed of 96°C for 10 seconds, 50°C for 5 seconds, and 60°C for

4 minutes; 4°C ∞. The reaction products were purified using EDTA 125 mM pH8 and EtOH. DNA sequencing was performed through a capillary electrophoresis using an ABI-3130 sequencer (Applied Biosystems), with 4 capillaries of 36 cm of length each, loaded with POP-7 polymer. Samples were allowed to run for about 1 h. Data were analysed using the FinchTV software.

2.14. Microsatellites Analysis. Loss of heterozygosity (LOH) analysis of chromosome 17 was assessed by means of PCR-based assays, as described in [7]. STR markers used are listed in Supplementary Table S6.

2.15. β Galactosidase Staining. GBM2 and G166 were grown on coverslips in 6-well plates and treated with 500 nM Danusertib. After one and two rounds of 48 h drug exposure, they were stained using the Cellular Senescence Assay Kit (Cell biolabs, San Diego, California, USA) according to the manufacturer's protocol. Stained cells were mounted using the ProLong Diamond mounting solution (Life technologies).

Random images were acquired on Axio Lb A1 (Zeiss) microscope equipped with an AxioCam ERc 5s (Zeiss, Oberkochen, Germany) and a 40x objective. At least 500 β galactosidase positive and negative cells were counted on a computer monitor for each condition and percentages of β galactosidase positive cells were calculated. The results are expressed as mean of two independent experiments.

2.16. Fluorescence In Situ Hybridization (FISH). Cells in exponential growth phase were treated with 500 nM Danusertib for one or two rounds of 48 h each. Cell suspension was retrieved from flask and dropped onto glass slides. Cells were fixed with fixative solution composed of 3:1 methanol:acetic acid and FISH analysis on interphase nuclei or metaphase chromosomes was performed using a commercial probe set targeting chromosomes X, Y, 13, 18, and 21 (FAST FISH Prenatal Enumeration Probe kit, CytoCell by Oxford Gene Technology, Begbroke, UK). Signals were counted in at least 50 cells per sample and the number of signals was used in order to predict the cell ploidy. All digital images were captured using a Leitz microscope (Leica DM 5000B) equipped with a CCD camera (Leica Microsystems, Wetzlar, Germany) and analyzed by means of Chromowin software (Tesi Imaging, Milano, Italy). The results are expressed as mean of two independent experiments.

2.17. Statistics. Statistical analyses were carried out performing Yates' chi-square test or t-test on raw data, by means of Excel spreadsheet (Microsoft Corporation). p value<0,05 was considered statistically significant.

3. Results

3.1. Assessment of Sensitivity and Resistance to Danusertib. To investigate the potential of Aurora kinases as therapeutic targets in GSCs, we initially verified the transcriptional and protein levels of Aurora kinases in a previously characterized GSCs panel [7]. We found that AURKA and AURKB are upregulated in all the cell lines of the panel and that AurKs are expressed in mitotic GSCs (Supplementary Figures S1A and S1B). Afterwards, we determined the effect of six increasing concentrations of Danusertib on the GSCs viability by MTT assay, after three time points of treatment. Dose-response curves, shown in Figure 1(a), suggest that the Danusertib inhibitory effect was heterogeneous among the cell lines (Figure 1(a), Supplementary Table S1). After 24 h of treatment, we observed a slight decrease of the cell viability in all the GSCs, which was mainly dose-dependent. After 48 and 72 h, this reduction was more evident in GBM2, G179, and G144 cell lines, showing a decrease of around 50% at the highest doses of Danusertib. The reduction values seemed not to be affected by the prolongation of the treatment, remaining almost the same after 48 h and 72 h of exposure. We also assessed the proliferation rates of the cells by mitotic index measurements (Figure 1(b)) and neurospheres formation assays (Figure 1(c)). These data revealed that Danusertib induced a significant dose-dependent reduction of cell viability and self-renewal potential only in some cell lines (Figures 1(b) and 1(c)). Based on the reduction of at least two of the parameters taken into consideration, we classified the cell lines in sensitive (GBM2, G179, and G144) and resistant (G166 and GliNS2).

3.2. Danusertib Induces Strong Changes in Cell and Nuclei Morphology in Sensitive GSCs. In the resistant cell lines, Danusertib did not induce any relevant modification in the cellular shape (Figure S2). On the contrary, Danusertib treatment caused morphological changes in the sensitive cell lines as shown in Figure 2(a). GBM2, G179, and G144 cells showed a dramatic increase in their size starting from 48 h of exposure to Danusertib 500 nM. Hence, we selected 48h and 500 nM, the earliest time point and the lowest concentration at which cells presented evident morphological changes reflecting the Aurora kinase inhibition, for the further experiments.

Additional analysis of nuclei morphology allowed us to distinguish between normally shaped and polymorphic nuclei and multinucleated and micronucleated cells (Figure 2(b), Table S2). A percentage of atypical nuclei, which are a hallmark of cancer, were already present in all the untreated GSCs. In the sensitive cell lines, there was a significant increase in the percentages of polymorphic nuclei and multinucleated cells after the treatment. Moreover, in GBM2, G179, and G144, Danusertib induced also the appearance of micronucleated cells. All these features could mirror the increased cell size previously reported. In the resistant G166, the nuclei morphology was already strongly altered in the control, while in GliNS2 there was only a slight increase in the percentages of polymorphic nuclei and multinucleated cells, but no micronuclei were observed.

3.3. Danusertib Inhibits Aurora Kinases and Causes Cytokinesis Failure in Both Sensitive and Resistant Cell Lines. A simple explanation for the difference in sensitivity within the GSCs panel could be the different levels of inhibition to AurKs in response to Danusertib, or difference in mitotic

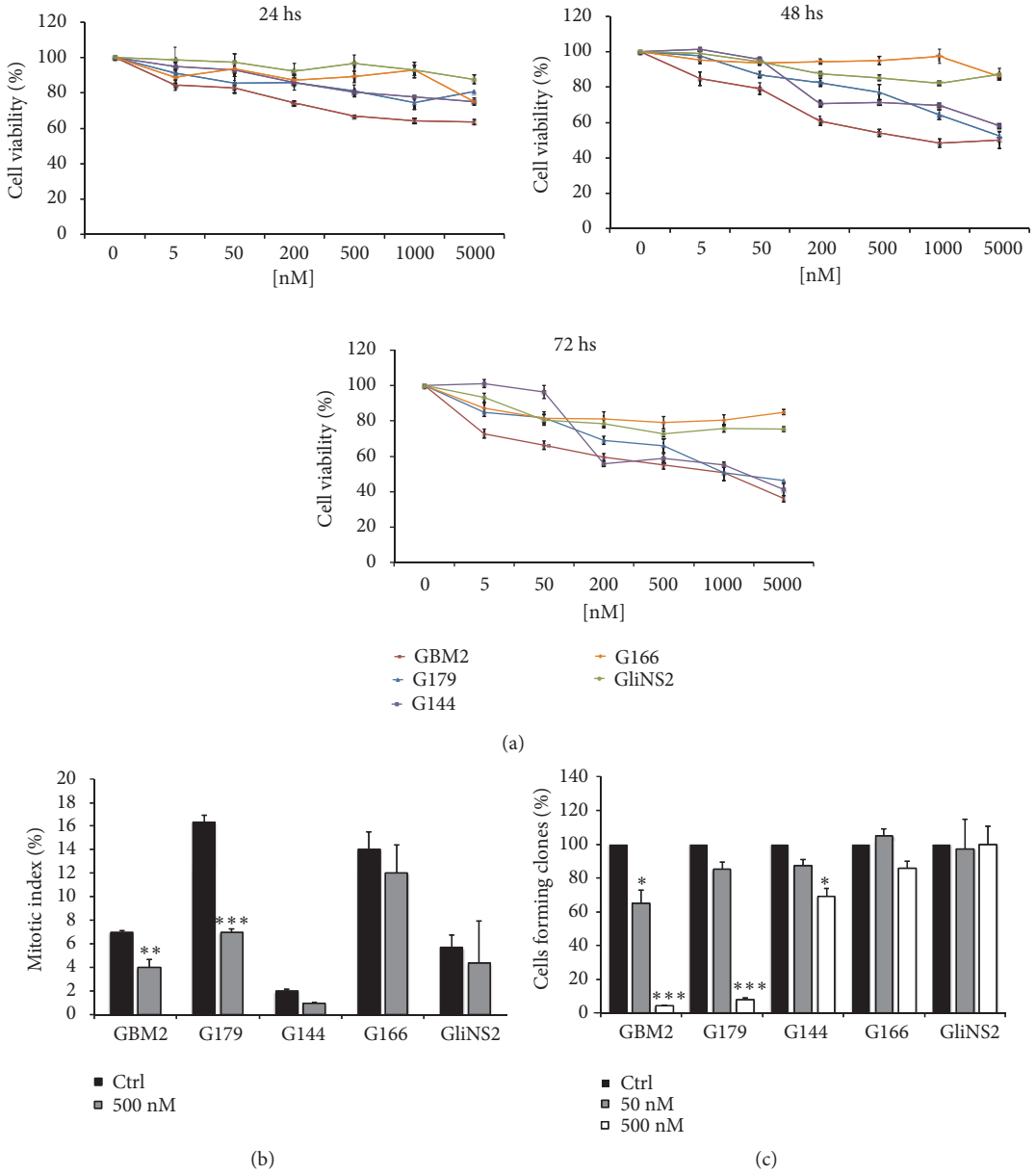

Figure 1: *Different sensitivity of GSCs to Danusertib exposure*. (a) Cell viability was analyzed in five GSC lines by MTT assay after exposure to escalating doses of Danusertib for 24, 48, and 72 h. Results represent the means from three different experiments performed in quadruplicate. Error bars represent SEM. For statistical analysis, see Supplementary Table S1. (b) Cell proliferation was evaluated through the determination of the mitotic index after exposure to Danusertib 500 nM for 48 h. Results are reported as percentages from the means of three independent experiments. Error bars represent SEM. Chi-square test on raw data was performed: ∗∗ $p<0,01$; ∗ ∗ ∗ $p<0,001$. (c) Clonogenic potential was evaluated after treatment for 48 h with Danusertib 50 nM and 500 nM. Results are reported in a bar graph as percentages of cell forming colonies in the treated samples over matching controls. Results are the means of three independent experiments. Error bars represent SEM. t-test was performed on raw data: ∗ $p<0,05$; ∗ ∗ ∗ $p<0,001$.

aberration following inhibition. In order to ascertain which type of mechanism determines the different behavior, we initially measured these responses to inhibitor treatment by quantitative fluorescence in mitotic cells and by live cell imaging. To assess AurKs activity, we used a phospho-specific antibody that cross-reacts with the T-loop autophosphorylation site in both Aurora-A, B, and C (residues: Thr288, Thr232, Thr198) [30]. We observed a significant reduction of the level of phosphorylated AurKs in all the cell lines suggesting that Danusertib inhibited these kinases in both sensitive and resistant cell lines (Figure 3, Supplementary Figure S3).

In order to better characterize the cell fate induced by Danusertib, we performed live cell imaging analyses in a sensitive (GBM2) and resistant (G166) cell lines (Supplementary Videos S1, S2, S3, and S4). Both cell lines responded to Danusertib with delayed mitotic exit and cytokinesis failure, both hallmarks of Aurora-B inhibition (Figures 4(a), 4(b),

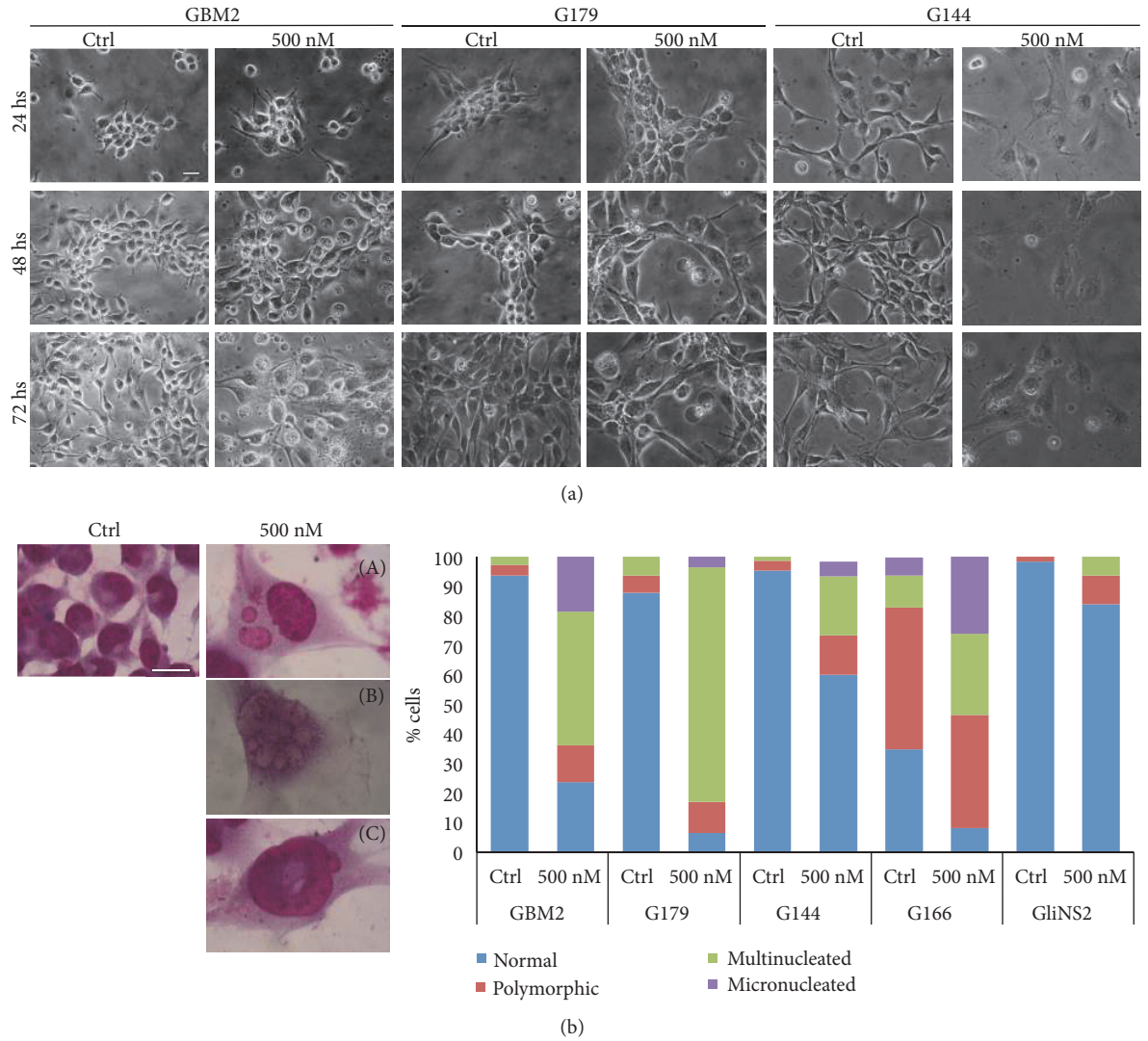

Figure 2: *Danusertib induces evident changes in cell and nuclei morphologies in sensitive GSCs.* (a) Representative images taken by phase contrast microscopy of GBM2, G179, and G144 cell lines treated with 500 nM Danusertib for 24, 48, and 72 h are reported. Drug treatment induced a significant increase in cell size starting from 48 h drug exposure. Scale bar = 100 μm. (b) Representative images of different nuclei shapes detected after 500 nM Danusertib treatment for 48 h and Giemsa staining. Sensitive cell lines highlighted the presence of a huge number of large multinucleated (A) and micronucleated (B) cells and polymorphic nuclei, such as ring-shaped nuclei (C). Scale bar = 100 μm. Quantitative data are reported in the graph. For statistical analysis, see Supplementary Table S2.

and 4(c), Table S3). Thus, the striking difference in cellular survival in response to AurKs inhibition in resistant and sensitive cells is not due to a different level of Auroras inhibition but must be due to a differential response to the failed cell division program in the different cell lines.

3.4. Danusertib Induces Ploidy Increase in GSC Lines. Given the highly penetrant cytokinesis defect following Danusertib treatment in both sensitive and resistant cell lines, we expected to observe an increase in ploidy following drug exposure. Measurement of chromosome content identified classes of ploidy and results were grouped according to this classification (Table 1). These data revealed that, even in untreated cells, Danusertib sensitive cell lines have a significantly higher chromosome content compared to the resistant ones. As expected, Danusertib induced an increase in the number of chromosomes in both sensitive and resistant cell lines. Only in GliNS2 cell line, the ploidy remained almost stable. Moreover, this increased DNA content was not fragmented, as demonstrated by the determination of the DNA integrity number (DIN) (Supplementary Figure S4A).

3.5. GSCs Response to Danusertib Is Not Dependent on TP53 Mutational Status. An obvious candidate to explain this differential response to polyploidisation is the mutational status of the TP53 gene, which has been shown to trigger cell cycle arrest following increases in ploidy [8]. However, sequencing of the TP53 mutational hot spot regions [31, 32] revealed that both sensitive and resistant cell lines, except for GliNS2, carried missense mutations in the DNA-binding

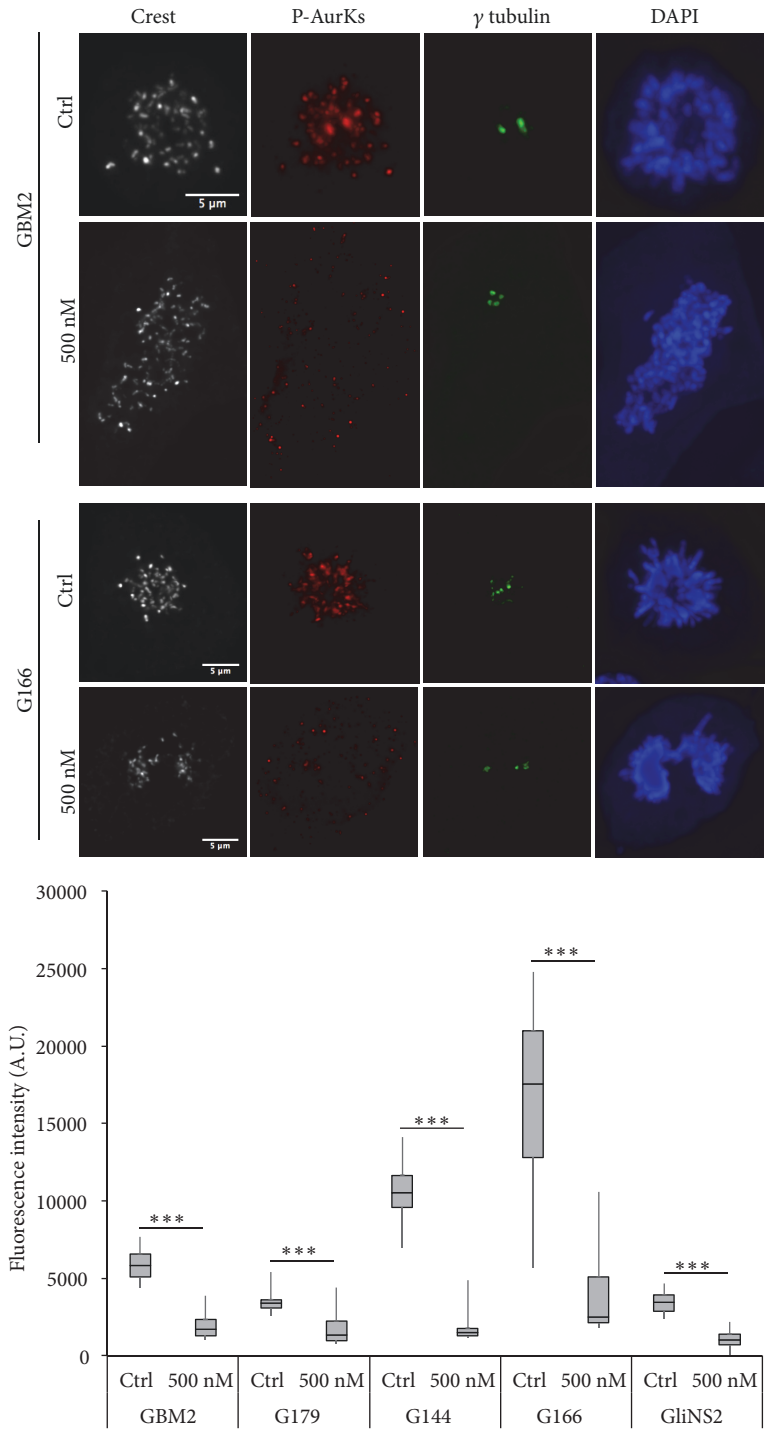

FIGURE 3: *Danusertib induces a reduction of phosphorylated Aurora kinases in all the GSCs.* Representative images (up) of untreated or 48 h 500 nM Danusertib treated sensitive (GBM2) and resistant (G166) GSC lines, synchronized with STLC and stained for Crest (white), phospho-Aurora kinases (red), γ tubulin (green), and DAPI (blue) are reported. Scale bar = 5 μm. Quantification of the pospho-Aurora kinases fluorescent signal in the nuclei of mitotic cells was performed by ImageJ software (bottom). Results are expressed as mean of two independent experiments. At least 25 cells were analyzed in each experiment. Error bars represent SEM. t- test was performed on raw data: $***$ $p<0{,}001$.

Table 1: *Ploidy evaluation after 48 h of treatment with 500 nM Danusertib.* Cells were divided into several classes based on the chromosome content. Danusertib induced an increase in the chromosomes content in both sensitive and resistant cell lines. Italic numbers indicate cell ploidy of untreated cells: sensitive cell lines have a significant higher chromosome content compared to the resistant ones. Chi square test (treated vs untreated): ∗p<0,05; ∗∗p<0,01; ∗ ∗ ∗p<0,001. t-test (ctrl sensitive vs ctrl resistant): #p<0,001.

		Class of ploidy (number of chromosomes/metaphase)											
Cell line	Treatment	hypo diploid 35-46	hyper diploid 47-57	hypo triploid 58-69	hyper triploid 70-80	hypo tetraploid 81-92	hyper tetraploid 93-103	near pentaploid 104-126	near hexaploid 127-149	near eptaploid 150-172	near octoploid 173-195	near nonaploid 196-218	near decaploid 219-241
GBM2	Ctrl[#]	*0,0*	*0,0*	*0,0*	*10,0*	*0,0*	*0,0*	*16,7*	*73,3*	*0,0*	*0,0*	*0,0*	*0,0*
	500 nM	0,0	0,0	0,0	0,0∗	6∗	3,0	12,0	36,4∗ ∗ ∗	39,4∗ ∗ ∗	0,0	0,0	3,0
G179	Ctrl[#]	*0,0*	*0,0*	*0,0*	*10,0*	*20,0*	*36,7*	*33,3*	*0,0*	*0,0*	*0,0*	*0,0*	*0,0*
	500 nM	0,0	0,0	0,0	3,3	0,0∗ ∗ ∗	6,7∗ ∗ ∗	3,3∗ ∗ ∗	16,7∗ ∗ ∗	13,3∗ ∗ ∗	30∗ ∗ ∗	6,7∗	20∗ ∗ ∗
G144	Ctrl[#]	*0,0*	*0,0*	*2,0*	*23,5*	*56,8*	*15,7*	*2,0*	*0,0*	*0,0*	*0,0*	*0,0*	*0,0*
	500 nM	0,0	0,0	16,7∗ ∗ ∗	33,3	33,3∗ ∗ ∗	0∗ ∗ ∗	0,0	3,3	6,6∗∗	3,3	0,0	0,0
G166	Ctrl	*0,0*	*66,7*	*33,3*	*0,0*	*0,0*	*0,0*	*0,0*	*0,0*	*0,0*	*0,0*	*0,0*	*0,0*
	500 nM	0,0	0∗ ∗ ∗	6,7∗ ∗ ∗	0,0	0,0	26,7∗ ∗ ∗	63,3∗ ∗ ∗	0,0	0,0	3,3∗	0,0	0,0
GliNS2	Ctrl	*50,0*	*33,3*	*0,0*	*0,0*	*16,7*	*0,0*	*0,0*	*0,0*	*0,0*	*0,0*	*0,0*	*0,0*
	500 nM	46,7	40,0	0,0	0,0	13,3	0,0	0,0	0,0	0,0	0,0	0,0	0,0

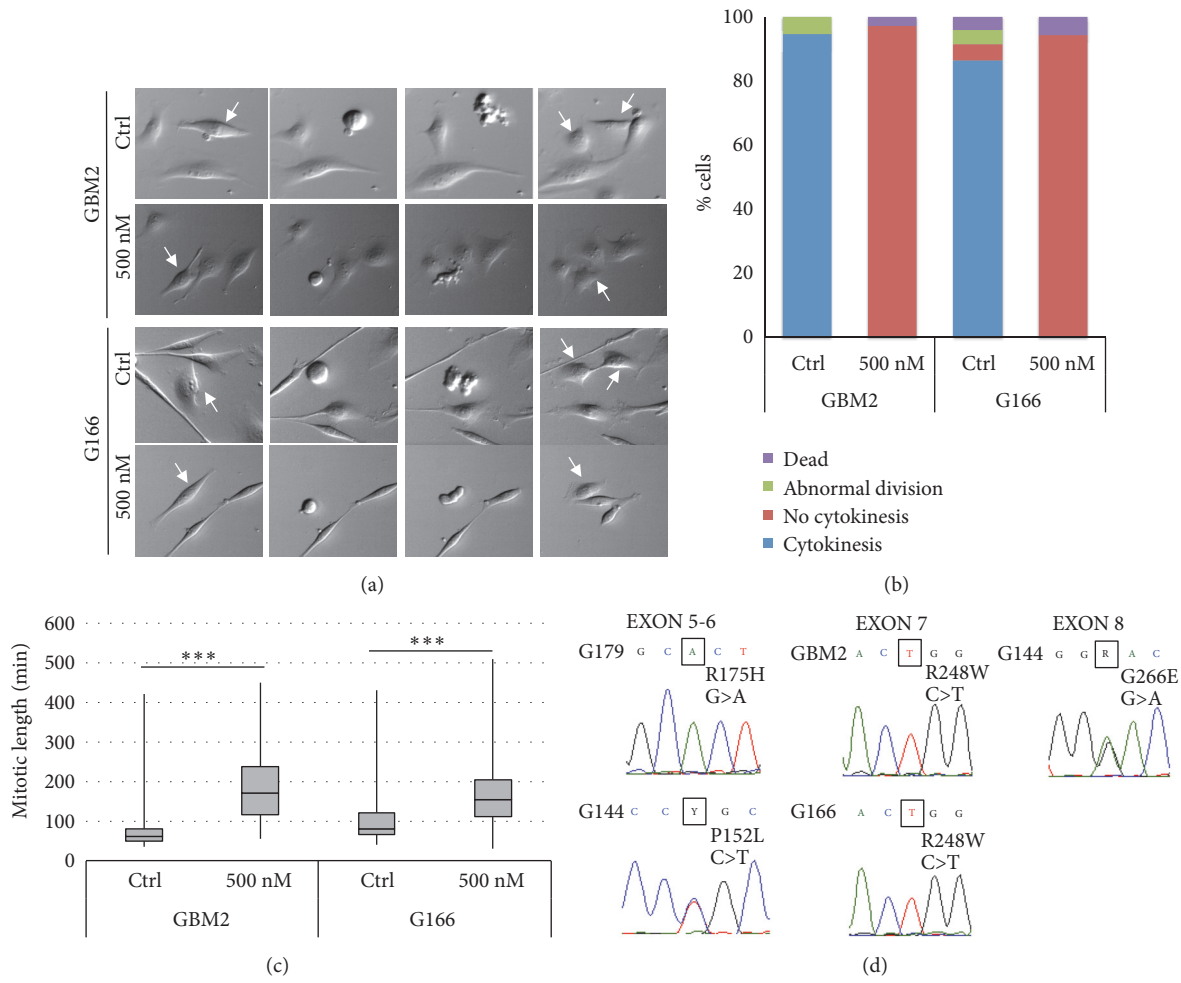

FIGURE 4: *Danusertib induces a cytokinesis failure and delayed mitotic exit in sensitive and resistant GSCs, independently of the T53 mutational status.* (a) Representative images of dividing cells (indicated by white arrows) detected by means of live cell imaging analysis (see also Supplementary Videos S1, S2, S3, and S4) show that GSCs were able to enter into mitosis after Danusertib exposure but not to divide through cytokinesis. (b) Quantitative data concerning the cells fate after treatment confirm that Danusertib 500 nM inhibited cytokinesis in sensitive and resistant GSCs. The other parameters evaluated, such as the cell death, did not show any relevant variations. Results represent the means from three different experiments. At least 100 cells were analyzed. For statistical analysis, see Supplementary Table S3. (c) Danusertib induced a significant increase in the mitotic length, determined analyzing the live cell movie by means of Image J. Results represent the means from three different experiments. At least 100 cells were analyzed. t-test was performed on raw data: $***p<0{,}001$. (d) Electropherograms of TP53 mutational hot spot regions highlighted that all the GSC lines carried missense mutations in the DNA-binding region of the protein, except for GliNS2 line, which was not affected by any mutation.

region of the protein (Figure 4(d) and Supplementary Table S4). This strongly suggests that GSCs sensitivity to Auroras inhibition is not TP53 mutational status-dependent. Interestingly, in all cell lines, except for G144, TP53 mutations were in homozygous state, suggesting a loss of heterozygosity (LOH) of whole or part of chromosome 17, as shown in Supplementary Figure S4B.

3.6. Danusertib Exposure Induces an Increase in Senescent/Autophagic Cells in Sensitive GSCs. Based on previous studies reporting the ability of Aurora inhibitors to induce senescence [33–35] and the association between senescence and autophagy in polyploid cells [36], we evaluated the levels of β-galactosidase and Beclin and the LC3-I/LC3-II ratio in two GSC lines with different sensitivity to Danusertib (GBM2 and G166). Beclin and LC3 have previously been used as markers of autophagy [37]. In particular, Beclin regulates the localization of specific proteins in the early autophagy stages [38], while LC3-I is converted to LC3-II during the activation of this process through lipidation by a ubiquitin-like system, allowing its association with autophagic vesicles [39]. After 48 h of exposure, Danusertib induced a significant increase in the percentage of senescent cells (79%), in the level of Beclin, and in the ratio of LC3-I and II in GBM2. G166 also showed an increase in the β-galactosidase positive cells (42%), but there was no variation in Beclin level or in the LC3-I/II ratio (Figures 5(a) and 5(b)).

3.7. Cell Ploidy Influences the Different GSCs Response to Danusertib. As described above, sensitive and resistant cell

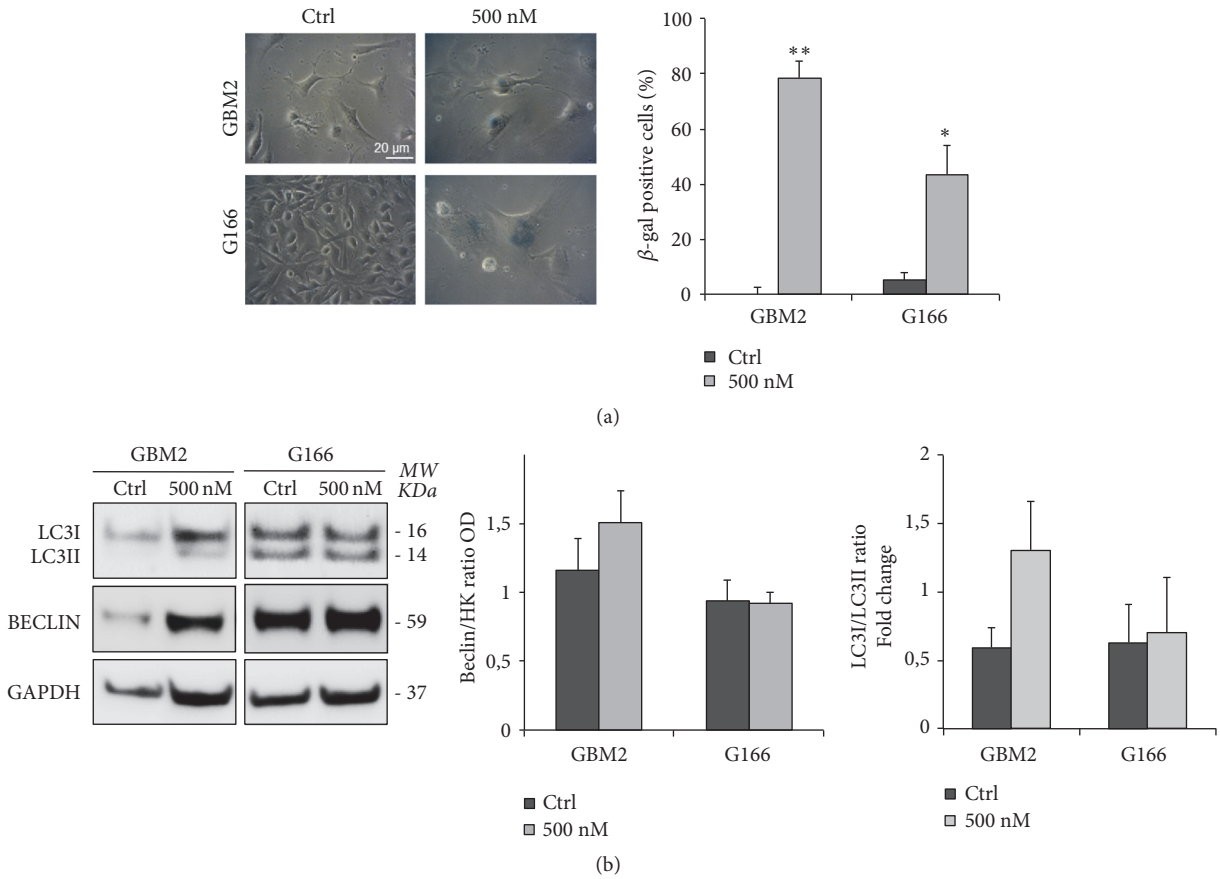

Figure 5: *Danusertib induces senescence/autophagy in sensitive cell line*. (a) GBM2 (sensitive) and G166 (resistant) cell lines were treated with 500 nM Danusertib for 48 h. After the incubation, they were fixed and stained for β-galactosidase to evaluate induction of senescence. Representative images showing β-galactosidase staining at baseline and after Danusertib treatment are reported. The graph shows the percentages of senescent cells in the two cell lines. Danusertib induced a significant and more relevant increase in the percentage of β-gal positive cells only in the sensitive cell line (GBM2). An average of 100 cells/condition/experiment were randomly imaged and scored. Results are representative of three independent experiments. Error bars represent SEM. t-test was performed on raw data: $*$ $p<0,05$; $**$ $p<0,01$. (b) Beclin level and LC3-I and LC3-II ratio were determined in untreated and 48 h 500 nM treated GBM2 (sensitive) and G166 (resistant) cell lines in order to evaluate the activation of an autophagic process. Representative images of Western blot analysis and quantitative data are reported. Beclin, LCR-I and II levels were determined and normalized on GAPDH. All the values are expressed in Arbitrary Unit (AU). Danusertib induced a non-statistically significant increase of Beclin level and LC3-I and LC3-II ratio only in the sensitive cell line (GBM2). Results are representative of three independent experiments. Error bars represent SEM.

lines are characterized by different ploidy, even in the untreated cells. This difference in chromosomes content could be an intrinsic feature of GSCs explaining their distinct fate after Danusertib exposure and suggesting a tolerable threshold in ploidy even in TP53 mutated cells. A direct consequence of this would be that resistant cell lines should also show a sensitization to Danusertib and undergo senescence/autophagy once reaching this threshold. This could be achieved by administering repeated rounds of Aurora inhibition, leading to a steady ploidy increase (Figure 6(a)).

We tested this hypothesis and found that the resistant cell line showed sensitization to Danusertib after the 2nd round of treatment, as demonstrated by the reduction of the cell viability and the self-renewal potential (Figures 6(b) and 6(c)). They underwent a similar senescent and autophagic response, which resulted in a significant increase in the percentage of β-galactosidase positive cells (Figure 6(d)), in the Beclin level, and in LC3-I and II ratio (Figure 6(e)). Finally, FISH analyses, performed with a diagnostic kit that detect, among the others, chromosome 21, which is not frequently altered in terms of number of copies in GBM [7, 40], highlighted that, after the 2nd round of Danusertib, the number of chromosomes per cell of the resistant cell line reached the same number observed in the sensitive one, already after 48 h of Danusertib exposure (Figure 6(f)). These data suggest that GBM2 cells reached the ploidy threshold already after 48 h of treatment, while G166 cells only after the 2nd round of Danusertib treatment.

4. Discussion

In this study, we analyzed the effects of Danusertib, a pan-Aurora kinases inhibitor with therapeutic potential against a variety of solid cancers [41], on five established GSC lines

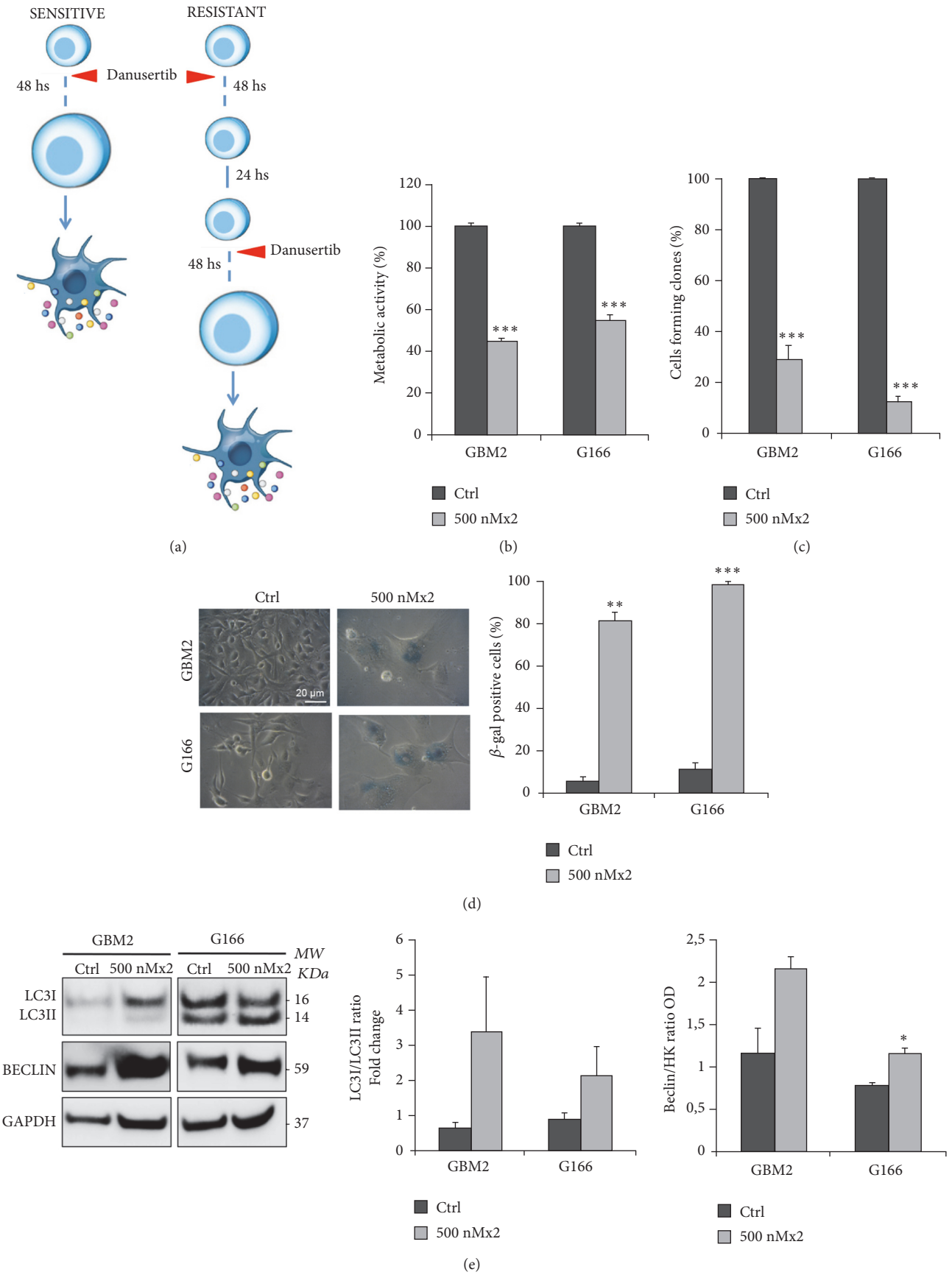

Figure 6: Continued.

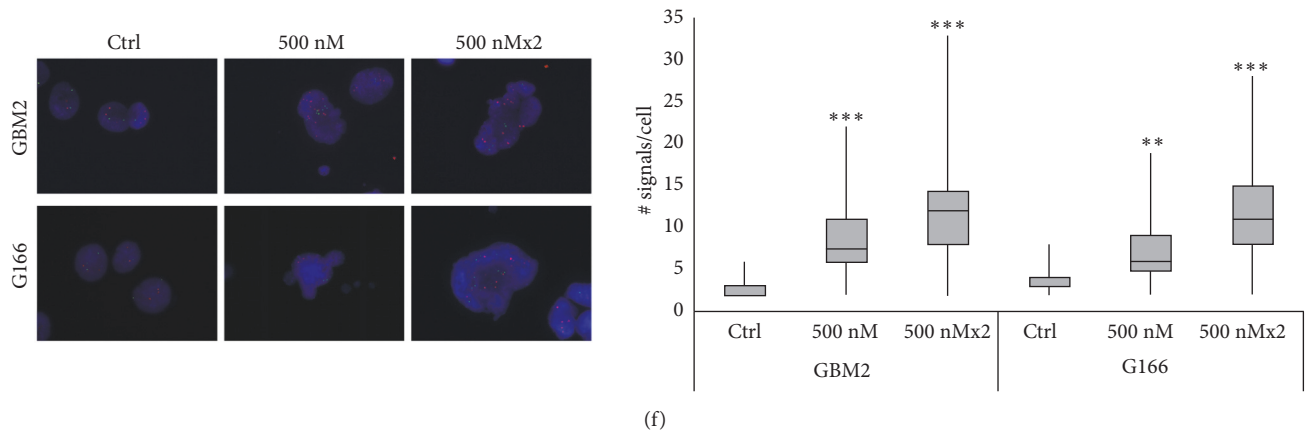

Figure 6: *Multiple rounds of exposure to Danusertib can sensitize the resistant cell line, inducing senescence/autophagy*. (a) Cell lines were subjected to multiple rounds of 48h treatment with Danusertib 500 nM. The sensitization of the resistant cell line (G166) to Aurora inhibition was reached already after two rounds of treatment with Danusertib 500 nM. This was confirmed by MTT assay (b) and the clonogenic assay (c). There was a significant decrease of the cell viability and the clonogenic potential in G166, which was similar to the one observed in GBM2, already after 48 h. Results are the means of three independent experiments. Error bars represent SEM. t- test was performed on raw data: $***$ p<0,001. (d) GBM2 (sensitive) and G166 (resistant) cell lines were treated with 500 nM Danusertib for two rounds of 48 h each. After the incubation, they were fixed and stained for β-galactosidase, to evaluate induction of senescence. Representative images showing β-galactosidase staining at baseline and after Danusertib treatment are reported. The graph shows the percentages of senescent cells in the two cell lines. An average of 100 cells/condition/experiment were randomly imaged and scored. After two rounds of exposure to Danusertib, there was a significant increase in the percentages of β–gal positive cells also in the resistant cell line (G166). Results are representative of three independent experiments. Error bars represent SEM. t- test was performed on raw data: $**$ p<0,01; $***$ p<0,001. (e) Beclin level and LC3-I and LC3-II ratio were determined in untreated and two rounds treated GBM2 and G166 cell lines in order to evaluate the activation of an autophagic process. Representative images of Western blot analysis and quantitative data are reported. Beclin, LCR-I, and II levels were determined and normalized on GAPDH. All the values are expressed in Arbitrary Unit (AU). After two rounds of Danusertib exposure, an increase of Beclin level and LC3-I and LC3-II ratio was detected also in G166 cell line. Results are representative of three independent experiments. t- test was performed on raw data: $*$ p<0,05. (f) Representative images of FISH analysis performed on GBM2 (sensitive) and G166 (resistant) cell lines after one and two rounds of 48 h treatment with Danusertib 500 nM are reported. Red signals correspond to chromosome 21, while green signals indicate chromosome 13. Scale bar = 100 μm. Quantitative analysis shows that Danusertib exposure induced a steady increase of the number of signals detected in both cell lines. The chromosome content detected in G166 after two rounds of Danusertib exposure is comparable to the one observed in GBM2 cell line already after one round of treatment. Results are expressed as mean of two independent experiments. At least 50 cells were analyzed in each experiment. t- test was performed on raw data: $***$ p<0,001.

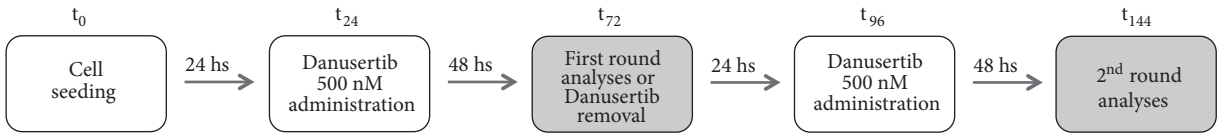

Figure 7: Danusertib administration schedule.

derived from GBM patients [7]. We discovered a strikingly heterogeneous response among GSC lines, even though Danusertib inhibited Aurora kinases to a similar extent in all the GSCs. Cell viability was significantly reduced only in three cell lines out of five (GBM2, G179, and G144), indicated as sensitive to Danusertib. In these cell lines, Danusertib induced a decrease of the proliferation and clonogenic potential and, above all, evident alterations in the cell and nuclei morphologies, with the appearance of bigger cells and multi- or micronucleated cells with an increased chromosome content. Interestingly, these ploidy alterations were also detected in the resistant cell lines even if they were not linked to relevant morphological alterations, probably because the level of ploidy they reached was not as high as the one detected in the sensitive ones. Live cell imaging analysis shed light on the mechanism underlying the increase in the chromosome number: in both sensitive and resistant cell lines, Danusertib allowed the cells to enter into mitosis but induced a block of the cytokinesis, leading to an increase in ploidy. All these findings confirm previously published data, which demonstrated that Danusertib is able to induce a cell cycle inhibition and endoreduplication in different cancer cells, causing a substantial increase in DNA content with 4N or even >4N cells subpopulations [41].

However, even if a failure of the cytokinesis and an alteration of the cell ploidy was observed in all the GSC lines after 48 h of treatment, sensitive and resistant cells were characterized by a different fate, with only the first ones undergoing a significant activation of a senescent/autophagic process. The senescent phenotype is intriguing and reminiscent of

published results [42]. Several studies showed that, after treatment with AurKs inhibition, cancer cells displayed a serial of senescent morphological and functional changes such as enlarged and flattened morphology, increased levels of p21 protein, and enhanced β-galactosidase staining, suggesting that, instead of apoptosis, senescence might be the mainly terminal outcome of Aurks inhibition in some tumor types [43]. Interestingly, recent studies also indicated that autophagy, a genetically regulated program responsible for the turnover of cellular proteins and damaged or superfluous organelles, can be a new effector mechanism of senescence, important for the rapid protein remodeling required to make the efficient transition from a proliferative to a senescent state [36]. In our case, the increase in misfolded proteins, caused by a polyploidy-induced proteomic strain, could be at the origin of proteotoxic stress, leading to the activation of an autophagic process, as demonstrated by the increased Beclin level and LC3-I/LC3-II ratio in the sensitive cell line.

A first explanation for cells responding differentially to an AurKs inhibitor has been recently suggested to be depending on the integrity of the p53-p21–dependent postmitotic checkpoint [44], even if several studies yielded conflicting results [45]. The analysis of the TP53 mutational status of our cells showed that both sensitive and resistant cell lines carried missense mutations, supporting the hypothesis that p53 status does not play a key role in determining the differential sensitivity of GSCs to AurKs inhibition.

However, an interesting cell feature that emerged to really differentiate between sensitive and resistant cell lines was the chromosome number observed in the untreated cells. We could group the GSC lines by their level of ploidy and correlate this with sensitivity to AurKs inhibition. A straightforward explanation for this result could be the presence of a ploidy threshold, that is intolerable even for p53 negative cell lines. This hypothesis is supported by our experiments with repeated rounds of Danusertib treatment in the resistant cell line (Figure 7). This leads to a further increase in ploidy and ultimately also triggered senescence/autophagy. These results are supported by previously published data, which showed that high amount of chromosome imbalances and alterations are associated with cell growth arrest. Cells with complex karyotype exhibit features of senescence and are even able to produce proinflammatory signals [46].

5. Conclusions

Our results suggest that a ploidy threshold is the main determinant of AurKs inhibition sensitivity in TP53 mutant glioma stem cells. Interestingly, previous cytogenetic screenings of GBM specimens have already highlighted that GBMs are characterized by a different chromosomes content [47], supporting the idea that cell ploidy could, indeed, be a promising prognostic factor to predict sensitivity to Danusertib treatment. Further research will be necessary to explore the mechanism of ploidy induced senescence and the precise reason why a particular ploidy threshold appears to trigger this response.

Abbreviations

GBM: Glioblastoma
GSCs: Glioma stem cells
CIN: Chromosomal instability
AurKs: Aurora kinases
MTT: 3-(4,5-Dimethylthiazol-2-yl)-2,5-Diphenyltetrazolium Bromide
FISH: Fluorescence in situ hybridization.

Data Availability

The data used to support the findings of this study are included within the article.

Conflicts of Interest

The authors declare that there are no conflicts of interest regarding the publication of this article.

Authors' Contributions

Chiara Cilibrasi, Angela Bentivegna, and Helfrid Hochegger conceived the studies and wrote the manuscript. Chiara Cilibrasi and Andrèe Guzzi conducted the majority of the experiments. Riccardo Bazzoni and Gabriele Riva performed some of the experiments. Helfrid Hochegger and Angela Bentivegna coordinated the study. Massimiliano Cadamuro, Helfrid Hochegger, and Angela Bentivegna provided a financial support. All authors read and approved the final manuscript.

Acknowledgments

The authors want to gratefully acknowledge Prof. Austin Smith (Wellcome Trust, Medical Research Council Stem Cell Institute, University of Cambridge, Cambridge, UK), Dr. Antonio Daga (IRCCS-AOU San Martino-IST, Genova, Italy), and Dr. Ida Biunno for kindly providing them with the cell lines used in this study, Dr. Eugenio Gautiero for his technical assistance, and Dr. Gessica Sala for the anti-Beclin antibody. This work was supported by 2013-ATE-0406 and 2013-ATE-0489 grants from University of Milano-Bicocca (to Angela Bentivegna), Grant no. 2014-1099 from Fondazione Cariplo (to Massimiliano Cadamuro), and CRUK senior research fellowship ID C28206/A14499 (to Helfrid Hochegger).

Supplementary Materials

Supplementary tables. *Supplementary legends*. *Supplementary Figure S1*. Transcriptional and protein levels of Aurora kinases in GSCs. *Supplementary Figure S2*. Danusertib does not induce evident changes in cell morphology in resistant GSCs. *Supplementary Figure S3*. Danusertib induces a reduction of phosphorylated Aurora kinases in all the GSCs. *Supplementary Figure S4*. *A* Danusertib does not induce any DNA fragmentation in GSC lines. *B* Detailed chromosome 17 LOH mapping of GSC lines. *Supplementary Video S1*.

Live cell imaging analysis of untreated GBM2. *Supplementary Video S2.* Live cell imaging analysis of 500 nM Danusertib treated GBM2. *Supplementary Video S3.* Live cell imaging analysis of untreated G166. *Supplementary Video S4.* Live cell imaging analysis of 500 nM Danusertib treated G166. *(Supplementary Materials)*

References

[1] D. N. Louis, A. Perry, G. Reifenberger et al., "The 2016 world health organization classification of tumors of the central nervous system: a summary," *Acta Neuropathologica*, vol. 131, no. 6, pp. 803–820, 2016.

[2] X. Zhang, W. Zhang, W. Cao, G. Cheng, and Y. Zhang, "Glioblastoma multiforme: molecular characterization and current treatment strategy (review)," *Experimental and Therapeutic Medicine*, vol. 3, no. 1, pp. 9–14, 2012.

[3] S. Bao, Q. Wu, R. E. McLendon et al., "Glioma stem cells promote radioresistance by preferential activation of the DNA damage response," *Nature*, vol. 444, no. 7120, pp. 756–760, 2006.

[4] S. K. Singh, C. Hawkins, I. D. Clarke et al., "Identification of human brain tumour initiating cells," *Nature*, vol. 432, no. 7015, pp. 396–401, 2004.

[5] T. N. Ignatova, V. G. Kukekov, E. D. Laywell, O. N. Suslov, F. D. Vrionis, and D. A. Steindler, "Human cortical glial tumors contain neural stem-like cells expressing astroglial and neuronal markers in vitro," *Glia*, vol. 39, no. 3, pp. 193–206, 2002.

[6] A. L. Vescovi, R. Galli, and B. A. Reynolds, "Brain tumour stem cells," *Nature Reviews Cancer*, vol. 6, no. 6, pp. 425–436, 2006.

[7] S. Baronchelli, A. Bentivegna, S. Redaelli et al., "Delineating the cytogenomic and epigenomic landscapes of glioma stem cell lines," *PLoS ONE*, vol. 8, no. 2, Article ID e57462, 2013.

[8] Y. Aylon and M. Oren, "p53: guardian of ploidy," *Molecular Oncology*, vol. 5, no. 4, pp. 315–323, 2011.

[9] A. J. Holland and D. W. Cleveland, "Boveri revisited: chromosomal instability, aneuploidy and tumorigenesis," *Nature Reviews Molecular Cell Biology*, vol. 10, no. 7, pp. 478–487, 2009.

[10] G. Vader and S. M. Lens, "The Aurora kinase family in cell division and cancer," *Biochimica et Biophysica Acta (BBA) - Reviews on Cancer*, vol. 1786, no. 1, pp. 60–72, 2008.

[11] W. Reichardt, V. Jung, C. Brunner et al., "The putative serine/threonine kinase gene STK15 on chromosome 20q13.2 is amplified in human gliomas," *Oncology Reports*, vol. 10, no. 5, pp. 1275–1279, 2003.

[12] H. Zhou, J. Kuang, L. Zhong et al., "Tumour amplified kinase STK15/BTAK induces centrosome amplification, aneuploidy and transformation," *Nature Genetics*, vol. 20, no. 2, pp. 189–193, 1998.

[13] W. F. Zeng, K. Navaratne, R. A. Prayson, and R. J. Weil, "Aurora B expression correlates with aggressive behaviour in glioblastoma multiforme," *Journal of Clinical Pathology*, vol. 60, no. 2, pp. 218–221, 2007.

[14] S. M. Quartuccio and K. Schindler, "Functions of aurora kinase C in meiosis and cancer," *Frontiers in Cell and Developmental Biology*, vol. 3, p. 50, 2015.

[15] A. Tang, K. Gao, L. Chu, R. Zhang, J. Yang, and J. Zheng, "Aurora kinases: novel therapy targets in cancers," *Oncotarget*, vol. 8, no. 14, pp. 23937–23954, 2017.

[16] M. Kollareddy, D. Zheleva, P. Dzubak, P. S. Brahmkshatriya, M. Lepsik, and M. Hajduch, "Aurora kinase inhibitors: progress towards the clinic," *Investigational New Drugs*, vol. 30, no. 6, pp. 2411–2432, 2012.

[17] N. Steeghs, F. A. Eskens, H. Gelderblom et al., "Phase I pharmacokinetic and pharmacodynamic study of the aurora kinase inhibitor danusertib in patients with advanced or metastatic solid tumors," *Journal of Clinical Oncology*, vol. 27, no. 30, pp. 5094–5101, 2009.

[18] R. B. Cohen, S. F. Jones, C. Aggarwal et al., "A phase I dose-escalation study of danusertib (PHA-739358) administered as a 24-hour infusion with and without granulocyte colony-stimulating factor in a 14-day cycle in patients with advanced solid tumors," *Clinical Cancer Research*, vol. 15, no. 21, pp. 6694–6701, 2009.

[19] H. J. Meulenbeld, J. P. Bleuse, E. M. Vinci et al., "Randomized phase II study of danusertib in patients with metastatic castration-resistant prostate cancer after docetaxel failure," *BJU International*, vol. 111, no. 1, pp. 44–52, 2013.

[20] P. Schoffski, B. Besse, T. Gauler et al., "Efficacy and safety of biweekly i.v. administrations of the Aurora kinase inhibitor danusertib hydrochloride in independent cohorts of patients with advanced or metastatic breast, ovarian, colorectal, pancreatic, small-cell and non-small-cell lung cancer: a multi-tumour, multi-institutional phase II study," *Annals of Oncology*, vol. 26, no. 3, pp. 598–607, 2015.

[21] G. Borthakur, H. Dombret, P. Schafhausen et al., "A phase I study of danusertib (PHA-739358) in adult patients with accelerated or blastic phase chronic myeloid leukemia and Philadelphia chromosome-positive acute lymphoblastic leukemia resistant or intolerant to imatinib and/or other second generation c-ABL therapy," *Haematologica*, vol. 100, no. 7, pp. 898–904, 2015.

[22] K. Fraedrich, J. Schrader, H. Ittrich et al., "Targeting aurora kinases with danusertib (PHA-739358) inhibits growth of liver metastases from gastroenteropancreatic neuroendocrine tumors in an orthotopic xenograft model," *Clinical Cancer Research*, vol. 18, no. 17, pp. 4621–4632, 2012.

[23] S. He, L. Shu, Z. Zhou et al., "Inhibition of aurora kinases induces apoptosis and autophagy via AURKB/p70S6K/RPL15 axis in human leukemia cells," *Cancer Letters*, vol. 382, no. 2, pp. 215–230, 2016.

[24] D. Zi, Z. Zhou, Y. Yang et al., "Danusertib induces apoptosis, cell cycle arrest, and autophagy but inhibits epithelial to mesenchymal transition involving PI3K/Akt/mTOR signaling pathway in human ovarian cancer cells," *International Journal of Molecular Sciences*, vol. 16, no. 11, pp. 27228–27251, 2015.

[25] S. M. Pollard, K. Yoshikawa, I. D. Clarke et al., "Glioma stem cell lines expanded in adherent culture have tumor-specific phenotypes and are suitable for chemical and genetic screens," *Cell Stem Cell*, vol. 4, no. 6, pp. 568–580, 2009.

[26] F. Griffero, A. Daga, D. Marubbi et al., "Different response of human glioma tumor-initiating cells to epidermal growth factor receptor kinase inhibitors," *The Journal of Biological Chemistry*, vol. 284, no. 11, pp. 7138–7148, 2009.

[27] N. Hégarat et al., "PP2A/B55 and Fcp1 regulate greatwall and ensa dephosphorylation during mitotic exit," *PLoS Genet*, vol. 10, no. 1, Article ID e1004004, 2014.

[28] C. Cilibrasi, G. Riva, G. Romano et al., "Resveratrol impairs glioma stem cells proliferation and motility by modulating the wnt signaling pathway," *PLoS ONE*, vol. 12, no. 1, Article ID e0169854, 2017.

[29] G. Riva, S. Baronchelli, L. Paoletta et al., "In vitro anticancer drug test: a new method emerges from the model of glioma stem cells," *Toxicology Reports*, vol. 1, pp. 188–199, 2014.

[30] C. J. Paller, M. D. Wissing, J. Mendonca et al., "Combining the pan-aurora kinase inhibitor AMG 900 with histone deacetylase inhibitors enhances antitumor activity in prostate cancer," *Cancer Medicine*, vol. 3, no. 5, pp. 1322–1335, 2014.

[31] M. S. Greenblatt, W. P. Bennett, M. Hollstein, and C. C. Harris, "Mutations in the p53 tumor suppressor gene: clues to cancer etiology and molecular pathogenesis," *Cancer Research*, vol. 54, no. 18, pp. 4855–4878, 1994.

[32] W. A. Freed-Pastor and C. Prives, "Mutant p53: one name, many proteins," *Genes & Development*, vol. 26, no. 12, pp. 1268–1286, 2012.

[33] G. Görgün, E. Calabrese, T. Hideshima et al., "A novel aurora-a kinase inhibitor MLN8237 induces cytotoxicity and cell-cycle arrest in multiple myeloma," *Blood*, vol. 115, no. 25, pp. 5202–5213, 2010.

[34] J. J. Huck, M. Zhang, A. McDonald et al., "MLN8054, an inhibitor of aurora a kinase, induces senescence in human tumor cells both in vitro and in vivo," *Molecular Cancer Research*, vol. 8, no. 3, pp. 373–384, 2010.

[35] Y. Liu, O. E. Hawkins, Y. Su et al., "Targeting aurora kinases limits tumour growth through DNA damage-mediated senescence and blockade of NF-κB impairs this drug-induced senescence," *EMBO Molecular Medicine*, vol. 5, no. 1, pp. 149–166, 2013.

[36] A. R. Young, M. Narita, M. Ferreira et al., "Autophagy mediates the mitotic senescence transition," *Genes & Development*, vol. 23, no. 7, pp. 798–803, 2009.

[37] D. Glick, S. Barth, and K. F. Macleod, "Autophagy: cellular and molecular mechanisms," *The Journal of Pathology*, vol. 221, no. 1, pp. 3–12, 2010.

[38] Y. Cao and D. J. Klionsky, "Physiological functions of Atg6/Beclin 1: a unique autophagy-related protein," *Cell Research*, vol. 17, no. 10, pp. 839–849, 2007.

[39] Y. Kabeya, N. Mizushima, T. Ueno et al., "LC3, a mammalian homologue of yeast Apg8p, is localized in autophagosome membranes after processing," *EMBO Journal*, vol. 19, no. 21, pp. 5720–5728, 2000.

[40] I. Crespo, A. L. Vital, A. B. Nieto et al., "Detailed characterization of alterations of chromosomes 7, 9, and 10 in glioblastomas as assessed by single-nucleotide polymorphism arrays," *The Journal of Molecular Diagnostics*, vol. 13, no. 6, pp. 634–647, 2011.

[41] P. Carpinelli, R. Ceruti, M. L. Giorgini et al., "PHA-739358, a potent inhibitor of aurora kinases with a selective target inhibition profile relevant to cancer," *Molecular Cancer Therapeutics*, vol. 6, no. 12, pp. 3158–3168, 2007.

[42] M. Mannino, N. Gomez-Roman, H. Hochegger, and A. J. Chalmers, "Differential sensitivity of Glioma stem cells to Aurora kinase A inhibitors: Implications for stem cell mitosis and centrosome dynamics," *Stem Cell Research*, vol. 13, no. 1, pp. 135–143, 2014.

[43] L. Wang, J. Wang, J. Chen et al., "Aurora A kinase inhibitor AKI603 induces cellular senescence in chronic myeloid leukemia cells harboring T315I mutation," *Scientific Reports*, vol. 6, no. 1, Article ID 35533, 2016.

[44] F. Gizatullin, Y. Yao, V. Kung, M. W. Harding, M. Loda, and G. I. Shapiro, "The aurora kinase inhibitor VX-680 induces endoreduplication and apoptosis preferentially in cells with compromised p53-dependent postmitotic checkpoint function," *Cancer Research*, vol. 66, no. 15, pp. 7668–7677, 2006.

[45] J. S. Nair, A. L. Ho, A. N. Tse et al., "Aurora B kinase regulates the postmitotic endoreduplication checkpoint via phosphorylation of the retinoblastoma protein at serine 780," *Molecular Biology of the Cell (MBoC)*, vol. 20, no. 8, pp. 2218–2228, 2009.

[46] S. Santaguida, A. Richardson, D. R. Iyer et al., "Chromosome mis-segregation generates cell-cycle-arrested cells with complex karyotypes that are eliminated by the immune system," *Developmental Cell*, vol. 41, no. 6, pp. 638–651.e5, 2017.

[47] H. S. Dahlback, P. Brandal, T. R. Meling, L. Gorunova, D. Scheie, and S. Heim, "Genomic aberrations in 80 cases of primary glioblastoma multiforme: pathogenetic heterogeneity and putative cytogenetic pathways," *Genes, Chromosomes and Cancer*, vol. 48, no. 10, pp. 908–924, 2009.

Hindawi
Journal of Oncology
Volume 2019, Article ID 9043675, 16 pages
https://doi.org/10.1155/2019/9043675

Research Article

Live Cell Imaging Supports a Key Role for Histone Deacetylase as a Molecular Target during Glioblastoma Malignancy Downgrade through Tumor Competence Modulation

Aline Menezes,[1] Gustavo Henrique dos Reis,[1] Maria Cecília Oliveira-Nunes,[1] Fernanda Mariath,[1] Mariana Cabanel,[1] Bruno Pontes,[2] Newton Gonçalves Castro,[3] José Marques de Brito ,[1] and Katia Carneiro [1]

[1]*Laboratório de Proliferação e Diferenciação Celular, Instituto de Ciências Biomédicas, Universidade Federal do Rio de Janeiro, Av. Carlos Chagas Filho 373, Bloco F Sala F2-01, Rio de Janeiro 21941-902, Brazil*
[2]*Laboratório de Pinças Ópticas, Instituto de Ciências Biomédicas, Universidade Federal do Rio de Janeiro, Av. Carlos Chagas Filho 373, Bloco F Sala F1-26, Rio de Janeiro 21941-902, Brazil*
[3]*Laboratório de Farmacologia Molecular, Instituto de Ciências Biomédicas, Universidade Federal do Rio de Janeiro, Av. Carlos Chagas Filho 373, Bloco J Sala J1-10, Rio de Janeiro 21941-902, Brazil*

Correspondence should be addressed to Katia Carneiro; kcarneiro@histo.ufrj.br

Aline Menezes and Gustavo Henrique dos Reis contributed equally to this work.

Received 28 December 2018; Accepted 3 July 2019; Published 8 August 2019

Academic Editor: Claudio Festuccia

Glioblastoma (GBM) is the most aggressive tumor of the central nervous system, and the identification of the mechanisms underlying the biological basis of GBM aggressiveness is essential to develop new therapies. Due to the low prognosis of GBM treatment, different clinical studies are in course to test the use of histone deacetylase inhibitors (iHDACs) in anticancer cocktails. Here, we seek to investigate the impact of HDAC activity on GBM cell behavior and plasticity by live cell imaging. We pharmacologically knock down HDAC activity using two different inhibitors (TSA and SAHA) in two different tumor cell types: a commercial GBM cell line (U87-MG) and primary tumor (GBM011). Upon 72 hours of *in vitro* iHDAC treatment, GBM cells presented a very unusual elongated cell shape due to tunneling tube formation and independent on TGF-β signaling epithelial to mesenchymal transition. Live cell imaging revealed that voltage-sensitive Ca^{++} signaling was disrupted upon HDAC activity blockade. This behavior was coupled to vimentin and connexin 43 gene expression downregulation, suggesting that HDAC activity blockade downgrades GBM aggressiveness mostly due to tumor cell competence and plasticity modulation *in vitro*. To test this hypothesis and access whether iHDACs would modulate tumor cell behavior and plasticity to properly respond to environmental cues *in vivo*, we xenografted GBM oncospheres in the chick developing the neural tube. Remarkably, upon 5 days in the developing neural tube, iHDAC-treated GBM cells ectopically expressed HNK-1, a tumor-suppressor marker tightly correlated to increased survivor of patients. These results describe, for the first time in the literature, the relevance of iHDACs for *in vivo* tumor cell morphology and competence to properly respond to environmental cues. Ultimately, our results highlight the relevance of chromatin remodeling for tumor cell plasticity and shed light on clinical perspectives aiming the epigenome as a relevant therapeutic target for GBM therapy.

1. Introduction

Glioblastoma (GBM) is the most aggressive tumor of the central nervous system (CNS). This tumor arises from glial cells and is classified as a grade IV glioma, causing focal or scattered anaplasia and presenting accelerated growth with histological diagnosis based on nuclear atypia and mitotic activity [1]. Despite many advances in research into the treatment of this type of cancer in the last decades, the prognosis is of 25 months after the first medical intervention and there has been an improvement in survival of only 2% in 5 years. GBM has been shown to be resistant to radiotherapy

and chemotherapy and invariably occurring following surgical resection followed by chemo/radiotherapy [2]. One of the reasons for GBM resistance to therapeutic intervention is the complexity of the tumor itself, which presents regions of pseudopalisade necrosis, hemorrhage, pleomorphic nuclei/cells, and microvascular proliferation. Indeed, following this line of reasoning, growing evidence indicates that rare populations of tumor cells, called tumor stem cells, play a significant role in GBM resistance mainly contributing to the high degree of phenotypic, cellular, genetic, and epigenetic heterogeneity. Cancer stem cells (CSCs) are crucial to boost invasive tumor growth and subsequent relapse [3].

GBM genetics is characterized by several deletions, amplifications, and point mutations that lead to the activation of different signal transduction pathways [4]. More deeply, epigenetic processes add layers of complexity on cancer biology, increasing heterogeneity, and complexity of tumors and, consequently, decreasing efficacy of treatment [5, 6]. Indeed, due to the low prognosis of GBM treatment, different clinical studies are in course to test the use of inhibitors of histone deacetylase (HDAC) activity in anticancer cocktails [7]. HDAC inhibitors (iHDACs) are among the most successful examples of epigenetic therapy for different types of malignancies, including GBM. In fact, preclinical studies have demonstrated the efficacy of different inhibitors of HDAC activity as antitumor agents, especially when associated with other therapies, including chemotherapy and radiation [8, 9]. Numerous studies have shown that there is a wide variety of iHDACs such as valproic acid (VPA), sodium butyrate, vorinostat, tricostatin A (TSA), panobinostat, and entinostat currently used in medical practice [10, 11]. In addition, several iHDACs are Food and Drug Administration (FDA) approved [12], including Vorinostat [13–16] and VPA [17], which are currently being tested in clinical trials on GBM as either monotherapies or combination therapies.

HDAC enzymes catalyze the removal of the acetyl radicals from the lysine residues of the N-terminal tail of the nucleosomal histones [18], resulting in electrostatic changes favoring chromatin compaction [7]. Due to this fact, the HDAC activity is mainly related to transcriptional repression [19]. In humans, 18 proteins with deacetylase domain are coded in the genome and are highly conserved among eukaryotes. Human HDACs are classified into four different classes: class I (HDACs 1, 2, 3, and 8), class IIa (HDACs 4, 5, 7, and 9), class IIb (HDACs 6 and 10), III (SIRT1–7), and IV (HDAC 11), according to structure similarity, enzymatic function, cell location, and expression pattern. Interestingly, HDACs have been inversely correlated to overall survival rates, also presenting a tight correlation with a poor prognosis in GBM patients [20]. In addition, it is very well documented that iHDACs also inhibit DNA damage repair response and influence the response of tumor cells to radiation, inducing cell cycle arrest, senescence, and autophagy [21]. For these reasons, iHDACs have emerged as excellent therapeutic targets for GBM therapy and, regardless all advances described above, the exact mechanisms for iHDACs are still poorly understood.

In this work, we uncovered a new aspect of iHDAC action at the cellular level in real time by time-lapse video microscopy and xenografts in the chick developing neural tube. We found that, after iHDAC treatment, GBM cells presented a very unusual elongated cell shape due to formation of actin- and/or tubulin-rich tunneling tubes in an independent epithelial to mesenchymal transition (EMT) fashion. HDAC activity was also necessary for GBM cell cycle progression, viability, and migration. This iHDAC-induced switch in tumor cell shape due to tunneling tube formation was followed by vimentin and connexin 43 gene expression downregulation, an increase in radio sensitization, and intracellular Ca^{2+} signaling disruption. When GBM oncospheres were placed in the developing neural tube, iHDAC-treated GBM cells expressed HNK-1, a molecular marker tightly correlated to tumor suppression and increased survival of patients. To date, this is the first report on HDAC-dependent HNK-1 expression in GBM cells. Our results describe the relevance of iHDACs for tumor cell morphology and competence highlighting the relevance of chromatin remodeling for tumor cell plasticity. These results shed light on clinical perspectives aiming the epigenome as a relevant therapeutic target for GBM therapy.

2. Materials and Methods

2.1. Cell Culture. GBM11 cells were isolated from a surgical biopsy of a 57-year-old male diagnosed with glioblastoma. The procedure was performed at the University Hospital of Clementino Fraga Filho (HUCFF) and was approved under the code Conselho Nacional de Saúde (CONEP) No. 2340 as previously described [22]. The GBM cell line U87-MG was obtained from the American tissue culture collection (ATCC) and properly genotyped and certified by the Laboratory of Macromolecular Metabolism Firmino Torres de Castro at UFRJ. GBM cells were cultured in 24-well plates at 2.5×10^5 cells with DMEM (low glucose), supplemented with 10% fetal bovine serum (FBS) and penicillin/streptomycin (PS). Cultures were maintained at 37°C and with 5% CO_2.

2.2. Drug Treatments. At 24 hours after seeding, U87-MG cells were treated with 100 nM TSA (Sigma T1952) or 500 nM SAHA (Sigma SML0061) or SB-431542 (Sigma S4317, diluted in DMSO) or DMSO, as the control group, for 72 h. GBM011 cells were treated with 200 nM TSA or 1 μM SAHA.

2.3. 3D Cell Culture. For the generation of oncospheres for morphometric analysis, sterile 96-well round bottom plates were pretreated with 1% agarose and the cells were cultured as described above for 72 or 144 hours. The wells containing oncospheres were photographed every 24 hours under an Olympus CKX41 inverted microscope. For the generation of oncospheres for xenografts, we used 1×10^6 U87-MG cells in suspension in 1 ml of culture medium on nonadherent sterile Petri dishes (60 mm) in the presence of 100 nM TSA or DMSO as control.

2.4. Morphometric Analysis of Oncospheres. The analyses were performed using the free AnaSP® software as previously described [23]. The area of each oncosphere was segmented to acquire an image in black and white binary mask format so that the morphological parameters were automatically extracted from each analyzed oncosphere. Three oncospheres of each condition were analyzed in the respective treatment times. The cultures were photographed after 72 hours of treatment to measure the diameter of the oncospheres. ImageJ software (https://imagej.nih.gov/ij/index.html) was used for image processing.

2.5. Xenograft in Chicken Embryo. Upon 72 hours, control and iHDAC (100 nM TSA) treated oncospheres were grafted into the neural tube lumen or on the neuroepithelium wall in the prosencephalic region of the developing chicken embryo at different embryonic stages ranging from 7 to 12 somites as previously described by our group [24]. The window opened on the egg was sealed with adhesive tape and incubated at 37°C for 5 days. At the end of this period, the eggs were opened and the embryos were removed and washed in 1x PBS. Embryonic membranes were removed, and the embryos were fixed in Fornoy (10% glacial acetic acid, 60% absolute ethanol, and 30% formol) for at least 24 hours. During the dehydration for histological processing, the embryos were photographed. The *in situ* hybridization and HNK-1 immunostaining were performed as previously described by our group [24].

2.6. Transwell Migration Assay. Comparative migration experiments were conducted using a conventional 24-well Transwell system (6.5 mm Transwell® (#3422), Corning, NY, USA) with each well separated by a microporous polycarbonate membrane (10 μm thickness; 8 μm pores) into an upper ("insert") and a lower chamber ("well"). U87-MG and GBM011 cells were plated as described above. Nutritional deprivation of the cells was induced by removing the medium with FBS and introducing the supplemental medium of 0.1% BSA and drugs. After 48 h under treatment, the cells were trypsinized, counted, and plated at the density of 10^5 cells/insert with medium supplemented with 0.1% BSA. In the lower bottom of the transwell, 600 μl of medium supplemented with 10% FBS was added. As a negative control was used SFB-free medium in the lower bottom of the well. In this way, cells completed 72 h of the treatment in the transwell. After 72 h, cells were fixed using 4% paraformaldehyde and stained with 1% of crystal violet for 10 minutes. Cells on the top surface of the insert were removed with a cotton swab. To quantify the cells that migrated and adhered to the underside of the membrane, five random fields per condition were photographed under an inverted optical microscope using a 10x magnification. A method of quantitation was performed as described by [25]. Migration was determined by calculating the average pixel/area of the five fields in triplicate.

2.7. Video Microscopy and FibrilTool Analysis. U87-MG cells were plated and treated as described above and transferred to a culture chamber under controlled conditions of CO_2 and temperature (5% and 37°C, respectively). The culture chamber was adapted to a Nikon Eclipse TE300 inverted microscope (Nikon, USA). Upon 72 hours, phase contrast images, from the same field of each experimental condition, were captured every minute by using a Hamamatsu C2400 CCD camera (Hamamatsu, Japan). After assembly of the frames, cell motility was quantified. Cells under the same video microscopy conditions were also cultured in coverslips for F-actin immunostaining, and the images were acquired in a confocal microscope at a 60x magnification and analyzed using the FibrilTool Plugin (ImageJ/National Institutes of Health, USA) [26]. For proliferation analyses, each cell performing mitosis was marked with a black dot using the ImageJ program. Then, the total number of dots for each image in the movie was counted and recorded in a table. Thus, it was possible to determine the number of dividing cells as a function of time, for each experimental situation. For cell motility analyses, dots were also marked to follow the position of a chosen cell over time. The trajectory of each marked cell was then tracked. Knowing the total time of the film (72 h) and the cell displacement in that period, it was possible to determine the cell velocity. At least 12 cells were followed, and a mean velocity value was determined for each experimental condition. The results were plotted using GraphPad Prism 6.0 software.

2.8. Conventional PCR. U87-MG and GBM011 cells were harvested, and their mRNAs were extracted with TRIzol (Life Technologies), precipitated in ethanol, and reverse transcribed using random hexamers. Qualitative conventional reverse-transcription polymerase chain reaction (PCR) with GoTaq DNA Polymerase was performed following the manufacturer's instructions (Promega). mRNA levels were standardized by parallel PCR using primers to the housekeeping gene, GAPDH (IDT).

2.9. Primers

GAPDH

F: ACCACAGTCCATGCCATCAC; R: TCCACCACCCTGTTGCTGTA

HDAC 1:

F: ACCGGGCAACGTTACGAAT; R: CTATCAAAGGACACGCCAAGTG

HDAC 2:

F: TCATTGGAAAATTGACAGCATAGT; R: CATGGTGATGGTGGTGAAGAAG

HDAC 3:

F: TTGAGTTCTGCTCGCGTTACA; R: CCCAGTTAATGGCAATATCACAGAT

HDAC 4:

F: ATTCTGAACCACTGCATTTCCA; R: GGTGGTTATAGGAGGTCGACACT

HDAC 5:

F: TTGGAGACGTGGAGTACCTTACAG; R: GACTAGGACCACATCAGGTGAGAAC

HDAC 6:

F: TGGCTATTGCATGTTCAACCA; R: GTCGAAGGTGAACTGTGTTCCT

HDAC 7:

F: CTGCATTGGAGGAATGAAGCT; R: CTGGCACAGCGGATGTTTG

HDAC 8:

F: TCCCGAGTATGTCAGTATATATGA; R: GCTTCAATCAAAGAATGCACCAT

Vimentin:

F: GCACATTCGAGCAAAGACAG; R: GAGGGCTCCTAGCGGTTTAG

E-cadherin:

F: TGCCCAGAAAATGAAAAAGG; R: GTGTATGTGGCAATGCGTTC;

Actin smooth muscle:

F: AATGGCTCTGGGCTCTGTAA; R: TGGTGATGATGCCATGTTCT;

Connexin 43:

F: TGGATTCAGCTTGAGTGCTG; R: TCTTTCCCTTAACCCGATCC;

P2X7:

F: GCAGCTGCAGTGATGTTTTC; R: CACCTCTGCTATCCCCTTCA;

CACNA1H T-type calcium:

F: CTGTCACTCATGGGCATCAC; R: ATGAAAAGAAGGCCCAGGTT

2.10. Flow Cytometry. U87-MG and GBM011 glioblastoma cells were treated as described above, and after 72 hours in culture, cells were harvested by trypsinization and collected for flow cytometry analysis. For the detection of intracellular antibodies, cells were fixed with 2% paraformaldehyde for 30 min, permeabilized with PBS + 1% BSA + 0.2% saponin for 15 min, stained with primary antibody, anti-Nodal (Santa Cruz Antibodies, polyclonal, sc-28913, 1 : 200) or anti-H4K16ac (Millipore, polyclonal, 07–329; 1 : 200), for 30 min, and diluted in PBS + 0.2% saponin solution. Cells were then washed once with PBS + 0.2% saponin and incubated with secondary antibody Alexa conjugated with fluorochrome 647 (Thermo Fisher Scientific, A-21443, 1 : 1000) or conjugated with fluorochrome 488 (Abcam, ab150077, 1 : 1000) and diluted in PBS + 0.2% saponin solution for 30 min. Cells were then washed twice with PBS + 0.2% saponin, resuspended in PBS, and transferred to FACS reading tubes. All samples were kept in ice and protected from the light. A total of 200.000 cells were acquired on a FACSCanto flow cytometer (BD Biosciences) and analyzed using FACSDiva software (version 8.0.1). Cell death was measured with annexin V-FITC apoptosis detection kit (BD Biosciences) according to the manufacturer. Cell cycle analysis by quantitation of DNA content was performed according to Vindelov's protocol (Vindelov, 1985). Briefly, GBM cells were resuspended in 400 μl propidium iodide solution (PBS, 0.1% Triton X-100, 0.1% RNAse, and 50 μg/ml propidium iodide) and incubated on ice for 15 min. Subsequently, cells were analyzed by flow cytometry, using a FACSCanto (BD Biosciences) operated by FACSDiva software, and at least 20,000 events were collected per sample. Cell doublets were gated out using FSC-A vs FSC-H profiles. All data were analyzed using FACSDiva software (Version 8.0.1).

2.11. Ionizing Radiation and Cell Proliferation Assay. U87-MG and GBM011 cells were treated for 72 h as described above and irradiated with 10 Gy in a single dose using a linear 6 MV accelerator with 25×25 cm^2 equivalent field adjusted to a window size and surface distance of 70 cm. After irradiation, MTT assays and flow cytometry were performed at 24 h, 48 h, and 72 h points, and MTT absorbance was read at 570 nm. Cell morphology was evaluated by bright-field and fluorescence microscopy with Falloidin 546 plus DAPI. The images were obtained under a Leica TCS SP5 AOBS confocal microscope.

2.12. Fluorimetry Assay. We have used Fluo-4 AM and Fura-2 AM (Molecular Probes F14201) to measure the intracellular increase in Ca^{2+} in U87-MG and GBM011 cells. U87-MG and GBM011 cells were plated as described above in round 15 mm coverslips (Fisher-545-102) coated with poly-L-lysine (Sigma P-2636) and treated with DMSO and iHDACs as described above for 72 hours. The culture medium was replaced by 1 ml of culture medium (DMEM) containing 1 mM probenecid, 0.04% pluoronic, 2 μM Fluo-4 AM (Molecular Probes), or 4 μM Fura 2-AM (to analyze the basal level of intracellular calcium by fluorescence intensity). Cells were incubated at 37°C for 45 minutes, washed with fluorimetry solution (145 mM NaCl, 5 mM KCl, 1.2 mM Na_2HPO_4, 4 mM $CaCl_2$, 1 mM $MgCl_2$, 5 mM HEPES, and 10 mM d-glucose) and transferred to a chamber (P-5 Platform, Warner Instruments, Hamden, CT) with perfusion and a capacity of 200 μl. The fluorescence of 100 cells was continuously monitored for approximately 300 seconds in a fluorescence microscope (Eclipse Ti-U; Nikon). Cells were continuously perfused with fluorimetry solution and stimulated with different solutions (20 mM potassium chloride and 1 mM ATP for Fluo-4 AM). The solutions were added to the cells by using a gravity infusion system, and the variation of intracellular Ca^{++}($[Ca^{2+}]$ I), was evaluated by the fluorescence emitted at 488 nm using a lambda DG4 illumination system (Sutter Instrument, Novato, CA, on a 40x objective and 510 nm band-pass filter (Semrock, Rochester, NY). The data were acquired using the software MetaFluor (Molecular Devices, Sunnyvale, CA). The

Fluo-4 AM data were processed by the software ClampFit (version 10.7.0.3, Molecular Devices). The Fura-2 AM data were processed by the software ImageJ, and the basal levels of intracellular calcium were assessed by fluorescence intensity (Integrated Density).

2.13. Statistical Analysis. GraphPad Prism (v6.0, La Jolla, CA) was used for ordinary one-way or two-way ANOVA analysis. If the ANOVA produced a significant result, post hoc pairwise comparisons were tested for significance in which the P value was adjusted ($P_{adj} < 0.05$) by Tukey's method for multiple comparisons inside each group and by Sidak's method for multiple comparisons among the individual groups. Results are presented as mean ± SD or mean ± SE, and statistical relevance was defined as $P < 0.05$.

3. Results

3.1. SAHA Treatment Leads to GBM Cell Cycle Arrest in G0/G1 and Decreased Cell Viability. Since HDACs have been reported to be expressed in GBM cells [28], we first performed a conventional PCR to detect the expression pattern of HDACs in commercial U87-MG and GBM011 primary tumor cells in culture. We found that HDACs 1–7 were constitutively expressed by U87-MG cells and HDACs 1–5 and 7 were constitutively expressed by GBM011 (Supplementary Figure S1(A, A')). We also performed flow cytometry to detect histone hyperacetylation upon iHDAC treatment. Indeed, upon 72 h of iHDAC treatment, there was an increase in the frequency of H4K16ac + U87-MG cells followed by a significant increase in fluorescence intensity per cell (Supplementary Figure S1(B-E)). These first results show that GBM cells express HDACs from classes I, IIa, and IIb, whose activity blockade leads to a hyperacetylated chromatin status.

Next, we monitored the effects of iHDAC treatment along the 72 hours of treatment. Here, we will be comparing the effects of two different iHDCAs, TSA and SAHA. While TSA is one of the most used iHDACs in experimental approaches, SAHA (Varinostat) has already been approved for clinical use [29]. Both U87-MG and GBM011 cells presented a similar behavior during cell cycle progression with respect to TSA treatment. The percentage of cells observed in the G0/G1 phase was similar to that of control groups along the time in TSA-treated cells (Supplementary Figure S2(A-E)). In contrast, HDAC activity was differentially necessary for cell progression when SAHA was added to the medium. While the percentage of U87-MG cells in the G0/G1 phase drastically decreased after 72 h of SAHA treatment, only a discrete decrease was observed in GBM011 cells (Supplementary Figure S2(B-F)). In agreement, cell viability was mostly similar between U87-MG and GBM011 upon TSA treatment (Supplementary Figure S3). Moreover, both U87-MG and GBM011 presented significant decrease in cell viability upon SAHA treatment (Supplementary Figure S3). We conclude that U87-MG and GBM011 present a similar response to TSA during cell cycle progression and cell viability maintenance. In contrast, cell cycle and viability were drastically affected by SAHA treatment in U87-MG while GBM011 was less affected.

Live cell imaging supports a key role for HDAC blockade during tunneling tube formation through F-actin cytoskeleton stabilization in glioblastoma cells.

However, upon 72 h hours of iHDAC treatment, we noticed an atypical elongated cell shape only in iHDAC-treated GBM cells. These changes in tumor cell shape were evidenced by time-lapse video microscopy and corroborated by morphometric analysis. Using time-lapse video microscopy, we observed in TSA-treated U87-MG cells that the membrane extensions of one cell touch the cell body of neighboring cells, interconnecting tumor cells (Supplementary Video S1, DMSO; Supplementary Video S2, iHDACs; Figure 1(D-G), white head arrow). As the cell body migrates, the established focal contact is stabilized causing a stretching of the cell membrane, resembling an elastic (Figure 1(A, B, D–H, M–O)). It is also possible to notice two active lateral membrane projections from the central (longer) one that are not stabilized and retract (Figure 1(C–E)). After losing contact with the neighboring cell, the membrane filament completely retracts (Figure 1(I–L)). It was possible to estimate that the membrane filament remained stretched for about 6 hours after loss of contact with the neighboring cell (Figure 1(E-H). In fact, morphometric analysis showed that iHDACs evoked a cell shape transition in both U87-MG (Figure 1(P)) and GBM011 tumor cells (Supplementary Figure S4). The elongation index was significantly higher in TSA-treated U87-MG cells than in the control group (Figure 1(R)). In addition, the anisotropy of TSA-treated U87-MG (Figure 1(S)) and GBM cells (Supplementary Figure S4) was higher than in the control group showing that HDAC activity is relevant to maintain cytoskeletal organization. Due to the similarity between the morphology of GBM cells upon iHDAC treatment and the morphological aspects conferred by epithelial to mesenchymal transition (ETM), we decided to test whether iHDAC would be modulating ETM in GBM cells. It has been shown that TGF-β1 signaling pathway plays an essential role in the EMT processes, leading to morphological changes closely related to the mesenchymal morphology [30]. In this sense, we decided to test whether the blockade of HDAC activity could regulate EMT by blocking the TGF-β signaling pathway with 25 μM SB-431542 (TGF-βi) in the presence of iHDAC. U87-MG cells were monitored for cell shape changes upon 72 h of TSA treatment. Interestingly, we noticed that the elongation index of iHDAC + iTGF-β treated cells did not present significant difference when compared to iHDACs (Figure 2(A-E)). These results indicate that HDAC activity is not at downstream to TGF-β signaling during tumor cell elongation. In addition, TSA treatment led to a suppression in the expression of vimentin, while smooth muscle actin (SMA) and E-cadherin were still constitutively expressed by U87-MG cells even upon TSA treatment (Figure 2(F)). In addition, TSA treatment led to suppression of connexin 43 expression, suggesting that cell coupling by gap junctions was also disrupted by HDAC activity blockade. Thus, this data set excludes the hypothesis that EMT is being modulated by the blockade of HDAC activity and strongly

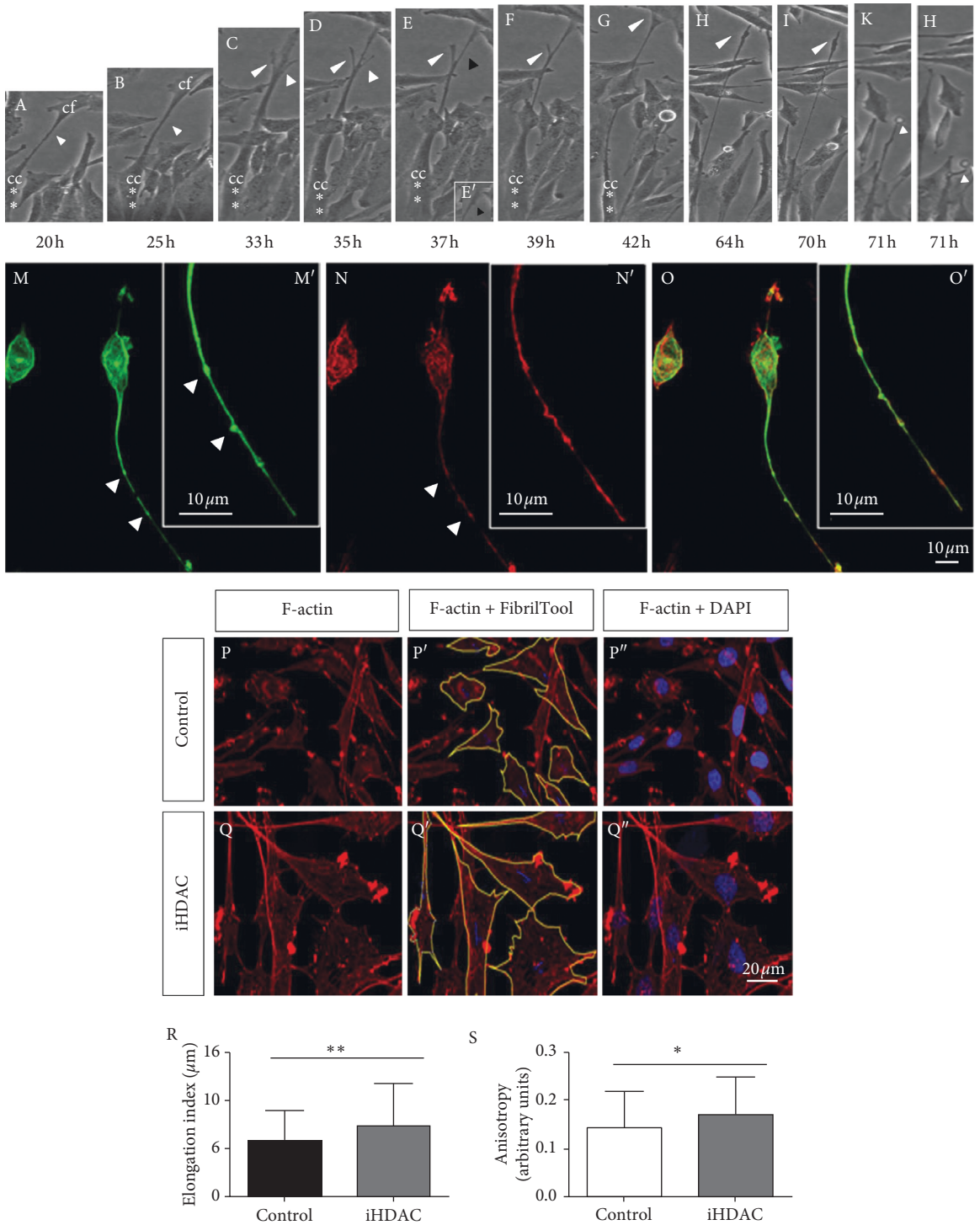

Figure 1: HDAC blockade leads to tunneling tube formation through F-actin cytoskeleton stabilization. (A–L) Time-lapse video microscopy of iHDAC-treated U87-MG cells during 72 h identified the formation of tunneling tubes starting at 20 h after treatment (A, white arrow; red asterisks evidence cell body). Membrane extensions of one cell touch the cell body of neighboring cells, interconnecting tumor cells starting at 35 h after treatment (D). At this time point, transitory membrane protrusions can be noticed (D, white head arrows). As the cell body migrates, it elongates (D, red asterisk) and the transitory membrane protrusion is retracted (E, black head arrow) at the same time that it is possible to note the formation of gondolas along the tunneling tube (E′, black head arrow). The tunneling tube now reaches a neighboring cell (E–G). After losing contact with the neighboring cell, the membrane filament completely retracts (H–L, white head arrow). It was possible to estimate that the membrane filament remained stretched for about 6 hours after loss of contact with the neighboring cell (I–L). iHDAC-treated cells presented type I (actin rich) and type II nanotubes (actin and tubulin rich) which also harbor gondolas (M–O, white head arrows). The elongation index was measured and iHDAC-treated cells (Q, R) were more elongated than DMSO group (P, R). Nanotubes formed in iHDAC-treated cells were more stable and organized than in the control group as found upon F-actin fibrillar structure and anisotropy analysis (S).

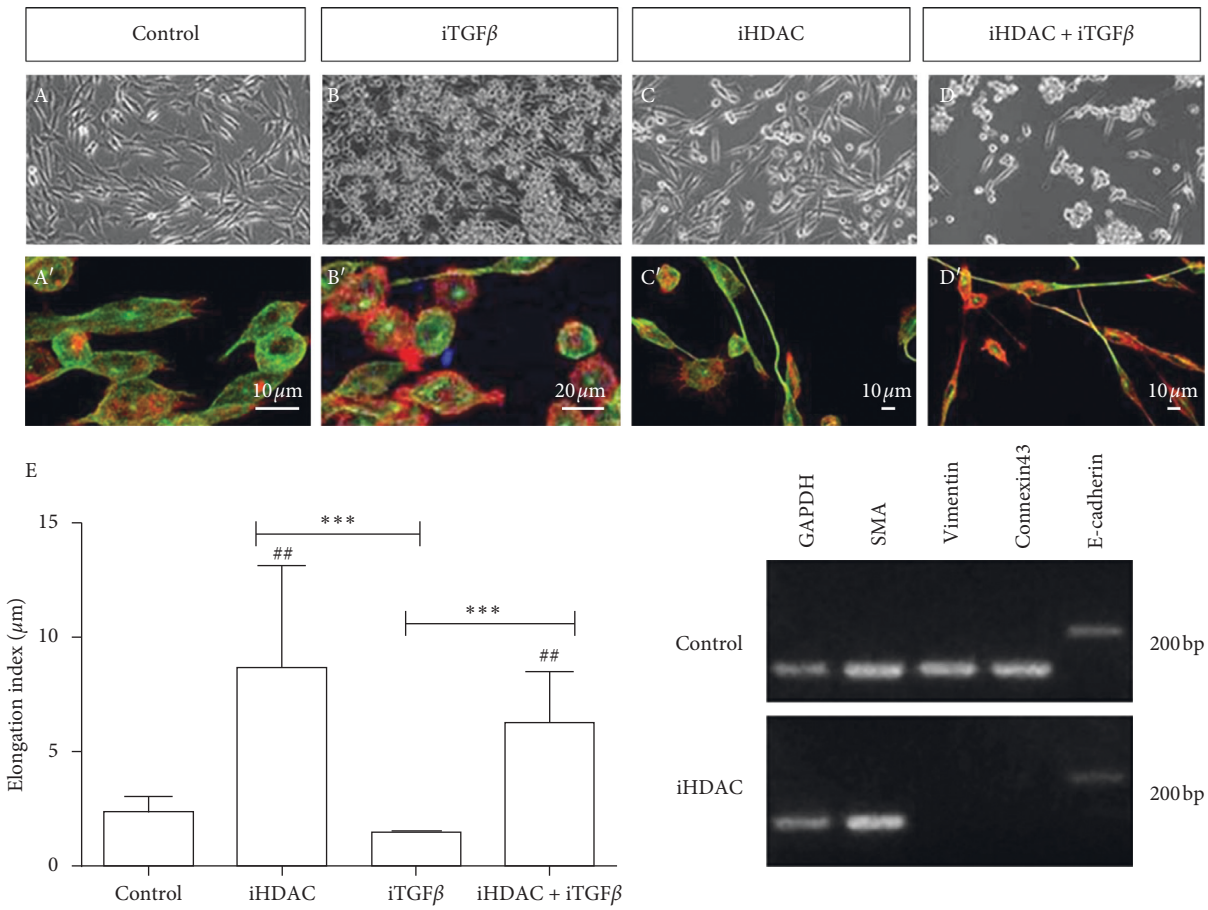

Figure 2: HDAC activity blockade leads to tumor cell shape changes in parallel to EMT and TGF-β signaling pathway through tunneling tube formation. U87-MG cells were treated with iTGF-β (25 μM SB-431542) in the presence or absence of iHDACs (100 nM TSA). Confocal microscopy characterized type I (C′, actin-rich nanotubes) and type II nanotubes (C′, actin- and tubulin-rich nanotubes) in iHDAC-treated cells. Elongation index showed that iHDAC + iTGF-β-treated cells displayed the same elongation index as that of iHDAC-treated cells (E). Qualitative RT-PCR performed with U87-MG cells treated with TSA 100 nM for 72 hours revealed that vimentin and connexin 43 expression was suppressed upon TSA treatment. Asterisks in F indicate comparisons made within the same experimental group at 24 h. $n = 3$, different experiments. $^{*}p < 0.05$; $^{**}p < 0.01$; $^{***}p < 0.001$.

suggests that the observed morphological differences between the groups are due to the structuring of tunneling tubes. Taking into account the features described above, we characterized type I and type II nanotubes in TSA-treated U87-MG cells. Type II nanotubes started growing as cells moved apart; they were enriched in actin and tubulin and harbored dilatations of the tube forming a gondola (Figure 1(M-O)). In fact, as observed by live cell imaging, nanotubes formed in iHDAC-treated GBM cells were more stable and organized than in the control group as found upon F-actin fibrillar structure and anisotropy analysis.

Next, we examined the effects of iHDAC treatment on GBM cell motility by time-lapse video microscopy and transwell migration assay. Upon 72 h of iHDAC treatment, U87-MG GBM cells presented a decrease in the velocity of migration that was corroborated by transwell assay. We detected a higher number of tumor cells retained in the transwell matrix after 72 hours when compared to the control group (Figure 3). This behavior was enhanced in the SAHA-treated group when compared to either the TSA or control group (Figure 3). In contrast, GBM011 cells did not present significative differences in cell velocity and migration to the control group when treated with TSA or SAHA (Supplementary Figure S5).

Thus, we conclude that HDAC activity blockade led to tumor cell shape changes through tunneling tube formation. We also conclude that tumor malignancy was downgraded because migration velocity was decreased, what may impact on tumor dissemination and infiltration.

3.2. HDAC Activity Is Necessary for GBM Radioresistance. According to the literature, GBM has been shown to be resistant to radiotherapy and invariably reoccurring after surgical resection. Previous work from the literature has also clearly demonstrated the relevance of iHDACs to increase GBM radiosensitization [11]. Thus, we compared the response of GBM cells to radiotherapy upon iHDAC treatment. U87-MG treated with TSA for 72 h showed a significant difference in the number of viable cells between control and TSA-treated cells (Figure 4(D, E)). In fact, we observed that the TSA-treated group showed no significant

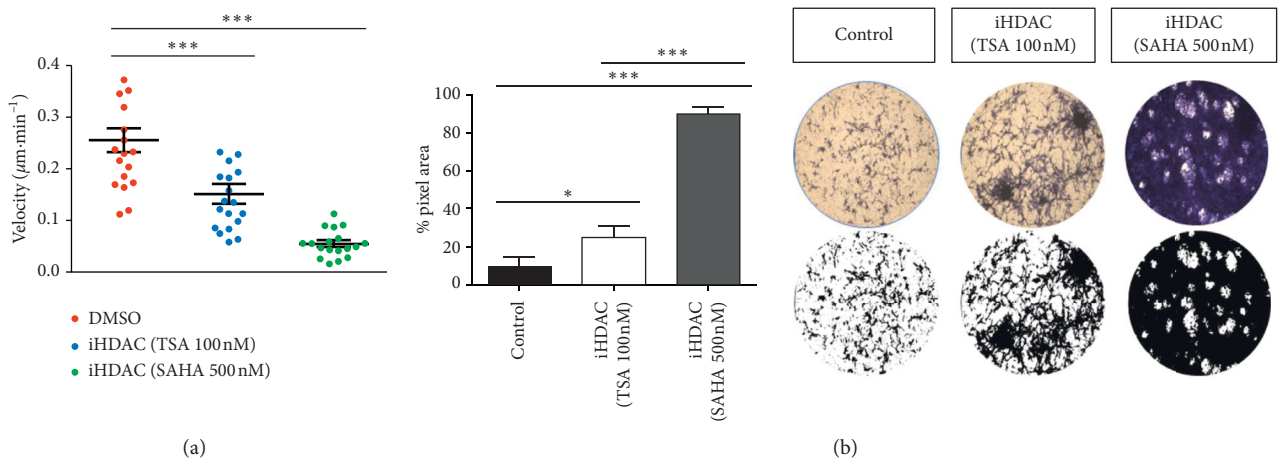

FIGURE 3: HDAC activity is required for the GBM migration velocity. U87-MG cells were treated for 72 hours with TSA or SAHA and were monitored by time-lapse video microscopy or submitted to the transwell assay. Treatment with TSA led to a significant decrease in the rate of cell migration that was corroborated by the transwell assay. It is possible to observe a larger number of cells retained in the transwell matrix in the TSA group than in the control group. The same effect was observed when the cells were treated with SAHA, but this effect was enhanced when compared to TSA. $n = 3$. $^{***}p < 0.001$; $^{****}p < 0.0001$.

increase in absorbance at 24 h and 48 h after irradiation, indicating that the treatment radiosensitized tumor cells (Figure 4(D, E)). In contrast to U87-MG cells, GBM011 cells still constitutively expressed SMA, vimentin, connexin 43, and E-cadherin when treated with TSA or SAHA (Supplementary Figure S6(A)). In fact, GBM011 cells treated with TSA did not present consistent differences in cell viability when compared to the control group 72 hours after irradiation (Supplementary Figure S6(C, E, G)). SAHA-treated GBM011, however, presented significative decrease in cell viability 72 h after irradiation (Supplementary Figure S6). We propose that HDAC-mediated radiosensitization of GBM cells is due to vimentin and connexin 43 expression downregulation.

3.3. Live Imaging of HDAC Blockade Uncovers Voltage-Sensitive Ca^{++} Signaling Disruption in GBM Cells. To test the functional status of GBM cells under iHDAC treatment, we investigated the efficiency of tumor cells in transducing Ca^{2+} signal through the cell membrane. Several studies have shown that intracellular calcium ($[Ca^{2+}]I$) concentration can significantly contribute to cell biochemical mitotic signaling, migration, apoptosis, cell cycle control, and cell volume regulation, all of them critical for cell survival and proliferation [31]. The main types of Ca^{2+} channels described in the literature and expressed by gliomas are voltage-dependent channels (Ca_v1 = Type L; Ca_v2 = Type P/Q, R, N; Ca_v3 = Type T) and purinergic receptors [32, 33]. Several studies suggest that the P2X7 receptor, the purinergic ionotropic receptor (P2X7R), and Type T low voltage play an important role in GBM behavior including glioma progression [34, 35]. Thus, we sought to better understand the biological significance of iHDACs in the context of Ca^{2+} signaling transduction. After 72 hours, the basal levels of intracellular Ca^{2+} were assessed by confocal microscopy in U87-MG and GBM011 cells under TSA and SAHA treatment. While significative differences in basal levels of intracellular Ca^{2+} were not detected in U87-MG cells (Figure 5(A)), GBM011 treated with SAHA presented a significative decrease (Supplementary Figure S7). Our results showed that control cells were responsive to both stimuli applied, KCl (20 mM and 50 mM), a depolarizing agent that acts on low-voltage channels, and ATP, an agonist that binds to that receptor and leads to cell depolarization. Quantitative analyses of $[Ca^{2+}]I$ showed that the control group presented a higher response to the stimuli than U87-MG cells treated with TSA (Figure 5(E-J)). In addition, control and TSA-treated U87-MG cells constitutively express P2X7 but do not express the alpha subunit 1H of the T-type calcium channel (Figure 5(K)). We conclude that iHDAC treatment disrupts intracellular Ca^{2+} upon stimulus even in the presence of similar basal levels of intracellular Ca^{2+} when compared to the control group.

3.4. HDAC Activity Blockade Downgrades GBM Malignance and Makes Tumor Cells Competent to Properly Respond to Environmental Cues In Vivo. Taken together, our results show that iHDAC treatment leads to tunneling tube formation and tumor malignance downgrade *in vitro*. Our interpretation relies on the fact that iHDAC-treated cells decrease the velocity of migration and downregulate vimentin and connexin 43 expression, and to test whether TSA-treated U87-MG cells in fact harbor the competence to properly respond to environmental cues and downregulate their malignant behavior, we used GBM oncospheres xenografted in the developing neural tube of the chick embryo. Oncospheres containing 1.5×10^3 cells were generated for the study of the morphometric properties after iHDAC treatment. Such oncospheres did not exceed 150 μm in diameter at the end of 4 days in culture (Supplementary Figure S8(A–C)), and iHDAC-treated oncospheres presented decreased diameter and volume when compared to

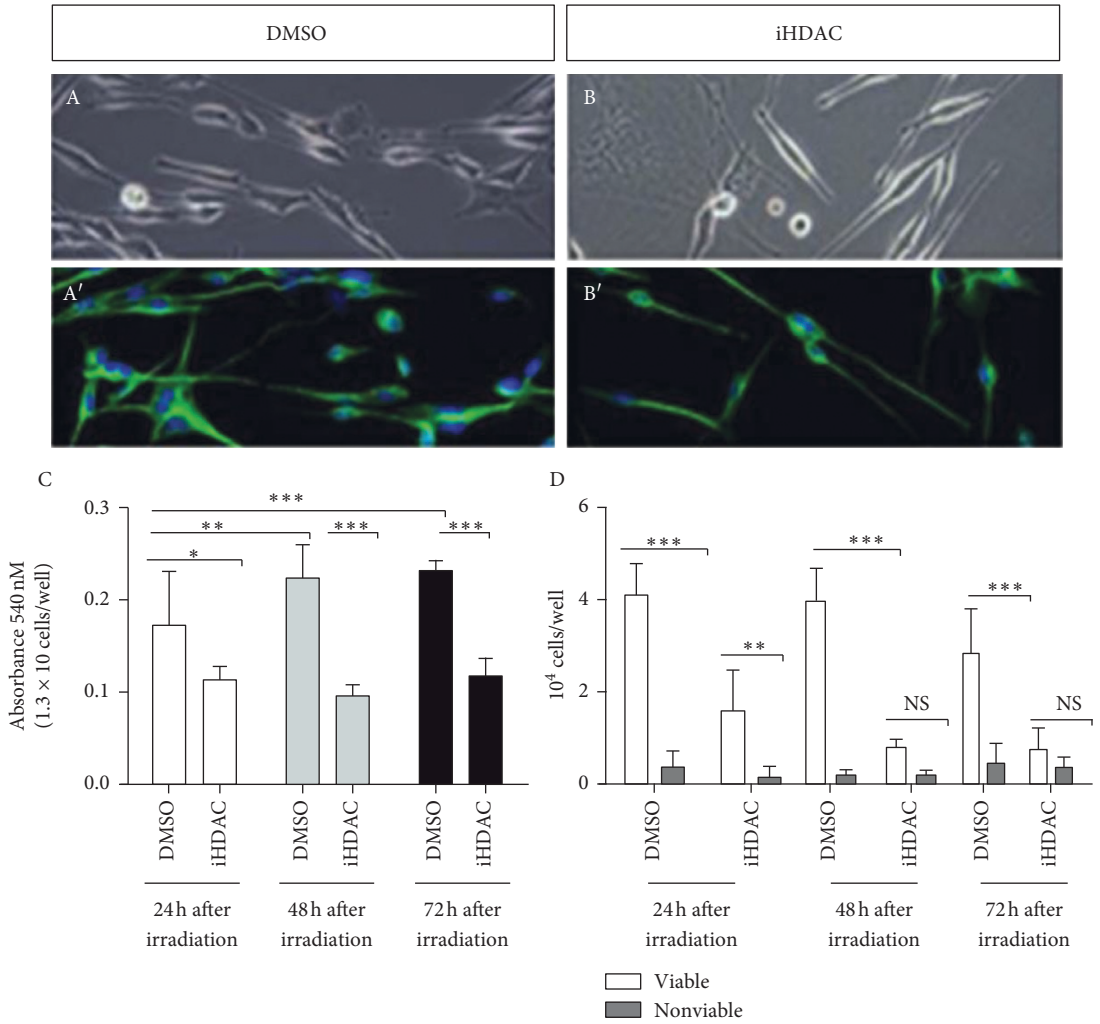

Figure 4: iHDAC treatment radiosensitizes U87-MG cells that, in turn, increase mitochondrial activity. U87-MG cells were irradiated (A, B), and MTT assay showed a significant increase in absorbance in the DMSO group at 24 h and 48 h after ionizing irradiation (C) and did not show significant differences, at the same time points, in iHDAC-treated cells (C). Cell counting using trypan blue at 24 h, 48 h, and 72 h time points after irradiation showed a significant decrease in cellular viability between the DMSO and iHDAC groups (D). $n = 9$; $^{*}p < 0.05$; $^{**}p < 0.01$; $^{***}p < 0.001$.

control oncospheres (Supplementary Figure S8(D)). When cell viability was assessed by MTT assay, we did not notice significant differences between control and TSA-treated oncospheres upon 72 hours (Supplementary Figure S8(F)). However, we were able to observe a significant decrease in cell viability at 96, 120, and 144 hours of prolonged treatment (Supplementary Figure S8(E)). This characterization is very relevant as upon xenograft, oncospheres will not be in contact with TSA anymore. For this reason, we monitored the morphometric properties upon TSA removal up to 72 hours after TSA had been removed. Despite the differences observed in the diameter and volume between control and TSA-treated oncospheres along the procedure (Supplementary Figure S8(G, H)), we did not notice significative changes in the morphometric parameters of iHDAC-treated oncospheres (Supplementary Figure S8(I, J)). So, we conclude that TSA treatment has a long-term effect even after inhibitor withdrawal. Then, we performed the xenograft of the control and TSA-treated oncospheres in the anterior prosencephalic region on the right wall of the neural tube shortly after its closure and the onset of neurogenesis (Figure 6(A)). Oncospheres were also placed in the neural tube lumen (Figure 6(B)). After 5 days of development (HH25; Figure 6(C)), the embryos were processed for histological analysis and paraffin sections were developed for *in situ* hybridization using the *Alu* probe for identification of the human cells and immune staining for HNK-1. First, in both groups, we observed that tumor cells successfully integrated into the embryonic mesenchyme and migrated over long distances (Figure 6(D)). By examining serial paraffin sections, we observed that TSA-treated cells migrated longer distances than control cells (Figure 6(D)). In fact, TSA-treated cells were found over a larger area than control cells since we found Alu^{+} nuclei at 196 μm beyond the xenograft point. In the control group, we were able to find Alu^{+} nuclei at 168 μm beyond the xenograft point (Figure 6(D)). This result bypasses the behavior observed *in vitro* since we found that iHDAC-treated cells presented a decrease in cell velocity

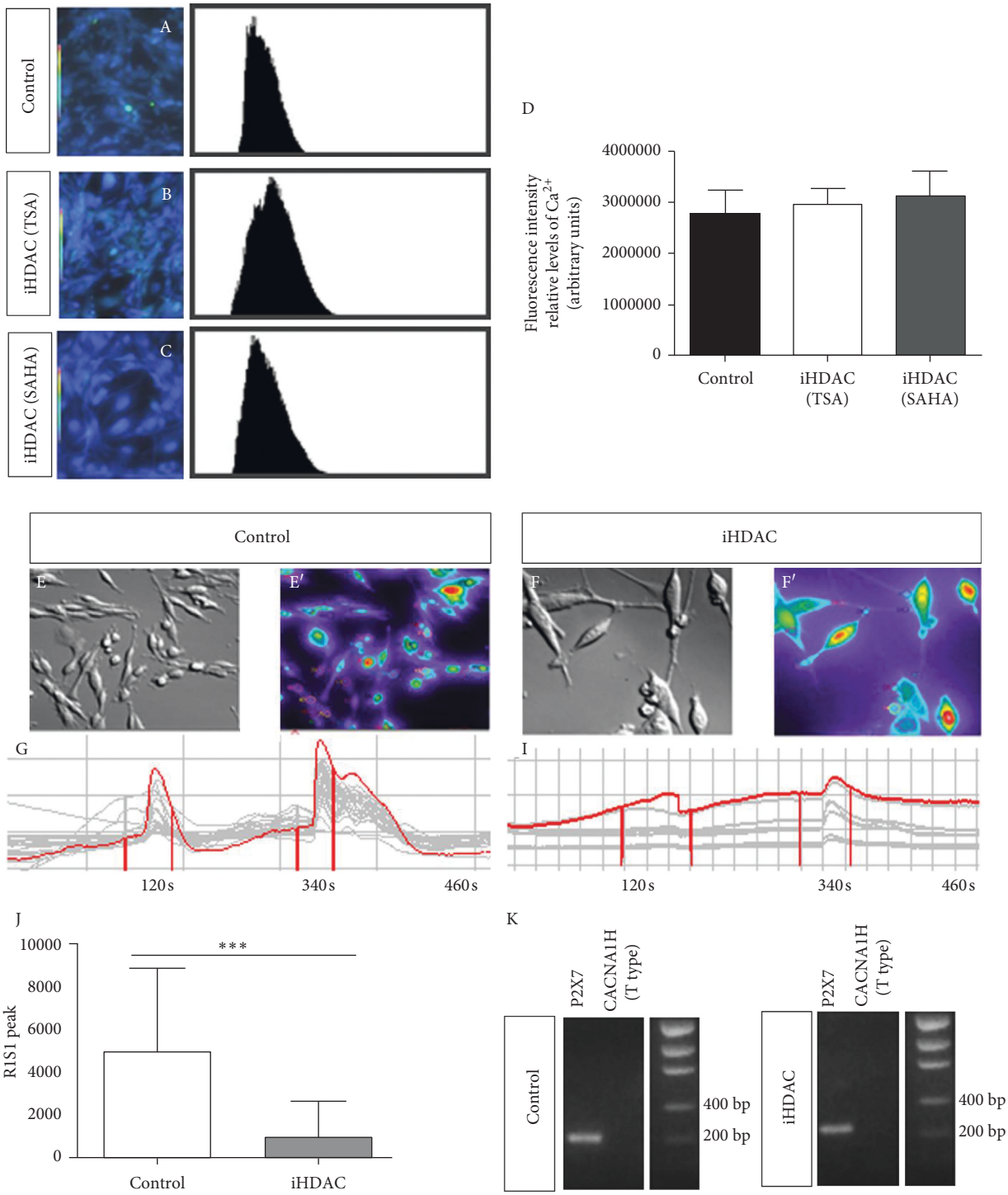

Figure 5: iHDAC treatment disrupts voltage-dependent Ca^{++} channels signaling by live cell imaging. iHDAC-treated U87-MG cells (100 nM TSA for 72 hours) were incubated with Fura 2-AM and analyzed by confocal microscopy. Significative differences in the basal levels of intracellular Ca^{2+} were not detected among the experimental groups (A–D). The fluorescence of 100 cells was continuously monitored for approximately 10 minutes in a fluorescence microscope (E-F). DMSO (E–G) or iHDAC (F–I) treated cells were continuously perfused with fluorimetry solution and stimulated with 20 mM KCl and 50 mM ATP. The variation of intracellular Ca^{++} ($[Ca^{2+}]I$) was evaluated by the fluorescence emitted at 488 nm. The responsiveness to KCL and ATP was quantified, and U87-MG cells treated with iHDACs were less responsive to KCl and ATP than DMSO-treated cells (J). Qualitative RT-PCR revealed constitutive expression of P2X7 in both control and iHDAC-treated groups. On the contrary, the alpha subunit 1H of the CACNA T-type calcium channel is not expressed by U87-MG cells. $^{***}p < 0.001$.

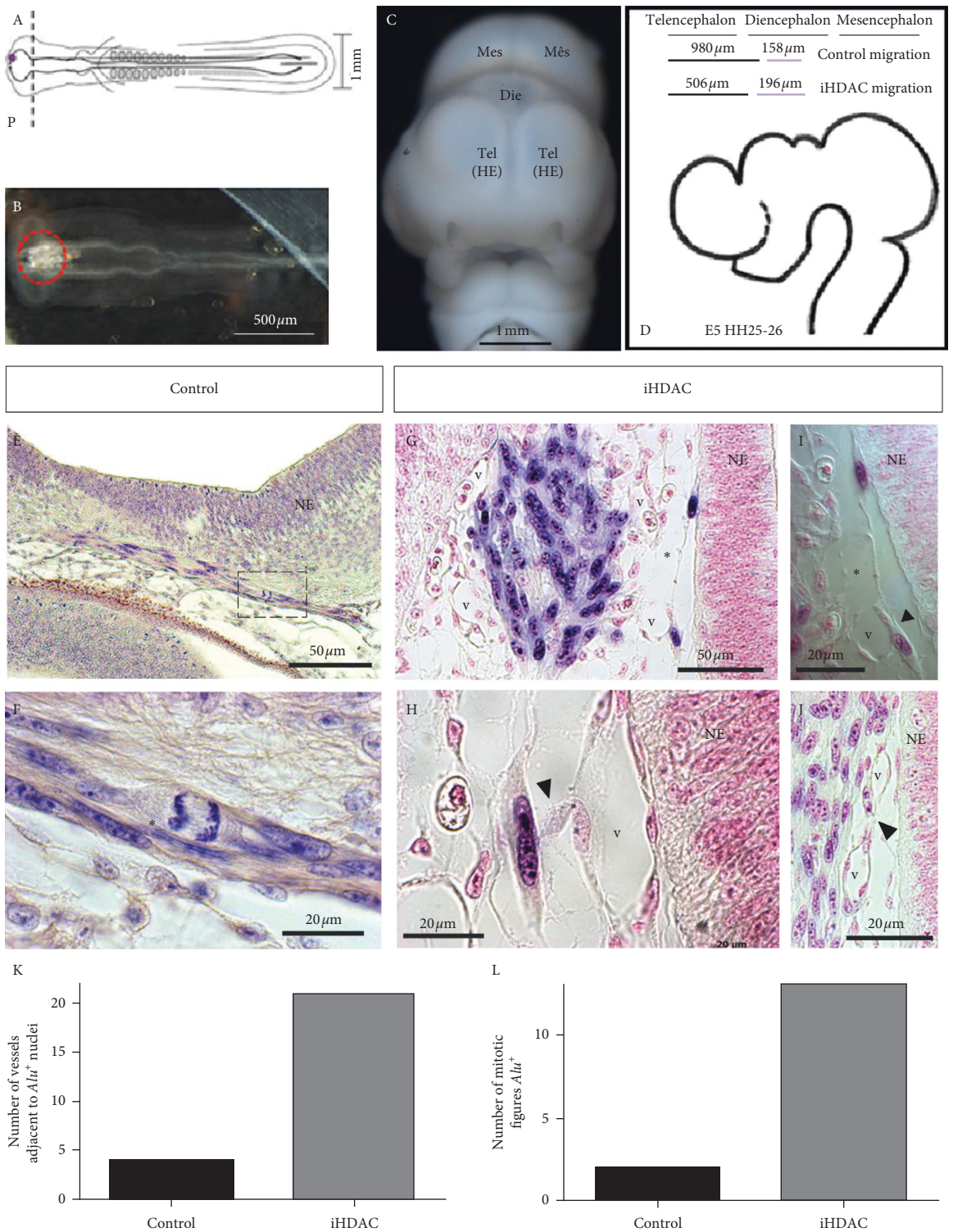

Figure 6: HDAC activity blockade in synergy with the developing embryo leads to tunneling tube formation in U87-MG cells. U87-MG oncospheres were generated *in vitro,* exposed to iHDACs (100 nM TSA) for 72 hours prior xenogaft and placed on the neuroepithelium wall (A) or inside the developing neural tube at the prosencephalic level (B). At E5 chick developmental stage (C), embryos were fixed and *in situ* hybridization was performed using *Alu* probe. *In situ* hybridization revealed that both control and iHDAC-treated U87-MG cells were integrated into the embryonic mesenchyme. iHDAC-treated cells spread for longer distances than control cells (D). The embryonic environment efficiently promoted cell proliferation in both control and iHDAC-treated cells (E and F, red asterisks), bypassing iHDAC inhibition of cell proliferation observed *in vitro* as more mitotic figures Alu^+ were found in the iHDAC group (K). Tunneling tube formation was observed *in vivo* only in iHDAC-treated cells (G and I, asterisks). Tunneling tubes connected neighboring tumor cells (G and I, asterisks) as well as tumor cells and embryonic vessels (H, arrow head). More embryonic vessels were found close to Alu^+ nuclei in iHDAC-treated cells than in control cells (J, L). NE = neuroepithelium; V = embryonic vessel.

when compared to the control group in the time-lapse video microscopy and transwell assay. The quantification of mitotic figures (Figure 6(E, F)) indicates that TSA-treated cells proliferated more than the cells in the control group (Figure 6(L)). We also observed that the association with embryonic vessels was greater in the TSA group than in the control group (Figure 6(K)), suggesting that human tumor cells maybe using the embryonic vessels as migratory routes to disperse in the mesenchyme. Interestingly, we also observed the formation of membrane protrusions similar to the ones observed *in vitro* only in the TSA group. These membrane protrusions were observed in the tumor cell-cell contact in migratory routes on the neuroepithelium (Figure 6(G, I)) and also in the contact between tumor cells and embryonic vessels (Figure 6(H, J)). We conclude that TSA-treated cells mostly recapitulated the behavior observed *in vitro* with respect to tunneling tube formation. However, the effects of TSA treatment on the migratory and proliferative behavior of tumor cells were reversed by the embryonic microenvironment.

We then hypothesized that TSA-treated cells harbor the competence to properly respond to environmental cues and downregulate their malignant behavior as we have mostly observed *in vitro*. To properly approach this question, we performed *in situ* hybridization followed by immune staining in serial sections for the HNK-1 marker, which is widely expressed by neuroepithelial cells and migratory neural crest cells during embryonic neurogenesis. In fact, we were able to detect HNK-1^+ cells only in the outermost layer of TSA-treated oncospheres placed in the neural tube lumen 5 days after the xenograft (Figure 7(A and B) (control); 7(C and D), TSA). In addition, we found HNK-1^+ cells dispersed into the embryonic mesenchyme but which were Alu^-, of embryonic origin therefore (Figure 7(E, F, I, J, M, N)). Surprisingly, only in the TSA group, we detected a colocalization of Alu^+ and HNK-1^+ cells (Figure 7(G, H, K, L, O, P)). Since we observed that oncospheres placed in the lumen of the neural tube and fixed immediately after the xenograft did not express HNK-1 (Figure 7(G, H, K, L, O, P) (control); 7(S and T) (TSA)), we concluded that the blockade of HDAC activity confers the competence to the tumor cell to properly respond to environmental cues and downregulate its malignant behavior *in vivo*.

4. Discussion

Several studies have reported the pattern of HDAC expression in both health and pathological brain tissue, showing that aberrant expression of HDACs correlates with a poor prognosis in different types of cancer [20]. It has been characterized that there is an increase in the mRNA expression levels of HDAC1, 3, and 6 in both GBM cells and primary GBM tissues [36]. Particularly, several HDAC classes have been reported to be correlated with GBM malignancy and radioresistance [28, 37, 38]. In this scenario, we have identified the HDACs from classes I, IIa, and IIb are expressed by U87-MG cells and primary GBM011 cells whose activity, when inhibited by TSA or SAHA, led to tumor cell shape changes associated with tunneling tube formation which correlated to disruption in the cell cycle and viability, Ca^{2+} responsiveness, and radiosensitization. We also successfully linked this behavior modulated by HDAC activity blockade to the downregulation of vimentin and connexin 43. Interestingly, it was recently reported the correlation among HDACs 4 and 6 and the DNA double-strand break repair machinery towards the maintenance of stemlike phenotype coupled to radioresistance in GBM cells [37]. In this paper, the authors studied samples from 31 GBM patients who underwent temozolomide and radiotherapy, which leads to an enrichment of more undifferentiated, stemlike GBM cells and, therefore, to a poor prognosis. Interestingly, the expression levels of HDAC 4 and HDAC 6 were upregulated in most of the cases and were directly related to a poor clinical prognosis. In addition, molecular ablation of HDACs 4 and 6 radiosensitized U87-MG cells predisposing GBM cells to radiation therapy-induced apoptosis [37]. Following this reasoning, the quantification of HDACs mRNA levels in the normal brain, astrocytoma grades I, II, and III, and GBM did not show significant differences in expression levels of HDACs 6 and 7 [39]. When the comparison was made among low- and high-grade gliomas and normal brain, only HDAC 4 mRNA was upregulated in high-grade gliomas. Comparisons made between GBM and grade III astrocytoma showed that HDACs 4, 6, and 7 were expressed at lower levels in GBM samples. These results suggest that HDACs 4, 6, and 7 expression patterns are restricted to a rare population of GBM cells and may be associated with a more-resistant GBM cell population which may be, at least in part, positively selected by usual radiotherapy and chemotherapy. This interpretation is corroborated by the fact that patients that underwent radiotherapy and chemotherapy presented an enrichment in mRNA levels of HDACs 4 and 6 associated with a stemlike phenotype [37]. These results from the literature corroborate our findings since we have shown that both U87-MG and GBM011 cells express HDACs 4 and 7 (Supplementary Figure S1) whose activity blockade leads to G2/M cell cycle arrest [40] and radiosensitization [37] as we have reported here.

However, our major finding is the report of HDAC-dependent tumor cell shape changes and tunneling tube formation never deeply explored in the literature before by live cell imaging. Plasma membrane protrusions can carry organelles and functionally couple tumor cells establishing a resistant population to radiation-induced cell death also presenting an invasive phenotype [41]. In this paper, the authors showed that tunneling tube formation was connexin 43-dependent and drove cell invasion, proliferation, and radioresistance. However, in contrast, our findings did not corroborate a role for connexin 43 during iHDAC-dependent tunneling tube formation. In fact, connexin 43 was downregulated after TSA treatment and was correlated to radiosensitization of U87-MG cells as previously reported [42]. In contrast, GBM011 cells still express connexin 43 what may contribute to radioresistance observed in TSA-treated GBM011 cells. In addition, we reported a GBM cell shape transition to mesenchymal morphology independent

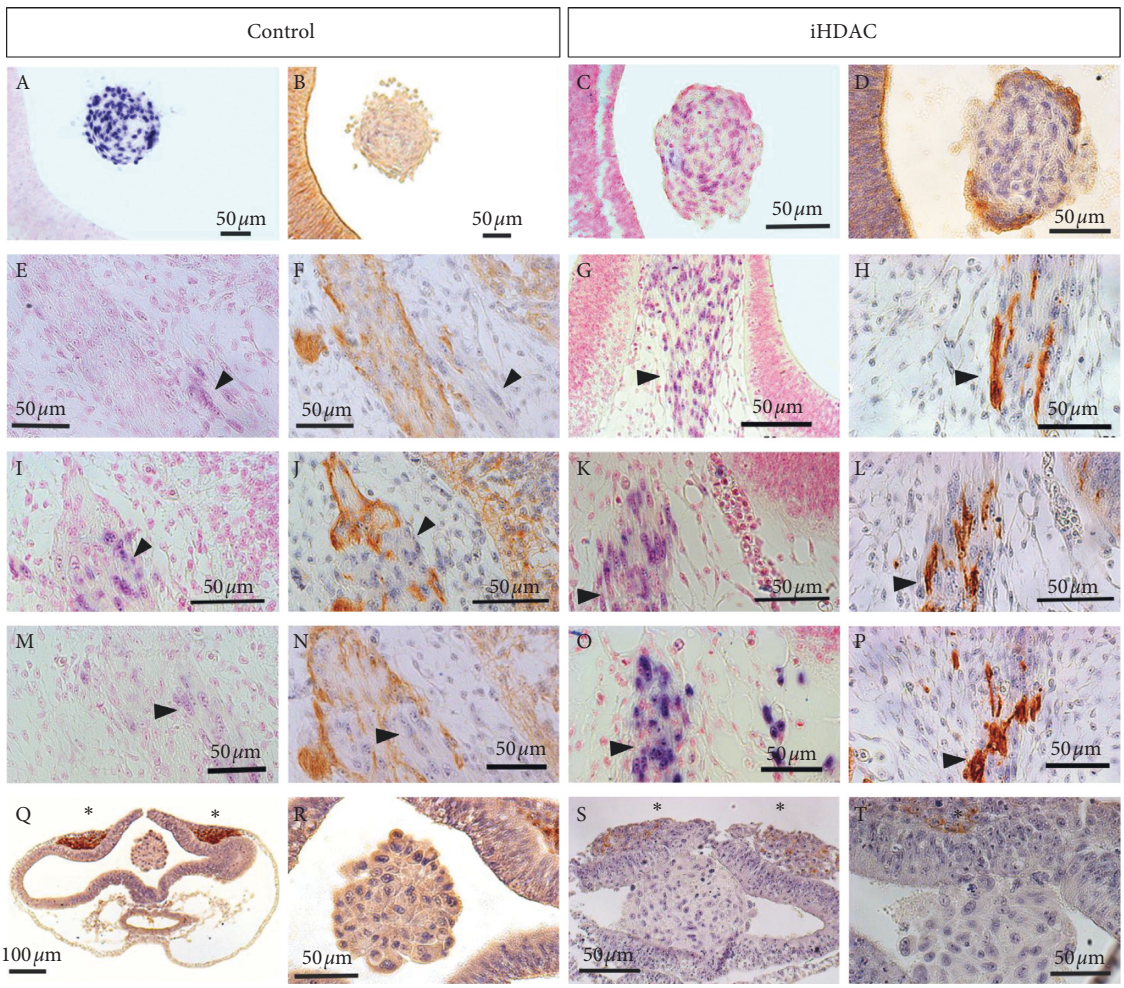

Figure 7: HDAC activity blockade downgrades GBM aggressiveness in synergy with the developing microenvironment. U87-MG oncopheres were cultured in the presence or absence of iHDACs (100 nM TSA) for 72 hours. After the xenograft, the embryos were allowed to develop until stage E5. *In situ* hybridization and immunostaining for HNK-1 revealed that when the oncospheres remained placed in the lumen of the developing neural tube, the outermost layer of cells expressed HNK-1 only in the iHDAC group: control oncospheres: (A) *Alu in situ* hybridization; (B) immunostaining for HNK-1 and iHDAC oncospheres: (C) *Alu in situ* hybridization; (D) immunostaining for HNK-1. The cells that were integrated into the embryonic mesenchyme were able to migrate and to associate with developing embryonic structures. In the control group, only embryonic cells expressed HNK-1 since Alu^+ nuclei did not colocalize with the HNK-1 (E–N, arrow heads). In iHDAC oncospheres, however, it was possible to observe the colocalization of Alu^+ nuclei and HNK-1 staining (G–P, arrow heads). In fact, control (Q, R) and iHDAC (S, T) treated oncospheres did not constitutively express HNK-1 since their placement in the developing neural tube lumen, followed immediately by fixation did not reveal HNK-1 staining in the oncospheres. Positive control for HNK-1 staining was done with migrating neural crest cells (Q–T, asterisks).

of TGF-β signaling and not related to EMT (Figure 2). Thus, once the regulation of EMT by blocking HDAC activity was excluded as a mechanism to promote the elongated morphology, we propose to morphologically characterize the cellular extensions observed in iHDAC-treated cells. To approach this issue, we started analyzing the F-actin fibrillar structure of control and iHDAC-treated cells by live imaging and anisotropy, an index that evaluates the cellular fibrillar organization. In fact, iHDAC-treated U87-MG and GBM011 cells presented a significant higher anisotropy index, indicating a more-organized fibrillar actin structure when compared to the control group (Figure 1). Such organization of the cytoskeleton in iHDAC-treated cells may respond, at least in part, by the elongated and stable morphology observed in the absence of HDAC activity (Figure 1). Dynamic protrusions of cell surfaces are well documented among different cell types and small membrane projections, such as filopodia and microvilli, as well as larger structures, such as lamellipodia, are largely documented in the literature. More recently, thin surface membrane projections have been described as key long-range mediators and named "membrane nanotubes or tunneling tubes" [43]. One interesting function described for nanotubes is focused on their ability to deliver proteins and organelles from one cell to a neighboring cell. Rustom [44] described, for the first time, the transfer of vesicles through nanotubes using neuronal and renal cells. In the context of tumor cell biology, it has been demonstrated that membrane nanotubes form a functional and resistant network to avoid damage caused by radiotherapy [41]. Our results showed that control cells

presented an elongated morphology upon radiotherapy, such as those observed in iHDAC-treated cells, suggesting that ionizing radiation modifies the morphology of GBM cells, which are known radioresistant. We also observed that after irradiation, there was an increase in mitochondrial activity, as demonstrated by the MTT, associated with decreased cell viability and total cell number (Figure 4). In fact, although there was a significant difference in the total number of viable and nonviable cells, 24 h after irradiation in the iHDAC group, at 48 h and 72 h after irradiation, it was not possible to observe significant differences.

Another parameter investigated by Osswald et al. [41], also evoked as a resistance mechanism in astrocytomas, was the maintenance of calcium homeostasis through the network communication formed by nanotubes. The authors then suggest that nanotubes are involved in Ca^{2+} signaling spreading from a single cell to neighboring cells. In our study, we aimed to characterize the relevance of Ca^{2+} channels in iHDAC-treated cells. We found that iHDAC cells presented a lower responsiveness to Ca^{2+} stimuli than control cells. Despite the similarities in the basal levels of intracellular Ca^{2+} between control and iHDAC-treated cells, control cells, however, responded to both T-type calcium channels and purinergic receptors (Figure 4). In fact, it has been shown that purinergic receptors (P2X7R) silencing reduces radiotherapy-induced GBM cell cytotoxicity in addition to a less-efficient radiotherapy-induced cell death, demonstrating that high P2X7 expression levels and function are a good prognostic factor for GBM radiosensitivity [34, 35]. In addition, Ca_v3 (Type T low) voltage-sensitive calcium-channel overexpression was already detected in GBM and pharmacological inhibition resulted in a decrease in cell viability, clonogenic potential, and induction of apoptosis [33].

Thus, our results argue in favor for HDAC blockade as an important hallmark for tumor malignancy downgrade. In fact, when placed in the developing neural tube U87-MG cells successfully integrated into the embryonic mesenchyme, proliferated, and migrated, establishing a close relationship with the embryonic vasculature (Figure 6). The identification of U87-MG cells in nonsequential caudal sections in the iHDAC group suggests the adoption of a possible migratory route. Detachment and the transition to the mesenchymal phenotype contribute to the migratory mechanism [45] and, in this sense, the mesenchymal morphology conferred by HDAC activity blockade may contribute to this kind of behavior. In fact, a recent work using the xenograft model showed that the embryonic microenvironment can orchestrate the cohesion and the detachment of neuroblastoma tumor cells from primary tumors formed in the adrenal medulla after the xenograft was performed in the region corresponding to adrenal sympathetic neural crest. It was possible to infer that there was a recapitulation of the metastatic behavior of these tumor cells both along peripheral nerves and also through the aorta artery during development [46]. In our study, the blockade of HDAC activity led to the formation of a primary aggregate between the telencephalic vesicles, where some cells were also observed, and the migratory process was initiated (Figure 6). In contrast, control U87-MG cells remained adjacent to the neuroepithelium in association with host cells (Figure 6). Finally, the immunostaining for HNK-1 showed that TSA-treated U87-MG cells were positives for this molecular marker. Interestingly, the levels of HNK-1 were found to be inversely proportional to patient survival. In addition, this same work also showed that HNK-1 is an important tumor suppressor for astrocytic tumors [47].

5. Conclusions

Thus, our results describe, for the first time in the literature, the relevance of iHDACs for tumor cell morphology, competence, and plasticity through an original approach using live cell imaging coupled to xenografts in the developing chick embryo. Indeed, regardless of our data corroborating with previous work from the literature showing the effects of iHDACs on proliferation, migration, and cell viability, we first connect the biological effects of iHDACs at the cellular level correlating morphological cell changes with functional outcomes, leading GBM cells to decrease the responsiveness to voltage-sensitive Ca^{2+} channels. In addition, we provided evidences that HDAC activity blockade made GBM cells competent to properly interact with the developing microenvironment and downgrade tumor malignancy. Taking into account that GBM stem cells still represent a therapeutic challenge due to the fact that they are resistant to radio and quimiotherapy, the use of iHDACs may represent an interesting strategy to promote GBM stem cell differentiation and consequently sensitization to current strategies used in the clinic. As a consequence, epigenetic mechanism HDAC-mediated may emerge as a tractable approach in GBM therapy and shed light on new clinical strategies for this malignancy.

Data Availability

All data generated or analyzed during this study are included in this published article or in the supplementary information files.

Conflicts of Interest

The authors declare that there are no conflicts of interest.

Authors' Contributions

Aline Menezes and Gustavo Henrique dos Reis contributed equally to this work.

Acknowledgments

The authors thank Grasiella Ventura and Gabriel Ferraz da Silva for confocal microscopy and calcium-signaling videomicroscopy support. The authors also thank scientific financial support agencies FAPERJ, CNPq, CAPES, and Fundação do Câncer Ary Frausino.

Supplementary Materials

Supplementary material contains experimental evaluation of HDACs mRNA expression pattern, flow cytometry, immunocytochemistry, conventional PCR, and morphometric analysis of iHDAC-treated oncospheres as follows: Supplementary Figure S1: U87-MG cells and GBM011 primary cells tumor constitutively express HDACs. Supplementary Figure S2: HDAC activity is necessary for cell cycle progression in GBM cells. Supplementary Figure S3: HDAC activity is necessary for GBM cell viability Supplementary Figure S4: HDAC blockade leads to F-actin cytoskeleton stabilization and tunneling tube formation in GBM011 cells. Supplementary Figure S5: HDAC blockade does not disrupt GBM011 migration pattern. Supplementary Figure S6: qualitative RT-PCR showed that GBM011 cells expressed smooth muscle actin (SMA), vimentin, connexin 43, and E-cadherin upon 72 hours of either TSA and SAHA treatment (A) Supplementary Figure S7: HDAC activity blockade disrupts basal levels of intracellular Ca^{2+} in GBM011 cells. Supplementary Figure S8: HDAC activity is necessary for U87-MG morphometric properties. (*Supplementary Materials*)

References

[1] D. N. Louis, A. Perry, G. Reifenberger et al., "The 2016 world health organization classification of tumors of the central nervous system: a summary," *Acta Neuropathologica*, vol. 131, no. 6, pp. 803–820, 2016.

[2] A. Bradshaw, A. Wickremesekera, H. D. Brasch et al., "Cancer stem cells in glioblastoma multiforme," *Frontiers in Surgery*, vol. 3, p. 48, 2016.

[3] A. R. Safa, M. R. Saadatzadeh, A. A. Cohen-Gadol, K. E. Pollok, and K. Bijangi-Vishehsaraei, "Glioblastoma stem cells (GSCs) epigenetic plasticity and interconversion between differentiated non-GSCs and GSCs," *Genes & Diseases*, vol. 2, no. 2, pp. 152–163, 2015.

[4] E. C. Holland, J. Celestino, C. Dai, L. Schaefer, R. E. Sawaya, and G. N. Fuller, "Combined activation of Ras and Akt in neural progenitors induces glioblastoma formation in mice," *Nature Genetics*, vol. 25, no. 1, pp. 55–57, 2000.

[5] M. Maleszewska and B. Kaminska, "Is glioblastoma an epigenetic malignancy?," *Cancers*, vol. 5, no. 3, pp. 1120–1139, 2013.

[6] P. A. Jones and S. B. Baylin, "The epigenomics of cancer," *Cell*, vol. 128, no. 4, pp. 683–692, 2007.

[7] M. Haberland, R. L. Montgomery, and E. N. Olson, "The many roles of histone deacetylases in development and physiology: implications for disease and therapy," *Nature Reviews Genetics*, vol. 10, no. 1, pp. 32–42, 2009.

[8] J. E. Shabason, P. J. Tofilon, and K. Camphausen, "Grand rounds at the National Institutes of Health: HDAC inhibitors as radiation modifiers, from bench to clinic," *Journal of Cellular and Molecular Medicine*, vol. 15, no. 12, pp. 2735–2744, 2011.

[9] P. Bezecny, "Histone deacetylase inhibitors in glioblastoma: pre-clinical and clinical experience," *Medical Oncology*, vol. 31, no. 6, p. 985, 2014.

[10] P. Chinnaiyan, G. Vallabhaneni, E. Armstrong, S.-M. Huang, and P. M. Harari, "Modulation of radiation response by histone deacetylase inhibition," *International Journal of Radiation Oncology ∗ Biology ∗ Physics*, vol. 62, no. 1, pp. 223–229, 2005.

[11] E. Adamopoulou and U. Naumann, "HDAC inhibitors and their potential applications to glioblastoma therapy," *Oncoimmunology*, vol. 2, no. 8, article e25219, 2013.

[12] K. J. Falkenberg and R. W. Johnstone, "Histone deacetylases and their inhibitors in cancer, neurological diseases and immune disorders," *Nature Reviews Drug Discovery*, vol. 13, no. 9, pp. 673–691, 2014.

[13] P. Chinnaiyan, S. Chowdhary, L. Potthast et al., "Phase I trial of vorinostat combined with bevacizumab and CPT-11 in recurrent glioblastoma," *Neuro-Oncology*, vol. 14, no. 1, pp. 93–100, 2012.

[14] B. B. Friday, S. K. Anderson, J. Buckner et al., "Phase II trial of vorinostat in combination with bortezomib in recurrent glioblastoma: a north central cancer treatment group study," *Neuro-Oncology*, vol. 14, no. 2, pp. 215–221, 2012.

[15] E. Galanis, K. A. Jaeckle, M. J. Maurer et al., "Phase II trial of vorinostat in recurrent glioblastoma multiforme: a north central cancer treatment group study," *Journal of Clinical Oncology*, vol. 27, no. 12, pp. 2052–2058, 2009.

[16] E. Galanis, S. K. Anderson, J. M. Lafky et al., "Phase II study of bevacizumab in combination with sorafenib in recurrent glioblastoma (N0776): a north central cancer treatment group trial," *Clinical Cancer Research*, vol. 19, no. 17, pp. 4816–4823, 2013.

[17] A. V. Krauze, S. D. Myrehaug, M. G. Chang et al., "A phase 2 study of concurrent radiation therapy, temozolomide, and the histone deacetylase inhibitor valproic acid for patients with glioblastoma," *International Journal of Radiation Oncology ∗ Biology ∗ Physics*, vol. 92, no. 5, pp. 986–992, 2015.

[18] C. A. Hassig, J. K. Tong, T. C. Fleischer et al., "A role for histone deacetylase activity in HDAC1-mediated transcriptional repression," *Proceedings of the National Academy of Sciences*, vol. 95, no. 7, pp. 3519–3524, 1998.

[19] Z. Wang, C. Zang, K. Cui et al., "Genome-wide mapping of HATs and HDACs reveals distinct functions in active and inactive genes," *Cell*, vol. 138, no. 5, pp. 1019–1031, 2009.

[20] A. C. West and R. W. Johnstone, "New and emerging HDAC inhibitors for cancer treatment," *Journal of Clinical Investigation*, vol. 124, no. 1, pp. 30–39, 2014.

[21] A. Newbold, K. J. Falkenberg, H. M. Prince, and R. W. Johnstone, "How do tumor cells respond to HDAC inhibition?," *FEBS Journal*, vol. 283, no. 22, pp. 4032–4046, 2016.

[22] M. C. Oliveira-Nunes, S. A. Kahn, A. L. D. O. Barbeitas et al., "The availability of the embryonic TGF-β protein nodal is dynamically regulated during glioblastoma multiforme tumorigenesis," *Cancer Cell International*, vol. 16, no. 1, p. 46, 2016.

[23] F. Piccinini, "AnaSP: a software suite for automatic image analysis of multicellular spheroids," *Computer Methods and Programs in Biomedicine*, vol. 119, no. 1, pp. 43–52, 2015.

[24] I. R. Cordeiro, D. V. Lopes, J. G. Abreu, K. Carneiro, M. I. D. Rossi, and J. M. Brito, "Chick embryo xenograft model reveals a novel perineural niche for human adipose-derived stromal cells," *Biology Open*, vol. 4, no. 9, pp. 1180–1193, 2015.

[25] R. Limame, A. Wouters, B. Pauwels et al., "Comparative analysis of dynamic cell viability, migration and invasion assessments by novel real-time technology and classic endpoint assays," *PLoS One*, vol. 7, no. 10, Article ID e46536, 2012.

[26] A. Boudaoud, A. Burian, D. Borowska-Wykręt et al., "FibrilTool, an ImageJ plug-in to quantify fibrillar structures

in raw microscopy images," *Nature Protocols*, vol. 9, no. 2, pp. 457–463, 2014.

[27] L. L. Vindelov, "Kits for quantitative flow cytometric analysis," *Cytometry*, vol. 6, p. 348, 1985.

[28] Z. Zhang, Y. Wang, J. Chen et al., "Silencing of histone deacetylase 2 suppresses malignancy for proliferation, migration, and invasion of glioblastoma cells and enhances temozolomide sensitivity," *Cancer Chemotherapy and Pharmacology*, vol. 78, no. 6, pp. 1289–1296, 2016.

[29] A. Bubna, "Vorinostat-an overview," *Indian Journal of Dermatology*, vol. 60, no. 4, p. 419, 2015.

[30] Y. Katsuno, S. Lamouille, and R. Derynck, "TGF-β signaling and epithelial-mesenchymal transition in cancer progression," *Current Opinion in Oncology*, vol. 25, no. 1, pp. 76–84, 2013.

[31] T. Calì, M. Brini, and E. Carafoli, "Regulation of cell calcium and role of plasma membrane calcium ATPases," *International Review of Cell and Molecular Biology*, vol. 332, pp. 259–296, 2017.

[32] N. C. K. Valerie, B. Dziegielewska, A. S. Hosing et al., "Inhibition of T-type calcium channels disrupts Akt signaling and promotes apoptosis in glioblastoma cells," *Biochemical Pharmacology*, vol. 85, no. 7, pp. 888–897, 2013.

[33] Y. Zhang, J. Zhang, D. Jiang et al., "Inhibition of T-type Ca^{2+} channels by endostatin attenuates human glioblastoma cell proliferation and migration," *British Journal of Pharmacology*, vol. 166, no. 4, pp. 1247–1260, 2012.

[34] M. P. Gehring, T. C. B. Pereira, R. F. Zanin et al., "P2X7 receptor activation leads to increased cell death in a radiosensitive human glioma cell line," *Purinergic Signalling*, vol. 8, no. 4, pp. 729–739, 2012.

[35] M. P. Gehring, F. Kipper, N. F. Nicoletti et al., "P2X7 receptor as predictor gene for glioma radiosensitivity and median survival," *International Journal of Biochemistry & Cell Biology*, vol. 68, pp. 92–100, 2015.

[36] M. Staberg, S. R. Michaelsen, R. D. Rasmussen, M. Villingshøj, H. S. Poulsen, and P. Hamerlik, "Inhibition of histone deacetylases sensitizes glioblastoma cells to lomustine," *Cellular Oncology*, vol. 40, no. 1, pp. 21–32, 2017.

[37] F. Marampon, F. Megiorni, S. Camero et al., "HDAC4 and HDAC6 sustain DNA double strand break repair and stem-like phenotype by promoting radioresistance in glioblastoma cells," *Cancer Letters*, vol. 397, pp. 1–11, 2017.

[38] Z. Wang, P. Hu, F. Tang et al., "HDAC6 promotes cell proliferation and confers resistance to temozolomide in glioblastoma," *Cancer Letters*, vol. 379, no. 1, pp. 134–142, 2016.

[39] A. K. Lucio-Eterovic, M. A. Cortez, E. T. Valera et al., "Differential expression of 12 histone deacetylase (HDAC) genes in astrocytomas and normal brain tissue: class II and IV are hypoexpressed in glioblastomas," *BMC Cancer*, vol. 8, no. 1, p. 243, 2008.

[40] M. Cornago, C. Garcia-Alberich, N. Blasco-Angulo et al., "Histone deacetylase inhibitors promote glioma cell death by G2 checkpoint abrogation leading to mitotic catastrophe," *Cell Death & Disease*, vol. 5, no. 10, article e1435, 2014.

[41] M. Osswald, E. Jung, F. Sahm et al., "Brain tumour cells interconnect to a functional and resistant network," *Nature*, vol. 528, no. 7580, pp. 93–98, 2015.

[42] S. F. Murphy, R. T. Varghese, S. Lamouille et al., "Connexin 43 inhibition sensitizes chemoresistant glioblastoma cells to temozolomide," *Cancer Research*, vol. 76, no. 1, pp. 139–149, 2016.

[43] D. M. Davis and S. Sowinski, "Membrane nanotubes: dynamic long-distance connections between animal cells," *Nature Reviews Molecular Cell Biology*, vol. 9, no. 6, pp. 431–436, 2008.

[44] A. Rustom, "Nanotubular highways for intercellular organelle transport," *Science*, vol. 303, no. 5660, pp. 1007–1010, 2004.

[45] M. Labelle and R. O. Hynes, "The initial hours of metastasis: the importance of cooperative host-tumor cell interactions during hematogenous dissemination," *Cancer Discovery*, vol. 2, no. 12, pp. 1091–1099, 2012.

[46] C. Delloye-Bourgeois, L. Bertin, K. Thoinet et al., "Microenvironment-driven shift of cohesion/detachment balance within tumors induces a switch toward metastasis in neuroblastoma," *Cancer Cell*, vol. 32, no. 4, pp. 427–443.e8, 2017.

[47] M. Suzuki-Anekoji, M. Suzuki, T. Kobayashi et al., "HNK-1 glycan functions as a tumor suppressor for astrocytic tumor," *Journal of Biological Chemistry*, vol. 286, no. 37, pp. 32824–32833, 2011.

Hindawi
Journal of Oncology
Volume 2019, Article ID 1232434, 10 pages
https://doi.org/10.1155/2019/1232434

Research Article

Oncosuppressive Role of RUNX3 in Human Astrocytomas

Giedrius Steponaitis, Arunas Kazlauskas, Paulina Vaitkienė, Vytenis P. Deltuva, Mykolas Mikuciunas, and Daina Skiriutė

Laboratory of Molecular Neurooncology, Neuroscience Institute, Lithuanian University of Health Sciences, Eiveniu Str. 4, 50161 Kaunas, Lithuania

Correspondence should be addressed to Giedrius Steponaitis; giedrius.steponaitis@lsmuni.lt

Received 11 January 2019; Revised 30 May 2019; Accepted 10 June 2019; Published 5 August 2019

Academic Editor: Claudio Festuccia

Background. Gliomas are the most common and aggressive among primary malignant brain tumours with significant inter- and intratumour heterogeneity in histology, molecular profile, and patient outcome. However, molecular targets that could provide reliable diagnostic and prognostic information on this type of cancer are currently unknown. Recent studies show that certain phenotypes of gliomas such as malignancy, resistance to therapy, and relapses are associated with the epigenetic alterations of tumour-specific genes. Runt-related transcription factor 3 (*RUNX3*) is feasible tumour suppressor gene since its inactivation was shown to be related to carcinogenesis. *Aim*. The aim of the study was to elucidate RUNX3 changes in different regulation levels of molecular biology starting from epigenetics to function in particular cases of astrocytic origin tumours of different grade evaluating significance of molecular changes of RUNX3 for patient clinical characteristics as well as evaluate RUNX3 reexpression effect to GBM cells. *Methods*. The methylation status and protein expression levels of RUNX3 were measured by methylation-specific PCR and Western blot in 136 and 72 different malignancy grade glioma tissues, respectively. Lipotransfection and MTT were applied for proliferation assessment in U87-MG cells. *Results*. We found that *RUNX3* was highly methylated and downregulated in GBM. *RUNX3* promoter methylation was detected in 69.4% of GBM (n=49) as compared to 0 to 17.2% in I-III grade astrocytomas (n=87). Weighty lower RUNX3 protein level was observed in GMB specimens compared to grade II-III astrocytomas. Correlation test revealed a weak but significant link among Runx3 methylation and protein level. Kaplan-Meier analysis showed that increased RUNX3 methylation and low protein level were both associated with shorter patient survival ($p<0.05$). Reexpression of RUNX3 in U87-MG cells significantly reduced glioma cell viability compared to control transfection. *Conclusions*. The results demonstrate that *RUNX3* gene methylation and protein expression downregulation are glioma malignancy dependent and contribute to tumour progression.

1. Introduction

Glial brain tumours originating from glial cells are intracranial solid neoplasms. According to classification system of the World Health Organisation (WHO) based on histological evaluation, brain tumour grade is determined by necrotic cells in the centre of the tumour, increased mitotic activity, the presence of nuclear pleomorphism, and angiogenesis. Brain tumour malignancy is associated with tumour heterogeneity, recurrence, patient survival, and therapy response [1]. For instance, grade I tumours, like pilocytic astrocytomas (according to the 4th edition of WHO classification), are curable glial tumours, while grade IV astrocytic tumours, glioblastomas, are rapidly progressive and lethal [2]. In the last years evidences indicating evolvement of epigenetic alterations in cancer development and in the response to therapy steadily accumulated. Although histology in neurooncology represents gold standard in diagnostics, the recently described identification of molecularly different glioblastoma oncotypes and its correlation with clinical characteristics is important step in patient stratification into clinically distinct subgroups that could eventually benefit from personalized therapeutic strategy [3–5].

RUNX3 protein is a transcription factor, containing a highly conserved DNA binding domain which binds to a DNA core motif of 5′ pyGpyGGT 3′ designated as a "runt domain, RD" which shares a sequence similarity with D. melanogaster RUNX. Three different mammalian

RUNX protein family members have been identified: RUNX1 (also called PEBP2AB, CBFA2/AML1), RUNX2 (PEBP2aA, CBFA1, AML3), and RUNX3 (PEBP2aC, CBFA3/AML2). All three family proteins physically associate with SMAD proteins, downstream targets of TGF-beta/BMP signalling, and play roles in mammalian development [7]. RUNX3 is the least studied and the least characterized of all RUNX members. During normal development, RUNX3 is found to be expressed in the hematopoietic system, in osteoblasts and chondrocytes and in neurotrophin-positive neurons of the dorsal root ganglia [8] indicating its role in neuronal development [9]. In adult organism RUNX3 expression persists in the hematopoietic system [8]; however, its biological function is largely unexplored. RUNX3 was also noticed to be involved into oncological events. RUNX3 has been variously described as a tumour suppressor or promoter, occasionally with a conflicting result in the same cancer and possible reflecting a complex role of RUNX3 in oncogenesis [10]. The study of loss of RUNX3 expression during progression to invasive gastric cancer compared to the normal gastric epithelium was the first suggesting tumour suppressive function for RUNX3 [11]. Later on, a number of studies meet the same results suggesting gene suppressor role for RUNX3 in other solid tumours such as colon [12], lung [13], breast [14], glioblastoma [15], renal cell [16], hepatocellular carcinomas [17], chondrosarcoma [18], etc. Many other cancer studies based on epigenetics have suggested that RUNX3 downregulation in cancers could be the result of hypermethylation of the promoter of RUNX3 [19–21]. Hypermethylation of RUNX3 promoter was also observed in glioblastoma cell lines and primary tumour tissue compared to normal human brain tissue [15, 22]. Moreover, RUNX3 methylation was considered as a potential biomarker of aggressiveness of gliomas [23].

Nevertheless, other studies showed opposite data and suggested tumour promoting or oncogenic role for RUNX3. High expression of RUNX3 was associated with ovarian cancer [24] as well as with poor histologic differentiation, metastasis, and invasion in head and neck squamous cell carcinoma [25], with pancreatic ductal adenocarcinoma [26] and basal cell carcinoma [27], with childhood acute myeloid leukaemia [28], and with inflammatory breast [29] and gastric cancers [30, 31].

In current study we aimed to evaluate *RUNX3* gene methylation and protein expression in only astrocytic origin tumours of different grade to estimate association between methylation frequency and protein expression, as well as evaluate the RUNX3 alteration effect on patient survival. In the present study for the first time RUNX3 promoter methylation and protein expression was analysed in the same specimens of brain tumour to reveal if the link of RUNX3 methylation and silencing which was shown in glioma cell lines meet the similar processes in astrocytoma specimens.

2. Material and Methods

2.1. Patients and Tissue Samples. In total 136 postoperative grade I-IV astrocytoma specimens were used for the analysis: 14 (10.3%) grade I pilocytic astrocytomas, 44 (32.4%) grade II diffuse astrocytomas, 29 (21.3%) grade III anaplastic astrocytomas, and 49 (36%) glioblastomas grade IV. All the specimens of astrocytoma were surgically resected from patients without prior treatment (no patients had received chemo- or radiotherapy before surgery) in Neurosurgery Clinics of Hospital (NCH) of Lithuanian University of Health Sciences Kaunas, Lithuania, during the period from 2003 to 2017. Brain tumour tissue specimens after dissection were snap-frozen in liquid nitrogen and stored until analysis. Written informed patient consent was obtained for every patient under the approval of Kaunas Regional Biomedical Research Bioethics Committee. The study was accomplished under the principles of Declaration of Helsinki. The clinical patient data such as age at the time of the tumour resection, gender, time of the last follow-up, were collected for each patient. The survival of the patients was calculated from the date of tumour resection to the date of death of the patient or database closure (September 2018) date if the patient was still alive.

Overall study sample of 136 glioma patients consisted of 44.8% (n=61) males and 55.1% (n=75) females, patient median age was 48 years (range 18-89 years), and median overall survival time after diagnosis was 30.9 months (range 0.2 to 154 months). Patient age does not differ between astrocytoma grade I to III (median age 37.6 years), but patients in those groups were significantly younger compared to glioblastoma group (median age 65 years, Kruskal-Wallis test, $p<0.001$).

2.2. Methylation-Specific PCR. DNA extraction from human brain tumour tissue applying modified salting-out method, DNA bisulfite modification using EpiJET Bisulfite Conversion Kit (Cat No: K1461, Thermo Scientific, Inc.), methylation-specific amplification using hot start polymerase (Cat No: K1052, Thermo Scientific Inc.), and methylation detection procedures were performed as previously described [32]. MSP primers designed and verified by Mueller, 2007, were applied for RUNX3 methylation analysis. MSP primers for methylated allele were 5'-TTACGAGGGGCGGTCGTACGCGGG-3' (sense) and 5'-AAAACGACCGACGCGAACGCCTCC-3' (antisense) and for unmethylated allele: 5'-TTATGAGGGGTGGTTGTATGTGGG-3' (sense) and 5'-AAAACAACCAACACAAACACCTCC-3' (antisense). 10 pmol of each primer in a total volume of 12 μl was used for MSP. MSP was carried out for 38 cycles applying at 95°C for 15 sec. for denaturation, 67°C for 30 sec. for annealing, and 72°C for 15 sec for the extension. The signals of the correct molecular weight of amplified DNA with primers for methylated or unmethylated sequence were registered as a methylated or unmethylated promoter of the gene (Figure 1(a)). In a case of amplification of both variants (methylated and unmethylated), gene promoter of the sample was considered as being methylated.

2.3. Whole-Tissue Protein Extract Preparation and Immunoblot Analysis. Preparation of whole-tissue extracts of the tumour specimens, SDS-PAGE, and protein transfer to nitrocellulose membrane procedures was done as previously described [32]. Primary rabbit antibody against RUNX3 (Antibodies-Online, cat no. ABIN739370) diluted 1:500 in

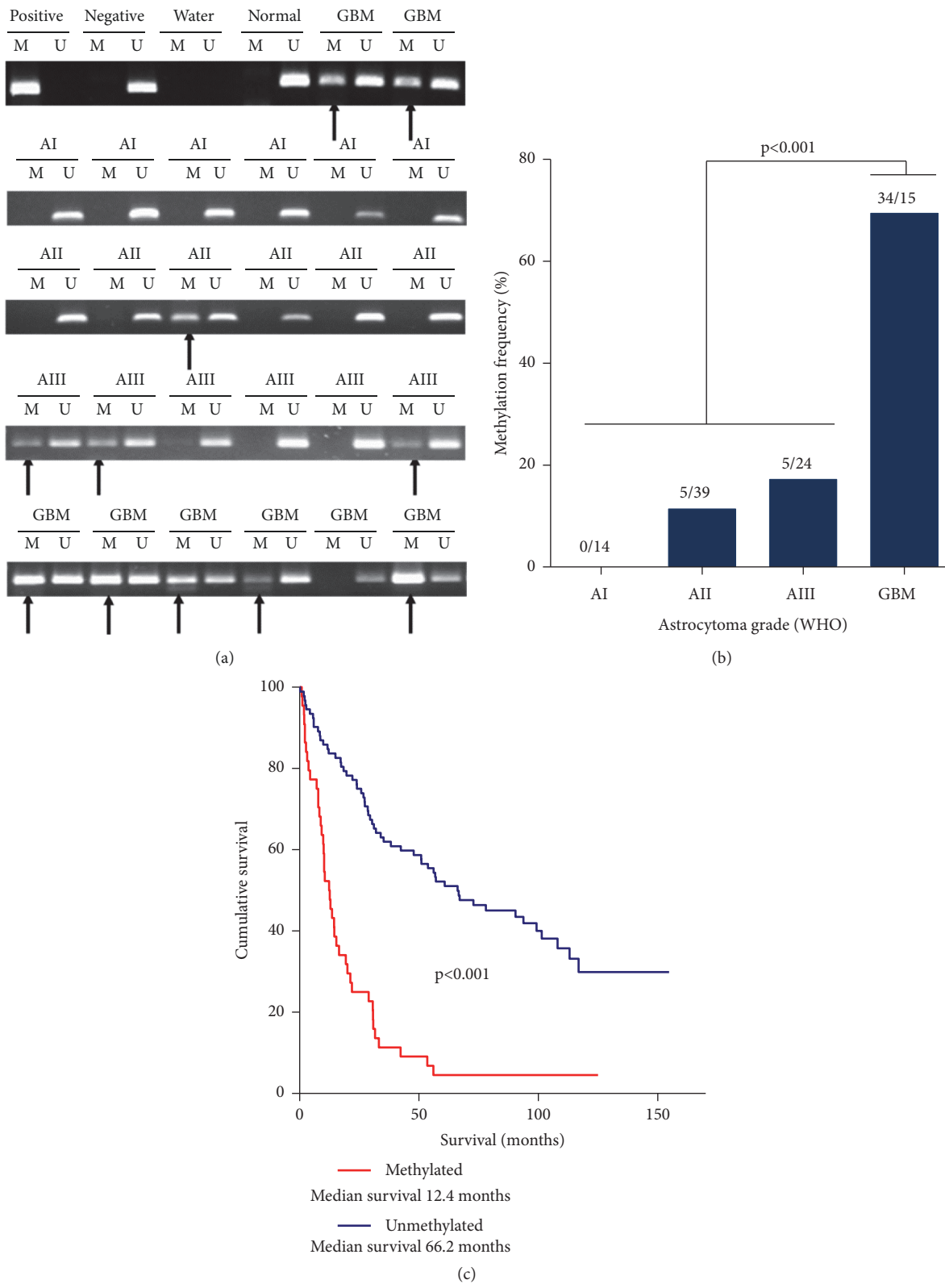

FIGURE 1: (a) Representative results for methylation-specific PCR of RUNX3 gene in different malignancy grade gliomas. M: PCR with primers for methylated RUNX3. U: PCR with primers for unmethylated RUNX3. Positive control: bisulfite converted universal methylated human DNA standard (Zymo Research, USA). Negative control: bisulfite converted normal lymphocyte DNA. Normal: "normal human brain DNA" (Zymo Research, cat. no. D5018). Arrows indicate methylated allele. (b) RUNX3 promoter methylation frequency in different astrocytoma grade. GBM revealed significant increase in RUNX3 gene promoter methylation frequency compared to I-III WHO grade astrocytomas ($p<0.001$, chi-square test). (c) Kaplan-Meier curves for survival (months) of all glioma patients (n=136) stratified by RUNX3 gene methylation status revealed significantly shorter survival of patients with RUNX3 methylated tumours (Log-rank test, $\chi^2=44.68$, df=1, $p<0.001$).

5% nonfat milk in PBS was used for RUNX3 protein detection applying 2-hour incubation on a platform shaker at room temperature. After washing in PBS buffer supplemented with 0.5% of Tween-20, membranes were incubated with the anti-rabbit secondary antibody conjugated with horseradish peroxidase (Life Technologies, cat no. 656120, dilution 1:2000) for 1-hour at room temperature. Signals were visualized using enhanced chemiluminescence reagent Ampliflu™ Red (Sigma-Aldrich, cat no. 90101) and recorded using gel visualization system GelDoc-It®2 imager (Analytik Jena AG). Detection assay of input control, ACTB, on the same membranes after mild stripping and reprobing was performed as previously described [32]. Values of RUNX3 and ACTB signals were calculated applying image analysis program ImageJ version 1.47 (National Institutes of Health, USA).

2.4. Cell Culturing and Proliferation Assay. Human glioblastoma cell line U87-MG was used for functional assessment of RUNX3. The U87-MG cell line was purchased from Sigma-Aldrich (source: European Collection of Authenticated Cell Culture, ECACC, cat. no: 89081402). Cells were cultivated in high glucose Dulbecco's Modified Eagle Medium (DMEM) with Phenol Red, "GlutaMAX™ " (Gibco, cat. no 10566016) supplemented with 10% (v/v) fetal bovine serum (FBS) (Gibco, cat. no 10566016) and 1% (v/v) Penicillin and Streptomycin (P/S). Cells were maintained at 37˚C in a humidified incubator containing 5% (v/v) CO2. Cells visualization was accomplished under Etaluma LS620 microscope (Lumascope) applying standard phase contrast microscopy for routine cell visualization and exited microscopy with a green filter (Excitation 473-491 nm, Emission 502-561 nm) for green fluorescent protein (GFP) detection. GFP plasmid (pcDNA4TO-GFP) transfected cell was applied to evaluate transfection efficiency. Expression vector pcDNA3 with RUNX3 gene (pcDNA3-RUNX3) was gifted from PhD Dominic Chih-Cheng Voon, Cancer Science Institute of Singapore, National University of Singapore. Cell viability was monitored applying the MTT assay (Invitrogen, cat. no M6494) in 96-well flat-bottomed microplates after 24-hours after transfection. Approximately 12.500 U87 cells per well were used for transfection with "Lipofectamine™ 3000 Transfection Reagent" (Invitrogen, cat. no. L3000015) and 100 ng of plasmid DNA according to the manufacturer's protocol. Microplates were analysed by the Multiskan™ GO Microplate Spectrophotometer measuring absorption at 550 nm (Formazan absorption) and at 620 nm (background normalization).

2.5. Statistical Analysis. Differences across two independent groups were analysed applying Mann-Whitney U test, and Kruskal-Wallis test was used for differences estimation across more than two independent groups. For categorical data sets analysis (such MSP data) chi-square test was applied. The Kaplan-Meier curves method was applied to estimate survival functions and the log-rank test used to compare the difference of survival between groups. Patient survival was calculated from the data of tumour resection to the date of patient death, or database closure date (September 2018). Cox regression model was applied to assess the independence of prognostic factors such as gender, age, and molecular factors such as RUNX3 methylation and protein expression which were first examined individually applying univariate Cox regression analysis, and all factors that had a strong impact on survival were then evaluated jointly in multivariate Cox regression analysis applying Backward Conditional method.

Statistical calculations were performed using GraphPad Prism for Windows (v. 6.0, GraphPad Software, Inc.) and SPSS statistics for Windows (v. 22.0, IBM) software packages. The value of $p<0.05$ was considered significant.

3. Results

3.1. RUNX3 Promoter Methylation Frequency Is Gradually Increasing along Astrocytoma Grade. MSP analysis revealed positive *RUNX3* promoter methylation (below in the text: *RUNX3* methylation) in 44 (32.4%) out 136 of glioma patient tumour specimens (Table 1). Should be noted that *RUNX3* gene promoter was unmethylated in normal brain tissue sample (Zymo Research, cat. no. D5018), Figure 1(a). *RUNX3* promoter methylation analysis showed gradually increasing RUNX3 methylation frequency along astrocytoma grade. No methylation signals in any tumour samples of astrocytoma grade I (0 from 14) was detected (Figure 1(b); Table 1). *RUNX3* methylation frequency increased to 11.4% and 17.2% in astrocytoma grade II and astrocytoma grade III tumours, respectively. The highest *RUNX3* methylation frequency was observed in glioblastoma tissue specimens and even 34 out of 49 samples were methylated (69.4%). Data analysis revealed significant increase in *RUNX3* methylation frequency in glioblastoma tumours as compared to grade I-III astrocytomas (Chi-square test, $p<0.001$), Figure 1(c).

3.2. RUNX3 Protein Expression Is Reduced in Glioblastomas. RUNX3 expression evaluation at protein level was performed on the same glioma samples applying Western blot (WB) analysis, and in a total 72 glioma specimens, among which 6 were astrocytoma grade I, 27 grade II, 17 grade III, and 22 grade IV (glioblastoma) were used (Table 1). In tumour specimens RUNX3 protein level showed variable pattern; the expression varied between highly expressed to very weak or not detectable at all, Figure 2(a). RUNX3 revealed significantly lower protein level in glioblastomas compared to grade II tumours (Kruskal-Wallis test, $p=0.005$) and a tendency of lower GBM RUNX3 protein level compared to grade III astrocytomas (Kruskal-Wallis test, $p=0.124$), Figure 2(b). RUNX3 protein expression reduction was observed in the majority of studied glioblastoma specimens as compared to lower-grade gliomas.

Significant association between RUNX3 gene methylation and protein expression was found (Kruskal-Wallis test, $p=0.026$) Figure 2(c). Correlation analysis revealed a weak but significant link among Runx3 methylation and protein level. (Spearman correlation coefficient -0.269, $p=0.024$, $n=72$).

3.3. Molecular RUNX3 Variations in Tumours Are Associated with Patient Clinicopathological Variables. Promoter methylation of *RUNX3* was closely associated with patient age

Table 1: Associations between grade I-IV astrocytoma patients' clinical data and RUNX3 gene molecular properties.

Variable	Methylation			Protein expression		
	Unmethylated % (n)	Methylated % (n)	*P* (χ^2; *df*)†	Low % (n)	High % (n)	*P*
Overall	67.6 (92)	32.4 (44)		48.6 (35)	51.4 (37)	
Grade						
I	100 (14)	0 (0)		66.7 (4)	33.3 (2)	
II	88.6 (39)	11.4 (5)	**<0.001** *(49.3; 3)*	25.9 (7)	74.1 (20)	**0.007**§
III	82.8 (24)	17.2 (5)		35.3 (6)	64.7 (11)	
IV (GBM)	30.6 (15)	69.4 (34)		81.8 (18)	18.2 (4)	
Gender						
Male	65.6 (40)	34.4 (21)	0.641 *(0.22; 1)*	48.8 (20)	51.2 (21)	0.707‡
Female	69.3 (52)	30.7 (23)		48.4 (15)	51.6 (16)	
Age, years						
<50	88.7 (63)	11.3 (8)	**<0.001** *(30.2; 1))*	32.5 (13)	67.5 (27)	**0.037**‡
≥50	44.6 (29)	55.4 (36)		68.8 (22)	31.2 (10)	
Survival, months						
<24	40 (22)	60 (33)	**<0.001** *(32.2; 1)*	80 (20)	20 (5)	**0.001**‡
≥24	86.4 (70)	13.6 (11)		31.9 (15)	68.1 (32)	
Methylation						
Unmethylated				39.2 (20)	60.8 (31)	**0.026**‡
Methylated				68.4 (13)	31.6 (6)	

†P-value estimated by Pearson Chi-square (χ^2) test.
§Kruskal-Wallis test.
‡Mann-Whitney U test.

(Mann-Whitney test, p<0.001), tumour malignancy grade (χ^2 test, p<0.001), and total patient survival (Mann-Whitney test, p<0.001) as well as patient 2-year patient survival after tumour resection (≤24 and >24 months; χ^2 test, p=0.001). Patient gender did not show any importance for RUNX3 methylation in tumours (χ^2 test, p>0.05), Table 1. *RUNX3* methylated gliomas were more likely to be high grade than low grade and gene methylation was associated with older patient age. Patients surviving more than 24 months were more likely having tumours without *RUNX3* gene methylation than patients surviving less than 24 months period. The clinicopathological significance of RUNX3 gene expression at protein level was evaluated by analysing its expression link with clinical parameters. Kruskal-Walis test revealed significant RUNX3 protein level associations with astrocytoma pathological grade (p=0.007), patient 2-year survival after tumour resection (≤24 and >24 months, p=0.001), and patient disease appearance age (≤50 and >50 years; p=0.037), but not gender (p=0.707), Table 1. Glioma patients who survived longer than 2-years more likely have highly RUNX3 expressed tumours than shorter surviving patients. Associations between RUNX3 methylation as well as protein level and patient clinicopathological characteristics are summarized in Table 1.

3.4. Astrocytoma Patient Survival Is Associated with RUNX3 Molecular Aberrations. The survival analysis encompassed all the analysed samples irrespective of tumour grade, thus eliminating obscure boundary when separating between grade II and III as well as grade III and IV astrocytomas. All astrocytoma patients were stratified (n=136) in two groups: having tumours with methylated *RUNX3* gene promoter and with unmethylated promoter. Among 136 patients 37 were alive at the end of the study (September 2018) and in statistical analysis were censored. The log-rank test showed that *RUNX3* gene methylation was strongly related to patient survival time (Log-rank test, χ^2=44.68, df=1, p<0.001; Figure 1). Similar results were obtained when analysing high grade tumours (grades III-IV) only (Log-rank test, χ^2=8.74, df=1, p=0.003, n=78; data not shown. More specifically, the patient median survival time in the group with unmethylated gene promoter was 66.17 months [95% CI 34.76-97.58], whereas the median survival time of those with methylated promoter was only 12.35 months [95% CI 8.69-16.02], Figure 1(b). The cumulative 3-year survival rate was 61.95% in RUNX3 unmethylated group, whereas in methylated gene group survival rate was only 11.62%.

Next, we analysed RUNX3 protein expression effect on glioma patient survival. For the purpose we stratified RUNX3 protein expression data into two expression groups based on ROC curve analysis (selecting 2-year overall survival as a state variable). The value of 0.54 of Relative Runx3/ACTB protein expression was selected as cut-off point. Among the 72 glioma specimen, low RUNX3 protein level was assigned for 48.6% (35 of 72), and 51.4% (37 of 72) of samples was assigned for high RUNX3 protein level group, Table 1. Among 72 patients

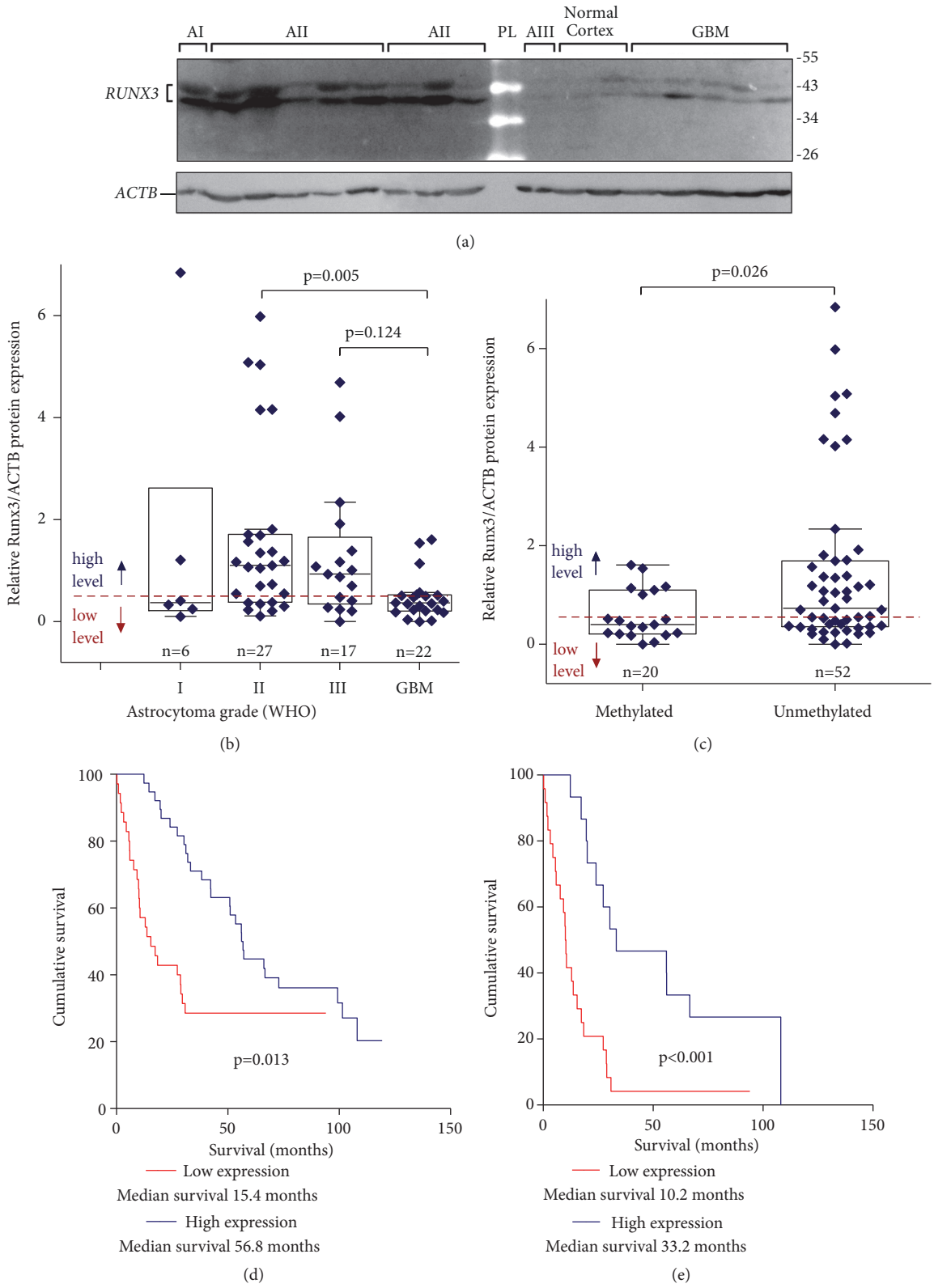

Figure 2: (a) Representative Western blot result of RUNX3 protein expression in astrocytomas. AI-AIII: astrocytoma malignancy grades I-III, respectively; GBM: glioblastoma. Two isoforms of RUNX3 were identified in all the specimens that is consistent with what has been described in the literature [6]. (b) RUNX3 protein expression levels in different astrocytoma grade. Protein expression was significantly downregulated in glioblastomas (GBM) as compared to grade II astrocytomas ($p<0.005$, Kruskal-Wallis test) and a tendency as compared to grade III astrocytomas ($p=0.124$, Kruskal-Wallis test). (c) Relative RUNX3 protein expression stratified by promoter methylation groups. Significant association between RUNX3 gene methylation and protein expression was found ($p=0.026$, Kruskal-Wallis test). (d) Kaplan-Meier curves for survival of all astrocytoma patients (n=72) stratified in two groups (low; high) according to protein expression revealed significant better survival rates for patient with high RUNX3 protein level (Log-rank test, $\chi 2=6.11$, df=1, $p=0.013$). (e) Kaplan-Meier survival curves of high malignancy grade (III-IV) astrocytoma patients only (n=39) (Log-rank test, $\chi 2=13.74$, df=1, $p<0.001$).

21 were alive at the end of the study and were censored in the analysis. Survival analysis showed significantly higher survival rates of astrocytoma patients having tumours with high RUNX3 protein level when analysing whole sample set (Log-rank test, χ^2=6.11, df=1, p=0.013, Figure 2(d)) and even stronger connection when analysing malignant astrocytomas (grades III-IV) only (Log-rank test, χ^2=13.74, df=1, p<0.001, Figure 2(e)). The median survival of patients with high RUNX3 protein expression reached 56.77 months [95% CI 41.81-71.74] while patient median survival with low RUNX3 levels reached only 15.37 months [95% CI 6.24-24.52], Figure 2(d).

To evaluate the independence of analysed molecular prognostic factors such as RUNX3 methylation and RUNX3 protein expression, the multivariate Cox regression analysis applying *Backward Conditional* method was performed combining patient age as a clinical covariate (patient gender was not associated with death risk, p>0.05). Multivariate analysis revealed that RUNX3 protein level and patient age but not RUNX3 methylation (p>0.05) were an independent indicators increasing the risk of patient death. Low RUNX3 protein level increases event risk by 1,33-fold (95%CI 1.61-1.08; p=0.004) while older patient age at disease appearance increases event risk by 1.07-fold (95%CI 1.04-1.09; p<0.001), Table 2.

3.5. Reexpression of RUNX3 in Glioblastoma U87-MG Cell Line Decreased Cell Viability. Since protein expression of RUNX3 is decreased in glioblastomas compared to lower-grade astrocytoma tumours we performed U87-MG cells proliferation analysis after RUNX3 reexpression. U87-MG cells were transfected with pcDNA3-RUNX3, pcDNA4TO-GFP, and empty pcDNA3 (control) plasmids. Transfection efficiency varied between 60 and 75%. 24-hours after transfection cells were subjected to cell proliferation, MTT assay. WB analysis showed that native U87-MG RUNX3 protein expression is barely detectable while RUNX3 promoter is fully methylated, Figures 3(a) and 3(b). Reexpression of RUNX3 in U87-MG cells significantly decreased cells viability as compared to control cells transfected with empty plasmid or plasmid with GFP (p<0.001, when 100 ng of plasmid used), Figure 3(c). Cell viability decreased to 40.2% using 100 ng of RUNX3 construct for transfection compared to nontransfected cell control (NTC), Figure 3(c).

4. Discussion

In present analysis we demonstrated that RUNX3 is starting to be deregulated from very onset of gliomagenesis at both epigenetic (methylation) and functional (protein expression) levels and these changes are tightly associated with patient age and survival as well as tumour pathological grade. Functional assessment revealed putative-oncosupressive acting of RUNX3 in astrocytomas since gene is methylated and silenced in GBM cell lines and restoration of RUNX3 expression weighty reduced tumour cell viability.

RUNX3 was first suggested to be a tumour suppressor in gastric cancer. The gastric mucosa of RUNX3 knock-out mouse exhibited hyperplasia due to stimulated proliferation and suppressed apoptosis of epithelial cells which showed resistance to the growth-inhibitory and apoptosis inducing action of TGF-β [11]. Since the discovery of the potential role of RUNX3 in gastric cancer, *RUNX3* has been found to be inactivated in various cancers, including colorectal, liver, lung, prostate, and breast as well as gliomas [12–15, 17, 18, 21, 33–35]. Few cancer epigenetic studies have suggested that RUNX3 downregulation could be the result of hypermethylation of the promoter of RUNX3 [15, 19, 20]. Mueller with colleagues were first to show that RUNX3 is hypermethylated in glioblastoma cell lines and primary glioma tumour tissue cells compared to normal human brain tissue. Moreover, they suggested that RUNX3 expression is regulated by promoter methylation since increased mRNA levels of RUNX3 following 5-aza-dC treatment were found in glioma U87 cells [15]. Nevertheless, low sample numbers and the lack of information about RUNX3 alterations in lower-grade gliomas decided the appearance of wider RUNX3 analysis in sample number-rich glioma studies. Mei and colleagues showed that RUNX3 protein expression is decreased in benign and malignant brain tumours as compared to normal or adjacent tissue. Nevertheless they did not found any associations between RUNX3 protein level and patient clinicopathological data [35]. In present study we found tight RUNX3 association with astrocytoma tumour grade as well as patient age and survival. We found that RUNX3 protein expression is reduced in glioblastomas as compared to grade II-III tumours and this reduction is associated with patient overall survival. Since Mei and colleagues combined very diverse origin brain tumours encompassing astrocytomas, ependymomas, and oligodendrogliomas in one analysis, they might have vanished very specific features of tumours of a particular origin. Current analysis revealed that grade I pilocytic astrocytomas (PA) showed different RUNX3 expression profile from other low grade tumours indicating possible distinct molecular features that operate at the onset of PA, since these tumours are the most common benign neoplasms in children or young adults [36]. Nevertheless, the result from both studies indicates that RUNX3 is important player from very beginning of tumorigenesis. Majchrzak-Celińska and colleagues showed RUNX3 promoter methylation changes in different grade gliomas where methylation frequency was consistently increasing along with glioma grade, 0%; 22%; 52%; 62.5%, grades I; II; III; IV, respectively. They also showed significant association between RUNX3 methylation and patients age as well as tumour grade [23]. Very similar data was showed in present study. Besides RUNX3 methylation association with tumour grade and patient age we found very strong association between RUNX3 methylation and patient survival what indicates prognostic importance of RUNX3. Similarly to our results, Saraiva-Esperon and colleagues showed that RUNX3 promoter methylation was associated with poorer patient survival [22]. Another study of RUNX3 methylation encompassing relatively small numbers of specimens (grades II-III-IV, 3-3-12 samples, respectively) failed to find any weighty tumour grade and methylation association; nevertheless they showed significant link between RUNX3 methylation and mRNA expression [37]. Functional study of RUNX3 revealed that reexpression of RUNX3 weighty

Table 2: Multivariate Cox regression analysis applying Backward Conditional method.

Step	Factor	Multivariate analysis		
		HR	95% CI	*P*-value
1	Patient Age	1.058	1.034-1.083	<0.001
	Runx3 methylation	1.579	0.755-3.3	0.225
	Runx3 protein level	0.777	0.633-0.953	0.015
2	Patient Age	1.065	1.044-1.087	<0.001
	Runx3 protein level	0.752	0.62-0.913	0.004

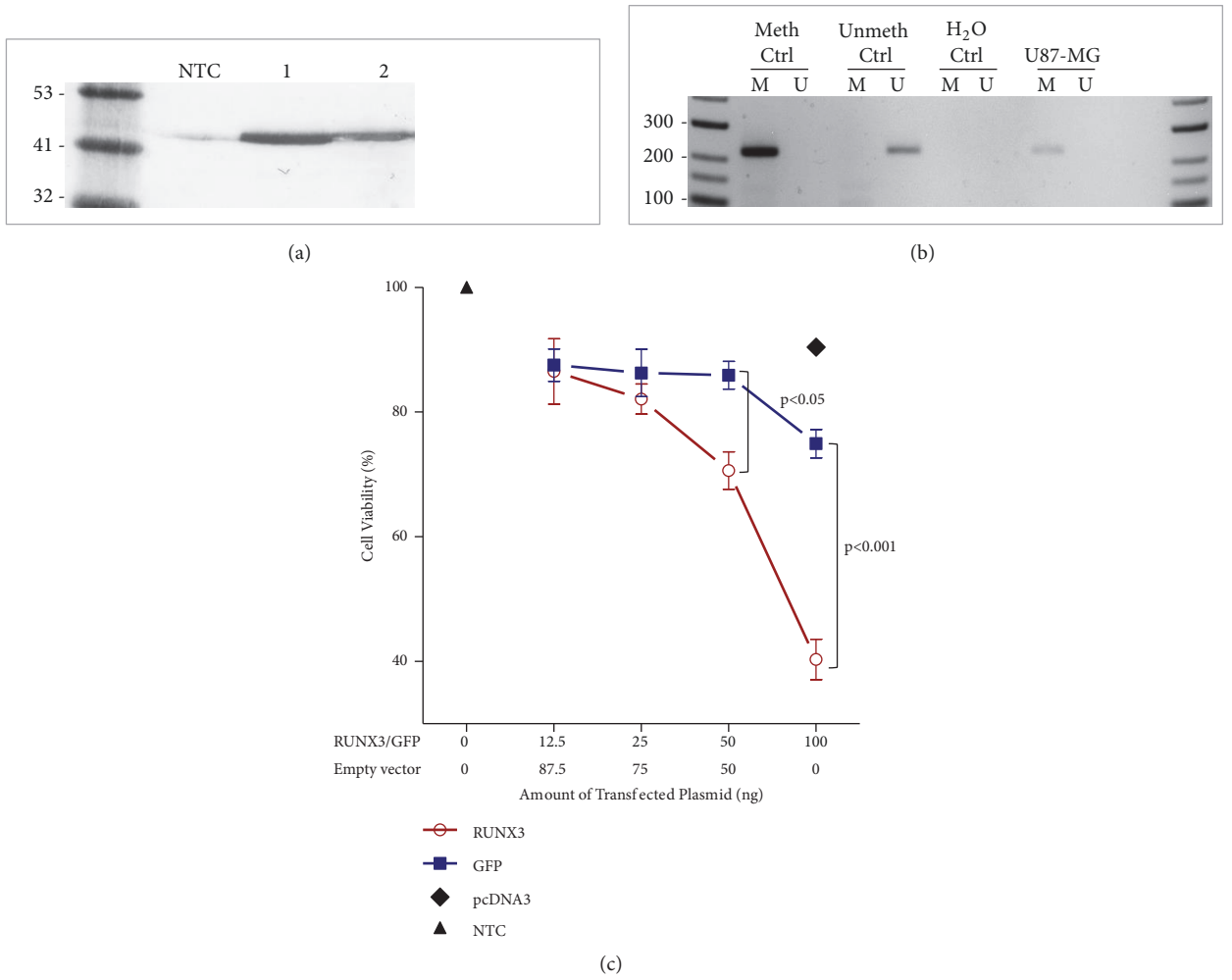

Figure 3: (a) WB of RUNX3 protein expression after U87-MG cells transfection with pcDNA3-RUNX3 construct. NTC: nontransfected cells lysate; 1: cells transfected with 100 ng of pcDNA3-RUNX3 vector; 2: cells transfected with 50 ng of pcDNA3-RUNX3 vector. Equal amount of total protein extract (60 μg) was loaded per each gel lane. The same amount of cell (b) RUNX3 promoter methylation status in U87-MG cells. (c) Results from glioblastoma U87-MG cells viability assay applying MTT test after 24 h of 100 ng of DNA transfection. RUNX3: RUNX3 gene in pcDNA3 expression vector (pcDNA3-RUNX3); GFP: green fluorescing protein in pcDNA4TO expression vector (pcDNA4TO-GFP); pcDNA3: empty (control) vector; NTC: nontransfected cell control. Overexpression of RUNX3 significantly decreased U87-MG cell viability starting from 50 ng of vector used as compared to the cells transfected with GFP vector. Moreover even bigger effect of decreased cell viability was obtained when 100 ng of RUNX3 was transfected.

reduces U87-MG glioblastoma cell viability indicating oncosupressive features of RUNX3. Similar data was shown by Mei et al. when restoration of RUNX3 significantly inhibited U87 and U251 cell invasion and migration abilities [35].

In conclusion, our study revealed that RUNX3 gene methylation frequency is increasing during gliomagenesis, while RUNX3 protein expression is significantly decreasing along with astrocytic origin tumours of different grade and such alterations are tightly associated with patient

clinicopathological features. Functional assessment revealed putative-oncosupressive acting of RUNX3 in astrocytomas what is in the line with expression data from astrocytoma specimen's analysis. Significant impact of RUNX3 on patient survival as well as other clinicopathological features indicates gene as potential prognostic marker in astrocytomas.

Data Availability

The data used to support the findings of this study are available from the corresponding author upon request.

Disclosure

The part of the data in this article was presented in Danube Scientific Conference on Epigenetics, Budapest, 2014, as a pilot study data of RUNX3 molecular changes during gliomagenesis.

Conflicts of Interest

The authors declare that there are no conflicts of interest regarding the publication of this paper.

Acknowledgments

We kindly thank Evaldas Simanavicius for technical help. This research was funded by a grant [no. LIG-11/2012] from the Research Council of Lithuania.

References

[1] D. N. Louis, H. Ohgaki, O. D. Wiestler et al., "The 2007 WHO classification of tumours of the central nervous system," *Acta Neuropathologica*, vol. 114, no. 2, pp. 97–109, 2007.

[2] C. Burkhard, P. Di Patre, D. Schüler et al., "A population-based study of the incidence and survival rates in patients with pilocytic astrocytoma," *Journal of Neurosurgery*, vol. 98, no. 6, pp. 1170–1174, 2003.

[3] J. Laffaire, S. Everhard, A. Idbaih et al., "Methylation profiling identifies 2 groups of gliomas according to their tumorigenesis," *Neuro-Oncology*, vol. 13, no. 1, pp. 84–98, 2010.

[4] R. Martinez, J. I. Martin-Subero, V. Rohde et al., "A microarray-based DNA methylation study of glioblastoma multiforme," *Epigenetics*, vol. 4, no. 4, pp. 255–264, 2009.

[5] H. Noushmehr, D. J. Weisenberger, K. Diefes et al., "Identification of a CpG island methylator phenotype that defines a distinct subgroup of glioma," *Cancer Cell*, vol. 17, no. 5, pp. 510–522, 2010.

[6] S. Moon, J. Y. Bae, H. Son et al., "RUNX3 confers sensitivity to pheophorbide a-photodynamic therapy in human oral squamous cell carcinoma cell lines," *Lasers in Medical Science*, vol. 30, no. 2, pp. 499–507, 2015.

[7] Y. Ito and K. Miyazono, "RUNX transcription factors as key targets of TGF-beta superfamily signaling," *Current Opinion in Genetics & Development*, vol. 13, no. 1, pp. 43–47, 2003.

[8] M. Wu, C. Li, G. Zhu et al., "Deletion of core-binding factor β (Cbfβ) in mesenchymal progenitor cells provides new insights into Cbfβ/Runxs complex function in cartilage and bone development," *Bone*, vol. 65, pp. 49–59, 2014.

[9] A. Illendula, J. Gilmour, J. Grembecka et al., "Small molecule inhibitor of CBFβ-RUNX binding for runx transcription factor driven cancers," *EBioMedicine*, vol. 8, pp. 117–131, 2016.

[10] M. C. Whittle and S. R. Hingorani, "Runx3 and cell fate decisions in pancreas cancer," in *Advances in Experimental Medicine and Biology*, vol. 962, pp. 333–352, 2017.

[11] Q.-L. Li, K. Ito, C. Sakakura et al., "Causal relationship between the loss of *RUNX3* expression and gastric cancer," *Cell*, vol. 109, no. 1, pp. 113–124, 2002.

[12] A. Goel, C. N. Arnold, P. Tassone et al., "Epigenetic inactivation ofRUNX3 in microsatellite unstable sporadic colon cancers," *International Journal of Cancer*, vol. 112, no. 5, pp. 754–759, 2004.

[13] K. Lee, Y. Lee, J. Lee et al., "Runx3 is required for the differentiation of lung epithelial cells and suppression of lung cancer," *Oncogene*, vol. 29, no. 23, pp. 3349–3361, 2010.

[14] B. Huang, Z. Qu, C. W. Ong et al., "RUNX3 acts as a tumor suppressor in breast cancer by targeting estrogen receptor α," *Oncogene*, vol. 31, no. 4, pp. 527–534, 2012.

[15] W. Mueller, C. L. Nutt, M. Ehrich et al., "Downregulation of RUNX3 and TES by hypermethylation in glioblastoma," *Oncogene*, vol. 26, no. 4, pp. 583–593, 2007.

[16] F. Chen, J. Bai, W. Li et al., "RUNX3 suppresses migration, invasion and angiogenesis of human renal cell carcinoma," *PLoS ONE*, vol. 8, no. 2, Article ID e56241, 2013.

[17] T. Mori, S. Nomoto, K. Koshikawa et al., "Decreased expression and frequent allelic inactivation of the RUNX3 gene at 1p36 in human hepatocellular carcinoma," *Liver International*, vol. 25, no. 2, pp. 380–388, 2005.

[18] Z. Jin, Y. Han, and X. Han, "Loss of RUNX3 expression may contribute to poor prognosis in patients with chondrosarcoma," *Journal of Molecular Histology*, vol. 44, no. 6, pp. 645–652, 2013.

[19] B. Kurklu, R. H. Whitehead, E. K. Ong et al., "Lineage-specific RUNX3 hypomethylation marks the preneoplastic immune component of gastric cancer," *Oncogene*, vol. 34, no. 22, pp. 2856–2866, 2015.

[20] W. Kim, E. Kim, P. Jeong et al., "*RUNX3* inactivation by point mutations and aberrant DNA methylation in bladder tumors," *Cancer Research*, vol. 65, no. 20, pp. 9347–9354, 2005.

[21] M. M. Subramaniam, J. Y. Chan, K. G. Yeoh, T. Quek, K. Ito, and M. Salto-Tellez, "Molecular pathology of RUNX3 in human carcinogenesis," *Biochimica et Biophysica Acta (BBA) - Reviews on Cancer*, vol. 1796, no. 2, pp. 315–331, 2009.

[22] U. Saraiva-Esperón, A. Ruibal, and M. Herranz, "The contrasting epigenetic role of RUNX3 when compared with that of MGMT and TIMP3 in glioblastoma multiforme clinical outcomes," *Journal of the Neurological Sciences*, vol. 347, no. 1-2, pp. 325–331, 2014.

[23] A. Majchrzak-Celińska, J. Paluszczak, M. Szalata et al., "The methylation of a panel of genes differentiates low-grade from high-grade gliomas," *Tumor Biology*, vol. 36, no. 5, pp. 3831–3841, 2015.

[24] S. H. Barghout, N. Zepeda, K. Vincent et al., "RUNX3 contributes to carboplatin resistance in epithelial ovarian cancer cells," *Gynecologic Oncology*, vol. 138, no. 3, pp. 647–655, 2015.

[25] T. Tsunematsu, Y. Kudo, S. Iizuka et al., "RUNX3 has an oncogenic role in head and neck cancer," *PLoS ONE*, vol. 4, no. 6, Article ID e5892, 2009.

[26] M. Whittle, K. Izeradjene, P. Rani et al., "RUNX3 controls a metastatic switch in pancreatic ductal adenocarcinoma," *Cell*, vol. 161, no. 6, pp. 1345–1360, 2015.

[27] M. Salto-Tellez, B. K. Peh, K. Ito et al., "RUNX3 protein is overexpressed in human basal cell carcinomas," *Oncogene*, vol. 25, no. 58, pp. 7646–7649, 2006.

[28] C. K. Cheng, L. Li, S. H. Cheng et al., "Transcriptional repression of the RUNX3/AML2 gene by the t(8;21) and inv(16) fusion proteins in acute myeloid leukemia," *Blood*, vol. 112, no. 8, pp. 3391–3402, 2008.

[29] F. M Robertson, K. Chu, S. V. Fernandez et al., "Genomic profiling of pre-clinical models of inflammatory breast cancer identifies a signature of epithelial plasticity and suppression of TGFβ signaling," *Journal of Clinical & Experimental Pathology*, vol. 02, no. 05, 2012.

[30] R. Carvalho, A. N. Milne, M. Polak, W. E. Corver, G. J. Offerhaus, and M. A. Weterman, "Exclusion of RUNX3 as a tumour-suppressor gene in early-onset gastric carcinomas," *Oncogene*, vol. 24, no. 56, pp. 8252–8258, 2005.

[31] J. Wen, T. Zheng, K. Hu, C. Zhu, L. Guo, and G. Ye, "Promoter methylation of tumor-related genes as a potential biomarker using blood samples for gastric cancer detection," *Oncotarget*, vol. 8, no. 44, pp. 77783–77793, 2017.

[32] G. Steponaitis, A. Kazlauskas, D. Skiriute, P. Vaitkiene, K. Skauminas, and A. Tamasauskas, "Significance of amphiregulin (AREG) for the outcome of low and high grade astrocytoma patients," *Journal of Cancer*, vol. 10, no. 6, pp. 1479–1488, 2019.

[33] G. H. Kang, S. Lee, H. J. Lee, and K. S. Hwang, "Aberrant CpG island hypermethylation of multiple genes in prostate cancer and prostatic intraepithelial neoplasia," *The Journal of Pathology*, vol. 202, no. 2, pp. 233–240, 2004.

[34] Y. Jiang, D. Tong, G. Lou, Y. Zhang, and J. Geng, "Expression of RUNX3 gene, methylation status and clinicopathological significance in breast cancer and breast cancer cell lines," *Pathobiology*, vol. 75, no. 4, pp. 244–251, 2008.

[35] P. Mei, J. Bai, H. Liu et al., "RUNX3 expression is lost in glioma and its restoration causes drastic suppression of tumor invasion and migration," *Journal of Cancer Research and Clinical Oncology*, vol. 137, no. 12, pp. 1823–1830, 2011.

[36] K. Kikuchi, A. Hiwatashi, O. Togao et al., "Usefulness of perfusion- and diffusion-weighted imaging to differentiate between pilocytic astrocytomas and high-grade gliomas: a multicenter study in Japan," *Neuroradiology*, vol. 60, no. 4, pp. 391–401, 2018.

[37] C. B. Avci, Y. Dodurga, S. Y. Susluer et al., "Promoter hypermethylation-mediated down-regulation of RUNX3 gene in human brain tumors," *Irish Journal of Medical Science*, vol. 183, no. 2, pp. 259–264, 2014.

Hindawi
Journal of Oncology
Volume 2019, Article ID 1740763, 16 pages
https://doi.org/10.1155/2019/1740763

Review Article

Molecular and Clinical Insights into the Invasive Capacity of Glioblastoma Cells

Carlos Velásquez,[1,2] **Sheila Mansouri**,[3] **Carla Mora**,[1] **Farshad Nassiri**,[2,3] **Suganth Suppiah**,[2,3] **Juan Martino**,[1] **Gelareh Zadeh**,[2,3] **and José L. Fernández-Luna**[4]

[1] *Department of Neurological Surgery and Spine Unit, Hospital Universitario Marqués de Valdecilla and Instituto de Investigación Marqués de Valdecilla (IDIVAL), Santander, Spain*
[2] *Division of Neurosurgery, Toronto Western Hospital, University Health Network, University of Toronto, Toronto, Canada*
[3] *MacFeeters-Hamilton Center for Neuro-Oncology Research, Princess Margaret Cancer Centre, Toronto, Canada*
[4] *Genetics Unit, Hospital Universitario Marqués de Valdecilla and Instituto de Investigación Marqués de Valdecilla (IDIVAL), Santander, Spain*

Correspondence should be addressed to Carlos Velásquez; carvelhn@gmail.com and José L. Fernández-Luna; joseluis.fernandezl@scsalud.es

Received 18 March 2019; Revised 1 July 2019; Accepted 7 July 2019; Published 29 July 2019

Academic Editor: Claudio Festuccia

The invasive capacity of GBM is one of the key tumoral features associated with treatment resistance, recurrence, and poor overall survival. The molecular machinery underlying GBM invasiveness comprises an intricate network of signaling pathways and interactions with the extracellular matrix and host cells. Among them, PI3k/Akt, Wnt, Hedgehog, and NFkB play a crucial role in the cellular processes related to invasion. A better understanding of these pathways could potentially help in developing new therapeutic approaches with better outcomes. Nevertheless, despite significant advances made over the last decade on these molecular and cellular mechanisms, they have not been translated into the clinical practice. Moreover, targeting the infiltrative tumor and its significance regarding outcome is still a major clinical challenge. For instance, the pre- and intraoperative methods used to identify the infiltrative tumor are limited when trying to accurately define the tumor boundaries and the burden of tumor cells in the infiltrated parenchyma. Besides, the impact of treating the infiltrative tumor remains unclear. Here we aim to highlight the molecular and clinical hallmarks of invasion in GBM.

1. Introduction

In adults, glioblastoma (GBM) is the most common primary tumor in the central nervous system, with an incidence of 4.5 cases per 100,000 inhabitants. The median survival remains 14 months despite highly aggressive standard treatment protocols [1]. One of the key hallmarks of GBM hindering effective therapy is the diffuse invasiveness of the tumor cells through the normal parenchyma, causing tumor recurrence in close proximity or distant from the original tumor site. This feature appears to be independent of tumor grade, as both higher and lower grade gliomas tend to recur as a result of invasion of tumor cells into surrounding brain tissue [2]. The mechanism of glioma cell invasion involves both biochemical and biophysical processes that regulate cell shape and its movement across the intercellular space, concurrent with rearrangement of the extracellular matrix (ECM). In the recent years several molecular pathways have been associated with glioma invasion and represent potential therapeutic targets and biomarkers for prognosis. Taking this into account, it is mandatory for oncologists, neurosurgeons, neurologists and neuroscientists to be familiar with the most important signaling processes underlying glioma invasion and understand the clinical manifestations of GBM invasion for appropriate treatment planning. Herein, we review key cellular pathways and processes that regulate glioma cell invasion and describe their relevance as potential therapeutic targets for management of gliomas.

2. The Molecular Hallmarks of Invasion in GBM

2.1. Adhesion Molecules. The first stage of glioma cell invasion is detachment from the surrounding tumor tissue, a process that involves cell surface adhesion molecules such as neuronal cell adhesion molecule (NCAM) and cadherins as key players in this process. It had been demonstrated that cadherin instability leads to glioma cell migration [3] and NCAMs modify the ECM by downregulating the expression of matrix metalloproteinases that degrade cadherins and, thereby, hinder tumor cell motility [4]. Furthermore, the expression of NCAMs is inversely related to glioma grade, which is in agreement with data showing that loss of this molecule enhances tumor cell migration [5]. Recent transcriptomic and proteomic analyses have reproduced these findings and have identified a new splice variant of NCAM1 with potential implications in cell signaling [6].

In addition to NCAMs, intercellular adhesion molecule-1 (ICAM1), a member of the immunoglobulin family of genes and expressed in several cell types, has recently been shown to contribute to glioma cell invasion [7]. ICAM1 is involved in several processes, including inflammatory cell movement, effector leukocyte activity, antigen-presenting cells adhesion to T lymphocytes, and signal transduction pathways through outside-in signaling processes. Upon induction of inflammation, leukocytes interact with ICAM1 on the endothelial cells, which allows them to cross the barrier vessel wall [8]. It has been shown that thalidomide can suppress ICAM1 expression and inhibit invasion mediated by ICAM1 in lung cancer [9]. In glioma, it was shown that radiation increased ICAM1 expression, thereby, promoting migration and invasion of the tumor cells [10]. Lin et al. reported that ICAM1 enhances the invasiveness of GBM cells into the healthy brain tissue and may, therefore, serve as a marker of invasion in GBM [11].

Integrins (ITGs) are another key component of the interface between tumor cells and other cells in the microenvironment and function as receptors that regulate cell adhesion to ECM proteins or cell surface proteins on other stromal cells [12]. They also play a central role in linking extracellular contacts with the intracellular cytoskeleton through two different signaling mechanisms; ITGs cluster in the membrane upon extracellular ligands binding and transduce intracellular signals through their cytoplasmic domain (β subunit) by activation of kinases such as Focal Adhesion Kinase (FAK), Integrin-Linked Kinase (ILK) and Rho-GTPases. Through this mechanism, ITGs then activate pathways leading expression of genes that modulate cell proliferation, survival, differentiation, and migration (outside-in signaling)[12]. It is also possible for cytoplasmic proteins to modulate the extracellular affinity of ITGs for their ligands (inside-out signaling) and contribute to cell migration and invasion [13].

ITGs are expressed by various cell types in the tumor microenvironment including endothelial cells, immune cells, and pericytes and promote tumorigenesis. In particular, ITGs regulate invasion and metastasis by providing the traction necessary for cell migration [14]. They also modulate the expression of proteases that play a role in remodelling the ECM. Involvement of several ITGs in epithelial to mesenchymal transition (EMT) has been described. For example, $\alpha v\beta 1$ ITG was shown to mediate an EMT-like program in GBM cells [15]. In addition, $\alpha v\beta 3/\alpha v\beta 5$ was shown to promote GBM cell migration and invasion by enhancing the adhesion of tumor cells to components of the ECM via fibronectin, vitronectin, osteopontin, or periostin [16–18] and activation of intracellular signaling pathways such as FAK, Rho-GTPases, Shc/MAP-Kinases, and Src Family Kinases [14, 19, 20]. $\alpha v\beta 3$ also enhances GBM invasion through the activation of matrix metalloproteinase 2 (MMP2) at the plasma membrane, which is thought to degrade components of the ECM and enhance cell motility [14]. Finally, inhibition of $\alpha v\beta 3/\alpha v\beta 5$ in mouse models reduces GBM cell migration and invasion [21]. Another study by Delamarre et al. has also shown that $\alpha 6\beta 1$ is associated with invasive phenotype in U87 GBM cell line *in vitro* and *in vivo* [22]. Therefore, targeting specific ITGs in GBM could inhibit tumor invasion and aggressive features.

2.2. ECM Composition and Invasion. ECM composition plays a critical role in the invasion process and the tumor-associated ECM is intrinsically different from the ECM within the normal parenchyma [23, 24]. For instance, hyaluronic acid (HA) enrichment in tumor microenvironment promotes cell invasion through positive feedback regulation of NFκB that may result from ionizing radiation or hypoxia [25–27]. On the other hand, it has been shown that a glycosylated chondroitin sulfate proteoglycans- (CSPGs-) enriched ECM is associated with non-invasive lesions. Upregulation of LAR-CSPG binding complexes results in strong binding of the tumor cells to the ECM, preventing cell invasion, and high levels of CSPGs elicit an astrocyte/microglia-mediated anti-invasion response. On the contrary, diffusely infiltrating tumor ECM lacks glycosylated CSPGs [28]. Interestingly, recent animal models suggest that temozolomide/dexamethasone combination therapy affects proteoglycan levels in the parenchymal ECM, potentially resulting in a proinvasive microenvironment [29].

Glioma cells also degrade the surrounding ECM to favor their migration. Proteases, among others, are the enzymes that tumor cells use to perform this activity. Matrix metalloproteinases, such as MMP-2 and MMP-9, are related to the tumor grade and the invasive capacity of glioma [30]. Other molecules involved in the degradation of the ECM are cysteine proteases, A disintegrin and metalloproteinases (ADAMs), and urokinase-type plasminogen activator (uPA). However, since low-grade gliomas with normal proteases levels are capable of invading the surrounding tissue, the role of proteases in the invasion of gliomas remains uncertain [31]. Nevertheless, in vitro assays show that a high migration capacity is associated with expression of MMP-2, MMP-9, uPA, and tissue plasminogen activator (tPA)[32].

2.3. Epithelial to Mesenchymal Transition. Epithelial to mesenchymal transition (EMT) is a biochemical process through which the cytoskeleton of polarized epithelial cells is remodelled, and they shift to a nonpolarized mesenchymal phenotype. Extensive evidence suggests that EMT is an essential process for tissue remodelling, wound repair and cancer

metastasis. While in an epithelial state cells are held tightly and are anchored to the basement membrane, mesenchymal cells are mainly spindle-shaped and are loosely attached to the ECM through interaction with focal adhesion molecules. Specific transcription factors such as Snail and Slug, the zinc-finger E-box-binding homeobox (ZEB)1/2, and Twist1/2 are considered the main regulators of the EMT process, as they regulate transcription of genes, including N-cadherin, vimentin, and fibronectin that are typically expressed in mesenchymal cells [33]. These factors simultaneously suppress the expression of epithelial markers such as E-cadherin, claudins, occludins, and cytokeratins. Loss of E-cadherin, in turn, results in Wnt signaling and accumulation of β-catenin, which leads to increased transcription of genes that promote cell proliferation and invasion [34]. In GBM cell lines, it was shown that silencing SNAIL reduced invasion, migration and proliferation [35], and expression level of Slug correlated with tumor grade [36]. Additionally, ZEB1/ZEB2 expression correlated with invasiveness and decreased survival of GBM patients [37]. Furthermore, Twist1 and Twist 2, which typically regulate stemness, were found to be associated with the invasive properties of GBM cell lines as they regulate the expression of key EMT-regulating genes such as MMP2, Slug, and HGF [38].

It is important to note that the role of cadherin switch as a hallmark of EMT in carcinomas is not well established in GBM, as these tumors are not epithelial in nature. E-cadherin is expressed at very low levels in neural tissues and is found only in a small proportion of aggressive GBM cells. On the other hand, N-cadherin is absent in epithelial tumors before the initiation of EMT, while it is highly expressed in astrocytes and regulates cell polarity and migration, resulting in a less regulated cell movement [37]. It was also shown that expression of N-cadherin negatively correlated with GBM tumor cell invasiveness, and its overexpression *in vitro* reduced cell migration and restored cell polarity [3, 39]. In addition, several studies showed that radiation treatment or anti-angiogenic therapy of primary GBMs resulted in transition to a mesenchymal phenotype in the recurrent tumors [40, 41]. In fact, radio-resistant glioma cells display upregulated expression of genes involved in the EMT pathway [40, 42]. This is further supported by an *in vivo* study in xenograft mouse models of GBM, demonstrating that the gene expression profile of proneural GBM shifted towards a mesenchymal signature upon radiation treatment [41].

In addition to the master regulators, several cytokines play a role in EMT. In particular, Tumor Necrosis Factor-α (TNFα) activation through NFκB is essential for EMT induction [43]. In addition, interleukins such as IL6 contribute to stimulation of EMT. Other signals that regulate the EMT and originate from the tumor include growth factors including HGF, EGF, and PDGF and these are thought to activate EMT-related transcription factors [44–46].

2.4. Cytoskeletal Remodelling and Cell Motility. Cytoskeletal remodelling is a key process in the formation of invadopodia and lamellipodia that are necessary for tumor cell motility [47]. Glioma cells typically show a mesenchymal pattern of migration and passage through extracellular spaces that are smaller than their own nuclei. Mechanistically, glioma cells become polarized and fibroblast-like, with characteristic leading and trailing edges on the opposite ends of the cell. This leads to the outward extension of the cell membrane at the leading edge (pseudopod), which is in contact with the ECM through ITGs localized on the cell membrane. ITGs interact with adaptor molecules and signaling proteins, activating signals inside the cell (phosphorylation/dephosphorylation via focal adhesion kinase, FAK) [48]. Subsequently, membrane-type MMPs are recruited at the focal contacts to degrade and restructure the ECM via the production of soluble matrix metalloproteases, including MMP-2 and MMP-9. Finally, the cells contract by the acto-myosin complex engagement, resulting in focal contact disassembly, integrin recycling, detachment of the trailing edge, and, ultimately, cell invasion [49, 50].

Other important factors that regulate acto-myosin complex engagement during EMT include RHO GTPases, among which RHOA promotes formation of actin stress fibres. RAC1 and CDC42, on the other hand, regulate the formation of lamellipodia and filopodia. Following the activation of GTPases, the RHO-associated kinase (ROCK) cooperates with the formin diaphanous 1 (DIA1) to enhance actin polymerization and also induces the phosphorylation of myosin light chain to promote acto-myosin contraction and activation of LIM kinase (LIMK)[51]. Once activated by RAC1 or CDC42, the p21-activated kinase 1 (PAK1) activates target proteins that are involved in cell spreading and motility [52]. In glioma cells, RHO GTPases including RHOA and RAC regulate cytoskeletal rearrangements resulting in ameboid and mesenchymal cell motility and have been shown to promote migration and growth of glioma cells *in vitro* and *ex vivo* [53]. Furthermore, it has been described that transmembrane ion cotransporters induce cell migration and EMT through downstream activation of RHOA and RAC pathways [54]. Besides, several pathways including Wnt, PI3K/Akt, and ODZ1 have been shown to be associated with RhoA to regulate cytoskeletal changes that allows migration [55–57].

It is important to note that glioma cell motility is not only influenced by the biochemical processes associated with the ECM but also by biophysical properties such as cell density and the rigidity and geometry of the ECM [58]. Ulrich et al. demonstrated that increased rigidity of the ECM in gliomas results in formation of stress fibres and focal adhesions that enable more rapid migration of the cells [59]. Another component of the tumor microenvironment that plays a role in cell invasion is blood vessels. Notably, glioma cells do not intravasate the vessels but instead associate with the vascular walls and migrate along the vessels. It has been shown that bradykinin is secreted by the brain endothelial cells and functions as a chemotactic signal for glioma cells through binding to its receptor (BR-2) on the glioma cell surface resulting in subsequent intracellular Ca2+ oscillations [60]. Changes in Ca2+ levels in turn, regulate cell motility through acto-myosin-mediated contraction, regulation of tubulin dynamics, and controlling the activation of focal adhesion kinases that mediate cell adhesion to substrates in the ECM [61]. Movement of glioma cells along the vascular walls in turn alters the organization of the brain vasculature where

astrocyte endfeet are closely associated with endothelial cells through anchorage with basement membrane [62]. Migration of glioma cells leads to displacement of astrocytes endfeet via degradation of the basement membrane around the blood vessel environment. This results in disruption and breakdown of the blood-brain barrier (BBB) and alterations in blood vessel diameter [62]. This enables glioma cells to gain access to oxygen and nutrients from the bloodstream. In addition to the cytoskeletal rearrangement, regulation of cell volume by voltage-gated chloride and potassium channels is another mechanism that regulates glioma cell migration [63].

2.5. Cross-Talk with Host Cells and Immune Modulation. Tumor cells integrate with supportive stromal cells that are components of the tumor microenvironment. Stromal cells secrete growth factors and molecules that have the capacity to alter the milieu in which neoplastic cells proliferate. In fact, the microenvironment has been demonstrated to play key regulatory roles in response to therapy and tumor progression [64]. It has recently been shown that astrocytic and oligodendrogliotic gliomas share similar glial lineages and that difference in bulk expression profiles between these glial tumors is primarily driven by composition of the tumor microenvironment [65]. Alterations in local immune and vascular networks have been shown to facilitate tumor growth in GBM thereby highlighting the exciting opportunity for immunomodulatory therapies.

Nearly a third of GBM mass is composed of glioma-associated macrophages (GAMs). Due to the breakdown of the blood-brain barrier, these GAMs are derived primarily from bone-marrow derived cells and, to a lesser extent, from local resident inflammatory cells [66]. Macrophages either adopt a proinflammatory M1 phenotype or anti-inflammatory M2 phenotype. Glioma cells release chemo-attractans, such as monocyte chemo-attractant protein-1 (MCP-1), fractalkine (CX3CL1), glial cell–derived neurotrophic factor (GDNF), and colony stimulating factor-1 (CSF)-1) that recruit GAMs to tumor tissue [67]. CSF-1 plays a key role as it also promotes recruited macrophages to adopt M2 phenotype that contributes to tumor invasion. In fact, immunomodulation of CSF-1 signaling using a CSF-1R inhibitor has demonstrated to shift macrophages back to M1 phenotype with promising preclinical utility that requires further assessment [68].

Extensive body of literature suggests that GAMs are not simple passenger cells in the tumor microenvironment as they play a key role in regulating tumor growth and invasion with complex interactions with many other cell types [69, 70]. Importantly, GAMs secrete several factors with primary effects on tumor cells. For example, when exposed to glioma cells, GAMs upregulate expression of membrane type 1–matrix metalloproteinase (MT1-MMP) that cleaves pro-MMP2 to facilitate degradation of the extracellular matrix and GBM invasion. Moreover, GAMs secrete several oncogenic factors such as transforming growth factor beta (TGFß), which enhances glioma cell migration by upregulating integrin expression and contributes to the degradation of extra-cellular matrix components by inducing MMP2 expression and suppressing the expression of tissue inhibitor of metalloproteinases (TIMP)-2 [71, 72]. Although the interaction between neoplastic and stromal cells is complex, more thorough understanding of this crosstalk facilitates exploration of immune-modulatory compounds for GBM treatment.

2.6. Molecular Pathways in GBM Invasion. Large-scale genetic analyses have demonstrated that multiple signaling networks are employed by GBM cells to promote tumor growth and invasion. The most comprehensively studied pathways involved in GBM invasion include *PI3K/Akt*, Wnt/ß-catenin, Hedegehog, TGFß, and Tyrosine kinase receptors, which are involved in the activation of EMT-related cellular processes to promote tumor cell dissemination and invasion [73, 74]. Furthermore, as the structure of function of the ECM is critical for tumor cell invasion, dysfunction of ECM and its cognate receptor integrins may lead to aberrant activation of signaling pathways including Ras/Raf/MAPK, Raf/JNK, Rho/Rac/PAK, and PI3K/Akt/mTOR, which shape the tumor microenvironment and regulating tumor growth, angiogenesis, and invasion [75].

2.6.1. Receptor Tyrosine Kinases. Many of the signal transduction pathways that regulate the tumor microenvironment, including Ras/Raf/MAPK, Raf/JNK, Rho/Rac/PAK, and PI3K/Akt/mTOR, are convergent downstream signaling pathways of RTKs, implicating their role in GBM invasiveness and aggressiveness [76]. Furthermore, as ECM serves as a reservoir for several growth factors including VEGF, EGF, PDGF, and TGF-β, secretion of these factors and their interaction with their receptors may lead to the activation of these signaling pathways, resulting in uncontrolled cell behaviors in tumor growth, angiogenesis, and invasion [77].

The Phosphoinositide-3-kinase (PI3K) signaling cascade is one of the main canonical pathways that have been implicated in GBM pathogenesis. This pathway transduces extracellular signals via receptor tyrosine kinases (RTKs) to regulate a series of biological processes such as cellular metabolism, growth, survival, and invasion. The PI3K pathway can be activated through interaction of ligands such as the epidermal growth factor (EGF) and TGFß with their respective RTKs. Induction of PI3K leads to activation of Akt family of kinases that regulate cell growth and survival. Regulation of the PI3K-Akt signaling pathway occurs through the tumor suppressor phosphatase and tensin homolog (PTEN) protein that dephosphorylates and, thereby, inactivates Akt [78].

Constitutional activation of the PI3K-Akt pathway is implicated in many cancers. In GBM, this pathway is activated by two frequent alterations, an in-frame deletion of amino acids 6–273 in EGFRvIII resulting in a mutant EGFR protein which is present in more than 50% of high grade gliomas and its activation is ligand-independent [79] and oncogenic mutations in PTEN detected in up to 40% of adult gliomas [80]. Both alterations result in increased expression of matrix metalloproteinases including MMP-2 and MMP9 that facilitate degradation of ECM and lead to tumor invasiveness [79]. The PI3K pathway is also activated by gain-of-function mutations in the PI3K catalytic subunit gene

(PIK3CA). These mutations occur in up to 10% of GBMs and result in constitutive activation of the pathway with downstream effects similar to those promoted by *EGFRvIII* and *PTEN* mutations [81]. The key role of PI3K-Akt pathway in oncogenesis has sparked increasing interest in using small molecular inhibitors to target this pathway.

Additionally, the RTK c-Met and its ligand hepatocyte growth factor (HGF)/Scatter factor are overexpressed in gliomas and they have been shown to play a role in cell proliferation, invasion, angiogenesis and survival in several cancers [82]. EGFR and c-Met are known to trigger similar signal transduction pathways and their crosstalk in solid tumors affects the duration and strength of the response [83] and overall tumor malignancy. Notably, coexpression of EGFR and c-Met in GBM leads to deregulated EGFR signaling and increased HGF binding to c-Met, which in turn, promotes cell invasion [84].

In addition to EGFR and cMET, Wang et al. have demonstrated that the RTK Mer (MerTK) is overexpressed in GBM and this is accompanied with increased invasiveness [85]. Their results indicate that MerTK expression is maintained in primary GBM-derived tumour cells grown in stem cell cultures but is reduced significantly in serum-containing culture conditions, accompanied with downregulation of Nestin and Sox2. Furthermore, depletion of MerTK disrupts the round morphology of glioma cells and decreases their invasiveness. Additionally, the expression and phosphorylation of myosin light chain strongly correlated with activation of MerTK, suggesting that the effect of MerTK on glioma cell invasion is mediated by the ability of acto-myosin to contract. Importantly, DNA damage resulted in upregulation and phosphorylation of MerTK, protecting the cells from apoptosis. Collectively, RTKs appear as attractive therapeutic targets for the treatment of the malignant gliomas.

2.6.2. Wnt (Canonical and ß-Catenin-Independent Pathways). WNT signaling pathway is a crucial regulator of proliferation, migration and cell fate in the central nervous system during embryogenesis [86]. However, deregulation of this pathway also has oncogenic properties in mature cells. Abnormal WNT pathway activation is implicated in various cancers, including GBMs [87, 88]. Proteins of the WNT family bind to transmembrane Frizzled receptors [86] and downstream events can be divided into canonical ß-catenin-dependent and ß-catenin-independent pathways.

Activation of the canonical WNT pathway leads to disassembly of the transmembrane receptors of the ß-catenin destruction complex, consisting of the GSK3B, AXIN and adenomatous polyposis coli (APC) [86]. As a result, ß-catenin accumulates in the cytoplasm and translocates into the nucleus where it regulates TCF-LEF-dependent transcription. The classical targets of the canonical WNT pathway include cyclin D1 (CCND1), c-myc, COX2, and SOX2. Studies have demonstrated that the canonical pathway is important for glioma stem cell maintenance [89, 90]. In contrast, the ß-catenin independent pathway mainly regulates cell motility and polarity. This pathway is activated through WNT2, WNT4, WNT5A, WNT6, and WNT11 factors and leads to upregulation of the planar cell polarity (PCP) and calcium pathways [86].

In addition, WNT signaling is a major factor in epithelial-mesenchymal transition (EMT) and tumor invasion. Several studies have demonstrated that WNT pathway activation enhances the motility of cancer cells [87, 91]. Specifically, in GBMs constitutive activation of ß-catenin leads to increased tumor invasion, while inhibition of ß-catenin suppressed cell proliferation and invasion [87]. Furthermore, knockdown of WNT5A downregulated expression of MMP and suppressed glioma cell migration and invasion [91]. The building evidence of WNT pathway in GBM invasion provides a therapeutic rationale for targeting this pathway. Kahlert et al. found that the Wnt/β-catenin pathway is mainly activated within cells located at the invasive edge of the mesenchymal tumors. Furthermore, they found that this pathway mainly promotes tumor cell migration *in vitro* by inducing the expression of Zeb1, Twist1, and Slug [87].

2.6.3. Hedegehog-GLI1. Similar to WNT pathway, the Hedgehog pathway plays a crucial role in the development of the central nervous system. Hedgehog pathway dysfunction during embryogenesis leads to congenital defects such as microcephaly or cyclopia. In many cancers including glioma, the Hedgehog pathway is upregulated and plays a role in tumorigenesis and tumor progression. Generally, Sonic hedgehog (SHH), Indian hedgehog (IHH), and Desert hedgehog (DHH) ligands can activate the Hedgehog pathway by binding to the transmembrane protein Patched (PTCH1). Hedgehog pathway activation leads to upregulation of GLI1, PTCH1, cyclin D2 (CCND2), Bcl-2, and VEGF. In addition, Hedgehog pathway modulates the expression of stemness genes, such as NANOG, OCT4, and SOX [92].

Although GLI1 amplification is relatively rare in GBMs, a novel truncated isoform, tGLI1, has been linked to increased cell motility and tumor invasion in GBM and breast cancer [93, 94]. This isoform is the result of alternative splicing and lacks exon 3 and part of exon 4. The tGLI1 isoform is undetectable in normal cells but expressed in GBM [93]. Furthermore, tGLI1 upregulates heparanase expression, which remodels the ECM and releases angiogenic factors [95]. The inhibition of hedgehog pathway with cyclopamine and RNA interference techniques inhibited glioma cell migration and tumor invasion [96, 97].

Epigenetic modulators may also play a role in hedgehog pathway activation. Bromodomain-containing protein 4 (BRD4) is a critical regulator of GLI1 transcription through direct occupancy of the gene promoter [98, 99]. In addition, lysine acetyltransferase 2B (KAT2B) is a positive cofactor in the Hedgehog pathway and depletion of KAT2B led to reduced expression of Hedgehog target genes [100]. Therefore, therapeutic strategies targeting the epigenetic modulators, such as BET-inhibitors and acetyltransferase inhibitors, are promising therapeutic options.

2.6.4. Nuclear Factor-κB. NF-κB is a designation used for a family of highly regulated dimer transcription factors. They are usually elevated in GBM and contribute to the survival of migratory tumor cells [101]. Signaling pathways

Table 1: Pre- and intraoperative methods to assess GBM's invasive capacity.

Preoperative methods	Intraoperative methods
MRI-based	*Fluorescence-guidance*
T2/FLAIR hyperintensity	5-aminolevulinic acid (5-ALA)
DTI	Fluorescein sodium (Fl-Na)
DWI (ADC and FA)	*iMRI-based T2/FLAIR*
Perfusion	*Intraoperative Ultrasound*
Spectroscopy	Contrast enhanced US
Quantitative MR	Elastosonography
Radiomics radiophenotype	*Intraoperative confocal microscopy*
PET-based	Fluorescein
Fluorothymidine	Indocyanine green
Fluoroethylthyrosine	Acriflavine hydrochloride
Tryptophan	*Optical coherence tomography*
Methionine	

MRI= Magnetic Resonance Imaging, FLAIR= fluid attenuated inversion recovery, DTI= Diffusion tensor imaging, PET= Positron emission tomography, and iMRI= intraoperative MRI.

triggered by growth factor receptors, including EGFR and PDGFR, contribute to tumor development in GBM and NF-κB plays key roles in these pathways [102, 103]. Among GBM subtypes, the mesenchymal phenotype is the most aggressive because it is highly invasive and radio-resistant [104] and associates with poor patient outcome. A transition of GBM cells from less aggressive phenotypes (i.e., proneural) to cells with mesenchymal features can be promoted by activation of NFκB signaling [105]. Moreover, NFκB activation in mesenchymal GBM cells mediates cell migration and tumor invasion through upregulation of NFκB target genes, including cell chemoattractants (IL-8, MCP-1) and matrix metalloproteinases (MMP-9) [106]. This signaling pathway can be activated by a number of stimuli, including ECM components such as hyaluronic acid, through binding to TLR4, differentiation of GBM stem-like cells [27, 107], and cytokines that may be released by infiltrating monocytes/macrophages or surrounding parenchymal cells. To this end, when RANKL, a member of the TNF family, is upregulated in GBM cells, it activates neighbouring astrocytes through NFκB signaling which leads to secretion of cytokines, such as TGFß, and promotes GBM cell invasion [108]. Thus, NFκB-mediated invasiveness may occur when this signaling pathway is activated either in GBM cells or in cells in the tumor microenvironment.

3. The Clinical Implications of GBM Invasiveness

Invasiveness is one of the key features that allow GBM to overcome the current treatment strategies [109]. GBM initiating cells with enhanced invasive capacity have been identified in the peritumoral parenchyma. This cell subpopulation has a distinctive molecular profile [110, 111] and they are considered to be responsible for tumor recurrence, progression, and resistance to treatment [112, 113]. Furthermore, they could be involved in the gliomagenesis process [114].

Targeting tumor invasion and infiltration is a major clinical challenge. Novel pre- and intraoperative imaging techniques are being developed to accurately assess the extent of parenchymal infiltration in the clinical setting. Besides, new insights into potential therapeutic approaches have been recently reported.

3.1. Assessment of GBM Invasion in the Clinical Setting

3.1.1. Imaging GBM Invasion. The radiological definition of infiltrated parenchyma remains unclear and the current imaging techniques, summarized in Table 1, are limited to accurately recognize the extent of tumor invasion. This is particularly relevant in focal therapies, such as surgical resection, radiotherapy, or local chemotherapeutic agents, to precisely define the peritumoral area that requires treatment in order to obtain significant responses.

GBM-induced T2/FLAIR hyperintensity in the MRI represents the area of peritumoral oedema and tumor-induced alterations in the parenchyma. It is a result of changes in the composition of the ECM and impairment of the blood-brain barrier in a process associated with the expression of endogenous tenascin-C [115].

It has been widely demonstrated that glioma cells infiltrate the peritumoral T2/FLAIR high signal region beyond the contrast enhancement on the preoperative MRI [116, 117]. The peritumoral invasion results in a gradient of the apparent diffusion coefficient (ADC) and in a higher relative Cerebral Blood Volume (rCBV), due to the peritumoral hypercellularity and the consequent increase in perfusion [118].

Nevertheless, the distinction of the diffuse nonenhancing tumor invasion from the peritumoral vasogenic oedema can be challenging in the clinical practice [119, 120]. Several alternative MRI-based methods have been described to overcome this limitation, including multi-parametric machine-learning [121] and DTI-based imaging analyses [122]. For instance, the distinction between oedema and tumor invasion is feasible by using quantitative MR methods [119] or by combining

changes in the ADC value and the signal intensity on FLAIR images [120].

Moreover, considering GBM's diffuse infiltration, the burden of tumor cell invasion in the "normal" brain is not yet possible by using imaging techniques [123]. It is well known that invading tumor cell can be found as far as the contralateral hemisphere [124] and current imaging techniques are limited in fully assessing, at the microscopic level, the tumor cells invading the parenchyma beyond the limits of the T2/FLAIR abnormalities [125]. Besides, it has been suggested that GBM invasive margin can be identified by using a combination of DTI, perfusion, and spectroscopy [122, 126].

Radiomic analyses have focused on the invasion-related radio-phenotype applying quantitative volumetric to assess the correlation between specific radiological invasion features and IDH mutation status, outcome, or response to surgery [127, 128]. Besides, MRI-based mathematical models incorporating invasion features are capable to classify nodular and diffuse GBMs, two groups with different outcome and response to treatment [129]. Alternatively, MRI DWI-based models use the ADC value as a measure of cellular density predicting the spatial microscopic tumor growth dynamics and generating maps of cell diffusion and proliferation rates [130].

Other imaging methods, as Positron Emission Tomography (PET), have been used to assess the parenchymal response to tumor invasion [131] and, more recently, to assess the infiltrative tumor volume [132–134]. For instance, [18] fluorothymidine (FLT)-PET-CT, a proliferation marker, shows that the tumor infiltration can extend up to 24 mm beyond the MRI-based T2 abnormality volume and it was useful to distinguish between infiltrative tumor and peritumoral oedema [132]. Similar results have been described by using other PET amino acid markers as Fluoroethylthyrosine [133], Tryptophan [134], and methionine [135].

3.1.2. Intraoperative Identification of GBM Invasion. Intraoperatively, the tumor infiltrating the adjacent parenchyma maintains the macroscopic aspect of normal or oedematous brain parenchyma. Therefore, it is critical to develop and validate methods to accurately define the boundaries of the infiltrative tumor.

In the last two decades, the 5-aminolevulinic acid (5-ALA), an intermediate metabolite in the porphyrin intracellular pathway that results in the accumulation of fluorescent protoporphyrin IX molecule inside tumor cells, has been used to intraoperatively define the infiltrative tumor [136, 137]. Although 5-ALA fluorescence represents contrast-enhanced tumor in the MRI, an accurate correlation with T2/FLAIR changes remains unclear. It is widely accepted that 5-ALA fluorescence depicts more accurately the tumor burden than gadolinium; however its capacity to identify the infiltrative tumor is not fully understood due to a low negative predictive value [138, 139].

Moreover, the concordance between 5-ALA fluorescence and intraoperative MRI (iMRI) findings is still poorly understood. For instance, residual contrast enhancement in the iMRI after 5-ALA fluorescence-guided resection can be found in the majority of cases. Histopathological analysis of these regions revealed tumor core or tumor infiltration in 39 and 25% of cases, respectively [140, 141]. In other histopathological correlation studies, 5-ALA predicted tumor in strong and weak fluorescence regions. However, tumor tissue was still observed in fluorescence-negative regions in approximately half of the cases [142]. Besides, although the use of iMRI and 5-ALA fluorescence-guided surgery may increase the extent of resection, a significant impact in survival has not been established [143].

On the other hand, preoperative 18F-fluoroethyl-L-tyrosine (FET)-PET can predict 5-ALA fluorescence [144]. However, more recent analyses have shown contradictory results. Roessler at al. described that 5-ALA had higher sensitivity than 18F-FET-PET to detect the infiltrative tumor surrounding the contrast-enhanced region [145]. On the contrary, Floeth et al. concluded that 18F-FET PET is more sensitive to detect glioma tissue than 5-ALA fluorescence [146]. Further research is needed to fully understand the correlation between both techniques.

Fluorescein sodium (Fl-Na) is another marker used in fluorescence-guided surgery. Despite a good correlation of Fl-Na and histopathological [147], 5-ALA has demonstrated to be superior in identifying tumor cells in the peri-tumoral area beyond the contrast-enhanced tumor when compared to Fl-Na. While Fl-NA accumulation is associated with blood-brain barrier disruption, 5-ALA is mainly dependent on the protoporphyrin tumor cell pathway [148].

Intraoperative ultrasound (US) is another intraoperative resource used to assess tumor extension [149, 150]. In brightness mode (B-Mode) GBM appears as a heterogeneous echogenic mass with hyperechogenic boundaries and, in the majority of LGG, the B-mode hyperechogenicity overlaps with the preoperative T2/FLAIR MRI hyper-intensity [150–152]. Nevertheless, in both cases, the distinction between infiltrative tumor and associated oedema can be challenging, especially in advanced stages of the resection when surgery-related oedema and other artefacts may interfere with the US imaging [153]. Although intraoperative US is a promising tool to assess the infiltrative tumor, a better understanding of the underlying mechanisms is needed along with the development of multimodal intraoperative US imaging approaches integrating contrast-enhanced ultrasound [152, 154] and elastosonography [151].

Among other techniques described to identify the boundaries of the infiltrative GBM during the surgical resection, intraoperative confocal microscopy is an emerging approach capable of identifying fluorescein-, indocyanine green-, or acriflavine hydrochloride-enhanced differences in cell density and cellular morphology corresponding with the T2 hyper-intensity on MR imaging [117, 155–157]. Furthermore, this technique can potentially identify the tumor margins at a microscopic level and distinguish them from perilesional parenchyma [155].

Finally, optical coherence tomography, a real-time tissue microstructure imaging technique based on low-coherence interferometry in the near infra-red range of wavelengths, is another promising tool for assessing the tumor infiltrative margin in gliomas. It provides comprehensive qualitative and quantitative analysis of the tumor and the peritumoral

tissue, generating color-coded maps that correlate with the histological findings and help to accurately identify the tumor boundaries [158–161].

3.2. Therapeutic Approaches Targeting GBM Invasion. The current standard of care for patients with GBM involves surgical resection and adjuvant chemo-radiation with temozolomide [1]. It is widely accepted that the infiltrated parenchyma is associated with recurrence and resistance to treatment, thereby playing a central role in each step of the treatment [162].

3.2.1. Surgical Resection of the Infiltrative Tumor. In GBM, tumor cell invasiveness can lead to the infiltration or destruction of surrounding parenchyma resulting in neurological deficits [63, 163]. It has been proven that gross total resection of the contrast-enhanced tumor improves overall outcome [164, 165]. However, this approach might disregard the tumor burden invading the surrounding parenchyma, which could be potentially resected if eloquent areas are not compromised [166].

Thus far, several studies have shown that resection of the infiltrative portion of the tumor, based on DTI, ADC, or T2/FLAIR abnormalities is associated with longer progression-free survival (PFS) and overall survival (OS) [166–170]. However, a recent analysis of 245 primary GBMs did not find a significant difference in recurrence and survival associated with the postoperative FLAIR volume [171].

Although there is evidence supporting that resection of the infiltrative tumor can result in better outcomes, opposite results highlight the need for further research, as it remains unclear the more appropriate method to identify the areas of the surrounding parenchyma with greater tumor cell density and to distinguish them from the oedematous brain [120].

3.2.2. Radiation Therapy Targeting GBM Invasiveness. Accurate tumor volume definition is critical in conformal or intensity-modulated radiotherapy (IMRT) planning. Analogously to surgical approaches, a subtherapeutic radiation dose within the tumor may result in treatment failure and recurrence, whereas whole-brain dose increments may lead to radiation-induced toxicity [133]. Moreover, a sublethal irradiation dose may enhance invasion in GBM [172, 173]. Another suggested mechanism of tumor recurrence is the proinvasive ECM remodelling in the tumor microenvironment in response to ionizing radiation [25].

Despite the infiltrative nature of GBM, radiation planning protocols have evolved from whole brain radiotherapy towards more tailored tumor volume targets, partially based on that the great majority of recurrences arise within 2 cm from the primary site [174, 175]. In this context, it remains unclear if targeting the MRI-defined infiltrative tumor results in better PFS and OS. Moreover, in clinical practice there is a considerable variation in target volume definition without significant differences in outcome, from using a 2-3 cm margin on the T1 contrast-enhanced tumor to a 2 cm margin on the T2/FLAIR hyper-intensity, as recommended by the European Organization for Research and Treatment of Cancer or the Radiation Therapy Oncology Group, respectively [176, 177]. In fact, by targeting the tumor area with a margin of 2 cm and without using the peritumoral oedema as tumor volume, Chang et al. achieved similar recurrence pattern results [175]. Further research is needed to assess whether this is a result of the overall lack of benefit from radiation therapy or if targeting the infiltrative tumor burden with radiation does not significantly impact the outcome [177].

On the other hand, the use of DTI-based clinical target volumes (CTV) has been proposed, as they are smaller than the ones based on the T2-hyperintensity, sparing the peritumoral oedema. Besides, this reduction in the CTVs could allow dose escalation [178, 179]. Furthermore, approaches taking into account tumor growth dynamics have been developed, by defining the CTVs based on DTI-derived mathematical growth models. Although this approach could be more effective at targeting cancer cells and preserving healthy tissue, further research is warranted to assess its outcome and tumor recurrence [123, 180]

Other approaches for CTV definition are based on PET findings. For instance, a higher dose coverage of 18F-FET-PET tumor regions is positively correlated with time to progression and PET-based CTVs better-predicted failure sites when compared to MRI-based CTVs [133, 181], although current ongoing protocols are trying to better define the impact of PET-based tumor delineation in outcome [182].

3.2.3. Therapeutic Targets in GBM Invasion. Overall, current commonly used therapies for GBM, including alkylating agents as Temozolomide (TMZ) and the anti-VEGF compound Bevacizumab, failed in targeting glioma cell invasion. Although TMZ can potentially inhibit invasion in vitro [183], this effect is not significant in the clinical practice and several resistance mechanisms to alkylating agents have been proposed [184]. Among them, the lack of blood-brain permeability in T2/FLAIR hyperintensity areas [185, 186] and the resistance mechanisms intrinsic to GSC in the infiltrative tumor are intimately associated with the GBM invasive capacity [112, 187]. On the other hand, Bevacizumab could lead to a hypoxic environment resulting in enhanced glioma cell invasion of the normal parenchyma [188, 189].

Considering the lack of an effective therapeutic approach against GBM invasiveness, further research is warranted to better understand the invasion pathways contributing to glioma cell infiltration and, consequently, to develop new therapeutic agents. An effective therapeutic strategy should target both infiltrative GBM cells and the tumor cell-stroma interaction [190].

Up to now, no clinically transferable results have been achieved after trying to target some of the mechanisms involved in GBM invasion, including cytoskeleton reorganization and cell motility, cell adhesion, and degradation of ECM [57, 162]

Current areas of research include several potential targets in glioma cell invasion pathways. Glutamate-mediated infiltration inhibition has been assessed in several Phases I-II trials with promising results. Besides, the role of different tumor cell ion channels and transporters, microtubule-based tumor cell network, microRNA-related invasion, and the mechanisms involved in the interaction between the tumor

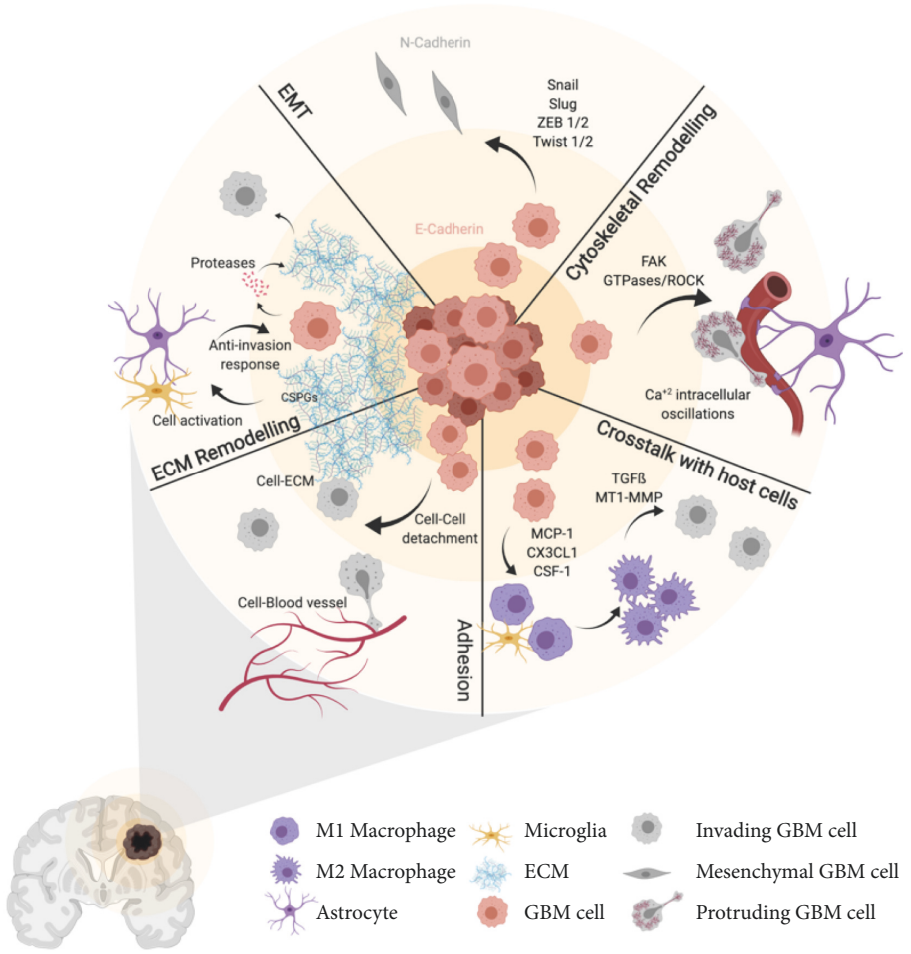

Figure 1: *Cellular processes involved in GBM cell invasion*. Schematic summary of the processes involved in the invasive capacity of GBM cells including cell-to-cell and cell-to-ECM adhesion, ECM remodelling, EMT, cytoskeletal remodelling, and cross-talk with host cells. See text for details (created with Biorender.com).

and the host open potential opportunities for targeted therapy approaches [109, 162, 190]

4. Conclusion

The GBM invasiveness capacity is one of the main features contributing to tumor recurrence, treatment resistance, and low survival rates. It results from an intricate combination of several signalling routes, mainly receptor tyrosine kinases and transcriptional pathways and also cellular processes that include cytoskeletal remodelling and interactions with ECM components and host cells (Figure 1). Although significant advances have been made in the last decade, the complexity of this protein interaction network and the lack of understanding about the contribution of each one of these mechanisms to glioma cell invasiveness have hampered the translation of novel therapeutic strategies into the clinic. Further research integrating key elements in the process of invasion will be needed to unravel efficient combination therapies to avoid tumor progression. Novel preoperative and intraoperative imaging techniques have been recently developed to help the clinician to recognize and treat the infiltrative portion of the GBM. Nevertheless, this portion of the tumor remains elusive to these methods. Therefore, improvement in revealing the presence of invasive tumor cells would be needed in the clinical practice to significantly impact the prognosis of patients with GBM.

Conflicts of Interest

The authors declare that they have no conflicts of interest.

Authors' Contributions

Carlos Velásquez and Sheila Mansouri contributed equally to this work.

Acknowledgments

This work received funding from Instituto de Salud Carlos III, grant PI17/01399.

References

[1] R. Stupp, W. P. Mason, M. J. van den Bent et al., "Radiotherapy plus concomitant and adjuvant temozolomide for glioblastoma," *The New England Journal of Medicine*, vol. 352, no. 10, pp. 987–996, 2005.

[2] R. Soffietti, B. G. Baumert, L. Bello et al., "Guidelines on management of low-grade gliomas: report of an EFNS-EANO Task Force," *European Journal of Neurology*, vol. 17, no. 9, pp. 1124–1133, 2010.

[3] K. Asano, C. D. Duntsch, Q. Zhou et al., "Correlation of N-cadherin expression in high grade gliomas with tissue invasion," *Journal of Neuro-Oncology*, vol. 70, no. 1, pp. 3–15, 2004.

[4] A. Claes, A. J. Idema, and P. Wesseling, "Diffuse glioma growth: a guerilla war," *Acta Neuropathologica*, vol. 114, no. 5, pp. 443–458, 2007.

[5] P. Duenisch, R. Reichart, U. Mueller et al., "Neural cell adhesion molecule isoform 140 declines with rise of WHO grade in human gliomas and serves as indicator for the invasion zone of multiform glioblastomas and brain metastases," *Journal of Cancer Research and Clinical Oncology*, vol. 137, no. 3, pp. 399–414, 2011.

[6] S. Jayaram, L. Balakrishnan, M. Singh et al., "Identification of a Novel Splice Variant of Neural Cell Adhesion Molecule in Glioblastoma Through Proteogenomics Analysis," *OMICS: A Journal of Integrative Biology*, vol. 22, no. 6, pp. 437–448, 2018.

[7] J. A. Yu, M. R. Sadaria, X. Meng et al., "Lung cancer cell invasion and expression of intercellular adhesion molecule-1 (ICAM-1) are attenuated by secretory phospholipase A_2 inhibition," *The Journal of Thoracic and Cardiovascular Surgery*, vol. 143, no. 2, pp. 405–411, 2012.

[8] P. G. Frank and M. P. Lisanti, "ICAM-1: role in inflammation and in the regulation of vascular permeability," *American Journal of Physiology-Heart and Circulatory Physiology*, vol. 295, no. 3, pp. H926–H927, 2008.

[9] Y. Lin, C. Shun, M. Wu, and C. Chen, "A novel anticancer effect of thalidomide: inhibition of intercellular adhesion molecule-1-mediated cell invasion and metastasis through suppression of nuclear factor- B," *Clinical Cancer Research*, vol. 12, no. 23, pp. 7165–7173, 2006.

[10] D. Kesanakurti, C. Chetty, D. Rajasekhar Maddirela, M. Gujrati, and J. S. Rao, "Essential role of cooperative NF-κB and Stat3 recruitment to ICAM-1 intronic consensus elements in the regulation of radiation-induced invasion and migration in glioma," *Oncogene*, vol. 32, no. 43, pp. 5144–5155, 2013.

[11] J. Lin, J. Tsai, T. Chao, H. Ma, and W. Liu, "Musashi-1 enhances glioblastoma migration by promoting ICAM1 translation," *Neoplasia*, vol. 21, no. 5, pp. 459–468, 2019.

[12] Y. Takada, X. Ye, and S. Simon, "The integrins," *Genome Biology*, vol. 8, no. 5, article 215, 2007.

[13] M. Paolillo, M. Serra, and S. Schinelli, "Integrins in glioblastoma: Still an attractive target?" *Pharmacological Research*, vol. 113, pp. 55–61, 2016.

[14] J. S. Desgrosellier and D. A. Cheresh, "Integrins in cancer: biological implications and therapeutic opportunities," *Nature Reviews Cancer*, vol. 10, no. 1, pp. 9–22, 2010.

[15] G. Renner, F. Noulet, M.-C. Mercier et al., "Expression/activation of $\alpha 5\beta 1$ integrin is linked to the β-catenin signaling pathway to drive migration in glioma cells," *Oncotarget* , vol. 7, no. 38, pp. 62194–62207, 2016.

[16] E. Serres, F. Debarbieux, F. Stanchi et al., "Fibronectin expression in glioblastomas promotes cell cohesion, collective invasion of basement membrane in vitro and orthotopic tumor growth in mice," *Oncogene*, vol. 33, no. 26, pp. 3451–3462, 2014.

[17] A. M. Mikheev, S. A. Mikheeva, A. D. Trister et al., "Periostin is a novel therapeutic target that predicts and regulates glioma malignancy," *Neuro-Oncology*, vol. 17, no. 3, pp. 372–382, 2015.

[18] Q. Ding, J. J. Stewart, C. W. Prince et al., "Promotion of malignant astrocytoma cell migration by osteopontin expressed in the normal brain: differences in integrin signaling during cell adhesion to osteopontin versus vitronectin," *Cancer Research*, vol. 62, no. 18, pp. 5336–5343, 2002.

[19] S. Hehlgans, M. Haase, and N. Cordes, "Signalling via integrins: Implications for cell survival and anticancer strategies," *Biochimica et Biophysica Acta (BBA) - Reviews on Cancer*, vol. 1775, no. 1, pp. 163–180, 2007.

[20] C. D. Lawson and K. Burridge, "The on-off relationship of Rho and Rac during integrin-mediated adhesion and cell migration," *Small GTPases*, vol. 5, no. 1, Article ID e27958, 2014.

[21] C. Scaringi, G. Minniti, P. Caporello, and R. M. Enrici, "Integrin inhibitor cilengitide for the treatment of glioblastoma: A brief overview of current clinical results," *Anticancer Reseach*, vol. 32, no. 10, pp. 4213–4224, 2012.

[22] E. Delamarre, S. Taboubi, S. Mathieu et al., "Expression of integrin alpha6beta1 enhances tumorigenesis in glioma cells," *The American Journal of Pathology*, vol. 175, no. 2, pp. 844–855, 2009.

[23] M. Herrera-Perez, S. L. Voytik-Harbin, and J. L. Rickus, "Extracellular matrix properties regulate the migratory response of glioblastoma stem cells in three-dimensional culture," *Tissue Engineering Part A*, vol. 21, no. 19-20, pp. 2572–2582, 2015.

[24] M. C. de Gooijer, M. Guillén Navarro, R. Bernards, T. Wurdinger, and O. van Tellingen, "An experimenter's guide to glioblastoma invasion pathways," *Trends in Molecular Medicine*, vol. 24, no. 9, pp. 763–780, 2018.

[25] K. Yoo, Y. Suh, Y. An et al., "Proinvasive extracellular matrix remodeling in tumor microenvironment in response to radiation," *Oncogene*, vol. 37, no. 24, pp. 3317–3328, 2018.

[26] J. E. Chen, J. Lumibao, A. Blazek, H. R. Gaskins, and B. Harley, "Hypoxia activates enhanced invasive potential and endogenous hyaluronic acid production by glioblastoma cells," *Biomaterials Science*, vol. 6, no. 4, pp. 854–862, 2018.

[27] E. Ferrandez, O. Gutierrez, D. S. Segundo, and J. L. Fernandez-Luna, "NFκB activation in differentiating glioblastoma stem-like cells is promoted by hyaluronic acid signaling through TLR4," *Scientific Reports*, vol. 8, no. 1, 2018.

[28] Y. Kim, H. Kang, G. Powathil et al., "Role of extracellular matrix and microenvironment in regulation of tumor growth and LAR-mediated invasion in glioblastoma," *PLoS ONE*, vol. 13, no. 10, p. e0204865, 2018.

[29] A. Y. Tsidulko, C. Bezier, G. de La Bourdonnaye et al., "Conventional anti-glioblastoma chemotherapy affects proteoglycan composition of brain extracellular matrix in rat experimental model in vivo," *Frontiers in Pharmacology*, vol. 9, article 1104, 2018.

[30] M. Wang, T. Wang, S. Liu, D. Yoshida, and A. Teramoto, "The expression of matrix metalloproteinase-2 and -9 in human gliomas of different pathological grades," *Brain Tumor Pathology*, vol. 20, no. 2, pp. 65–72, 2003.

[31] S. S. Lakka, C. S. Gondi, N. Yanamandra et al., "Inhibition of cathepsin B and MMP-9 gene expression in glioblastoma cell

line via RNA interference reduces tumor cell invasion, tumor growth and angiogenesis," *Oncogene*, vol. 23, no. 27, pp. 4681–4689, 2004.

[32] P. Kaphle, Y. Li, and L. Yao, "The mechanical and pharmacological regulation of glioblastoma cell migration in 3D matrices," *Journal of Cellular Physiology*, vol. 234, no. 4, pp. 3948–3960, 2019.

[33] U. D. Kahlert, J. V. Joseph, and F. A. Kruyt, "EMT- and MET-related processes in nonepithelial tumors: importance for disease progression, prognosis, and therapeutic opportunities," *Molecular Oncology*, vol. 11, no. 7, pp. 860–877, 2017.

[34] P. D. McCrea and C. J. Gottardi, "Beyond β-catenin: prospects for a larger catenin network in the nucleus," *Nature Reviews Molecular Cell Biology*, vol. 17, no. 1, pp. 55–64, 2016.

[35] J. K. Myung, S. A. Choi, S.-K. Kim, K.-C. Wang, and S.-H. Park, "Snail plays an oncogenic role in glioblastoma by promoting epithelial mesenchymal transition," *International Journal of Clinical and Experimental Pathology*, vol. 7, no. 5, pp. 1977–1987, 2014.

[36] H. W. Yang, L. G. Menon, P. M. Black, R. S. Carroll, and M. D. Johnson, "SNAI2/Slug promotes growth and invasion in human gliomas," *BMC Cancer*, vol. 10, no. 1, 2010.

[37] F. A. Siebzehnrubl, D. J. Silver, B. Tugertimur et al., "The ZEB1 pathway links glioblastoma initiation, invasion and chemoresistance," *EMBO Molecular Medicine*, vol. 5, no. 8, pp. 1196–1212, 2013.

[38] S. A. Mikheeva, A. M. Mikheev, A. Petit et al., "TWIST1 promotes invasion through mesenchymal change in human glioblastoma," *Molecular Cancer*, vol. 9, article 194, 2010.

[39] E. Camand, F. Peglion, N. Osmani, M. Sanson, and S. Etienne-Manneville, "N-cadherin expression level modulates integrin-mediated polarity and strongly impacts on the speed and directionality of glial cell migration," *Journal of Cell Science*, vol. 125, pp. 844–857, 2012.

[40] R. Mahabir, M. Tanino, A. Elmansuri et al., "Sustained elevation of Snail promotes glial-mesenchymal transition after irradiation in malignant glioma," *Neuro-Oncology*, vol. 16, no. 5, pp. 671–685, 2014.

[41] J. Halliday, K. Helmy, S. S. Pattwell et al., "In vivo radiation response of proneural glioma characterized by protective p53 transcriptional program and proneural-mesenchymal shift," *Proceedings of the National Acadamy of Sciences of the United States of America*, vol. 111, no. 14, pp. 5248–5253, 2014.

[42] Y. Kim, K. Yoo, Y. Cui et al., "Radiation promotes malignant progression of glioma cells through HIF-1alpha stabilization," *Cancer Letters*, vol. 354, no. 1, pp. 132–141, 2014.

[43] G. Storci, P. Sansone, S. Mari et al., "TNFalpha up-regulates SLUG via the NF-kappaB/HIF1alpha axis, which imparts breast cancer cells with a stem cell-like phenotype," *Journal of Cellular Physiology*, vol. 225, no. 3, pp. 682–691, 2010.

[44] J. Kim, J. Kong, H. Chang, H. Kim, and A. Kim, "EGF induces epithelial-mesenchymal transition through phospho-Smad2/3-Snail signaling pathway in breast cancer cells," *Oncotarget* , vol. 7, no. 51, pp. 85021–85032, 2016.

[45] F. Liu, S. Song, Z. Yi et al., "HGF induces EMT in non-small-cell lung cancer through the hBVR pathway," *European Journal of Pharmacology*, vol. 811, pp. 180–190, 2017.

[46] Q. Wu, X. Hou, J. Xia et al., "Emerging roles of PDGF-D in EMT progression during tumorigenesis," *Cancer Treatment Reviews*, vol. 39, no. 6, pp. 640–646, 2013.

[47] S. S. Stylli, A. H. Kaye, and P. Lock, "Invadopodia: At the cutting edge of tumour invasion," *Journal of Clinical Neuroscience*, vol. 15, no. 7, pp. 725–737, 2008.

[48] R. O. Hynes, "Integrins: bidirectional, allosteric signaling machines," *Cell*, vol. 110, no. 6, pp. 673–687, 2002.

[49] E. M. Tam, Y. I. Wu, G. S. Butler, M. S. Stack, and C. M. Overall, "Collagen binding properties of the membrane type-1 matrix metalloproteinase (MT1-MMP) hemopexin C domain," *The Journal of Biological Chemistry*, vol. 277, no. 41, pp. 39005–39014, 2002.

[50] M. A. Wear, D. A. Schafer, and J. A. Cooper, "Actin dynamics: Assembly and disassembly of actin networks," *Current Biology*, vol. 10, no. 24, pp. R891–R895, 2000.

[51] S. Narumiya, M. Tanji, and T. Ishizaki, "Rho signaling, ROCK and mDia1, in transformation, metastasis and invasion," *Cancer and Metastasis Reviews*, vol. 28, no. 1-2, pp. 65–76, 2009.

[52] A. Whale, F. N. Hashim, S. Fram, G. E. Jones, and C. M. Wells, "Signaling to cancer cell invasion through PAK family kinases," *Front Biosci (Landmark Ed)*, vol. 16, pp. 849–864, 2011.

[53] H. Wang, M. Han, W. Whetsell et al., "Tax-interacting protein 1 coordinates the spatiotemporal activation of Rho GTPases and regulates the infiltrative growth of human glioblastoma," *Oncogene*, vol. 33, no. 12, pp. 1558–1569, 2014.

[54] H. Ma, T. Li, Z. Tao et al., "NKCC1 promotes EMT-like process in GBM via RhoA and Rac1 signaling pathways," *Journal of Cellular Physiology*, vol. 234, no. 2, pp. 1630–1642, 2019.

[55] G. Liu, T. Yan, and X. Li, "Daam1 activates RhoA to regulate Wnt5ainduced glioblastoma cell invasion," *Oncology Reports*, vol. 39, no. 2, pp. 465–472, 2018.

[56] A. Talamillo, L. Grande, P. Ruiz-Ontañon et al., "ODZ1 allows glioblastoma to sustain invasiveness through a Myc-dependent transcriptional upregulation of RhoA," *Oncogene*, pp. 1–12, 2016.

[57] J. Drappatz, A. D. Norden, and P. Y. Wen, "Therapeutic strategies for inhibiting invasion in glioblastoma," *Expert Review of Neurotherapeutics*, vol. 9, no. 4, pp. 519–534, 2014.

[58] D. E. Discher, P. Janmey, and Y. L. Wang, "Tissue cells feel and respond to the stiffness of their substrate," *Science*, vol. 310, no. 5751, pp. 1139–1143, 2005.

[59] T. A. Ulrich, E. M. de Juan Pardo, and S. Kumar, "The Mechanical Rigidity of the Extracellular Matrix Regulates the Structure, Motility, and Proliferation of Glioma Cells," *Cancer Research*, vol. 69, no. 10, pp. 4167–4174, 2009.

[60] V. Montana and H. Sontheimer, "Bradykinin Promotes the Chemotactic Invasion of Primary Brain Tumors," *The Journal of Neuroscience*, vol. 31, no. 13, pp. 4858–4867, 2011.

[61] F. J. Martini and M. Valdeolmillos, "Actomyosin Contraction at the Cell Rear Drives Nuclear Translocation in Migrating Cortical Interneurons," *The Journal of Neuroscience*, vol. 30, no. 25, pp. 8660–8670, 2010.

[62] S. Watkins, S. Robel, I. F. Kimbrough, S. M. Robert, G. Ellis-Davies, and H. Sontheimer, "Disruption of astrocyte–vascular coupling and the blood–brain barrier by invading glioma cells," *Nature Communications*, vol. 5, article 4196, 2014.

[63] V. A. Cuddapah, S. Robel, S. Watkins, and H. Sontheimer, "A neurocentric perspective on glioma invasion," *Nature Reviews Neuroscience*, vol. 15, no. 7, pp. 455–465, 2014.

[64] E. Hirata and E. Sahai, "Tumor Microenvironment and Differential Responses to Therapy," *Cold Spring Harbor Perspectives in Medicine*, vol. 7, no. 7, p. a026781, 2017.

[65] A. S. Venteicher, I. Tirosh, and C. Hebert, "Decoupling genetics, lineages, and microenvironment in IDH-mutant gliomas by single-cell RNA-seq," *Science*, vol. 355, no. 6332, 2017.

[66] M. De Palma, "Origins of brain tumor macrophages," *Cancer Cell*, vol. 30, no. 6, pp. 832-833, 2016.

[67] D. Hambardzumyan, D. H. Gutmann, and H. Kettenmann, "The role of microglia and macrophages in glioma maintenance and progression," *Nature Neuroscience*, vol. 19, no. 1, pp. 20–27, 2016.

[68] S. M. Pyonteck, L. Akkari, A. J. Schuhmacher et al., "CSF-1R inhibition alters macrophage polarization and blocks glioma progression," *Nature Medicine*, vol. 19, no. 10, pp. 1264–1272, 2013.

[69] S. K. Biswas and A. Mantovani, "Macrophage plasticity and interaction with lymphocyte subsets: cancer as a paradigm," *Nature Immunology*, vol. 11, no. 10, pp. 889–896, 2010.

[70] F. Hu, O. D. a Dzaye, A. Hahn et al., "Glioma-derived versican promotes tumor expansion via glioma-associated microglial/macrophages Toll-like receptor 2 signaling," *Neuro-Oncology*, vol. 17, no. 2, pp. 200–210, 2015.

[71] D. S. Markovic, K. Vinnakota, S. Chirasani et al., "Gliomas induce and exploit microglial MT1-MMP expression for tumor expansion," *Proceedings of the National Acadamy of Sciences of the United States of America*, vol. 106, no. 30, pp. 12530–12535, 2009.

[72] A. Wesolowska, A. Kwiatkowska, L. Slomnicki et al., "Microglia-derived TGF-β as an important regulator of glioblastoma invasion—an inhibition of TGF-β-dependent effects by shRNA against human TGF-β type II receptor," *Oncogene*, vol. 27, no. 7, pp. 918–930, 2008.

[73] S. K. Singh, C. Hawkins, I. D. Clarke et al., "Identification of human brain tumour initiating cells," *Nature*, vol. 432, no. 7015, pp. 396–401, 2004.

[74] D. Hanahan and R. A. Weinberg, "Hallmarks of cancer: the next generation," *Cell*, vol. 144, no. 5, pp. 646–674, 2011.

[75] I. Manini, F. Caponnetto, A. Bartolini et al., "Role of microenvironment in glioma invasion: what we learned from in vitro models," *International Journal of Molecular Sciences*, vol. 19, no. 1, p. 147, 2018.

[76] C. H. Streulli and N. Akhtar, "Signal co-operation between integrins and other receptor systems," *Biochemical Journal*, vol. 418, no. 3, pp. 491–506, 2009.

[77] S. V. Plotnikov, A. M. Pasapera, B. Sabass, and C. M. Waterman, "Force fluctuations within focal adhesions mediate ECM-rigidity sensing to guide directed cell migration," *Cell*, vol. 151, no. 7, pp. 1513–1527, 2012.

[78] C. Liu, H. Wu, Y. Li et al., "SALL4 suppresses PTEN expression to promote glioma cell proliferation via PI3K/AKT signaling pathway," *Journal of Neuro-Oncology*, vol. 135, no. 2, pp. 263–272, 2017.

[79] A. Lal, C. A. Glazer, H. M. Martinson et al., "Mutant epidermal growth factor receptor up-regulates molecular effectors of tumor invasion," *Cancer Research*, vol. 62, no. 12, pp. 3335–3339, 2002.

[80] C. W. Brennan, R. G. Verhaak, and A. McKenna, "The somatic genomic landscape of glioblastoma," *Cell*, vol. 155, no. 2, pp. 462–477, 2013.

[81] R. S. McNeill, E. E. Stroobant, E. Smithberger et al., "PIK3CA missense mutations promote glioblastoma pathogenesis, but do not enhance targeted PI3K inhibition," *PLoS ONE*, vol. 13, no. 7, p. e0200014, 2018.

[82] A. Gentile, L. Trusolino, and P. M. Comoglio, "The Met tyrosine kinase receptor in development and cancer," *Cancer and Metastasis Reviews*, vol. 27, no. 1, pp. 85–94, 2008.

[83] L. Trusolino, A. Bertotti, and P. M. Comoglio, "MET signalling: principles and functions in development, organ regeneration and cancer," *Nature Reviews Molecular Cell Biology*, vol. 11, no. 12, pp. 834–848, 2010.

[84] K. K. Velpula, V. R. Dasari, S. Asuthkar, B. Gorantla, and A. J. Tsung, "EGFR and c-Met Cross Talk in Glioblastoma and Its Regulation by Human Cord Blood Stem Cells," *Translational Oncology*, vol. 5, no. 5, pp. 379–IN18, 2012.

[85] Y. Wang, G. Moncayo, P. Morin et al., "Mer receptor tyrosine kinase promotes invasion and survival in glioblastoma multiforme," *Oncogene*, vol. 32, no. 7, pp. 872–882, 2013.

[86] J. P. Dijksterhuis, J. Petersen, and G. Schulte, "WNT/Frizzled signalling: Receptor-ligand selectivity with focus on FZD-G protein signalling and its physiological relevance: IUPHAR Review 3," *British Journal of Pharmacology*, vol. 171, no. 5, pp. 1195–1209, 2014.

[87] U. D. Kahlert, D. Maciaczyk, S. Doostkam et al., "Activation of canonical WNT/β-catenin signaling enhances in vitro motility of glioblastoma cells by activation of ZEB1 and other activators of epithelial-to-mesenchymal transition," *Cancer Letters*, vol. 325, no. 1, pp. 42–53, 2012.

[88] C. Cui, X. Zhou, W. Zhang, Y. Qu, and X. Ke, "Is β-catenin a druggable target for cancer therapy?" *Trends in Biochemical Sciences*, vol. 43, no. 8, pp. 623–634, 2018.

[89] G. Bhuvanalakshmi, N. Gamit, M. Patil et al., "Stemness, pluripotentiality, and Wnt antagonism: sFRP4, a Wnt antagonist mediates pluripotency and stemness in glioblastoma," *Cancers*, vol. 11, no. 1, 2018.

[90] G. Wang, J. Shen, J. Sun et al., "Cyclophilin a maintains glioma-initiating cell stemness by regulating Wnt/β-catenin signaling," *Clinical Cancer Research*, vol. 23, no. 21, pp. 6640–6649, 2017.

[91] M. Kamino, M. Kishida, T. Kibe et al., "Wnt-5a signaling is correlated with infiltrative activity in human glioma by inducing cellular migration and MMP-2," *Cancer Science*, vol. 102, no. 3, pp. 540–548, 2011.

[92] R. L. Carpenter and H. Lo, "Identification, functional characterization, and pathobiological significance of GLI1 isoforms in human cancers," *Vitamins and Hormones*, vol. 88, pp. 115–140, 2012.

[93] T. K. Rimkus, R. L. Carpenter, S. Sirkisoon et al., "Truncated glioma-associated oncogene homolog 1 (tGLI1) mediates mesenchymal glioblastoma via transcriptional activation of CD44," *Cancer Research*, vol. 78, no. 10, pp. 2589–2600, 2018.

[94] S. R. Sirkisoon, R. L. Carpenter, T. Rimkus et al., "Interaction between STAT3 and GLI1/tGLI1 oncogenic transcription factors promotes the aggressiveness of triple-negative breast cancers and HER2-enriched breast cancer," *Oncogene*, vol. 37, no. 19, pp. 2502–2514, 2018.

[95] R. L. Carpenter, I. Paw, H. Zhu et al., "The gain-of-function GLI1 transcription factor TGLI1 enhances expression of VEGF-C and TEM7 to promote glioblastoma angiogenesis," *Oncotarget*, vol. 6, no. 26, pp. 22653–22665, 2015.

[96] K. Wang, L. Pan, X. Che, D. Cui, and C. Li, "Sonic Hedgehog/GLI1 signaling pathway inhibition restricts cell migration and invasion in human gliomas," *Neurological Research*, vol. 32, no. 9, pp. 975–980, 2010.

[97] H. Uchida, K. Arita, S. Yunoue et al., "Role of sonic hedgehog signaling in migration of cell lines established from CD133-positive malignant glioma cells," *Journal of Neuro-Oncology*, vol. 104, no. 3, pp. 697–704, 2011.

[98] Y. Wang, X. Sui, Y. Sui et al., "BRD4 induces cell migration and invasion in HCC cells through MMP-2 and MMP-9 activation

mediated by the Sonic hedgehog signaling pathway," *Oncology Letters*, vol. 10, no. 4, pp. 2227–2232, 2015.

[99] Y. Tang, S. Gholamin, and S. Schubert, "Epigenetic targeting of Hedgehog pathway transcriptional output through BET bromodomain inhibition," *Nature Medicine*, vol. 20, no. 7, pp. 732–740, 2014.

[100] M. Malatesta, C. Steinhauer, F. Mohammad, D. P. Pandey, M. Squatrito, and K. Helin, "Histone Acetyltransferase PCAF Is Required for Hedgehog-Gli-Dependent Transcription and Cancer Cell Proliferation," *Cancer Research*, vol. 73, no. 20, pp. 6323–6333, 2013.

[101] D. Smith, T. Shimamura, S. Barbera, and B. E. Bejcek, "NF-κB controls growth of glioblastomas/astrocytomas," *Molecular and Cellular Biochemistry*, vol. 307, no. 1-2, pp. 141–147, 2008.

[102] A. H. Shih and E. C. Holland, "Platelet-derived growth factor (PDGF) and glial tumorigenesis," *Cancer Letters*, vol. 232, no. 2, pp. 139–147, 2006.

[103] R. Bonavia, M. M. Inda, S. Vandenberg et al., "EGFRvIII promotes glioma angiogenesis and growth through the NF-κB, interleukin-8 pathway," *Oncogene*, vol. 31, no. 36, pp. 4054–4066, 2012.

[104] M. S. Carro, W. K. Lim, M. J. Alvarez et al., "The transcriptional network for mesenchymal transformation of brain tumours," *Nature*, vol. 463, no. 7279, pp. 318–325, 2010.

[105] K. P. L. Bhat, V. Balasubramaniyan, B. Vaillant et al., "Mesenchymal differentiation mediated by NF-κB promotes radiation resistance in glioblastoma," *Cancer Cell*, vol. 24, no. 3, pp. 331–346, 2013.

[106] A. Tchoghandjian, C. Jennewein, I. Eckhardt, K. Rajalingam, and S. Fulda, "Identification of non-canonical NF-κB signaling as a critical mediator of Smac mimetic-stimulated migration and invasion of glioblastoma cells," *Cell Death & Disease*, vol. 4, no. 3, pp. e564–e564, 2013.

[107] L. Nogueira, P. Ruiz-Ontañon, A. Vazquez-Barquero et al., "Blockade of the NFκB pathway drives differentiating glioblastoma-initiating cells into senescence both in vitro and in vivo," *Oncogene*, vol. 30, no. 32, pp. 3537–3548, 2011.

[108] J. Kim, X. Jin, Y. Sohn et al., "Tumoral RANKL activates astrocytes that promote glioma cell invasion through cytokine signaling," *Cancer Letters*, vol. 353, no. 2, pp. 194–200, 2014.

[109] A. Vehlow and N. Cordes, "Invasion as target for therapy of glioblastoma multiforme," *Biochimica et Biophysica Acta (BBA)—Reviews on Cancer*, vol. 1836, no. 2, pp. 236–244, 2013.

[110] B. J. Gill, D. J. Pisapia, H. R. Malone et al., "MRI-localized biopsies reveal subtype-specific differences in molecular and cellular composition at the margins of glioblastoma," *Proceedings of the National Academy of Sciences of the United States of America*, vol. 111, no. 34, pp. 12550–12555, 2014.

[111] S. Darmanis, "Single-cell RNA-Seq analysis of infiltrating neoplastic cells at the migrating front of human glioblastoma," *Cell Reports*, vol. 21, no. 5, pp. 1399–1410, 2017.

[112] P. Ruiz-Ontañon, J. L. Orgaz, B. Aldaz et al., "Cellular plasticity confers migratory and invasive advantages to a population of glioblastoma-initiating cells that infiltrate peritumoral tissue," *Stem Cells*, vol. 31, no. 6, pp. 1075–1085, 2013.

[113] S. Bao, Q. Wu, R. E. McLendon et al., "Glioma stem cells promote radioresistance by preferential activation of the DNA damage response," *Nature*, vol. 444, no. 7120, pp. 756–760, 2006.

[114] C. Angelucci, A. D'Alessio, G. Lama et al., "Cancer stem cells from peritumoral tissue of glioblastoma multiforme: the possible missing link between tumor development and progression," *Oncotarget* , vol. 9, no. 46, 2018.

[115] O. Eidel, S. Burth, J. Neumann et al., "Tumor infiltration in enhancing and non-enhancing parts of glioblastoma: a correlation with histopathology," *PLoS ONE*, vol. 12, no. 1, Article ID e0169292, 2017.

[116] P. J. Kelly, C. Daumas-Duport, D. B. Kispert, B. A. Kall, B. W. Scheithauer, and J. J. Illig, "Imaging-based stereotaxic serial biopsies in untreated intracranial glial neoplasms," *Journal of Neurosurgery*, vol. 66, no. 6, pp. 865–874, 1987.

[117] N. L. Martirosyan, D. D. Cavalcanti, J. M. Eschbacher et al., "Use of in vivo near-infrared laser confocal endomicroscopy with indocyanine green to detect the boundary of infiltrative tumor," *Journal of Neurosurgery*, vol. 115, no. 6, pp. 1131–1138, 2011.

[118] P. Lemercier, S. P. Maya, J. T. Patrie, L. Flors, and C. Leiva-Salinas, "Gradient of apparent diffusion coefficient values in peritumoral edema helps in differentiation of glioblastoma from solitary metastatic lesions," *American Journal of Roentgenology*, vol. 203, no. 1, pp. 163–169, 2014.

[119] I. Blystad, J. B. Warntjes, Ö. Smedby et al., "Quantitative MRI for analysis of peritumoral edema in malignant gliomas," *PLoS ONE*, vol. 12, no. 5, p. e0177135, 2017.

[120] P. D. Chang, D. S. Chow, P. H. Yang, C. G. Filippi, and A. Lignelli, "Predicting glioblastoma recurrence by early changes in the apparent diffusion coefficient value and signal intensity on FLAIR images," *American Journal of Roentgenology*, vol. 208, no. 1, pp. 57–65, 2017.

[121] H. Akbari, L. Macyszyn, X. Da et al., "Imaging surrogates of infiltration obtained via multiparametric imaging pattern analysis predict subsequent location of recurrence of glioblastoma," *Neurosurgery*, vol. 78, no. 4, pp. 572–580, 2016.

[122] K. Kallenberg, T. Goldmann, J. Menke et al., "Glioma infiltration of the corpus callosum: early signs detected by DTI," *Journal of Neuro-Oncology*, vol. 112, no. 2, pp. 217–222, 2013.

[123] E. Konukoglu, O. Clatz, P. Bondiau, H. Delingette, and N. Ayache, "Extrapolating glioma invasion margin in brain magnetic resonance images: Suggesting new irradiation margins," *Medical Image Analysis*, vol. 14, no. 2, pp. 111–125, 2010.

[124] G. Nagashima, R. Suzuki, H. Hokaku et al., "Graphic analysis of microscopic tumor cell infiltration, proliferative potential, and vascular endothelial growth factor expression in an autopsy brain with glioblastoma," *Surgical Neurology*, vol. 51, no. 3, pp. 292–299, 1999.

[125] J. Pallud, P. Varlet, B. Devaux et al., "Diffuse low-grade oligodendrogliomas extend beyond MRI-defined abnormalities," *Neurology*, vol. 74, no. 21, pp. 1724–1731, 2010.

[126] S. J. Price, A. M. Young, W. J. Scotton et al., "Multimodal MRI can identify perfusion and metabolic changes in the invasive margin of glioblastomas," *Journal of Magnetic Resonance Imaging*, vol. 43, no. 2, pp. 487–494, 2016.

[127] A. L. Baldock, K. Yagle, D. E. Born et al., "Invasion and proliferation kinetics in enhancing gliomas predict IDH1 mutation status," *Neuro-Oncology*, vol. 16, no. 6, pp. 779–786, 2014.

[128] J. Pérez-Beteta, D. Molina-García, J. A. Ortiz-Alhambra et al., "Tumor surface regularity at MR imaging predicts survival and response to surgery in patients with glioblastoma," *Radiology*, vol. 288, no. 1, pp. 218–225, 2018.

[129] P. R. Jackson, J. Juliano, A. Hawkins-Daarud, R. C. Rockne, and K. R. Swanson, "Patient-specific mathematical neuro-oncology: using a simple proliferation and invasion tumor model to inform clinical practice," *Bulletin of Mathematical Biology*, vol. 77, no. 5, pp. 846–856, 2015.

[130] B. M. Ellingson, T. F. Cloughesy, A. Lai, P. L. Nghiemphu, and W. B. Pope, "Cell invasion, motility, and proliferation level estimate

(CIMPLE) maps derived from serial diffusion MR images in recurrent glioblastoma treated with bevacizumab," *Journal of Neuro-Oncology*, vol. 105, no. 1, pp. 91–101, 2011.

[131] A. Bauer, K. J. Langen, and H. Bidmon, "18F-CPFPX PET identifies changes in cerebral A1 adenosine receptor density caused by glioma invasion," *The Journal of Nuclear Medicine*, vol. 46, no. 3, pp. 450–454, 2005.

[132] F. Zhao, M. Li, Z. Wang et al., "18F-Fluorothymidine PET-CT for Resected Malignant Gliomas before Radiotherapy: Tumor Extent according to Proliferative Activity Compared with MRI," *PLoS ONE*, vol. 10, no. 3, p. e0118769, 2015.

[133] M. Harat, B. Malkowski, I. Wiatrowska, R. Makarewicz, and K. Roszkowski, "Relationship between glioblastoma dose volume parameters measured by dual time point Fluoroethylthyrosine-PET and clinical outcomes," *Frontiers in Neurology*, vol. 8, p. 756, 2017.

[134] M. Christensen, D. O. Kamson, M. Snyder et al., "Tryptophan PET-defined gross tumor volume offers better coverage of initial progression than standard MRI-based planning in glioblastoma patients," *Journal of Radiation Oncology*, vol. 3, no. 2, pp. 131–138, 2014.

[135] I. H. Lee, M. Piert, D. Gomez-Hassan et al., "Association of 11C-methionine PET uptake with site of failure after concurrent temozolomide and radiation for primary glioblastoma multiforme," *International Journal of Radiation Oncology, Biology, Physics*, vol. 73, no. 2, pp. 479–485, 2009.

[136] S. J. Smith, M. Diksin, S. Chhaya, S. Sairam, M. A. Estevez-Cebrero, and R. Rahman, "The invasive region of glioblastoma defined by 5ALA guided surgery has an altered cancer stem cell marker profile compared to central tumour," *International Journal of Molecular Sciences*, vol. 18, no. 11, 2017.

[137] W. Stummer, U. Pichlmeier, T. Meinel, O. D. Wiestler, F. Zanella, and H.-J. Reulen, "Fluorescence-guided surgery with 5-aminolevulinic acid for resection of malignant glioma: a randomised controlled multicentre phase III trial," *The Lancet Oncology*, vol. 7, no. 5, pp. 392–401, 2006.

[138] D. W. Roberts, P. A. Valdés, B. T. Harris et al., "Coregistered fluorescence-enhanced tumor resection of malignant glioma: relationships between δ-aminolevulinic acid-induced protoporphyrin IX fluorescence, magnetic resonance imaging enhancement, and neuropathological parameters: clinical article," *Journal of Neurosurgery*, vol. 114, no. 3, pp. 595–603, 2011.

[139] M. J. Colditz and R. L. Jeffree, "Aminolevulinic acid (ALA)–protoporphyrin IX fluorescence guided tumour resection. Part 1: Clinical, radiological and pathological studies," *Journal of Clinical Neuroscience*, vol. 19, no. 11, pp. 1471–1474, 2012.

[140] S. B. Hauser, R. A. Kockro, B. Actor, J. Sarnthein, and R. Bernays, "Combining 5-aminolevulinic acid fluorescence and intraoperative magnetic resonance imaging in glioblastoma surgery," *Neurosurgery*, vol. 78, no. 4, pp. 475–483, 2016.

[141] J. Quick-Weller, S. Lescher, M. Forster, J. Konczalla, V. Seifert, and C. Senft, "Combination of 5-ALA and iMRI in re-resection of recurrent glioblastoma," *British Journal of Neurosurgery*, vol. 30, no. 3, pp. 313–317, 2016.

[142] B. Kiesel, M. Mischkulnig, A. Woehrer et al., "Systematic histopathological analysis of different 5-aminolevulinic acid–induced fluorescence levels in newly diagnosed glioblastomas," *Journal of Neurosurgery*, vol. 129, no. 2, pp. 341–353, 2018.

[143] M. D. Jenkinson, D. G. Barone, A. Bryant et al., "Intraoperative imaging technology to maximise extent of resection for glioma," *Cochrane Database of Systematic Reviews*, vol. 1, article CD012788, 2018.

[144] F. Stockhammer, M. Misch, P. Horn, A. Koch, N. Fonyuy, and M. Plotkin, "Association of F18-fluoro-ethyl-tyrosin uptake and 5-aminolevulinic acid-induced fluorescence in gliomas," *Acta Neurochirurgica*, vol. 151, no. 11, pp. 1377–1383, 2009.

[145] K. Roessler, A. Becherer, M. Donat, M. Cejna, and I. Zachenhofer, "Intraoperative tissue fluorescence using 5-aminolevolinic acid (5-ALA) is more sensitive than contrast MRI or amino acid positron emission tomography ((18)F-FET PET) in glioblastoma surgery," *Neurological Research*, vol. 34, no. 3, pp. 314–317, 2012.

[146] F. W. Floeth, M. Sabel, C. Ewelt et al., "Comparison of 18F-FET PET and 5-ALA fluorescence in cerebral gliomas," *European Journal of Nuclear Medicine and Molecular Imaging*, vol. 38, no. 4, pp. 731–741, 2011.

[147] J. A. Neira, T. H. Ung, and J. S. Sims, "Aggressive resection at the infiltrative margins of glioblastoma facilitated by intraoperative fluorescein guidance," *Journal of Neurosurgery*, vol. 127, no. 1, pp. 111–122, 2017.

[148] H. Yano, N. Nakayama, N. Ohe, K. Miwa, J. Shinoda, and T. Iwama, "Pathological analysis of the surgical margins of resected glioblastomas excised using photodynamic visualization with both 5-aminolevulinic acid and fluorescein sodium," *Journal of Neuro-Oncology*, vol. 133, no. 2, pp. 389–397, 2017.

[149] A. V. Moiyadi, P. M. Shetty, A. Mahajan, A. Udare, and E. Sridhar, "Usefulness of three-dimensional navigable intraoperative ultrasound in resection of brain tumors with a special emphasis on malignant gliomas," *Acta Neurochirurgica*, vol. 155, no. 12, pp. 2217–2225, 2013.

[150] O. Solheim, T. Selbekk, A. S. Jakola, and G. Unsgård, "Ultrasound-guided operations in unselected high-grade gliomas—overall results, impact of image quality and patient selection," *Acta Neurochirurgica*, vol. 152, no. 11, pp. 1873–1886, 2010.

[151] M. Del Bene, "Advanced ultrasound imaging in glioma surgery: beyond gray-scale B-mode," *Frontiers in Oncology*, vol. 8, p. 576, 2018.

[152] F. Prada, L. Mattei, and M. D. Bene, "Intraoperative cerebral glioma characterization with contrast enhanced ultrasound," *BioMed Research International*, vol. 2014, Article ID 484261, 9 pages, 2014.

[153] D. Lindner, C. Trantakis, C. Renner et al., "Application of intraoperative 3D ultrasound during navigated tumor resection," *Minimally Invasive Neurosurgery*, vol. 49, no. 4, pp. 197–202, 2006.

[154] F. Prada, V. Vitale, M. Del Bene et al., "Contrast-enhanced MR imaging versus contrast-enhanced US: a comparison in glioblastoma surgery by using intraoperative fusion imaging," *Radiology*, vol. 285, no. 1, pp. 242–249, 2017.

[155] N. Sanai, J. Eschbacher, G. Hattendorf et al., "Intraoperative confocal microscopy for brain tumors: a feasibility analysis in humans," *Operative Neurosurgery*, vol. 68, no. 2, pp. ons282–ons290, 2011.

[156] H. Schlosser, O. Suess, P. Vajkoczy, F. K. Landeghem, M. Zeitz, and C. Bojarski, "Confocal Neurolasermicroscopy in Human Brain – Perspectives for Neurosurgery on a Cellular Level (including additional Comments to this article)," *Central European Neurosurgery*, vol. 71, no. 01, pp. 13–19, 2010.

[157] T. Sankar, P. M. Delaney, R. W. Ryan et al., "Miniaturized handheld confocal microscopy for neurosurgery," *Neurosurgery*, vol. 66, no. 2, pp. 410–418, 2010.

[158] K. S. Yashin, E. B. Kiseleva, A. A. Moiseev et al., "Quantitative nontumorous and tumorous human brain tissue assessment

using microstructural co- and cross-polarized optical coherence tomography," *Scientific Reports*, vol. 9, no. 1, 2019.

[159] C. Kut, K. L. Chaichana, J. Xi et al., "Detection of human brain cancer infiltration ex vivo and in vivo using quantitative optical coherence tomography," *Science Translational Medicine*, vol. 7, no. 292, Article ID 292ra100, 2015.

[160] W. Yuan, C. Kut, W. Liang, and X. Li, "Robust and fast characterization of OCT-based optical attenuation using a novel frequency-domain algorithm for brain cancer detection," *Scientific Reports*, vol. 7, no. 1, 2017.

[161] H. J. Böhringer, E. Lankenau, F. Stellmacher, E. Reusche, G. Hüttmann, and A. Giese, "Imaging of human brain tumor tissue by near-infrared laser coherence tomography," *Acta Neurochirurgica*, vol. 151, no. 5, pp. 507–517, 2009.

[162] F. Lefranc, E. Le Rhun, R. Kiss, and M. Weller, "Glioblastoma quo vadis: Will migration and invasiveness reemerge as therapeutic targets?" *Cancer Treatment Reviews*, vol. 68, pp. 145–154, 2018.

[163] E. Mandonnet, L. Capelle, and H. Duffau, "Extension of paralimbic low grade gliomas: toward an anatomical classification based on white matter invasion patterns," *Journal of Neuro-Oncology*, vol. 78, no. 2, pp. 179–185, 2006.

[164] K. L. Chaichana, I. Jusue-Torres, R. Navarro-Ramirez et al., "Establishing percent resection and residual volume thresholds affecting survival and recurrence for patients with newly diagnosed intracranial glioblastoma," *Neuro-Oncology*, vol. 16, no. 1, pp. 113–122, 2014.

[165] D. S. Xu, A. Awad, C. Mehalechko et al., "An extent of resection threshold for seizure freedom in patients with low-grade gliomas," *Journal of Neurosurgery*, vol. 128, no. 4, pp. 1084–1090, 2018.

[166] Y. M. Li, D. Suki, K. Hess, and R. Sawaya, "The influence of maximum safe resection of glioblastoma on survival in 1229 patients: Can we do better than gross-total resection?" *Journal of Neurosurgery*, vol. 124, no. 4, pp. 977–988, 2016.

[167] J. Yan, A. van der Hoorn, T. J. Larkin, N. R. Boonzaier, T. Matys, and S. J. Price, "Extent of resection of peritumoral diffusion tensor imaging–detected abnormality as a predictor of survival in adult glioblastoma patients," *Journal of Neurosurgery*, vol. 126, no. 1, pp. 234–241, 2017.

[168] F. Pessina, P. Navarria, L. Cozzi et al., "Maximize surgical resection beyond contrast-enhancing boundaries in newly diagnosed glioblastoma multiforme: is it useful and safe? A single institution retrospective experience," *Journal of Neuro-Oncology*, vol. 135, no. 1, pp. 129–139, 2017.

[169] A. Elson, E. Paulson, J. Bovi, M. Siker, C. Schultz, and P. S. Laviolette, "Evaluation of pre-radiotherapy apparent diffusion coefficient (ADC): patterns of recurrence and survival outcomes analysis in patients treated for glioblastoma multiforme," *Journal of Neuro-Oncology*, vol. 123, no. 1, pp. 179–188, 2015.

[170] R. Grossman, N. Shimony, D. Shir et al., "Dynamics of FLAIR volume changes in glioblastoma and prediction of survival," *Annals of Surgical Oncology*, vol. 24, no. 3, pp. 794–800, 2017.

[171] D. Mampre, J. Ehresman, G. Pinilla-Monsalve et al., "Extending the resection beyond the contrast-enhancement for glioblastoma: feasibility, efficacy, and outcomes," *British Journal of Neurosurgery*, vol. 32, no. 5, pp. 528–535, 2016.

[172] J. Pei, I. Park, H. Ryu et al., "Sublethal dose of irradiation enhances invasion of malignant glioma cells through p53-MMP 2 pathway in U87MG mouse brain tumor model," *Journal of Radiation Oncology*, vol. 10, no. 1, 2015.

[173] A. Zaboronok, T. Isobe, T. Yamamoto et al., "Proton beam irradiation stimulates migration and invasion of human U87 malignant glioma cells," *Journal of Radiation Research*, vol. 55, no. 2, pp. 283–287, 2014.

[174] G. Minniti, D. Amelio, M. Amichetti et al., "Patterns of failure and comparison of different target volume delineations in patients with glioblastoma treated with conformal radiotherapy plus concomitant and adjuvant temozolomide," *Radiotherapy & Oncology*, vol. 97, no. 3, pp. 377–381, 2010.

[175] E. L. Chang, S. Akyurek, and T. Avalos, "Evaluation of peritumoral edema in the delineation of radiotherapy clinical target volumes for glioblastoma," *International Journal of Radiation Oncology, Biology, Physics*, vol. 68, no. 1, pp. 144–150, 2007.

[176] A. R. Cabrera, J. P. Kirkpatrick, J. B. Fiveash et al., "Radiation therapy for glioblastoma: executive summary of an american society for radiation oncology evidence-based clinical practice guideline," *Practical Radiation Oncology*, vol. 6, no. 4, pp. 217–225, 2016.

[177] A. Wernicke, A. W. Smith, S. Taube, and M. P. Mehta, "Glioblastoma: Radiation treatment margins, how small is large enough?" *Practical Radiation Oncology*, vol. 6, no. 5, pp. 298–305, 2016.

[178] J. Berberat, J. McNamara, L. Remonda, S. Bodis, and S. Rogers, "Diffusion tensor imaging for target volume definition in glioblastoma multiforme," *Strahlentherapie und Onkologie*, vol. 190, no. 10, pp. 939–943, 2014.

[179] R. Jena, S. J. Price, and C. Baker, "Diffusion tensor imaging: possible implications for radiotherapy treatment planning of patients with high-grade glioma," *Clinical Oncology Journal (The Royal College of Radiologists)*, vol. 17, no. 8, pp. 581–590, 2005.

[180] M. B. Jensen, T. L. Guldberg, A. Harbøll, S. Lukacova, and J. F. Kallehauge, "Diffusion tensor magnetic resonance imaging driven growth modeling for radiotherapy target definition in glioblastoma," *Acta Oncologica*, vol. 56, no. 11, pp. 1639–1643, 2017.

[181] M. Harat, B. Małkowski, and R. Makarewicz, "Pre-irradiation tumour volumes defined by MRI and dual time-point FET-PET for the prediction of glioblastoma multiforme recurrence: A prospective study," *Radiotherapy & Oncology*, vol. 120, no. 2, pp. 241–247, 2016.

[182] O. Oehlke, M. Mix, E. Graf et al., "Amino-acid PET versus MRI guided re-irradiation in patients with recurrent glioblastoma multiforme (GLIAA) – protocol of a randomized phase II trial (NOA 10/ARO 2013-1)," *BMC Cancer*, vol. 16, no. 1, 2016.

[183] W. Wick, A. Wick, J. B. Schulz, J. Dichgans, H. P. Rodemann, and M. Weller, "Prevention of irradiation-induced glioma cell invasion by temozolomide involves caspase 3 activity and cleavage of focal adhesion kinase," *Cancer Research*, vol. 62, no. 6, pp. 1915–1919, 2002.

[184] S. Hombach-Klonisch, M. Mehrpour, S. Shojaei et al., "Glioblastoma and chemoresistance to alkylating agents: Involvement of apoptosis, autophagy, and unfolded protein response," *Pharmacology & Therapeutics*, vol. 184, pp. 13–41, 2018.

[185] J. N. Sarkaria, L. S. Hu, I. F. Parney et al., "Is the blood–brain barrier really disrupted in all glioblastomas? A critical assessment of existing clinical data," *Neuro-Oncology*, vol. 20, no. 2, pp. 184–191, 2018.

[186] L. Goldwirt, K. Beccaria, A. Carpentier et al., "Preclinical impact of bevacizumab on brain and tumor distribution of irinotecan and temozolomide," *Journal of Neuro-Oncology*, vol. 122, no. 2, pp. 273–281, 2015.

[187] M. Safari and A. Khoshnevisan, "Cancer stem cells and chemoresistance in glioblastoma multiform: A review article," *Journal of Stem Cells*, vol. 10, no. 4, pp. 271–285, 2015.

[188] O. Keunen, M. Johansson, A. Oudin et al., "Anti-VEGF treatment reduces blood supply and increases tumor cell invasion in glioblastoma," *Proceedings of the National Academy of Sciences of the United States of America*, vol. 108, no. 9, pp. 3749–3754, 2011.

[189] M. Rahman, H. Azari, L. Deleyrolle, S. Millette, H. Zeng, and B. A. Reynolds, "Controlling tumor invasion: bevacizumab and BMP4 for glioblastoma," *Future Oncology*, vol. 9, no. 9, pp. 1389–1396, 2013.

[190] Q. Xie, S. Mittal, and M. E. Berens, "Targeting adaptive glioblastoma: An overview of proliferation and invasion," *Neuro-Oncology*, vol. 16, no. 12, pp. 1575–1584, 2014.

Hindawi
Journal of Oncology
Volume 2019, Article ID 9342796, 13 pages
https://doi.org/10.1155/2019/9342796

Review Article

Convection-Enhanced Delivery in Malignant Gliomas: A Review of Toxicity and Efficacy

Minghan Shi[1] **and Léon Sanche**[2]

[1]*Department of Radiation Oncology, The Second Affiliated Hospital of Zhejiang University, School of Medicine, Hangzhou, China*
[2]*Department of Nuclear Medicine and Radiobiology, Université de Sherbrooke, Sherbrooke, QC, Canada*

Correspondence should be addressed to Minghan Shi; minghan_shi@zju.edu.cn

Received 14 March 2019; Revised 6 May 2019; Accepted 25 June 2019; Published 22 July 2019

Academic Editor: Claudio Festuccia

Malignant gliomas are undifferentiated or anaplastic gliomas. They remain incurable with a multitude of modalities, including surgery, radiation, chemotherapy, and alternating electric field therapy. Convection-enhanced delivery (CED) is a local treatment that can bypass the blood-brain barrier and increase the tumor uptake of therapeutic agents, while decreasing exposure to healthy tissues. Considering the multiple choices of drugs with different antitumor mechanisms, the supra-additive effect of concomitant radiation and chemotherapy, CED appears as a promising modality for the treatment of brain tumors. In this review, the CED-related toxicities are summarized and classified into immediate, early, and late side effects based on the time of onset, and local and systemic toxicities based on the location of toxicity. The efficacies of CED of various therapeutic agents including targeted antitumor agents, chemotherapeutic agents, radioisotopes, and immunomodulators are covered. The phase III trial PRECISE compares CED of IL13-PE38QQR, an interleukin-13 conjugated to *Pseudomonas aeruginosa* exotoxin A, to Gliadel® Wafer, a polymer loaded with carmustine. However, in this case, CED had no significant median survival improvement (11.3 months vs. 10 months) in patients with recurrent glioblastomas. In phase II studies, CED of recombinant poliovirus (PVSRIPO) had an overall survival of 21% vs. 14% for the control group at 24 months, and 21% vs. 4% at 36 months. CED of Tf-diphtheria toxin had a response rate of 35% in recurrent malignant gliomas patients. On the other hand, the TGF-β2 inhibitor Trabedersen, HSV-1-tk ganciclovir, and radioisotope ^{131}I-chTNT-1/B mAb had a limited response rate. With this treatment, patients who received CED of the chemotherapeutic agent paclitaxel and immunomodulator, oligodeoxynucleotides containing CpG motifs (CpG-ODN), experienced intolerable toxicity. Toward the end of this article, an ideal CED treatment procedure is proposed and the methods for quality assurance of the CED procedure are discussed.

1. Introduction

Despite the fast development of several modalities for cancer treatment, such as chemotherapy, immunotherapy, and targeted therapy, pharmaceutical agents available for brain tumor treatment remain rare. The failure of the application of these agents in brain tumor is partially due to the existence of the blood-brain barrier (BBB), which prevents them from entering the tumor site. This problem led to the development of strategies to open temporarily the BBB, including osmotic and ultrasonic BBB disruption [1–4]. During the osmotic BBB disruption procedure, hyperosmotic agents such as mannitol are infused and a temporary cell membrane retraction is induced, creating a physical opening between the endothelium cells [1–3]. In the case of ultrasonic BBB disruption, pulsed ultrasound is applied in combination with infusion of microbubbles to disrupt the BBB, thus increasing the intratumoral concentration of the therapeutic agents [4]. Rather than disrupting the BBB, another strategy consists of bypassing the BBB. In the early 1990s, Oldfield and his research team proposed a new technique to traverse the BBB, convection-enhanced delivery (CED) [5], by which interstitial infusion of the agent by a syringe pump creates a pressure gradient, permitting enhanced distribution of the brain. The technical parameters of the CED procedure have been reviewed by Allard E. et al. [6].

With the emergence of novel radiation therapy techniques, such as intensity-modulated radiation therapy (IMRT), volumetric-modulated arc therapy (VMAT), and 4π radiation therapy (RT) [7], the precision of target volume delineation has largely improved, which in some aspects could make CED of therapeutic agents less attractive. However, the rationale behind CED remains a potentially useful way to enhance drug delivery to the brain. Besides increased tumor uptake of antitumor agents, by penetration of the BBB [8], the localization of the drug provides an effective condition for concomitant chemoradiation therapy and the benefits of its supra-additive effect [8, 9].

2. Preclinical Studies

In animal studies, two delivery systems were commonly employed for safety and efficiency evaluation. (1) A micro infusion syringe connected to a micro infusion pump: Our group optimized this technique by using flat tip 33 Ga needle gas-tight Hamilton syringe, to inject 10 μL of therapeutic agent at an infusion rate of 0.5 μl/min, for a duration of 20 mins [8]. These parameters prevented reflux from the injection site, permitting a large distribution volume in the tumor site of a rat brain. (2) An ALZET® osmotic pump, a device embedded subcutaneously: It provides an infusion time of up to a week [10, 11] and hence has the advantage of long-term infusion without recurrent operations. The longer infusion time means less reflux and a larger diffusion volume, which is a key parameter for brain tumor CED in humans. Since the brain volume of a rat at 8 weeks is only ~600 mm^3 [12], the difference in the distribution volume, after 20 mins infusion, with a syringe or an osmotic pump can be indistinguishable. Yang et al. compared survival after CED injection of carboplatin in F98 glioma bearing rats with a syringe, to that obtained with an ALZET® osmotic pump. The median survival time (MeST) for controls was 23 days after cell implantation. CED of carboplatin with the syringe extended the MeST to 46 days, whereas the ALZET® osmotic pump further increased it to 59 days. However, the osmotic pump delivered 84 μg of carboplatin, as opposed to 20 μg by the CED with the syringe [13], suggesting that prolonged administration is therapeutically more effective.

In experimental studies, catheter design plays an important role in reducing the reflux of the infusate and increasing the convection volume [14]. The most common is the one port catheter, which consists of a cannula with one port at the tip. This catheter has been well studied in gels and is widely used in animal studies [15–17]. The computational and experimental studies in gels and rats showed that reflux decreases as the diameter of the needle decreases [15, 18, 19]. Thus, to prevent reflux within the catheter, a diameter smaller than 30 Ga was usually chosen, which limited the flow rate to 0.5 μL/min [20, 21]. To further reduce reflux, Krauze and his colleagues designed a stepped cannula [22]. Compared to a simple 32 gauge needle, the step-design cannula was able to increase the reflux-free flow rate from 5 μL/min to 50 μL/min in agarose gel and from 0.5 μL/min to <50 μL/min in the rat brain [15, 17, 19]. To increase the distribution volume, multiple-pore catheter was designed. It has five pores of 0.2 mm diameter on opposite sides of the tip [23]. Computational analysis predicted that the drug distribution from the multiple pores design in the caudate nucleus increased the distribution volume by 26%. However, an experimental study with this type of catheter in gels has shown that the infusate can only be released from the proximal pores leaving the rest of the pores useless [24]. Another design increased the distribution volume by using a hollow fiber catheter, with millions of nanoscale pores (450 nm) [25]. Seunguk and his colleagues found that the distribution volume of a dye injected in a gel by such a hollow fiber catheter was 2.7 times larger than that obtained with a one port catheter. However, further studies are required for clinical applications, because longer catheters would be required in humans, and the physical characteristics of the drug distribution may change. In clinical settings, before the administration of chemotherapy, a cavity is left by tumor resection, which makes the administration of a chemotherapeutic agent by CED complicated. To alleviate the problem, a balloon-tipped catheter with an inflatable balloon attached to the tip of the catheter was designed. The inflatable balloon fills the resection cavity and thus reduces reflux [26, 27].

Halle et al. systemically reviewed preclinical CED studies and found that methodological parameters such as catheter design, infusion rate, and infusion duration varied among different studies. Data on endpoint measurements of drug diffusion and adverse effects are often missing in many preclinical studies [28]. These parameters are crucial for carrying out preclinical investigations and further clinical studies based on promising results from animal experiments. The authors also suggested that *in vivo* studies with larger animal brains should be carried out before undertaking clinical trials.

Besides the different techniques employed in CED, different types of medications have been tested: chemotherapeutic drugs, antibodies, toxins, vaccines, etc. The standard treatment of glioblastomas (GBM), the most common and aggressive glioma in adults, is composed of several combined modalities, which may include surgery, RT, concomitant and adjuvant temozolomide (TMZ) chemotherapy, and more recently alternating electric field therapy. The current standard treatment includes concurrent and adjuvant TMZ chemotherapy and it is therefore reasonable to compare CED with this agent in preclinical studies. Saito et al. in 2004 studied CED delivery of tumor necrosis factor-related apoptosis-inducing ligand (TRAIL) and systemic delivery of TMZ in a U87MG intracranial xenograft rat model [29]. Both CED of TRAIL and systemic delivery of TMZ increased survival. More importantly, the synergistic effect of the chemotherapeutic agent cisplatin and TRAIL has been demonstrated in a glioma model. In this study, a combination of CED of TRAIL with systemic delivery of TMZ further increased the survival ($P = 0.032$) [30]. Barth and his research team in 2011 studied RT plus oral delivery of TMZ in daily doses of 80 mg/ kg body weight for 5 d or CED of 1.5 mg TMZ in 15 μL at a flow rate of 0.5 μL/min for 30 min in F98 glioma bearing Fischer rats [13]. Radiation

was performed at 6, 7, and 8 days after implantation with a daily dose of 5 Gy. They obtained an MeST of 23 days for oral TMZ plus radiation and 27 days for CED of TMZ plus radiation, compared to 21 days for radiation alone. Although a modest increase of MeST in the CED group was observed, no significant difference was found. Indeed, due to its inherent ability for crossing the BBB, TMZ may not be a good candidate for CED and the study of Barth and his research group confirmed this hypothesis. Other studies focused on a nanocarrier for the delivery of TMZ by CED, i.e., the polymeric nanoparticle vector [31], TMZ-loaded photopolymerizable PEG-DMA-based hydrogel [32], and liposomes [33]. They all demonstrated various degrees of antitumor efficacy compared to free TMZ or reduced toxicity to normal brain, but failed to demonstrate the advantage of CED of TMZ over oral delivery of TMZ, which is the standard method of administration in the clinic.

The well-studied chemotherapeutic agents by CED are platinum-based drugs, such as cisplatin, carboplatin, and oxaliplatin, delivered in glioma bearing rats which were largely investigated by the groups of Barth and Elleaume [11, 13, 20, 21, 34–36], Lonser [17], Tomita [37], and ours [8, 38, 39]. These authors measured the combined effect of radiation and platinum drugs. However, due to differences in tumor model, doses of infusion, and protocol design, the effectiveness of these drugs cannot be determined from a comparison of the results of the different groups. Moreover, CED of these drugs was not compared to other routes of delivery such as intra-arterial injection and intravenous infusion. For this reason, in our laboratory, we performed a series of studies comparing intravenous (iv), intra-arterial (ia), and CED of different platinum drugs, as well as their combinational effect with radiation [8, 39–41]. It was further observed that carboplatin was the most effective platinum drug compared to cisplatin and oxaliplatin. When encapsulated within a liposome, carboplatin still had the advantage over the others; however, the other platinum drugs were not encapsulated nor designed for CED.

There are four main theories regarding the mechanisms of the synergistic action of platinum drugs and radiation: radiation sensitization of the hypoxic cells by platinum drugs [42–45]; fixing by platinum drugs of the radiation-induced sublethal DNA damage [46, 47]; radiation-induced formation of toxic platinum adducts [48, 49]; and direct radiation sensitization by platinum drugs [50–54].

Tippayamontri et al. studied the amount of DNA-platinum adducts formed in the nucleus of cancer cells over time, both in vitro and in vivo. The efficiency of RT was found to be proportional to the amount of the Pt drug bound to the DNA of the cancer cells. When mice bearing a human colorectal HCT116 tumor were irradiated at the time of highest yields of DNA-platinum adducts, the synergy between radiation and cisplatin or oxaliplatin and their liposomal formulation was the largest [55, 56]. Based on their findings, CED of these agents was carried out to further increase tumor uptake. However, survival increase of F98 glioma bearing Fisher rats was not significant. This may reflect the ceiling of radiation enhancement based on DNA-platinum yield [8].

3. Clinical Studies

3.1. Clinical Protocols. Before carrying out clinical trials with CED, a carefully designed clinical protocol is surely a prerequisite to achieve significant results, especially for new treatment techniques, where many parameters need to be adjusted from animal to human protocols. The catheter designs and placement, flow rate, choice of therapeutic agent, infusion volume, and visualization of the infusion volume are all key parameters that need to be accurately assessed. Considering the problems encountered in the setting of these parameters, but not limited to them, the PRECISE phase III clinical trial failed to demonstrate an advantage of CED over standard-of-care treatment [57].

Ren et al. in 2003 designed and published a phase I/II protocol of CED of a liposomally encapsulated replication-disabled Semliki Forest virus vector, carrying the human interleukin 12 gene (LSFV-IL12). This protocol involved treatment of recurrent or progressive GBM to evaluate the safety, maximum tolerated dose (MTD), and antitumor efficacy [58]. They designed an infusion volume of 11 mL at a maximum infusion rate of 0.5 mL/h for a total of 24 h. However, the results of this study were not further analyzed and disseminated.

Another phase I clinical trial protocol was proposed by White et al. in 2012, after a series of successful animal studies of CED of carboplatin [59]. The principal research objectives were to determine the safety, tolerability, and MTD, via dose escalation and further facilitate the safe application of a phase II protocol. In addition, the efficacy, carboplatin distribution, and visualization of infusate will also be evaluated with a carboplatin delivery of 8 h/d for 3 consecutive days at a maximum infusion rate of 0.6 mL/h for no more than 20 mL of infusate per day.

3.2. Toxicity Studies in Clinical Trials. The safety and tolerability of various therapeutic agents, including antibodies, targeted toxins, interleukins, chemotherapeutic drugs, targeted radioisotopes, and vaccines (Table 1), have been studied in clinical trials in the last two decades.

Based on their results of intratumoral injection of monoclonal antibodies in patients with advanced malignant glioma, Wersall et al. classified side effects as immediate (<2 h) or late (5-48 h) and we believe that CED could have a similar evolution [60]. On the other hand, Kunwar S. et al. defined three phases of toxicity based on the time of onset: pre-CED, peri-CED, and post-CED [61]. Here, based on their classifications and the review of all published CED clinical trials, we reclassify CED-related toxicities as immediate, early, and late side effects.

(a) Immediate side effects occur within hours of the placement of catheters. Physical damage to the brain tissue and cerebral hemorrhage by the catheter are possible causes related to symptoms such as headache, seizure, and neurological toxicities [61].

(b) Early side effects occur hours to days after CED. Mechanical stress caused by the infusion of fluid leads to common complaints such as headache, seizure, worsening of neurological symptoms, shivering, and mild fever [62, 63].

Table 1: Summary of clinical studies of CED in the treatment of malignant gliomas.

Reference	Therapeutic agent	Trial phase	Diagnosis (n)	Infusion volume	Infusion rate	Treatment responders (n/total pts)	MeST	Drug-related adverse events (rate)
Laske et al., 1997 [64]	Tf-CRM107 (TransMID)	I/II	GBM (9) AA (5) AO (1)	5-180 mL	0.24-0.6 mL/h	9/15	74 wks (responders) 36 wks (non-responders)	Seizures (27%), local toxicity (20%), transit elevation of ALT, AST (93%), mild hypoalbuminemia (80%)
Weaver et al., 2003 [70]	Tf-CRM107 (TransMID)	II	Recurrent AA/GBM (44)	5-180 mL	0.2 mL/h/catheter 2 catheters	12/34	37 wks	Symptomatic progressive cerebral edema (24%), seizure (9%)
Rand et al., 2000 [65]	IL-4 PE38KDEL (NBI-3001)	I	GBM (9)	30-185 mL	0.3-0.6 mL/h	-	-	Headache (11%), seizures (22%), anomia (11%), dysphasia (11%), communicating hydrocephalus (22%), weakness (22%), nausea (11%)
Weber et al., 2001 [66] Weber et al., 2003 [90]	IL-4 PE38KDEL (NBI-3001)	I	GBM (25) AA (6)	40-100 mL		-	-	Headache (45%), seizures (84%), weakness (32%), aphasia (23%), speech disorder (10%), hypoesthesia (16%), coma (10%), wound infection (10%), pyrexia (10%), nausea (23%)
Kunwar et al., 2003 [68] Kunwar et al., 2006 [61] Kunwar et al., 2007 [80]	IL13-PE38QQR	I	MG (5) GBM (46)	19.2-51.8 mL 72 mL	0.4-0.54 mL/h intratumoral 0.75 mL/h intraparenchymal	-	-	Headache (41 %), convulsion (14 %), sensory disturbance (25 %), aphasia/speech disorder (18 %), asthenia (16 %), hemiparesis (14 %), facial paresis (12 %), memory impairment (8 %), pyrexia (8 %), nausea (8 %)
Vogelbaum et al., 2007 [81]	IL13-PE38QQR	I	GBM (22) anaplastic mixed OA (1)	72 mL	0.75 mL/h	-	-	Headache (50%), fatigue (73%), nausea (41%), convulsion (14%), confusion (14%), aphasia (14%), dyspepsia (14%), pyrexia (14%)
Kunwar et al., 2010 [57]	IL13-PE38QQR	III	Recurrent GBM (296)	72 mL	0.75 mL/h	Not reported	36.4 wks IL13-PE38QQR vs. 35.5 wks Gliadel wafer	Headache (0.4%), aphasia (1.2%), hemiparesis (0.8 %), Monoparesis (0.5%), hemiplegia (0.3%), gait disturbance (0.3%), coordination abnormal (0.3%), mental status changes (0.3%)
Sampson et al., 2003 [91] Sampson et al., 2008 [92]	TP-38	I	GBM (17), AO (1), GSC (1), Metastasis (1)	40 mL	0.4 mL/h	-	-	Headache (47%), hemiparesis (20%), speech (20%), constitutional (20%), ocular/visual (13%), seizure (8%)
Voges et al., 2003 [62]	LIPO-HSV-1-*tk* GCV	I/II	GBM (8)	3.5 mL	0.025-0.6 mL/h	2/8	28.1 ± 3.0 wks	Transient worsening of motor aphasia (25%), fever (25%), leukocytosis (25%), ALT (37.5%), AST (25%), LDH (12.5%), CRP (25%)

Table 1: Continued.

Reference	Therapeutic agent	Trial phase	Diagnosis (n)	Infusion volume	Infusion rate	Treatment responders (n/total pts)	MeST	Drug-related adverse events (rate)
Lidar et al., 2004 [67]	Paclitaxel	I/II	GBM (13), AA/AO (1), Mixed AO (1)	6-6.6 mL	0.3 mL/h	11/15	32.1 wks	Chemical meningitis (40%), neurological deterioration due to peritumoral edema and necrosis (20%)
Pöpperl et al., 2005 [69] Tanner et al., 2007 [72]	Paclitaxel	II	Recurrent GBM (8)	36 mL	0.3 mL/h	0/8	42.9 wks	Temporary worsening of (pre-existing) neurological symptoms (63%), poor wound healing (25%), neurological deterioration (25%)
Patel et al., 2005 [76]	^{131}I-chTNT-1/B mAb (Cotara)	I/II	Recurrent GBM (37) primary GBM (8) AA (6)	4.5-18 mL	0.18-0.72 mL/h	1/12	37.9 wks	headache (14%), convulsions (6%), simple partial seizures (4%), aphasia (6%), weakness (6%), hemiparesis (14%), facial palsy (4%), short-term memory loss (2%), fatigue (6%), nausea (4%)
Sampson et al., 2006 [93]	I^{131}-Ch81C6		Recurrent GBM (10)	4.5-18 mL	0.18 mL/h	3/10	30.3 wks	
Pandit-Taskar et al., 2018 [77]	I^{124}-8H9	I	Diffuse intrinsic pontine glioma	0.25-4 mL	0.05-0.45 mL/h	-	-	Headache (50%), ataxia (29%), facial palsy (36%), diplopia (25%), muscle weakness (22%), dysarthria (15%), anaemia (32%), platelet count decreased (25%), white blood cells decreased (67%), ALT (32%), AST (25%), hypoalbuminaemia (61%), rash (11%), skin infection (8%), vomiting (18%)
Boiardi et al., 2005 [73]	Mitoxantrone	0	Recurrent MG (12)			-	-	Procedure problem (25%), infection (8%)
Carpentier et al., 2006 [63]	CpG-ODN	I	Recurrent GBM (24)	1 mL/catheter	0.2 mL/h/catheter	-	-	Worsening of previous neurological condition (21%), partial seizures (21%), somnolence (8%), fever (21%), fatigue (25%), nausea (4%), lymphopenia (46%), ALT (25%), AST (4%)

Table 1: Continued.

Reference	Therapeutic agent	Trial phase	Diagnosis (n)	Infusion volume	Infusion rate	Treatment responders (n/total pts)	MeST	Drug-related adverse events (rate)
Carpentier et al., 2010 [74]	CpG-ODN	II	Recurrent GBM (31)	1 mL/catheter 2 catheters	0.2 mL/h/catheter	3/31	28 wks	Worsening of previous neurological condition (65%), partial seizures (42%), general seizures (16%), fever (grade 2) (3%), fatigue (grade 2) (6%), hemorrhage leading to death 8 days after treatment (3%), lymphopenia (grade 2) (71%), lymphopenia (grade 3) (48%), ALT (10%)
Hau et al., 2007 [86]	TGF-β2 inhibitor Trabedersen	I/II	AA (5) GBM (19)	23-81 mL/cycle up to 10 cycles	0.24-0.32 mL/h	24	146.6 wks AA 44.0 wks GBM	Serious adverse events central and peripheral nervous system disorders (92%)
Bogdahn et al., 2011 [75]	TGF-β2 inhibitor Trabedersen	IIb	Recurrent/ refractory GBM, AA (145)	40 mL/cycle up to 11 cycles	0.24 mL/h	Not reported	AA: 39.1 mos (10 μM) vs. 35.2 mos (80 μM) vs. 21.7 mos (TMZ or PCV) GBM: 7.3 mos (10 μM) vs. 10.9 mos (80 μM) vs. 10 mos (TMZ or PCV)	Headache (10%), nervous system disorders (59-66%), depressed level of consciousness (4-12%), hemiparesis (22-27%), aphasia (10-15%), neurological symptom (8-17%), convulsion (8-12%), injury poisoning, and procedural complications (16-17%), infections and infestations brain abscess (7-12%), psychiatric disorders (6-12%), blood and lymphatic system disorders (5-8%)
Bruce et al., 2011 [78]	Topotecan	Ib	Recurrent GBM (10), AA (2), AE (2), AO (2)	40 mL	0.2 mL/h	-	-	Headache (31%), seizure (31%), worsened hemiparesis (31%), right-hand dyscoordination (13%), upper-extremity weakness (6%), poor wound healing (13%), intracerebral hemorrhage (6%), thrombocytopenia/leukopenia (13%), gastrointestinal symptoms (25%)
Desjardins et al., 2018 [87]	Recombinant poliovirus	II	Recurrent GBM (61)	3.25 mL	0.5 mL/h	-	12.5 mos (PVSRIPO) vs. 11.3 mos (Historical control)	Headache (52%), hemiparesis (50%), seizure (45%), dysphasia (28%), cognitive disturbance (25%), hemianopia (19%), confusion (18%), paresthesia (13%), fatigue (12%), nausea (10%)

Abbreviations. AA: anaplastic astroglioma; AE: anaplastic ependymoma; ALT: alanine aminotransferase; AST: aspartate aminotransferase; AO: anaplastic oligodendroglioma; GSC: gliosarcoma; MG: malignant glioma; n: number of patients; OA: oligoastrocytoma; pts: patients.

(c) Late side effects include mainly neurological toxicity, due to the toxicity from delivered drugs, occurring days to weeks after infusion [64–67].

Depending on the location of the toxicities related to CED, we summarized them into two categories.

(a) Local Toxicities (Common and Severe). These comprise neurological toxicities due to inflammatory reactions, necrosis, and peritumor edema [64]. Depending on the location of the tumor and site of infusion, patients could manifest different types of neurological toxicity symptoms: headache, seizure, nausea, pyrexia, sensory disturbance, upper motor neuron lesion, aphasia/speech disorder, and memory impairment [68]. The reaction can be severe and cannot be satisfactorily controlled by steroids, and debulking is needed to reduce the mass effect [65]. In the study by Rand et al., nine patients received 30-185 mL of IL-4(38-37)-PE38KDEL and seven of them required craniotomy due to uncontrollable cerebral edema. The reaction seems not related to the infusion rate, infusion volume, total infused dose, and number of catheters. The edema appeared 10-97 days after CED procedure; thus, it was not procedure-related. However, edema could be well controlled by steroids [64, 69] in other trials. In the procedure of Weaver and Laske, 5-180 mL of Tf-CRM107, a targeting toxin, was infused in patients with anaplastic oligodendroglioma (AO)/anaplastic astroglioma (AA)/GBM. The symptoms related to the edema and mass effect were fewer (i.e., 3 in 44 treatments) and well controlled by steroids and hyperosmolar therapy. Their phase II clinical trial demonstrated a similar toxicity and showed that cerebral edema can be well controlled by medical treatment [70]. With a similar pretreatment and treatment conditions, such large differences in the rate and severity of local toxicity can only be explained by the infused agent.

Local infection is related to the placement of the catheter and infusion time. Klatzmann et al. identified the pathogens to be gram negative and staphylococcus bacteria, due to the catheter and CSF leak to the skin. These infections were controllable with antibiotics [67, 69, 71–75]. Complications such as subdural empyema and bacterial meningitis were diagnosed in the study by Lidar et al. [67]. Chemical meningitis happens when chemotherapeutic agents, such as Taxol, reflux from the infusion site (i.e., 40% of patients experienced chemical meningitis) [67].

(b) Systemic Toxicities (Rare and Transitory). Studies with TP-38 or IL13, IL4, and Trabedersen did not show any systemic toxicity. General toxicities expressed as fever, fatigue, and erythema were observed [74, 76, 77], as well as gastrointestinal symptoms (nausea, vomiting) [76–78]. Hematological changes (decreased WBC, platelet, lymphopenia [63, 77, 78]) and liver enzyme perturbations (elevated AST, ALT, LDH, CRP, hypoalbuminemia [63, 64, 74, 77]) were also observed.

3.3. Efficacy Studies in Phase II and Phase III Clinical Trials. The efficacy of CED clinical studies in GBM treatments was reviewed by Jahangiri in 2017 [79]. Our section includes, in addition to all clinical trials reviewed by this author, more recent ones published after 2017 and those related to other malignant gliomas.

3.3.1. Targeted Antitumor Agents

Tf-CRM107 (TransMID) (Tf-Diphtheria Toxin) [64, 70]. This agent is a human transferrin, which targets receptors on the surface of tumor cells fused to a diphtheria toxin. In the phase I/II study of Laske group, out of 15 evaluated recurrent malignant gliomas patients, seven had partial response (PR) and two even had a complete response (CR) to Tf-CRM107 with a dose of 0.5-199 μg per treatment at a maximum infusion rate of 0.24-0.6 mL/h, giving a total volume of 5-180 mL. The tumor response appeared to be dose-dependent, with two out of five of the evaluated patients having PR at the dose of 0.5-12.8 μg, while in the higher dose groups, seven patients out of 10 had PR or even CR. Thus, the same group carried out the phase II study at a total dose of 26.8 μg per treatment, at an infusion rate of 0.4 mL/h, for a total of 40 mL. In the 34 evaluated patients, five patients had CR, seven had PR, which was a 35% response rate. However, all patients enrolled had a progressive disease and the progression of 9 of them was halted due to the response to treatment. Moreover, the magnetic resonance imaging (MRI) response rate was correlated with the survival analysis, with a median survival of 37 weeks. Due to these encouraging results, a phase III clinical trial of recurrent GBM was planned.

IL13- PE38QQR [57]. This agent is a human interleukin-13 (IL13) conjugated to a modified form of *Pseudomonas aeruginosa* exotoxin A (PE38QQR). The tolerable toxicity profile and efficacy over control groups, demonstrated by a series of phase I studies, led to the design of a phase III trial, also known as the PRECISE trial [61, 68, 80, 81]. It compared survival of CED of IL13-PE38QQR with tumor cavity placement of Gliadel® Wafer (GW). There were 296 recurrent GBM patients recruited; 192 were assigned to the CED group and 104 to the GW group. Infusion was performed at rate of 0.75 mL/h for 96 hours with a concentration of 0.5 μg/mL, which is the MTD assigned from safety studies. Unfortunately, of the patients evaluable for efficacy, the median survival for the CED group was 11.3 months compared to a median survival of 10 months in the GW group. No statistical significance was found (P = 0.310; hazard ratio 0.81; 95% CI = 0.67-1.18).

The underlying reason of the failure of this multicenter study was further analyzed [82]. Catheter positioning data were retrieved and the distribution volume of the infusate was predicted through iPlan® Flow software from Brainlab. The prediction showed that only 20.1% of peritumoral area was covered by IL13- PE38QQR. However, the effect size of the catheter score and the number of optimally positioned catheters on PFS are small. Thus, before carrying out further clinical protocols, the technical problems must be solved and quality control must be first assured, especially the optimization of parameters, such as geometry of the infusion

catheter, flexibility of protocol, and determination of drug distribution.

HSV-1-tk GCV [71, 83–85]. This regimen was a two-step treatment modality. Herpes simplex virus thymidine kinase (HSV-tk) gene was first transduced to the glioblastoma cells by either intratumoral injection or CED, then ganciclovir (GCV) was delivered systemically. Several investigations with intracerebral infusion of HSV-1-tk failed to demonstrate survival benefits due to limited diffusion volume of HSV-1-tk. Later in 2003, Voges et al. designed a liposome encapsulated HSV-1-tk and delivered it through CED with the expectation of an augmented distribution volume [62]. Unfortunately, it was not the case: their large and positively charged liposomes remained at the site of infusion, as observed in our recent study [39]. As a result, only two patients out of eight had PR.

TGF-β2 Inhibitor Trabedersen (AP 12009) [75, 86]. This compound is a transforming growth factor 2 (TGF-β2) inhibitor. It was evaluated in 145 recurrent/refractory AA/GBM patients by Bogdahn et al. Patients were assigned to 2 different dose groups, 2.48 mg for 10 μM group and 19.81 mg for 80 μM group at an infusion rate of 0.24 mL/h for 7 days [75]. In the subgroup analysis, compared to conventional chemotherapy (TMZ or procarbazine/CCNU/vincristine (PCV)), Trabedersen increased the MeST of the AA subgroup from 21.7 months with conventional chemotherapy to 39.1 months (but not significant); similar MeST CED and conventional chemotherapy were also obtained from the GBM subgroup.

Recombinant Poliovirus (PVSRIPO) [87]. This is an attenuated poliovirus type 1 vaccine. Poliovirus receptor CD115 is expressed in glioblastoma and the recombinant poliovirus can recognize CD115 and infect the tumor cells creating a cytotoxic effect. Sixty-one recurrent GBM patients were recruited in this phase II trial, during which, PVSRIPO was infused at a rate of 0.5mL/h for 6.5 hours. The results were compared to a historical control group of 104 patients. Although no significant improvement of the median survival time was observed for CED of PVSRIPO (12.5 months) compared to the control group (11.3 months), the survival of the PVSRIPO group reached a plateau starting at 24 months. The overall survival at 24 months is 21% for CED of PVSRIPO vs. 14% for control group, and at 36 months it is 21% vs. 4%. Moreover, two of them had survived over 69 months after infusion. Thus, further investigations on this vaccine are warranted.

3.3.2. Chemotherapeutic Agent

Paclitaxel [67, 69, 72]. This agent is a conventional chemotherapeutic drug that interferes with microtubules during cell division. Its antitumor effects on brain tumors have been reported in preclinical studies. Since it does not pass the BBB, it was considered as an interesting compound for treatment via CED. In the study by Lidar et al., 11 out of 15 patients had either PR or CR. The distribution volume after CED was confirmed by diffusion-weighted MRI (DW-MRI). They infused paclitaxel 3.6-7.2 mg/day for 5 days at an infusion rate of 0.3 mL/h. However, 40% of patients had chemical meningitis and 20% had neurological deterioration. Another group performed a similar study but followed with 18F-fluoro-ethyl-tyrosine-positron emission tomography (18F-FET-PET) [69, 72]. They employed similar parameters as Lidar et al., i.e., a total dose of 18 mg (0.5 mg/mL) or 9 mg (0.25 mg/mL) at an infusion rate of 0.3 mL/h for 120 hours. Six out of eight patients had a temporally stable disease. They also demonstrated that FET-EPT is better than MRI to follow-up patients and that an increase in FET uptake almost always implies a recurrence of the tumor.

3.3.3. Radioisotopes

^{131}I-chTNT-1/B mAb (Cotara) [76]. This compound is a ^{131}I-labeled chimeric monoclonal antibody that targets the intracellular antigen histone H1, which is exposed in the necrotic core of gliomas. In a phase II clinical trial, 39 patients were recruited, but only 12 recurrent glioblastoma patients who had received a dose in the therapeutic range (1.25-2.5 mCi/m^3) were evaluated. Among the 12 patients, only one patient had PR and 6 patients had stable disease. Necrotic tumors, which can be pathologically distinguished through features such as fibrinoid necrosis of blood vessel wall, white matter necrosis, and telangiectasis [88], were seen in several reoperated patients, which proved that Cotara has radiation effect on tumor, but its efficacy needs further evaluation.

3.3.4. Immunomodulators

Oligodeoxynucleotides Containing CpG Motifs (CpG-ODN) [74]. CpG-ODN is a strong immunomodulator, which activates both innate immunity (natural killing cells and macrophages) and adaptive immunity with the expectation of targeting tumor cells by the immune system. In the studies carried out by Carpentier et al. [63], CpG-ODN was infused at a rate of 0.2 mL/h for 5 hours. The phase I study demonstrated a tolerated dose of 20 mg [63]. In the following phase II trials, there was only one partial responder and three minor responders in 31 patients. Even worse, 13 patients out of 31 had treatment related seizure, among whom 3 had generalized seizure.

Overall, few efficacy studies demonstrated superior survivals over standard treatment regimen. Future investigations should adjust and standardize methodological parameters. Distribution volume prediction and validation should be implanted. Besides the above-mentioned reasons, another possible contributing factor for the failure of the clinical trials is related to the fact that CED augments the interstitial pressure, which could enhance the invasion of glioma cells [89].

4. Discussion

4.1. Choice of Agent. As we mentioned above, the advantages of CED compared with modern RT depend on the type of agents, i.e., those with different functions, such as

targeted toxins, radiosensitizing chemotherapeutic agents, radioisotopes, and so on. CED of these agents aims to gain local control of tumor progression, as does RT, with a different approach, which includes tumor cell targeting and radiosensitization. A choice of a suitable agent can add valuable antitumor efficacy to traditional RT. Such agents should have the ability to selectively target the tumor cells in infiltrative areas and thus spare normal brain cells. In this case, higher local doses can be obtained in cancerous tissue compared to conventional RT, where toxicity of normal tissue is a major concern. In fact, the recurrent tumor usually emerges from the peritumoral area. When compared to recently developed immunotherapeutic methods, CED offers a novel approach for the application of those therapeutic agents to malignant gliomas [94, 95].

4.2. Treatment Planning. Under ideal conditions, the medical team planning clinical studies employing CED should be similar to that in charge of radiation treatments. In the latter, radiation oncologists delineate the gross tumor volume (GTV) based on CT scans and/or MRI, clinical targeting volume (CTV) 1 and 2 for high and low risk area and organs, respectively. They assign the treatment dose to each target volume restricting, as much as possible, the dose to organs at risk. Medical physicists or dosimetrists then calculate and design a treatment plan to meet the requirements of radiation oncologists. The dose planning is based on the angle and number of the radiation fields, CT value of the tissue, and so on. While in the future treatment planning for CED will first be based on MRI, many other parameters will have to be considered. These should include GTV, peritumoral area, organs at risk, such as brain stem, hippocampus, and other areas related to functions that influence the quality of life. Treatment would benefit from software, such as iPlan® Flow, based on the DW-MRI, probably with appropriate input parameters such as placement of catheters, surface charge and quantity of drug, viscosity of the infusate, and infusion rate and volume, to simulate the dose assigned for each CTV [96].

4.3. Monitoring the Distribution of the Infusate. After treatment planning and simulation, monitoring and validation of the placement of catheters and distribution of infusate are equally important. This procedure is again similar to RT; before each delivery we use cone beam computerized tomography (CBCT) system to ensure that the targeted tumor is positioned in the planned coordinates. For this purpose, many techniques have been investigated. Coinfusion of gadolinium with therapeutic agents is an easy approach to monitor the infusate distribution, assuming that gadolinium diffuses in the tumor in the same manner as the infusate [97–99]. Loading of gadolinium and drugs in the same vector, such as a liposome, represents another approach to monitoring the distribution [100, 101]. This approach has the advantage of revealing the "true image" of the drug distribution, as long as gadolinium does not leak due to the convection pressure. Methods that do not utilize additional gadolinium appear more attractive, but they may compromise the drug efficacy. Multivoxel ^{1}H-MR Spectroscopy through analysis of metabolites ratio of Cho/Cr and Cho/NAA is able to describe the tumor site with and without CED infusion [102], but the resolution of this technique needs to be increased for adequate analysis in the future. DW-MRI is another noninvasive approach that can monitor the response of CED delivery of Taxol [103]. The response can be detected within 24-48 hours with DW-MRI, which is 1-2 days earlier than conventional imaging methods. However, none of the CED clinical trials assessed the distribution efficacy, which may be one of the factors that caused the failure of phase III clinical trial.

5. Conclusion

Regardless of emergence of novel therapeutic agents, their application in malignant gliomas remains rare, possibly due to the existence of the BBB. CED bypasses the BBB, increases the tumor uptake, and reduces the systemic toxicity. It has made progress during the past 25 years, since its invention, up to phase III clinical trial. It is a clinically feasible procedure with mostly local and tolerable toxicity, although grade III and IV adverse effects have been reported. Phase II clinical trials of PVSRIPO, Tf-diphtheria toxin, hold promise for future CED studies. Nevertheless, the phase III clinical trial failed to demonstrate survival improvements in the treatment of brain tumors. Analysis of the failure of these clinical trials showed the importance of catheter placement and distribution volume prediction and validation in performing CED treatments. Thus, it appears imperative to carefully analyze the methodological parameters to predict and validate the distribution volume for future clinical studies to be successful.

Conflicts of Interest

The authors declare that they have no conflicts of interest.

Acknowledgments

Minghan Shi would like to thank Dr. David Fortin for leading him to the field of CED. This review was supported in part by the Natural Science Foundation of Zhejiang Province under grant number LQ18H160013.

References

[1] S. I. Rapoport, M. Hori, and I. Klatzo, "Testing of a hypothesis for osmotic opening of the blood-brain barrier," *American Journal of Physiology-Endocrinology and Metabolism*, vol. 223, no. 2, pp. 323–331, 1972.

[2] E. A. Neuwelt, *Implications of the Blood-Brain Barrier and Its Manipulation*, vol. 1: Basic Science aspects, Springer, Boston, Mass, USA, 1989.

[3] D. Fortin, A. Desjardins, A. Benko, T. Niyonsega, and M. Boudrias, "Enhanced chemotherapy delivery by intraarterial infusion and blood-brain barrier disruption in malignant brain tumors: the Sherbrooke experience," *Cancer*, vol. 103, no. 12, pp. 2606–2615, 2005.

[4] A. Carpentier, M. Canney, A. Vignot et al., "Clinical trial of blood-brain barrier disruption by pulsed ultrasound," *Science Translational Medicine*, vol. 8, no. 343, p. 343re2, 2016.

[5] R. Hunt Bobo, D. W. Laske, A. Akbasak, P. F. Morrison, R. L. Dedrick, and E. H. Oldfield, "Convection-enhanced delivery of macromolecules in the brain," *Proceedings of the National Acadamy of Sciences of the United States of America*, vol. 91, no. 6, pp. 2076–2080, 1994.

[6] E. Allard, C. Passirani, and J.-P. Benoit, "Convection-enhanced delivery of nanocarriers for the treatment of brain tumors," *Biomaterials*, vol. 30, no. 12, pp. 2302–2318, 2009.

[7] V. Y. Yu, A. Landers, K. Woods et al., "A prospective 4π radiation therapy clinical study in recurrent high-grade glioma patients," *nternational Journal of Radiation Oncology Biology Physics*, vol. 101, no. 1, pp. 144–151, 2018.

[8] M. Shi, D. Fortin, L. Sanche, and B. Paquette, "Convection-enhancement delivery of platinum-based drugs and LipoplatinTM to optimize the concomitant effect with radiotherapy in F98 glioma rat model," *Investigational New Drugs*, vol. 33, no. 3, pp. 555–563, 2015.

[9] P. Bernhardt, W. Friedland, and H. Paretzke, "The role of atomic inner shell relaxations for photon-induced DNA damage," *Radiation and Environmental Biophysics*, vol. 43, no. 2, pp. 77–84, 2004.

[10] F. Theeuwes and S. I. Yum, "Principles of the design and operation of generic osmotic pumps for the delivery of semisolid or liquid drug formulations," *Annals of Biomedical Engineering*, vol. 4, no. 4, pp. 343–353, 1976.

[11] J. Rousseau, R. F. Barth, M. L. Moeschberger, and H. Elleaume, "Efficacy of intracerebral delivery of carboplatin in combination with photon irradiation for treatment of F98 glioma-bearing rats," *International Journal of Radiation Oncology • Biology • Physics*, vol. 73, no. 2, pp. 530–536, 2009.

[12] B. Sahin, H. Aslan, and B. Unal, "Brain volumes of the lamb, rat and bird do not show hemispheric asymmetry: a stereological study," *Image Analysis & Stereology*, vol. 20, no. 1, p. 9, 2011.

[13] W. Yang, T. Huo, R. F. Barth et al., "Convection enhanced delivery of carboplatin in combination with radiotherapy for the treatment of brain tumors," *Journal of Neuro-Oncology*, vol. 101, no. 3, pp. 379–390, 2011.

[14] W. Debinski and S. B. Tatter, "Convection-enhanced delivery for the treatment of brain tumors," *Expert Review of Neurotherapeutics*, vol. 9, no. 10, pp. 1519–1527, 2014.

[15] P. F. Morrison, M. Y. Chen, R. S. Chadwick, R. R. Lonser, and E. H. Oldfield, "Focal delivery during direct infusion to brain: Role of flow rate, catheter diameter, and tissue mechanics," *American Journal of Physiology-Regulatory, Integrative and Comparative Physiology*, vol. 277, no. 4 Pt 2, pp. R1218–R1229, 1999.

[16] R. R. Lonser, S. Walbridge, K. Garmestani et al., "Successful and safe perfusion of the primate brainstem: in vivo magnetic resonance imaging of macromolecular distribution during infusion," *Journal of Neurosurgery*, vol. 97, no. 4, pp. 905–913, 2002.

[17] J. W. Degen, S. Walbridge, A. O. Vortmeyer, E. H. Oldfield, and R. R. Lonser, "Safety and efficacy of convection-enhanced delivery of gemcitabine or carboplatin in a malignant glioma model in rats," *Journal of Neurosurgery*, vol. 99, no. 5, pp. 893–898, 2003.

[18] M. Y. Chen, R. R. Lonser, P. F. Morrison, L. S. Governale, and E. H. Oldfield, "Variables affecting convection-enhanced delivery to the striatum: a systematic examination of rate of infusion, cannula size, infusate concentration, and tissue—cannula sealing time," *Journal of Neurosurgery*, vol. 90, no. 2, pp. 315–320, 1999.

[19] M. T. Krauze, R. Saito, C. Noble et al., "Reflux-free cannula for convection-enhanced high-speed delivery of therapeutic agents," *Journal of Neurosurgery*, vol. 103, no. 5, pp. 923–929, 2005.

[20] M. Biston, A. Joubert, J. Adam et al., "Cure of fisher rats bearing radioresistant F98 glioma treated with cis-platinum and irradiated with monochromatic synchrotron X-rays," *Cancer Research*, vol. 64, no. 7, pp. 2317–2323, 2004.

[21] J. Rousseau, C. Boudou, R. F. Barth, J. Balosso, F. Esteve, and H. Elleaume, "Enhanced survival and cure of F98 glioma bearing rats following intracerebral delivery of carboplatin in combination with photon irradiation," *Clinical Cancer Research*, vol. 13, no. 17, pp. 5195–5201, 2007.

[22] M. T. Krauze, J. Forsayeth, D. Yin, and K. S. Bankiewicz, "Chapter 18 convection-enhanced delivery of liposomes to primate brain," *Methods in Enzymology*, vol. 465, no. C, pp. 349–362, 2009.

[23] A. A. Linninger, M. R. Somayaji, M. Mekarski, and L. Zhang, "Prediction of convection-enhanced drug delivery to the human brain," *Journal of Theoretical Biology*, vol. 250, no. 1, pp. 125–138, 2008.

[24] R. Raghavan, M. L. Brady, M. I. Rodríguez-Ponce, A. Hartlep, C. Pedain, and J. H. Sampson, "Convection-enhanced delivery of therapeutics for brain disease, and its optimization," *Neurosurgical Focus*, vol. 20, no. 4, p. E12, 2006.

[25] S. OH, R. Odland, S. R. Wilson et al., "Improved distribution of small molecules and viral vectors in the murine brain using a hollow fiber catheter," *Journal of Neurosurgery*, vol. 107, no. 3, pp. 568–577, 2007.

[26] S. B. Tatter, E. G. Shaw, M. L. Rosenblum et al., "An inflatable balloon catheter and liquid 125I radiation source (GliaSite Radiation Therapy System) for treatment of recurrent malignant glioma: multicenter safety and feasibility trial," *Journal of Neurosurgery*, vol. 99, no. 2, pp. 297–303, 2003.

[27] J. J. Olson, Z. Zhang, D. Dillehay, and J. Stubbs, "Assessment of a balloon-tipped catheter modified for intracerebral convection-enhanced delivery," *Journal of Neuro-Oncology*, vol. 89, no. 2, pp. 159–168, 2008.

[28] B. Halle, K. Mongelard, and F. Poulsen, "Convection-enhanced drug delivery for glioblastoma: a systematic review focused on methodological differences in the use of the convection-enhanced delivery method," *Asian Journal of Neurosurgery*, vol. 14, no. 1, pp. 5–14, 2019.

[29] R. Saito, J. R. Bringas, A. Panner et al., "Convection-enhanced delivery of tumor necrosis factor-related apoptosis-inducing ligand with systemic administration of temozolomide prolongs survival in an intracranial glioblastoma xenograft model," *Cancer Research*, vol. 64, no. 19, pp. 6858–6862, 2004.

[30] M. Nagane, G. Pan, J. J. Weddle, V. M. Dixit, W. K. Cavenee, and S. Huang, "Increased death receptor 5 expression by chemotherapeutic agents in human gliomas causes synergistic cytotoxicity with tumor necrosis factor- related apoptosis-inducing ligand in vitro and in vivo," *Cancer Research*, vol. 60, no. 4, pp. 847–853, 2000.

[31] G. M. Bernal, M. J. LaRiviere, N. Mansour et al., "Convection-enhanced delivery and in vivo imaging of polymeric nanoparticles for the treatment of malignant glioma," *Nanomedicine: Nanotechnology, Biology and Medicine*, vol. 10, no. 1, pp. 149–157, 2014.

[32] T. Fourniols, L. D. Randolph, A. Staub et al., "Temozolomide-loaded photopolymerizable PEG-DMA-based hydrogel for the treatment of glioblastoma," *Journal of Controlled Release*, vol. 210, pp. 95–104, 2015.

[33] M. M. Nordling-David, R. Yaffe, D. Guez et al., "Liposomal temozolomide drug delivery using convection enhanced delivery," *Journal of Controlled Release*, vol. 261, pp. 138–146, 2017.

[34] J. Rousseau, R. F. Barth, M. Fernandez et al., "Efficacy of intracerebral delivery of cisplatin in combination with photon irradiation for treatment of brain tumors," *Journal of Neuro-Oncology*, vol. 98, no. 3, pp. 287–295, 2010.

[35] R. F. Barth, W. Yang, T. Huo et al., "Comparison of intracerebral delivery of carboplatin and photon irradiation with an optimized regimen for boron neutron capture therapy of the F98 rat glioma," *Applied Radiation and Isotopes*, vol. 69, no. 12, pp. 1813–1816, 2011.

[36] W. Yang, R. F. Barth, T. Huo et al., "Radiation therapy combined with intracerebral administration of carboplatin for the treatment of brain tumors," *Journal of Radiation Oncology*, vol. 9, no. 1, p. 25, 2014.

[37] Y. Tange, A. Kondo, M. J. Egorin et al., "Interstitial continuous infusion therapy in a malignant glioma model in rats," *Child's Nervous System*, vol. 25, no. 6, pp. 655–662, 2009.

[38] M. Shi, D. Fortin, B. Paquette, and L. Sanche, "Convection-enhancement delivery of liposomal formulation of oxaliplatin shows less toxicity than oxaliplatin yet maintains a similar median survival time in F98 glioma-bearing rat model," *Investigational New Drugs*, vol. 34, no. 3, pp. 269–276, 2016.

[39] M. Shi, M. Anantha, M. Wehbe et al., "Liposomal formulations of carboplatin injected by convection-enhanced delivery increases the median survival time of F98 glioma bearing rats," *Journal of Nanobiotechnology*, vol. 16, no. 1, pp. 1–12, 2018.

[40] G. Charest, L. Sanche, D. Fortin, D. Mathieu, and B. Paquette, "Glioblastoma treatment: Bypassing the toxicity of platinum compounds by using liposomal formulation and increasing treatment efficiency with concomitant radiotherapy," *International Journal of Radiation Oncology • Biology • Physics*, vol. 84, no. 1, pp. 244–249, 2012.

[41] G. Charest, L. Sanche, D. Fortin, D. Mathieu, and B. Paquette, "Optimization of the route of platinum drugs administration to optimize the concomitant treatment with radiotherapy for glioblastoma implanted in the Fischer rat brain," *Journal of Neuro-Oncology*, vol. 115, no. 3, pp. 365–373, 2013.

[42] R. C. Richmond and E. L. Powers, "Radiation Sensitization of Bacterial Spores by cis-Dichlorodiammineplatinum(II)," *Journal of Radiation Research*, vol. 68, no. 2, pp. 251–257, 1976.

[43] E. B. Douple and R. C. Richmond, "Platinum complexes as radiosensitizers of hypoxic mammalian cells," *The British Journal of Cancer*, vol. 3, pp. 98–102, 1978.

[44] I. J. Stratford, C. Williamson, and G. E. Adams, "Combination studies with misonidazole and a cis-platinum complex: cytotoxicity and radiosensitization in vitro," *British Journal of Cancer*, vol. 41, no. 4, pp. 517–522, 1980.

[45] R. C. Richmond, A. R. Khokhar, B. A. Teicher, and E. B. Douple, "Toxic variability and radiation sensitization by Pt(II) analogs in salmonella typhimurium cells," *Journal of Radiation Research*, vol. 99, no. 3, pp. 609–626, 1984.

[46] A. Dritschilo, A. J. Piro, and A. D. Kelman, "The effect of cis-platinum on the repair of radiation damage in plateau phase CHINESE hamster (V-79) cells," *International Journal of Radiation Oncology • Biology • Physics*, vol. 5, no. 8, pp. 1345–1349, 1979.

[47] L. Dewit, "Combined treatment of radiation and cisdiamminedichloroplatinum (II): a review of experimental and clinical data," *International Journal of Radiation Oncology • Biology • Physics*, vol. 13, no. 3, pp. 403–426, 1987.

[48] L. Yang, E. B. Douple, and H. Wang, "Irradiation enhances cellular uptake of carboplatin," *International Journal of Radiation Oncology • Biology • Physics*, vol. 33, no. 3, pp. 641–646, 1995.

[49] J. Kopyra, C. Koenig-Lehmann, I. Bald, and E. Illenberger, "A single slow electron triggers the loss of both chlorine atoms from the anticancer drug cisplatin: implications for chemoradiation therapy," *Angewandte Chemie International Edition*, vol. 48, no. 42, pp. 7904–7907, 2009.

[50] B. Behmand, J. R. Wagner, L. Sanche, and D. J. Hunting, "Cisplatin intrastrand adducts sensitize DNA to base damage by hydrated electrons," *The Journal of Physical Chemistry B*, vol. 118, no. 18, pp. 4803–4808, 2014.

[51] Y. Zheng, D. J. Hunting, P. Ayotte, and L. Sanche, "Role of secondary low-energy electrons in the concomitant chemoradiation therapy of cancer," *Physical Review Letters*, vol. 100, no. 19, pp. 1–4, 2008.

[52] M. Rezaee, D. J. Hunting, and L. Sanche, "New insights into the mechanism underlying the synergistic action of ionizing radiation with platinum chemotherapeutic drugs: The role of low-energy electrons," *International Journal of Radiation Oncology • Biology • Physics*, vol. 87, no. 4, pp. 847–853, 2013.

[53] Z. Li, P. Cloutier, L. Sanche, and J. R. Wagner, "Low-energy electron-induced damage in a trinucleotide containing 5-bromouracil," *The Journal of Physical Chemistry B*, vol. 115, no. 46, pp. 13668–13673, 2011.

[54] Q. Bao, Y. Chen, Y. Zheng, and L. Sanche, "Cisplatin radiosensitization of DNA irradiated with 2-20 eV electrons: role of transient anions," *The Journal of Physical Chemistry C*, vol. 118, no. 28, pp. 15516–15524, 2014.

[55] T. Tippayamontri, R. Kotb, B. Paquette, and L. Sanche, "Efficacy of cisplatin and lipoplatin™ in combined treatment with radiation of a colorectal tumor in nude mouse," *Anticancer Reseach*, vol. 33, no. 8, pp. 3005–3014, 2013.

[56] T. Tippayamontri, R. Kotb, B. Paquette, and L. Sanche, "New therapeutic possibilities of combined treatment of radiotherapy with oxaliplatin and its liposomal formulations (LipoxalTM) in colorectal cancer using nude mouse xenograft," *Anticancer Research*, vol. 5312, pp. 5303–5312, 2014.

[57] S. Kunwar, S. Chang, M. Westphal et al., "Phase III randomized trial of CED of IL13-PE38QQR vs Gliadel wafers for recurrent glioblastoma," *Neuro-Oncology*, vol. 12, no. 8, pp. 871–881, 2010.

[58] H. Ren, T. Boulikas, K. Lundstrom, A. Söling, P. C. Warnke, and N. G. Rainov, "Immunogene therapy of recurrent glioblastoma multiforme with a liposomally encapsulated replication-incompetent Semliki forest virus vector carrying the human interleukin-12 gene–a phase I/II clinical protocol," *Journal of Neuro-Oncology*, vol. 64, no. 1-2, pp. 147–154, 2003.

[59] E. White, A. Bienemann, J. Pugh et al., "An evaluation of the safety and feasibility of convection-enhanced delivery of carboplatin into the white matter as a potential treatment for high-grade glioma," *Journal of Neuro-Oncology*, vol. 108, no. 1, pp. 77–88, 2012.

[60] P. Wersäll, I. Ohlsson, P. Biberfeld et al., "Intratumoral infusion of the monoclonal antibody, mAb 425, against the epidermal-growth-factor receptor in patients with advanced malignant glioma," *Cancer Immunology, Immunotherapy*, vol. 44, no. 3, pp. 157–164, 1997.

[61] S. Kunwar, S. M. Chang, M. D. Prados et al., "Safety of intraparenchymal convection-enhanced delivery of cintredekin besudotox in early-phase studies," *Neurosurgical Focus*, vol. 20, no. 3, p. E15, 2006.

[62] J. Voges, R. Reszka, A. Gossmann et al., "Imaging-guided convection-enhanced delivery and gene therapy of glioblastoma," *Annals of Neurology*, vol. 54, no. 4, pp. 479–487, 2003.

[63] A. Carpentier, F. Laigle-Donadey, S. Zohar et al., "Phase 1 trial of a CpG oligodeoxynucleotide for patients with recurrent gliobastoma," *Neuro-Oncology*, vol. 8, no. 1, pp. 60–66, 2006.

[64] D. W. Laske, R. J. Youle, and E. H. Oldfield, "Tumor regression with regional distribution of the targeted toxin TF- CRM107 in patients with malignant brain tumors," *Nature Medicine*, vol. 3, no. 12, pp. 1362–1368, 1997.

[65] R. W. Rand, R. J. Kreitman, N. Patronas, F. Varricchio, I. Pastan, and R. K. Puri, "Intratumoral administration of recombinant circularly permuted interleukin-4-Pseudomonas exotoxin in patients with high-grade glioma," *Clinical Cancer Research*, vol. 6, no. 6, pp. 2157–2165, 2000.

[66] F. Weber, A. L. Asher, R. Bucholz et al., "Tolerability and tumor response of IL4-toxin (NBI-3001) in patients with recurrent malignant glioma," *Neurosurgery*, vol. 49, no. 2, p. 525, 2001.

[67] Z. Lidar, Y. Mardor, T. Jonas et al., "Convection-enhanced delivery of paclitaxel for the treatment of recurrent malignant glioma: a phase I/II clinical study," *Journal of Neurosurgery*, vol. 100, no. 3, pp. 472–479, 2004.

[68] S. Kunvvar, "Convection enhanced delivery of IL13-PE38QQR for treatment of recurrent malignant glioma: Presentation of interim findings from ongoing phase 1 studies," *Acta Neurochirurgica, Supplementum*, no. 88, pp. 105–111, 2003.

[69] G. Pöpperl, R. Goldbrunner, F. J. Gildehaus et al., "O-(2-[18F]fluoroethyl)-l-tyrosine PET for monitoring the effects of convection-enhanced delivery of paclitaxel in patients with recurrent glioblastoma," *European Journal of Nuclear Medicine and Molecular Imaging*, vol. 32, no. 9, pp. 1018–1025, 2005.

[70] M. Weaver and D. W. Laske, "Transferrin receptor ligand-targeted toxin conjugate (Tf-CRM107) therapy of malignant gliomas," *Journal of Neuro-Oncology*, vol. 65, no. 1, pp. 3–13, 2003.

[71] D. Klatzmann, C. A. Valéry, G. Bensimon et al., "A phase I/II study of herpes simplex virus type 1 thymidine kinase 'Suicide' gene therapy for recurrent glioblastoma," *Human Gene Therapy*, vol. 9, no. 17, pp. 2595–2604, 1998.

[72] P. G. Tanner, M. Holtmannspötter, J. Tonn, and R. Goldbrunner, "Effects of drug efflux on convection-enhanced paclitaxel delivery to malignant gliomas: technical note," *Neurosurgery*, vol. 61, no. 4, pp. E880–E882, 2007.

[73] A. Boiardi, M. Eoli, A. Salmaggi et al., "Local drug delivery in recurrent malignant gliomas," *Neurological Sciences*, vol. 26, no. S1, pp. s37–s39, 2005.

[74] A. Carpentier, P. Metellus, R. Ursu et al., "Intracerebral administration of CpG oligonucleotide for patients with recurrent glioblastoma: a phase II study," *Neuro-Oncology*, vol. 12, no. 4, pp. 401–408, 2010.

[75] U. Bogdahn, P. Hau, G. Stockhammer et al., "Targeted therapy for high-grade glioma with the TGF-β2 inhibitor trabedersen: results of a randomized and controlled phase IIb study," *Neuro-Oncology*, vol. 13, no. 1, pp. 132–142, 2011.

[76] S. J. Patel, W. R. Shapiro, D. W. Laske et al., "Safety and feasibility of convection-enhanced delivery of Cotara for the treatment of malignant glioma: Initial experience in 51 patients," *Neurosurgery*, vol. 56, no. 6, pp. 1243–1252, 2005.

[77] M. M. Souweidane, K. Kramer, N. Pandit-Taskar et al., "Convection-enhanced delivery for diffuse intrinsic pontine glioma: a single-centre, dose-escalation, phase 1 trial," *The Lancet Oncology*, vol. 19, no. 8, pp. 1040–1050, 2018.

[78] J. N. Bruce, R. L. Fine, P. Canoll et al., "Regression of recurrent malignant gliomas with convection-enhanced delivery of topotecan," *Neurosurgery*, vol. 69, no. 6, pp. 1272–1280, 2011.

[79] A. Jahangiri, A. T. Chin, P. M. Flanigan, R. Chen, K. Bankiewicz, and M. K. Aghi, "Convection-enhanced delivery in glioblastoma: a review of preclinical and clinical studies," *Journal of Neurosurgery*, vol. 126, no. 1, pp. 191–200, 2017.

[80] S. Kunwar, M. D. Prados, S. M. Chang et al., "Direct intracerebral delivery of cintredekin besudotox (IL13-PE38QQR) in recurrent malignant glioma: a report by the cintredekin besudotox intraparenchymal study group," *Journal of Clinical Oncology*, vol. 25, no. 7, pp. 837–844, 2007.

[81] M. A. Vogelbaum, J. H. Sampson, S. Kunwar et al., "Convection-enhanced delivery of cintredekin besudotox (interleukin-13-PE38QQR) followed by radiation therapy with and without temozolomide in newly diagnosed malignant gliomas: phase 1 study of final safety results," *Neurosurgery*, vol. 61, no. 5, pp. 1031–1038, 2007.

[82] J. H. Sampson, G. Archer, C. Pedain et al., "Poor drug distribution as a possible explanation for the results of the PRECISE trial," *Journal of Neurosurgery*, vol. 113, no. 2, pp. 301–309, 2010.

[83] Z. Ram, K. W. Culver, E. M. Oshiro et al., "Therapy of malignant brain tumors by intratumoral implantation of retroviral vector-producing cells," *Nature Medicine*, vol. 3, no. 12, pp. 1354–1361, 1997.

[84] N. G. Rainov, "A phase III clinical evaluation of herpes simplex virus type 1 thymidine kinase and ganciclovir gene therapy as an adjuvant to surgical resection and radiation in adults with previously untreated glioblastoma multiforme," *Human Gene Therapy*, vol. 11, no. 17, pp. 2389–2401, 2000.

[85] N. Shand, F. Weber, L. Mariani et al., "A phase 1-2 clinical trial of gene therapy for recurrent glioblastoma multiforme by tumor transduction with the herpes simplex thymidine kinase gene followed by ganciclovir," *Human Gene Therapy*, vol. 10, no. 14, pp. 2325–2335, 1999.

[86] P. Hau, P. Jachimczak, R. Schlingensiepen et al., "Inhibition of TGF-beta2 with AP 12009 in recurrent malignant gliomas: from preclinical to phase I/II studies," *Oligonucleotides*, vol. 17, no. 2, pp. 201–212, 2007.

[87] A. Desjardins, M. Gromeier, J. E. Herndon et al., "Recurrent glioblastoma treated with recombinant poliovirus," *The New England Journal of Medicine*, vol. 379, no. 2, pp. 150–161, 2018.

[88] A. Na, N. Haghigi, and K. J. Drummond, "Cerebral radiation necrosis," *Asia-Pacific Journal of Clinical Oncology*, vol. 10, no. 1, pp. 11–21, 2014.

[89] J. M. Munson, R. V. Bellamkonda, and M. A. Swartz, "Interstitial flow in a 3D microenvironment increases glioma invasion by a CXCR4-dependent mechanism," *Cancer Research*, vol. 73, no. 5, pp. 1536–1546, 2013.

[90] F. W. Weber, F. Floeth, A. Asher et al., "Local convection enhanced delivery of IL4-Pseudomonas exotoxin (NBI-3001) for treatment of patients with recurrent malignant glioma," *Acta Neurochirurgica*, vol. 88, pp. 93–103, 2003.

[91] J. H. Sampson, G. Akabani, G. E. Archer et al., "Progress report of a Phase I study of the intracerebral microinfusion of a recombinant chimeric protein composed of transforming growth factor (TGF)-α and a mutated form of the Pseudomonas

exotoxin termed PE-38 (TP-38) for the treatment of malignant brain," *Journal of Neuro-Oncology*, vol. 65, no. 1, pp. 27–35, 2003.

[92] J. H. Sampson, G. Akabani, G. E. Archer et al., "Intracerebral infusion of an EGFR-targeted toxin in recurrent malignant brain tumors," *Neuro-Oncology*, vol. 10, no. 3, pp. 320–329, 2008.

[93] J. H. Sampson, G. Akabani, A. H. Friedman et al., "Comparison of intratumoral bolus injection and convection-enhanced delivery of radiolabeled antitenascin monoclonal antibodies," *Neurosurgical Focus*, vol. 20, no. 4, p. E14, 2006.

[94] N. Hilf, S. Kuttruff-Coqui, K. Frenzel et al., "Actively personalized vaccination trial for newly diagnosed glioblastoma," *Nature*, vol. 565, no. 7738, pp. 240–245, 2019.

[95] D. B. Keskin, A. J. Anandappa, J. Sun et al., "Neoantigen vaccine generates intratumoral T cell responses in phase Ib glioblastoma trial," *Nature*, vol. 565, no. 7738, pp. 234–239, 2019.

[96] j. H. Sampson, R. Raghavan, M. L. Brady et al., "Clinical utility of a patient-specific algorithm for simulating intracerebral drug infusions," *Neuro-Oncology*, vol. 9, no. 3, pp. 343–353, 2007.

[97] N. Sharma, K. S. Bankiewicz, M. T. Krauze et al., "Image-guided convection-enhanced delivery of GDNF protein into monkey putamen," *NeuroImage*, vol. 54, pp. S189–S195, 2011.

[98] J. H. Sampson, M. Brady, R. Raghavan et al., "Colocalization of gadolinium-diethylene triamine pentaacetic acid with high-molecular-weight molecules after intracerebral convection-enhanced delivery in humans," *Neurosurgery*, vol. 69, no. 3, pp. 668–676, 2011.

[99] M. Watanabe, T. Kumabe, R. Saito, K. Nagamatsu, T. Tominaga, and Y. Sonoda, "Regression of recurrent glioblastoma infiltrating the brainstem after convection-enhanced delivery of nimustine hydrochloride," *Journal of Neurosurgery: Pediatrics*, vol. 7, no. May, pp. 522–526, 2016.

[100] M. T. Krauze, T. R. Mcknight, Y. Yamashita et al., "Real-time visualization and characterization of liposomal delivery into the monkey brain by magnetic resonance imaging," *Brain Research Protocols*, vol. 16, no. 1-3, pp. 20–26, 2005.

[101] M. T. Krauze, J. Forsayeth, J. W. Park, and K. S. Bankiewicz, "Real-time Imaging and Quantification of Brain Delivery of Liposomes," *Pharmaceutical Research*, vol. 23, no. 11, pp. 2493–2504, 2006.

[102] D. I. Guisado, R. Singh, S. Minkowitz et al., "A novel methodology for applying multivoxel MR spectroscopy to evaluate convection-enhanced drug delivery in diffuse intrinsic pontine gliomas," *American Journal of Neuroradiology*, vol. 37, no. 7, pp. 1367–1373, 2016.

[103] Y. Mardor, Y. Roth, A. Orenstein et al., "Monitoring response to convection-enhanced taxol delivery in brain tumor patients using diffusion-weighted magnetic resonance imaging," *Cancer Research*, vol. 61, no. 13, pp. 4971–4973, 2001.

Hindawi
Journal of Oncology
Volume 2019, Article ID 2964783, 10 pages
https://doi.org/10.1155/2019/2964783

Review Article

Treatment Strategies Based on Histological Targets against Invasive and Resistant Glioblastoma

Akira Hara,[1] **Tomohiro Kanayama**,[1] **Kei Noguchi**,[1] **Ayumi Niwa**,[1] **Masafumi Miyai**,[1,2] **Masaya Kawaguchi**,[1,3] **Kazuhisa Ishida**,[1,4] **Yuichiro Hatano**,[1] **Masayuki Niwa**,[5] **and Hiroyuki Tomita**[1]

[1]*Department of Tumor Pathology, Gifu University Graduate School of Medicine, 1-1 Yanagido, Gifu City, Gifu 501-1194, Japan*
[2]*Department of Neurosurgery, Gifu University Graduate School of Medicine, 1-1 Yanagido, Gifu City, Gifu 501-1194, Japan*
[3]*Department of Radiology, Gifu University Graduate School of Medicine, 1-1 Yanagido, Gifu City, Gifu 501-1194, Japan*
[4]*Department of Oral and Maxillofacial Science, Gifu University Graduate School of Medicine, 1-1 Yanagido, Gifu City, Gifu 501-1194, Japan*
[5]*Medical Science Division, United Graduate School of Drug Discovery and Medical Information Sciences, Gifu University, 1-1 Yanagido, Gifu City, Gifu 501-1194, Japan*

Correspondence should be addressed to Akira Hara; ahara@gifu-u.ac.jp

Received 13 March 2019; Accepted 2 June 2019; Published 20 June 2019

Academic Editor: San-Lin You

Glioblastoma (GBM) is the most common and the most malignant primary brain tumor and is characterized by rapid proliferation, invasion into surrounding normal brain tissues, and consequent aberrant vascularization. In these characteristics of GBM, invasive properties are responsible for its recurrence after various therapies. The histomorphological patterns of glioma cell invasion have often been referred to as the "secondary structures of Scherer." The "secondary structures of Scherer" can be classified mainly into four histological types as (i) perineuronal satellitosis, (ii) perivascular satellitosis, (iii) subpial spread, and (iv) invasion along the white matter tracts. In order to develop therapeutic interventions to mitigate glioma cell migration, it is important to understand the biological mechanism underlying the formation of these secondary structures. The main focus of this review is to examine new molecular pathways based on the histopathological evidence of GBM invasion as major prognostic factors for the high recurrence rate for GBMs. The histopathology-based pharmacological and biological targets for treatment strategies may improve the management of invasive and resistant GBMs.

1. Introduction

Glioblastoma (GBM) is the most invasive, infiltrative, and lethal brain tumor with high proliferative potential [1]. Malignant gliomas, also called as high-grade gliomas and including GBM (WHO grade IV gliomas) and anaplastic gliomas (WHO grade III gliomas), are currently incurable despite aggressive surgery and are resistant to conventional therapies. Patient outcome following standard therapies including radiation and chemotherapy for GBM remains poor, with a median overall survival of only 12–14 months [2]. The highly invasive tumor cells predominantly migrate out of the tumor mass into the surrounding normal central nervous system. And they escape surgical resection and resist conventional treatments such as radiation and temozolomide, both of which are the first line of treatment for GBM patients following surgery. The surviving glioma cells after conventional therapies that target proliferating cells are principally responsible for tumor recurrence. Therefore, the effective treatment strategies which improve the management of invasive and resistant GBM cells are urgently needed to manage this malignancy. Histopathologically, infiltrated GBM cells show some specific morphological patterns, characterized as diffuse invasion. In general, glioma cells migrate along existing brain structures such as the brain parenchyma, blood vessels, white matter tracts, and subpial

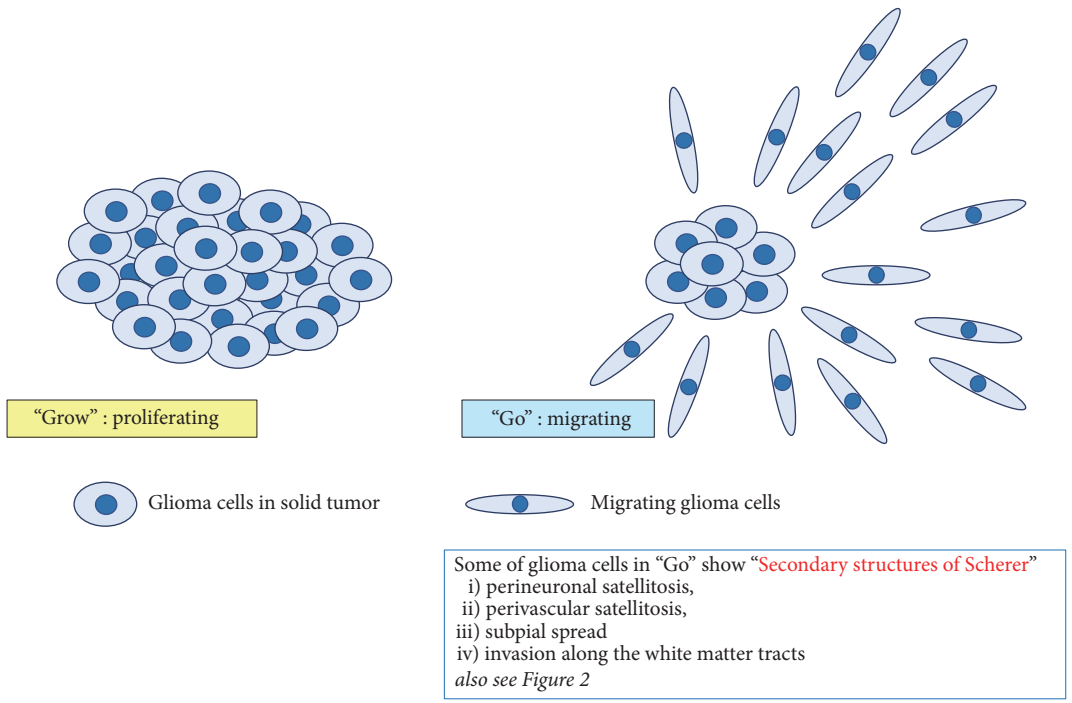

Figure 1: Illustration of "Go or Grow" theory in malignant gliomas. Malignant gliomas often consist of two subpopulations of cells, which mutually interact and mutually change, that are characterized by uncontrolled-proliferation and by abnormal migration. One subpopulation of cells is rapidly proliferating and forming a stationary tumor mass, while the other subpopulation is actively migrating and moves into surrounding brain without cell division. Some of glioma cells in "Go" stage show characteristic morphological patterns of tumor cell migration, referred to as "secondary structures of Scherer." These "secondary structures of Scherer," which are also shown in Figure 2, have been classified into histological patterns: (i) perineuronal satellitosis, (ii) perivascular satellitosis, (iii) subpial spread, and (iv) invasion along the white matter tracts.

spaces. These characteristic morphological patterns of tumor cell migration from the growing tumor mass into the adjacent brain tissues have been described first by Hans Joachim Scherer in 1938 [3] and referred to as "secondary structures of Scherer." These "secondary structures of Scherer" have been classified into histological patterns: (i) perineuronal satellitosis, (ii) perivascular satellitosis, (iii) subpial spread, and (iv) invasion along the white matter tracts (Figures 1 and 2). Careful observations of these histomorphological features have revealed the important contributions of the microenvironment that influence glioma cell migration. It is possible that invasive glioma cells showing "secondary structures of Scherer" mimic key intracellular processes of both proliferation and migration that occur in neural stem cells or glial progenitor cells within the developing central nervous system [4].

2. Similarities between Tumor Invasiveness of GBMs and Migrating Characteristics of Stem Cells

2.1. Stem Cells in Normal Brain. During neural development, neurons and glia are generated from developmental stage-specific and rapidly-dividing progenitor cells, and then quiescent, multipotent stem cells remain stable throughout adulthood [5]. During the formation of embryonic cerebral cortex, newly formed neuronal and glial progenitor cells migrate from the originating periventricular zone toward their specified physiological locations throughout the central nervous system [6–8]. Even in the adult mammalian brain, the subventricular zone (SVZ) contains neural stem cells (NSCs) or progenitor cells, which continue to produce neurons or glia for the maintenance of the central nervous system [7]. The SVZ of rodents, monkeys, and humans is a source of NSCs during adult neurogenesis. Some pathophysiological conditions, such as epilepsy [9], stimulate neurogenesis in the rostral forebrain SVZ of adult rats. Following ischemic insult, neural progenitors in caudal SVZ migrate to the hippocampus and contribute to the pyramidal cell regeneration in hippocampal CA1 [9]. Furthermore, some recent studies [10] suggest that the SVZ may also provide a source of brain tumor stem cells, which are morphologically and physiologically similar to NSCs producing neurons, astrocytes, and oligodendrocytes.

2.2. Relationship between SVZ and Brain Tumors. Unlike in normal brain development, tumor progenitor and quiescent tumor stem cell populations have yet to be understood in brain tumors [5]. A similarity between production of NSC in SVZ and the generation of malignant gliomas has been suggested [10]. While the underlying mechanisms remain

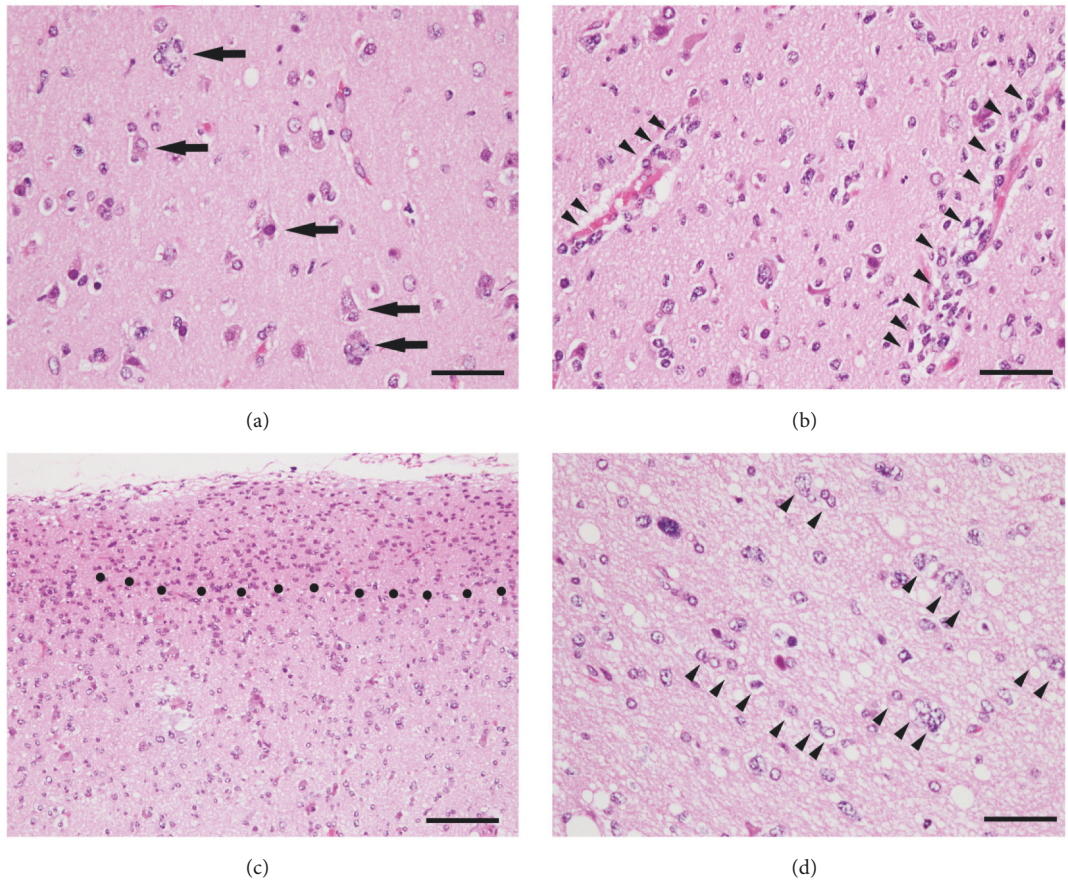

Figure 2: Specific histomorphological patterns of diffuse invasion, so-called "secondary structures of Scherer" in glioblastoma. As a rule, glioma cells migrate along existing brain structures such as brain parenchyma, blood vessels, white matter tracts, and subpial spaces. The secondary structures of Scherer are referred to four criteria as (a) perineuronal satellitosis (indicated by arrows), (b) perivascular satellitosis (indicated by arrow heads), (c) subpial spread (region above black dots), and (d) invasion along the white matter tracts (indicated by arrow heads). Hematoxylin and eosin staining. Scale bars in (a), (b), and (d) are 50 μm; scale bar in (c), 100 μm.

unclear, it has been suggested that increased tumor invasiveness, early recurrence, and mortality are worse in those patients whose malignant gliomas infiltrate or contact with the SVZ [11, 12]. It is hypothesized the SVZ has a unique role of contribution to GBM tumorigenesis in adult brain. Thus, these findings strongly suggest that the invasiveness of malignant glioma is derived from the migratory nature of NSCs in the adult human brain and that the morphological structures formed by invasive GBM, the "secondary structures of Scherer," are based on the functional similarities of invasive GBM to developing NSCs.

2.3. Glioma-Derived Cancer Stem Cells. Evidence suggests that the invasiveness of malignant gliomas, which mimic the migration attributes of NSCs, could be therapeutically controlled by modifying the intracellular systems or molecular pathways. Moreover, glioma-derived cancer stem cells (CSCs), which are regarded to be a counterpart of primary NSCs in normal brain, have subsequently been shown to be resistant to chemotherapy [13] and radiotherapy [14]. Glioma CSCs are key players in tumor initiation, therapeutic resistance, and tumor recurrence [4, 15–22] and are also related to glioblastoma heterogeneity. GBM is genotypically and phenotypically heterogeneous, which is a major factor in its poor response to various therapies. It is reported that even single cell-derived subclones from a patient can produce phenotypically heterogeneous self-renewing progenies in both *in vitro* and *in vivo* settings [23]. Several therapeutic strategies targeting glioma CSCs have been proposed to effectively control the disease progression [24–30].

3. Gliomatosis Cerebri and GBM

3.1. Gliomatosis Cerebri. Gliomatosis cerebri (GC) is an extremely rare neoplasm which shows diffuse infiltration of glioma cells within central nervous system including brain as well as spinal cord. Since clinical manifestations are various and focal neurological signs are usually recognized late in the course of the disease, the early recognition of this disease is difficult [31, 32], and no standard of care is usually available for the treatment of GC patients. Historically, histopathologic diagnosis of GC has been determined using standard hematoxylin and eosin staining and immunohistochemistry, with GC being defined as a distinct pathologic entity in "World

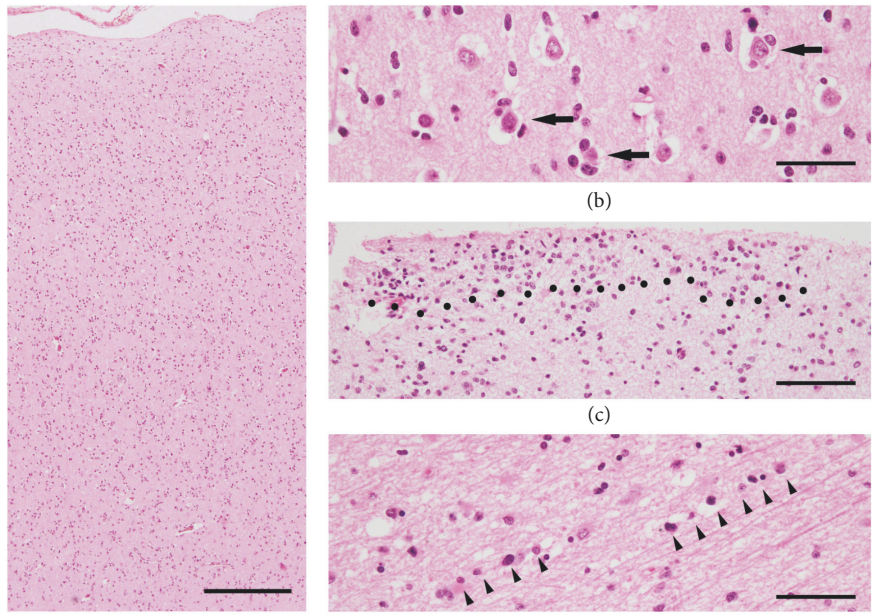

Figure 3: Representative images showing histomorphological structures of GC. Many histological features are similar to invasive patterns of GBM (secondary structures of Scherer in Figure 2). (a) Diffuse parenchymal infiltration of GC cells without the formation of a circumscribed tumor mass. The secondary structures of Scherer are seen also in GC as follows: (b) perineuronal satellitosis (indicated by arrows), (c) subpial spread (region above black dots), and (d) invasion along the white matter tracts (indicated by arrow heads). Hematoxylin and eosin staining. Scale bar in (a), 375 μm; scale bars in (b) and (d), 50 μm; scale bar in (c), 100 μm.

Health Organization (WHO) Classification of Tumors of the Central Nervous System" up to the 3rd edition. However, the scientific consensus now is that there is no common pathologic and radiographic consensus for its diagnosis, and in 2016, GC was eliminated from current WHO classification [33]. The reason of the elimination was based on overlap of discrete molecular alterations with other malignant gliomas and the absence of specific molecular markers [34, 35]. Many histomorphological features similar to infiltrative gliomas support the contention that GC is one variety of diffuse glioma including GBM. Therefore, GC is currently considered to be an extremely infiltrative subtype of diffusely growing malignant glioma, instead of a distinct histologic or molecular subtype of glioma.

3.2. Histological Findings of Gliomatosis Cerebri. GC has specific histological features, namely, tumor cells (i) that are elongated with diffuse and irregular parenchymal infiltration (without formation of a circumscribed tumor mass), (ii) with perivascular or perineuronal satellitosis, (iii) with subpial spread, and (iv) that infiltrate along myelinated tracts with the preserved neuronal axons (Figure 3). Neoplastic cells with elongated and fibrous cell processes were recognized easily with glial fibrillary acidic protein (GFAP) immunohistochemistry [31]. Since the anaplastic single cells infiltrate along myelinated axons and the basement membranes of blood vessels with distinct anatomic structures, typical features of GBM (e.g., neovascularization, necrosis, and mitotic activity) are usually absent in the lesions. The overall delineation of the histological findings for GC is similar to "secondary structures of Scherer" in the lesion of cell migration in malignant glioma.

3.3. Gliomatosis Cerebri and "Go or Grow". Usually, the neoplastic cells in GC do not have much proliferative activity, similar to that of low-grade gliomas [31, 36]. The fact that the neoplastic cells of GC infiltrate with low proliferative activity into brain tissues is very consistent with the following hypothesis, "Go or Grow" dichotomy theory.

4. "Go or Grow" Theory in Malignant Gliomas

4.1. Two Subpopulations. Malignant gliomas often consist of two subpopulations of cells, which mutually interact and mutually change, that are characterized by uncontrolled-proliferation and by abnormal migration. This has been termed the "Go or Grow" theory of gliomas (Figure 1). One subpopulation of cells is rapidly proliferating and forming a stationary tumor mass, while the other subpopulation is actively migrating and moves into surrounding brain without cell division (Figure 4). It has been hypothesized that cell proliferation and cell migration in gliomas are distinct and mutually exclusive, with a trade-off between them [37–43]. Tumor microenvironment and the metabolic stress (hypoxia; glucose deprivation) may regulate the switching between Go and Grow behaviors in GBM. It is possible that the surviving and invasive glioma cells after conventional therapies, which show "Go behavior," may later switch to a proliferative "Grow phenotype" at satellite lesions, forming rapid tumor mass.

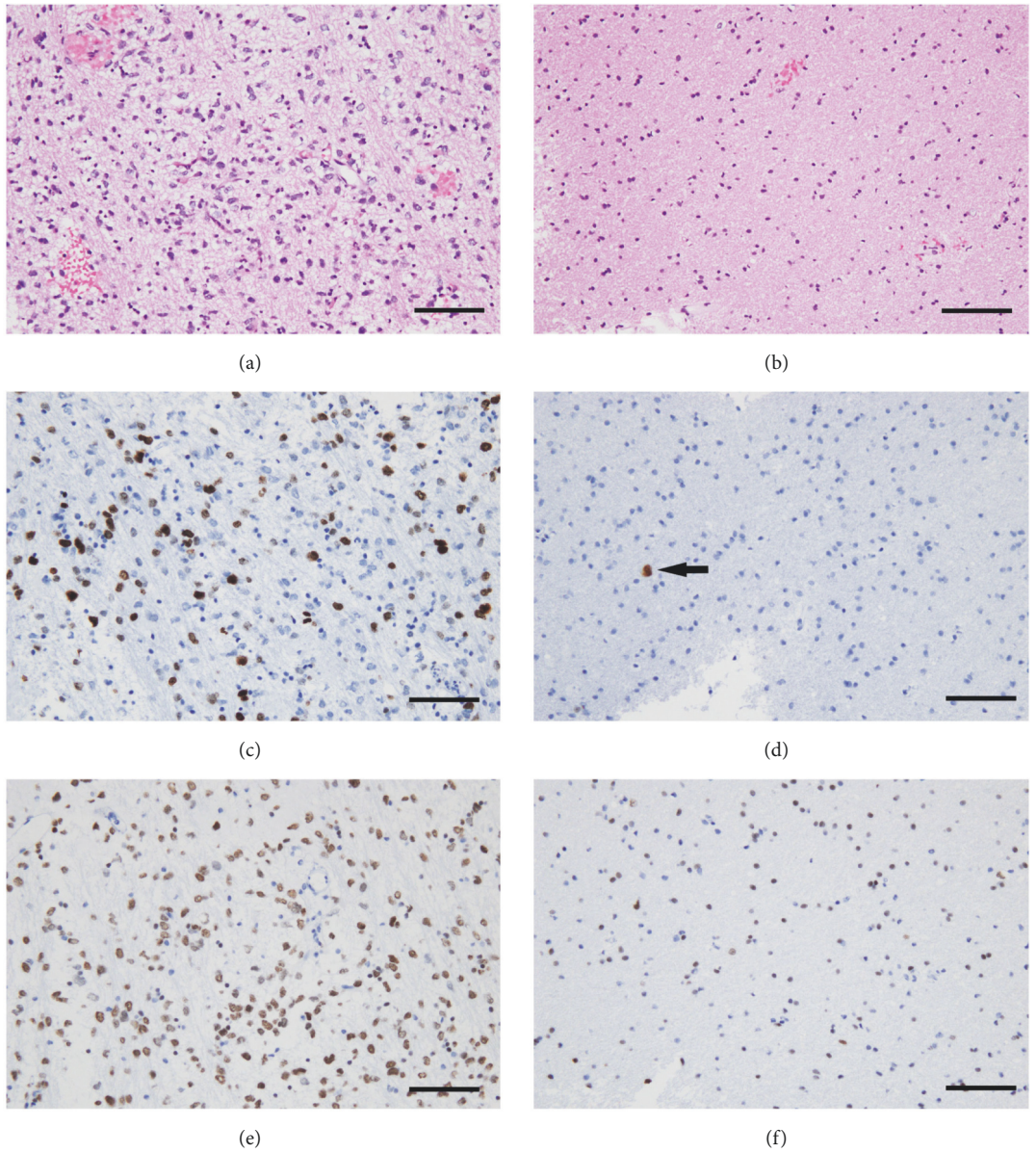

Figure 4: Representative histomorphological features of "Go or Grow" in GBM. The two subpopulations consist of uncontrolled-proliferating and abnormally migrating cells which interact mutually, which is so-called "Go or Grow" in gliomas. One subpopulation, rapidly proliferating cells, forms tumor mass being stationary (a, c, e). The other subpopulation, actively migrating cells, moves into surrounding brain without cell division (b, d, f). (a, b) Hematoxylin and eosin staining. (c, d) Immunohistochemistry for Ki-67 antigen, a marker of proliferating cells. The Ki-67 positive cells showing dark brown cell nuclei are detected as proliferating cells. (e, f) Immunohistochemistry for oligodendrocyte transcription factor (OLIG2), which is expressed universally in GBM cell nuclei. Vascular cells in GBM (observed in (e)) and normal glia cells (observed in (f)) are negative for OLIG2. Note that only one Ki-67 positive cell is detected in migrating GBM cells (arrow in (d)), whereas many OLIG2 positive GBM cells are seen in the same area (f). Also note that the sizes of cell nuclei recognized in (f) are smaller than that in (e). This means that migrating GBM cells into surrounding brain have smaller nuclei because they are actively moving. Scale bars, 100 μm.

4.2. Mechanism. This highly complex phenomenon involving molecular and cellular processes has been extensively studied. The mechanisms mediating uncontrolled-proliferation and abnormal migration of glioma cells have been investigated using glioma cell cultures. For example, the population of nonmotile glioma cells in standard cell culture conditions exhibits decreased intercellular space and high proliferating activity, indicating that the population is undergoing cell growth and division. In contrast, cells cultured on laminin exhibit activate migration, enlargement of the intercellular space, and spreading away from the proliferating growth site [44]. Glioma cells growing at the tumor core have a high proliferative activity, whereas migrating/invading cells around the tumor demonstrate a low proliferative activity,

with NF-kB activated in migration-stimulated GBM cells and c-Myc activated in migration-restricted GBM cells [40].

4.3. Spheroid Analysis. Glioma invasion *in vivo* and *in vitro* differs in several ways. Monolayer cell culture is typically employed for *in vitro* experiments for many kinds of tumor cells, but employing tumor cell spheroids in a three-dimensional culture is better model to mimic *in vivo* conditions. A spatiotemporal spheroid analysis of U87 glioma cells showing high invasiveness, using computational and experimental approaches, implicates intrinsic cellular mechanisms of glioma invasion: local cell density, radial oriented cell motion away from the spheroid, and intercellular repulsion dynamics are involved in glioma invasion [45].

4.4. Mathematical Model. Recently, a mathematical model based on the proliferation/migration dichotomy of glioma cells has been applied to investigate why modulatory interventions against glioma vascularization have not been successful at controlling glioma invasion [46]. The study found that cell proliferation/migration ratio was a critical determinant of glioma responses to vasomodulatory interventions against glioma vascularization [46].

4.5. Therapeutic Approach. The "Go or Grow" potential of gliomas is related to metabolic stress which mediates some neuropeptide-processing enzymes. Reduced expression of carboxypeptidase E (CPE), a neuropeptide-processing enzyme that is induced by environmental stressors such as hypoxia and glucose deprivation, contributes to GBM cell migration and invasion [47]. The study indicates that loss or reduction of CPE expression correlated with poor prognosis of GBM patients. The control of metabolic stress based on the "Go or Grow" hypothesis may be a potential target for future antiglioma therapeutic approach mediating glioma biology.

The mitotic kinesin, KIF11, is a driver of glioblastoma invasion, proliferation, and self-renewal [48]. Inhibition of KIF11 with a highly specific small-molecule inhibitor regulates GBM cell growth and motility, associated with intratumoral heterogeneity, suggesting that KIF11 is a therapeutic target for glioblastoma treatment.

Further analysis of the cellular, molecular, and genetic processes underlying the "Go or Grow" dichotomy is warranted to elucidate novel therapeutic approaches for glioma invasion.

5. Overview of Animal Model for Glioma

The invasiveness of human malignant brain tumors has been reproduced in several animal models in order to investigate detailed histopathological processes.

5.1. N-Ethyl-N-Nitrosourea-Induced Rat Glioma Model. One useful animal model is N-ethyl-N-nitrosourea- (ENU-) induced rat gliomas. A high incidence of CNS tumors including GBMs has been consistently induced in the offspring of rats treated with a single dose of transplacental ENU [49], and many aspects of this model have been studied [50–52]. A size-oriented classification for ENU-induced rat glial tumors has been established: early neoplastic proliferation (ENP), microtumors, and macrotumors [49, 52, 53]. ENP represents a focus of glial population less than 300 μm in diameter. Due to their small size, it is difficult to identify ENPs histomorphologically by conventional hematoxylin and eosin staining; therefore they are immunohistochemically using galectin-3 antibody [52]. Microtumors, exhibiting destructive histopathological features, are distinguished from macrotumors by their size, being between 300 and 500 μm in diameter. The macrotumors are considered to be an advanced stage of the neoplastic growth process, and when induced by ENU, they are used as endogenously produced gliomas for analyses of invasiveness [54].

5.2. Genetically Engineered Animal Models. Genetically engineered animals, one of the powerful tools for studying the biology of neoplasms and oncogene identification, have also been employed as developing mouse glioma models. Genetically engineered mice have been successfully used to investigate tumorigenesis and its progression within an intact living organ as animal models for human neoplasms. Weissenberger et al. [55] generated a transgenic mouse model showing the overexpression of v-src oncogene under the control of GFAP regulatory promotor. The transgenic mice produced low-grade astrocytomas in early phase and high-grade astrocytomas in later phase of glioma tumorigenesis. The morphological characteristics such as pseudopalisading cells surrounding necrotic areas were induced in GBM with high mitotic activity. Genetically engineered histone H3 K27M mutations in neonatal mice cooperate with activating platelet-derived growth factor receptor α (PDGFRα) mutant and Trp53 loss that may induce self-renewal of neural stem cell and develop diffuse intrinsic pontine glioma (DIPG) recapitulating human DIPG [56]. The histone H3 K27M mutation appears fundamental and important event in diffuse infiltration of glioma cells in DIPG.

5.3. Human Xenograft Glioma Models. Animal models of human GBMs have been established, including subcutaneous or orthotopic xenograft implantation of GBM cells into immunodeficient mice. Patient-derived orthotopic glioblastoma xenograft models using surgical samples of GBM from patients reproduce the histopathology of human glioblastomas. The advantage of the orthotopic GBM xenograft model, compared to subcutaneous xenograft implantation model, is that implanting GBM cells into their anatomical origin equivalent within a host animal provides a biologically suitable site for glioma-brain interactions and maintains genomic characteristics of original human GBMs. Soeda et al. [23] established patient-derived several subclones from a single tumor of a patient as GBM xenograft model. Differences of cell morphology, invasiveness, progression, and proliferative activities, which represented the glioblastoma heterogeneity, were revealed in a mouse model featuring orthotopic xenografts of the subclones [23]. The subclones

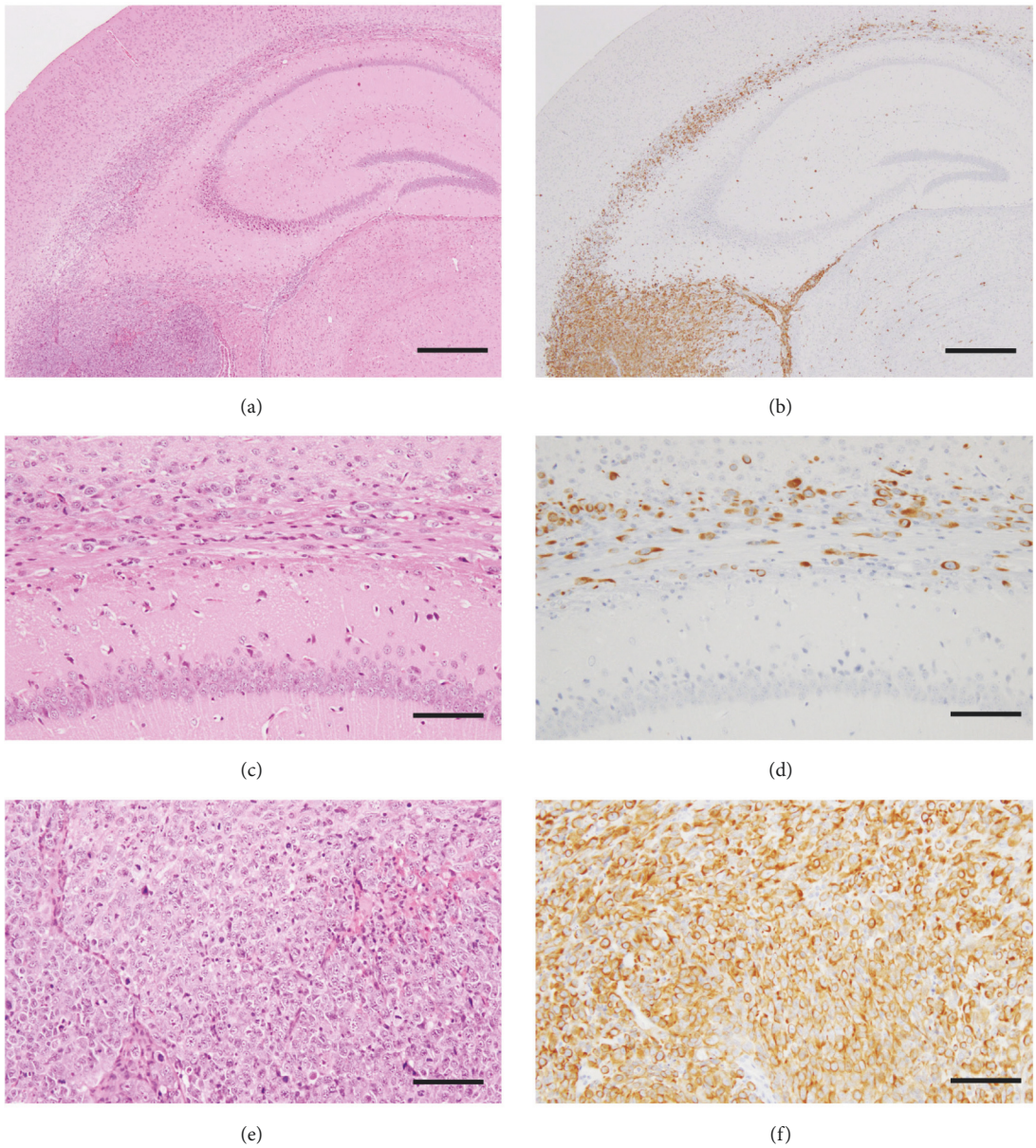

Figure 5: The human GBM orthotopic xenograft exhibiting invasive and extensive infiltration in NOD-scid mice. The nestin-expressing NSC-like GBM cells are highly invasive, showing diffuse infiltration into the brain including the corpus callosum, hippocampus, and the subependymal regions. (a, b) Photomicrographs of low-power field of human GBM orthotopic xenograft in NOD-scid mouse brain. (c, d) Photomicrographs of high-power field of corpus callosum infiltrated by human GBM. (e, f) Photomicrographs of high-power field of mass lesion of human GBM. (a, c, e) Hematoxylin and eosin staining. (b, d, f) Immunohistochemistry for nestin. Scale bars in (a) and (b), 500 μm; scale bars in (c), (d), (e), and (f), 100 μm.

exhibiting more invasive and extensive infiltration induced higher mortality. The nestin-expressing cells are able to differentiate into multiple cell types in CNS development, acting like neuroepithelial stem cells. Thus, nestin is a marker of NSCs or neural progenitor cell [57, 58]. Soeda et al. [23] demonstrated that the nestin-expressing NSC-like human GBM cells were highly invasive and showed diffuse infiltration into the brain, including to contralateral hemispheres via the corpus callosum (Figure 5).

Recently, induced pluripotent stem (iPS) cells derived from human fibroblasts have been used to reproduce glial tumorigenesis. In vivo transplantation of transformed neural iPS cells produced highly invasive tumors containing undifferentiated stem cells, and this model has been used to screen the effectiveness of anticancer compounds and revealed specific molecules targeting transformed neural iPS cells [59].

6. Conclusion

Specific molecular parameters, in addition to traditional histopathological analysis, have been used to define tumor

classification in the revised 4th edition of the WHO Classification of CNS tumors, published in 2016. Indeed, a large subset of glial tumors is now defined based on diagnostics of isocitrate dehydrogenase (IDH) mutation and 1p/19q codeletion, and histone H3 K27M mutation appears to be a fundamental event in diffuse infiltration of glioma cells in DIPG. As described in this review, currently GC is the only subtype of malignant glioblastoma developing a specific growth pattern. However, careful histomorphological examination is still important since, for example, the neoplastic cells within the GC can provide valuable insight into the mechanisms underlying glioma invasion. Furthermore, for example, morphological features such as "secondary structures of Scherer" are still important as diverse phenotypes of IDH(+) or IDH(-) glioma.

Detailed histopathological analysis based on the combination of molecular parameters with traditional analytical methods should be used for evaluating efficacy of targeted therapies against cellular and genetic heterogeneity within the invasive and resistant glioblastoma.

Conflicts of Interest

The authors declare that there are no conflicts of interest regarding the publication of this paper.

References

[1] T. A. Dolecek, J. M. Propp, N. E. Stroup, and C. Kruchko, "CBTRUS statistical report: primary brain and central nervous system tumors diagnosed in the United States in 2005-2009," *Neuro-Oncology*, vol. 14, no. 5, pp. v1–v49, 2012.

[2] T. F. Cloughesy, W. K. Cavenee, and P. S. Mischel, "Glioblastoma, from molecular pathology to targeted treatment," *Annual Review of Pathology*, vol. 9, pp. 25-10, 2014.

[3] H. J. Scherer, "Structural development in gliomas," *American Journal of Cancer*, vol. 34, no. 3, pp. 333–351, 1938.

[4] S. Mehta and C. Lo Cascio, "Developmentally regulated signaling pathways in glioma invasion," *Cellular and Molecular Life Sciences*, vol. 75, no. 3, pp. 385–402, 2018.

[5] D. H. Rowitch and A. R. Kriegstein, "Developmental genetics of vertebrate glial-cell specification," *Nature*, vol. 468, no. 7321, pp. 214–222, 2010.

[6] C. Klämbt, "Modes and regulation of glial migration in vertebrates and invertebrates," *Nature Reviews Neuroscience*, vol. 10, no. 11, pp. 769–779, 2009.

[7] F. T. Merkle and A. Alvarez-Buylla, "Neural stem cells in mammalian development," *Current Opinion in Cell Biology*, vol. 18, no. 6, pp. 704–709, 2006.

[8] K. Y. Kwan, N. Sestan, and E. S. Anton, "Transcriptional co-regulation of neuronal migration and laminar identity in the neocortex," *Development*, vol. 139, no. 9, pp. 1535–1546, 2012.

[9] J. M. Parent, N. von dem Bussche, and D. H. Lowenstein, "Prolonged seizures recruit caudal subventricular zone glial progenitors into the injured hippocampus," *Hippocampus*, vol. 16, no. 3, pp. 321–328, 2006.

[10] S. G. M. Piccirillo, I. Spiteri, A. Sottoriva et al., "Contributions to drug resistance in glioblastoma derived from malignant cells in the sub-ependymal zone," *Cancer Research*, vol. 75, no. 1, pp. 194–202, 2015.

[11] A. M. Mistry, A. T. Hale, L. B. Chambless, K. D. Weaver, R. C. Thompson, and R. A. Ihrie, "Influence of glioblastoma contact with the lateral ventricle on survival: a meta-analysis," *Journal of Neuro-Oncology*, vol. 131, no. 1, pp. 125–133, 2017.

[12] A. M. Mistry, M. C. Dewan, G. A. White-Dzuro et al., "Decreased survival in glioblastomas is specific to contact with the ventricular-subventricular zone, not subgranular zone or corpus callosum," *Journal of Neuro-Oncology*, vol. 132, no. 2, pp. 341–349, 2017.

[13] J. Chen, Y. Li, T.-S. Yu et al., "A restricted cell population propagates glioblastoma growth after chemotherapy," *Nature*, vol. 488, no. 7412, pp. 522–526, 2012.

[14] S. Bao, Q. Wu, R. E. McLendon et al., "Glioma stem cells promote radioresistance by preferential activation of the DNA damage response," *Nature*, vol. 444, no. 7120, pp. 756–760, 2006.

[15] J. D. Lathia, S. C. Mack, E. E. Mulkearns-Hubert, C. L. L. Valentim, and J. N. Rich, "Cancer stem cells in glioblastoma," *Genes & Development*, vol. 29, no. 12, pp. 1203–1217, 2015.

[16] T. M. Thomas and J. S. Yu, "Metabolic regulation of glioma stem-like cells in the tumor micro-environment," *Cancer Letters*, vol. 408, pp. 174–181, 2017.

[17] A. Roos, Z. Ding, J. C. Loftus, and N. L. Tran, "Molecular and microenvironmental determinants of glioma stem-like cell survival and invasion," *Frontiers in Oncology*, vol. 7, p. 120, 2017.

[18] M. A. Qazi, P. Vora, C. Venugopal et al., "Intratumoral heterogeneity: pathways to treatment resistance and relapse in human glioblastoma," *Annals of Oncology: Official Journal of the European Society for Medical Oncology*, vol. 28, no. 7, pp. 1448–1456, 2017.

[19] J. Bischof, M.-A. Westhoff, J. E. Wagner et al., "Cancer stem cells: The potential role of autophagy, proteolysis, and cathepsins in glioblastoma stem cells," *Tumour Biology: The Journal of the International Society for Oncodevelopmental Biology and Medicine*, vol. 39, no. 3, pp. 1–13, 2017.

[20] N. Colwell, M. Larion, A. J. Giles et al., "Hypoxia in the glioblastoma microenvironment: Shaping the phenotype of cancer stem-like cells," *Neuro-Oncology*, vol. 19, no. 7, pp. 887–896, 2017.

[21] D. Uribe, Á. Torres, J. D. Rocha et al., "Multidrug resistance in glioblastoma stem-like cells: Role of the hypoxic microenvironment and adenosine signaling," *Molecular Aspects of Medicine*, vol. 55, pp. 140–151, 2017.

[22] R. K. Balvers, C. M. F. Dirven, S. Leenstra, and M. L. M. Lamfers, "Malignant glioma in vitro models: on the utilization of stem-like cells," *Current Cancer Drug Targets*, vol. 17, no. 3, pp. 255–266, 2017.

[23] A. Soeda, A. Hara, T. Kunisada, S.-I. Yoshimura, T. Iwama, and D. M. Park, "The evidence of glioblastoma heterogeneity," *Scientific Reports*, vol. 5, no. 7979, 2015.

[24] S. Chiblak, Z. Tang, D. Lemke et al., "Carbon irradiation overcomes glioma radioresistance by eradicating stem cells and forming an antiangiogenic and immunopermissive niche," *JCI Insight*, vol. 4, no. 2, 2019.

[25] S. Sheikh, D. Saxena, X. Tian et al., "An integrated stress response agent that modulates DR5 dependent TRAIL synergy reduces patient derived glioma stem cell viability," *Molecular Cancer Research: MCR*, vol. 17, no. 5, 2019.

[26] R. Mooney, M. Hammad, J. Batalla-Covello, A. Abdul Majid, and K. S. Aboody, "Concise review: neural stem cell-mediated targeted cancer therapies," *Stem Cells Translational Medicine*, vol. 7, no. 10, pp. 740–747, 2018.

[27] G. S. Stoyanov, D. Dzhenkov, P. Ghenev, B. Iliev, Y. Enchev, and A. B. Tonchev, "Cell biology of glioblastoma multiforme: from basic science to diagnosis and treatment," *Medical Oncology*, vol. 35, no. 3, p. 27, 2018.

[28] S. Osuka and E. G. Van Meir, "Overcoming therapeutic resistance in glioblastoma: the way forward," *The Journal of Clinical Investigation*, vol. 127, no. 2, pp. 415–426, 2017.

[29] B. D. Liebelt, T. Shingu, X. Zhou, J. Ren, S. A. Shin, and J. Hu, "Glioma stem cells: signaling, microenvironment, and therapy," *Stem Cells International*, vol. 2016, Article ID 7849890, 10 pages, 2016.

[30] C. Maccalli and R. De Maria, "Cancer stem cells: perspectives for therapeutic targeting," *Cancer Immunology, Immunotherapy*, vol. 64, no. 1, pp. 91–97, 2015.

[31] A. Hara, N. Sakai, H. Yamada, T. Tanaka, and H. Mori, "Assessment of proliferative potential in gliomatosis cerebri," *Journal of Neurology*, vol. 238, no. 2, pp. 80–82, 1991.

[32] G. T. Armstrong, P. C. Phillips, L. B. Rorke-Adams, A. R. Judkins, A. R. Localio, and M. J. Fisher, "Gliomatosis cerebri: 20 years of experience at the childrens hospital of Philadelphia," *Cancer*, vol. 107, no. 7, pp. 1597–1606, 2006.

[33] D. N. Louis, A. Perry, G. Reifenberger et al., "The 2016 world health organization classification of tumors of the central nervous system: a summary," *Acta Neuropathologica*, vol. 131, no. 6, pp. 803–820, 2016.

[34] U. Herrlinger, D. T. W. Jones, M. Glas et al., "Gliomatosis cerebri: no evidence for a separate brain tumor entity," *Acta Neuropathologica*, vol. 131, no. 2, pp. 309–319, 2016.

[35] A. M. La Madrid, S. Ranjan, and K. E. Warren, "Gliomatosis cerebri: a consensus summary report from the Second International Gliomatosis cerebri Group Meeting, June 22–23, 2017, Bethesda, USA," *Journal of Neuro-Oncology*, vol. 140, no. 1, pp. 1–4, 2018.

[36] H. Nishioka, H. Ito, and T. Miki, "Difficulties in the antemortem diagnosis of gliomatosis cerebri: Report of a case with diffuse increase of gemistocyte-like cells, mimicking reactive gliosis," *British Journal of Neurosurgery*, vol. 10, no. 1, pp. 103–107, 1996.

[37] M. Cayre, P. Canoll, and J. E. Goldman, "Cell migration in the normal and pathological postnatal mammalian brain," *Progress in Neurobiology*, vol. 88, no. 1, pp. 41–63, 2009.

[38] A. Giese, M. A. Loo, N. Tran, D. Haskett, S. W. Coons, and M. E. Berens, "Dichotomy of astrocytoma migration and proliferation," *International Journal of Cancer*, vol. 67, no. 2, pp. 275–282, 1996.

[39] A. Kathagen-Buhmann, A. Schulte, J. Weller et al., "Glycolysis and the pentose phosphate pathway are differentially associated with the dichotomous regulation of glioblastoma cell migration versus proliferation," *Neuro-Oncology*, vol. 18, no. 9, pp. 1219–1229, 2016.

[40] H. D. Dhruv, W. S. M. Winslow, B. Armstrong et al., "Reciprocal activation of transcription factors underlies the dichotomy between proliferation and invasion of glioma cells," *PLoS ONE*, vol. 8, no. 8, p. e72134, 2013.

[41] S. D. Wang, P. Rath, B. Lal et al., "EphB2 receptor controls proliferation/migration dichotomy of glioblastoma by interacting with focal adhesion kinase," *Oncogene*, vol. 31, no. 50, pp. 5132–5143, 2012.

[42] S. Xia, B. Lal, B. Tung, S. Wang, C. R. Goodwin, and J. Laterra, "Tumor microenvironment tenascin-C promotes glioblastoma invasion and negatively regulates tumor proliferation," *Neuro-Oncology*, vol. 18, no. 4, pp. 507–517, 2016.

[43] Q. Xie, S. Mittal, and M. E. Berens, "Targeting adaptive glioblastoma: An overview of proliferation and invasion," *Neuro-Oncology*, vol. 16, no. 12, pp. 1575–1584, 2014.

[44] M. E. Berens and A. Giese, ""...those left behind." Biology and oncology of invasive glioma cells," *Neoplasia*, vol. 1, no. 3, Article ID 7900034, pp. 208–219, 1999.

[45] M. Tektonidis, H. Hatzikirou, A. Chauvière, M. Simon, K. Schaller, and A. Deutsch, "Identification of intrinsic in vitro cellular mechanisms for glioma invasion," *Journal of Theoretical Biology*, vol. 287, no. 1, pp. 131–147, 2011.

[46] J. C. L. Alfonso, A. Köhn-Luque, T. Stylianopoulos et al., "Why one-size-fits-all vaso-modulatory interventions fail to control glioma invasion: In silico insights," *Scientific Reports*, vol. 6, pp. 1–15, 2016.

[47] E. Höring, P. N. Harter, J. Seznec et al., "The "go or grow" potential of gliomas is linked to the neuropeptide processing enzyme carboxypeptidase E and mediated by metabolic stress," *Acta Neuropathologica*, vol. 124, no. 1, pp. 83–97, 2012.

[48] M. Venere, C. Horbinski, J. F. Crish et al., "The mitotic kinesin KIF11 is a driver of invasion, proliferation, and self-renewal in glioblastoma," *Science Translational Medicine*, vol. 7, no. 304, p. 304ra143, 2015.

[49] A. Koestner, J. A. Swenberg, and W. Wechsler, "Transplacental production with ethylnitrosourea of neoplasms of the nervous system in Sprague-Dawley rats," *The American Journal of Pathology*, vol. 63, no. 1, pp. 37–56, 1971.

[50] F. Yoshimura, T. Kaidoh, T. Inokuchi, and M. Shigemori, "Changes in VEGF expression and in the vasculature during the growth of early-stage ethylnitrosourea-induced malignant astrocytomas in rats," *Virchows Archiv: An International Journal of Pathology*, vol. 433, no. 5, pp. 457–463, 1998.

[51] H. Yano, A. Hara, J. Shinoda et al., "Immunohistochemical analysis of β-catenin in N-ethyl-N-nitrosourea-induced rat gliomas: implications in regulation of angiogenesis," *Neurological Research*, vol. 22, no. 5, pp. 527–532, 2000.

[52] N. H. Binh, K. Satoh, K. Kobayashi et al., "Galectin-3 in preneoplastic lesions of glioma," *Journal of Neuro-Oncology*, vol. 111, no. 2, pp. 123–132, 2013.

[53] G. Reifenberger, T. Bilzer, R. J. Seitz, and W. Wechsler, "Expression of vimentin and glial fibrillary acidic protein in ethylnitrosourea-induced rat gliomas and glioma cell lines," *Acta Neuropathologica*, vol. 78, no. 3, pp. 270–282, 1989.

[54] B. C. Zook, S. J. Simmens, and R. V. Jones, "Evaluation of ENU-induced gliomas in rats: nomenclature, immunochemistry, and malignancy," *Toxicologic Pathology*, vol. 28, no. 1, pp. 193–201, 2000.

[55] J. Weissenberger, J. P. Steinbach, G. Malin, S. Spada, T. Rulicke, and A. Aguzzi, "Development and malignant progression of astrocytomas in GFAP-v-src transgenic mice," *Oncogene*, vol. 14, no. 17, Article ID 1201168, pp. 2005–2013, 1997.

[56] J. D. Larson, L. H. Kasper, B. S. Paugh et al., "Histone H3.3 K27M accelerates spontaneous brainstem glioma and drives restricted changes in bivalent gene expression," *Cancer Cell*, vol. 35, no. 1, pp. 140–155.e7, 2019.

[57] A. P. Castillo, D. Aguilar-Morante, J. A. Morales-Garcia, and J. Dorado, "Cancer stem cells and brain tumors," *Clinical & Translational Oncology: Official Publication of the Federation of Spanish Oncology Societies and of the National Cancer Institute of Mexico*, vol. 10, no. 5, pp. 262–267, 2008.

[58] A. Bradshaw, A. Wickremsekera, S. T. Tan, L. Peng, P. F. Davis, and T. Itinteang, "Cancer stem cell hierarchy in glioblastoma multiforme," *Frontiers in Surgery*, vol. 3, no. 21, 2016.

[59] I. Sancho-Martinez, E. Nivet, Y. Xia et al., "Establishment of human iPSC-based models for the study and targeting of glioma initiating cells," *Nature Communications*, vol. 7, no. 1, article no. 10743, 2016.

Hindawi
Journal of Oncology
Volume 2019, Article ID 1805841, 10 pages
https://doi.org/10.1155/2019/1805841

Research Article

The SR-B1 Receptor as a Potential Target for Treating Glioblastoma

Ethan Berney,[1] Nirupama Sabnis,[1] Marlyn Panchoo,[1] Sangram Raut,[1] Rob Dickerman,[2] and Andras G. Lacko[1,3]

[1]*Lipoprotein Drug Delivery Laboratory, Department of Physiology/Anatomy, USA*
[2]*Neurosurgery, Presbyterian Hospital, Plano, TX, USA*
[3]*Department of Pediatrics, University of North Texas Health Science Center, Fort Worth, TX, USA*

Correspondence should be addressed to Andras G. Lacko; andras.lacko@unthsc.edu

Received 25 February 2019; Revised 22 April 2019; Accepted 12 May 2019; Published 3 June 2019

Academic Editor: Akira Hara

Purpose. The goal of these studies was to provide proof of concept for a novel targeted therapy for *Glioblastoma Multiforme (GBM)*. *Methods*. These studies involve the evaluation of reconstituted high density lipoprotein (rHDL) nanoparticles (NPs) as delivery agents for the drug, mammalian Target of Rapamycin (mTOR) inhibitor Everolimus (EVR) to GBM cells. Cytotoxicity studies and assessment of downstream effects, including apoptosis, migration, and cell cycle events, were probed, in relation to the expression of scavenger receptor B type 1 (SR-B1) by GBM cells. *Results*. Findings from cytotoxicity studies indicate that the rHDL/EVR formulation was 185 times more potent than free EVR against high SR-B1 expressing cell line (LN 229). Cell cycle analysis revealed that rHDL/EVR treated LN229 cells had a 5.8 times higher apoptotic cell population than those treated with EVR. The sensitivity of GBM cells to EVR treatment was strongly correlated with SR-B1 expression. *Conclusions*. These studies present strong proof of concept regarding the efficacy of delivering EVR and likely other agents, via a biocompatible transport system, targeted to the SR-B1 receptor that is upregulated in most cancers, including GBM. Targeting the SR-B1 receptor could thus lead to effective personalized therapy of GBM.

1. Introduction

Glioblastoma Multiforme (GBM) is a devastating disease with a very poor prognosis, as the survival of patients with GBM rarely extends beyond 3 years from the time of diagnosis [1–3]. Despite intensive research and new approaches to treatment, only limited improvements in patient outcomes have been achieved [4, 5]. New approaches, perhaps involving nanotechnology, are thus urgently needed to improve the survival and the quality of life for GBM patients.

GBM tumors undergo extensive metabolic reprogramming during their development, with epigenetic modifications that are also impacted by the tumor environment [6]. Postoperative hypoxia is likely to facilitate diffuse and invasive tumor growth [7] in addition to enhancing the expression of the scavenger receptor type B1 (SR-B1) [8]. Thus, targeting GBM with a high density lipoprotein (HDL) type drug transporter may be effective against the invasion of GBM tumors, facilitated by the SR-B1 receptor [9].

While nearly 165,000 publications listed in PubMed contain the keyword "nanoparticles" (NPs), the efficiency of payload delivery to oncogenic tissues on the average is only 0.7% [10]. This finding is still perceived as a major impediment to the development of clinical brain barrier application of nanotechnology. In addition, drug resistance to chemotherapy and drug delivery across the blood brain barrier (BBB) are major obstacles to the effective treatment of GBM [1]. Several therapeutic nanocarriers have been for the treatment of GBM including targeted nanoparticles to study the tumor microenvironment [11–14]. These studies demonstrated an enhanced permeability and retention (EPR)

effect, via selective targeting that enables the accumulation of therapeutic agents in tumor tissues.

In the last several years, research on lipoprotein-based drug delivery carriers has shown a dramatic increase [15–19]. Our laboratory and others have shown have emphasized the favorable properties of synthetic/reconstituted HDL and HDL mimicking nanomaterials due to their biocompatibility, small size, nonimmunogenicity, long circulation time, and selective uptake via SR-B1 receptors [20–25]. The rHDL NPs also seem suitable to cross the blood brain barrier (BBB) [21] and to subsequently deliver their therapeutic payload to the brain. Fung et al. [26] demonstrated that HDL is able to cross the BBB by transcytosis, a unique mechanism facilitated by the scavenger receptor B-1 (SR-B1). Others have described the ability of a major HDL component, Apolipoprotein A-I (Apo A-I), to cross the BBB [27–29]. Kadiyala et al. [30] studied the ability of synthetic HDL (sHDL) nanodiscs as a chemoimmunotherapy for delivery of CpG, a Toll-like receptor 9 (TLR9) agonist, together with docetaxel (DTX), to the GBM microenvironment and elicit tumor regression. This combination of DTX-sHDL-CpG treatment with radiation (IR) resulted in tumor regression and long-term survival in 80% of GBM-bearing animals.

Our laboratory was one of the first groups to develop an rHDL drug delivery platform that mimics the properties of endogenous HDL, a cholesterol transport vehicle [31]. These rHDL NPs also seem suitable to cross the blood brain barrier (BBB) and subsequently deliver their therapeutic payload to the brain. The purpose of this study was to obtain *proof of concept data to support more advanced preclinical studies and to facilitate the eventual translation of these findings toward clinical applications*. To accomplish these goals, the drug Everolimus (EVR) was chosen due to the recent clinical interest in EVR and regarding the off-target effects associated with mammalian Target of Rapamycin (mTOR) inhibitors [32]. EVR is an FDA approved mTOR inhibitor that has been used in combination with temozolomide (TMZ) in a recent Phase II clinical study with GBM patients [33].

With a partition coefficient ($X_{log}P$) value of 5.9, EVR is a suitable candidate to accumulate in the core regions of the rHDL "magic bullet" drug carrier [34]. The preferred payload for rHDL NPs appears to be hydrophobic compounds as their natural counterparts (HDL) transport primarily highly lipophilic cholesteryl esters as their core components [35]. The tumor selectivity of this drug delivery system is based on the overexpression of the SR-B1 receptor by cancer cells and tumors [36], including aggressive GBM cell lines. This feature provides enhanced targeting via the HDL type NPs for the SR-B1 receptor, thus limiting the off-target effects of chemotherapy [37].

2. Materials and Methods

Materials: Apolipoprotein A-I (Apo A-I) was purchased from MC Labs, San Francisco, CA. EVR and TMZ were purchased from Selleckchem, Houston, TX. Egg yolk phosphatidylcholine, free cholesterol and cholesterol oleate, and dimethylsulfoxide were obtained from Sigma Aldrich, St. Louis, MO.

2.1. Methods

2.1.1. Preparation of the rHDL/EVR Nanoparticles. rHDL/EVR nanoparticles were assembled via a modified cholate dialysis procedure [38] as follows. Briefly, the lipid ingredients, 15 mg egg yolk PC (EYPC), 0.035 mg free cholesterol (FC), and 0.15 mg cholesteryl oleate (CE), were dissolved in chloroform and combined with the drug (EVR). The mixture of the lipids (PC, FC, and CE) and the drug (EVE) were dried under N_2 to a thin film and dispersed in 60 μL dimethyl sulphoxide (DMSO). To this mixture, 5 mg of Apo A-I and 140 μL of 0.1 M sodium cholate were added and the volume was made up to 2 mL with Tris-EDTA buffer (10 mM Tris, 0.1 M KCl, and 1 mM EDTA pH 8.0). The final molar ratio of Apo A1: EYPC:FC:CE = 1:110:0.5:1.3. This procedure was optimized for EVR via a thermocycling/sonication step as follows. The EVR formulation was incubated at 50°C for 2 minutes and kept on ice for another 2 minutes. The formulation was then sonicated for 5 minutes with an Ultrasonic Processor™ at amplitude 25. The thermocycling/sonication procedure was repeated and the formulation was subsequently incubated for 12 hours at 4°C on a nutator shaker. Next the sample was dialyzed against 2 L of PBS, for 48 hours, with three buffer changes. The preparation was then centrifuged at 1000 rpm for 2 minutes and sterilized by passing it through a 0.2 μm syringe filter and kept in the dark at 4°C until used.

2.1.2. Characterization of rHDL/EVR Nanoparticles. The assembled, drug containing NPs were characterized with regard to physical properties and chemical composition. A bicinchoninic acid (BCA) assay (Thermo Fischer Scientific, Waltham, MA) was used to determine the Apo A-I. The Cholesterol E and Phospholipid C reagent kits (Wako Chemicals USA, Inc., Richmond, VA, USA) were used to determine the amount of cholesterol, cholesterol oleate, and EYPC in the NPs. These assays were conducted on a Cytation 3 Imaging reader Instrument (Bio-Tek, Winooski, VT, USA). The amount of EVR incorporated into the NPs was estimated by spectrophotometry at 277 nm (at the λ_{max} of EVR). To account for the interference by the Apo A1 protein (known to also absorb in this wavelength range), the absorbance of the empty rHDL NPs (containing the same amount of Apo A-I as the drug containing NPs) was subtracted from the rHDL/EVR absorbance.

The drug entrapment efficiency (DEE) was calculated using the equation

$$\text{DEE} = \left[\frac{(\text{drug incorporated into NPs})}{(\text{initial drug})}\right] \times 100\%. \quad (1)$$

The percentage of individual components is calculated by a formula

$$\%\ \text{Component} = \left(\frac{\text{Average mg/mL of the component}}{\sum\ \text{total mg/mL of all the components}}\right) \times 100 \quad (2)$$

2.1.3. Nanoparticle Size Measurements. To determine the diameter of the rHDL NPs, dynamic light scattering (DLS) was carried out using a DelsaNano HC Particle Analyzer (Beckman Coulter, Inc., Fullerton, CA). The data are reported as mean diameter $^{\pm}$ SD and poly-dispersity index (PDI) using number distribution analysis.

2.1.4. Transmission Electron Microscopy. The rHDL NP solution was dialyzed against distilled water for 18-24hr. Carbon coated 200 mesh Formvar grids were used for sample preparation. Diluted samples were drop coated on to discharged grids, followed by staining with 1% uranyl acetate for 1 min. TEM images were taken using TecnaiTM Spirit electron microscope (EMCF facility in University of Texas Southwestern Medical Center, Dallas, TX).

2.1.5. Cell Culture. A172, LN229, and LN18 cells were purchased from ATCC, Manassas, VA. Astrocytes and U87-MG were provided by Dr. Meharvan Singh (UNTHSC). Cells were cultured in DMEM, supplemented with 10% fetal bovine serum (FBS) and 1% (100 U/mL) Penicillin-Streptomycin. All cultures were incubated at 37°C in 5% CO_2 in 75 cm^2 flasks and passaged with 0.25% trypsin upon 80-90% confluency.

2.1.6. Western Blot and Densitometry. Antibodies for SR-B1 and beta actin were acquired from Abcam (Cambridge, MA). Anti-rabbit secondary antibody was purchased from Cell Signaling Technology, Inc. (Beverly, MA). Cells were first pelleted and then disrupted using a lysis buffer (50 mM Tris-HCl (pH 8.0), 150 mM NaCl, 0.02% Sodium Azide, 100 μg/ml PMSF, 1 μg/ml aprotinin, 1% NP-4D). The protein concentration of each sample was determined using a BCA assay. A sample containing 20 μg of protein (from each cell extract) was subjected to SDS electrophoresis. The isolated protein band was then transferred to a nitrocellulose membrane using the iBlot 2 system (Thermo Fisher Scientific, Carlsbad, CA) and probed with primary and secondary antibodies. Finally, the immune-complexes were visualized via chemiluminescence and were quantified using Image J software to yield the relative expression levels of SR-B1/Actin.

2.1.7. Cytotoxicity Assays and IC_{50} Determination. Cell lines were grown in DMEM medium and incubated at 37°C with 5% CO_2. Upon achieving the needed density, the cells were recovered, treated with trypan blue, and subsequently counted with a Cellometer mini (Nexcelom Bioscience, Lawrence, MA, USA). The cells were next seeded at a density of 5×10^4 cells/well in 96 well microtiter plates in DMEM+10%FBS+1% penicillin/streptomycin medium and incubated for 24 hours. Once the cells were attached, the medium was removed, and the cells were washed with sterile PBS. Each cell line was subsequently incubated with increasing amounts of the respective drug formulations in DMEM+1% FBS for 72 hours. The drug containing NPs was prepared fresh for each experiment and stored at −20°C if necessary. Drug formulations were diluted in DMEM+1% FBS on the day of the experiment to 0.1-100 μM. After incubation, 10 μL of tetrazolium salt solution from the Cell Counting Kit-8 (CCK-8, Dojindo Molecular Technologies, Inc. Gaithersburg MD) was added to the respective wells and incubated for 3 hours. The absorbance (for each well) at 450 nm was obtained on a microplate reader (PowerWave, Biotek Instruments Inc., Winooski, VT, USA). IC_{50} values were calculated by plotting cell viability vs. drug concentration, where the molar concentration of the drug inducing a 50% reduction in viability was designated as the IC_{50} value for each formulation.

2.1.8. Matrigel Invasion Assay. Corning BioCoat Matrigel Invasion Chambers (Corning, Bedford, MA) were used to assess the invasive limiting capabilities of the rHDL NPs, according to manufacturer's protocol. Typically, 25,000 cells/insert (0.5 ml) were placed onto rehydrated matrigel invasion chambers, which were then placed into a 24-well plate containing 0.75 ml of a chemoattractant (FBS). The cells were treated, respectively, with 5 μM rHDL/EVR or free EVR (control). The cell suspensions were then incubated for 22 hours (37°C, 5% CO_2). After incubation, noninvading cells were removed from the upper surface of the membrane by scrubbing with a cotton swab. The chambers were then removed from the wells, containing the chemoattractant, dipped in wells containing PBS for a quick wash, and immediately fixed with 100% methanol for 10 minutes. After drying the preparations were stained with crystal violet for 10 minutes. The membranes inside the chambers were then removed with a scalpel and placed onto an oil immersion slide to be viewed for invasion quantification. Fields in triplicate were randomly chosen for each treatment, and cells that invaded through the membrane were counted to assess the invasion.

2.1.9. Cell Cycle Analysis. The respective cell lines were seeded (800,000 cells/dish) in 60 mm dishes and grown to confluency in DMEM+10% FBS+1% penicillin/streptomycin medium. After 24 hours, the medium was removed, and the cells were washed 3 times with PBS, pH 7.4. The cells were then incubated in serum free DMEM medium with free drug, rHDL/EVR, or empty HDL, with a positive control (no drug treatment). A control experiment was run by adding the same amount of DMSO as used to dissolve the free drug. After 22 hours, the medium of each preparation was removed, and the cells were washed twice with PBS. These suspensions were isolated and added to the corresponding samples of medium to ensure that all cells were covered. The cells were then harvested using trypsin as described above, pelleted, and resuspended in PBS+0.1%, bovine serum albumin (BSA).

To this suspension, 3 ml of cold absolute ethanol was added dropwise while vortexing. The cells were then fixed at 4°C overnight and then were again centrifuged and washed with PBS. Next, propidium iodide staining solution (Sigma, P4170) was mixed with the cell pellet. RNaseA stock solution (Worthington Biochemical, LS005649) was then added to each suspension, and the respective preparations were incubated at 37°C for 30 minutes. Cell cycle analysis was then performed with an FC500 Cytometer, with the data presented under Results.

2.1.10. Stability Study. Aliquots of the rHDL/EVR NP formulations were placed into plastic vials and stored at either -20 or 4°C for 1, 15, and 30 days. At each time point, these aliquots were dialyzed as before and the percentage drug retention was determined.

3. Results

3.1. Physicochemical Properties of rHDL/EVR NPs. The chemical composition of the rHDL/EVR nanoparticles is shown in Table 1. The EVR loading efficiency into the rHDL NPs was similar to formulations described earlier [22]. The entrapment efficiency (EE) of EVR into the rHDL NPs was 57±5.6% while the most abundant component was phospholipid (60.7%) followed by protein (20.1%), cholesterol 10%, and EVR (9.3%).

The particle diameter analyses obtained from DLS measurements for the rHDL/ EVR NPs (Figure 1) show a mean diameter of 20.6 nm ± 5.8 nm. The polydispersity index (PDI) of the formulation was 0.253. The morphology and size of the particles were confirmed via transmission electron microscopy (see inset in Figure 1) where most of the NPs were observed to be smaller than 40 nm.

3.2. Storage Stability. The storage stability of the rHDL/EVR NPs was tested at two different temperatures 4°C and −20°C at 3 different time points (Table 2). The % drug recovery is calculated as % encapsulation efficiency (EE). At 4°C, the drug recovery dropped from 99% to 91% over a month. At −20°C almost 96% of the drug was recovered after one month (Table 2).

3.3. SR-B1 Expression in GBM Cells. A panel of GBM cells as well as primary astrocytes was probed for SR-B1 expression (Figure 2(a)) via a Western blot and densitometric analysis (Figure 2(b)). The LN229 cells, derived from an epithelial cell line, were found to have a relatively high SR-B1 expression, while U87-MG, a cerebellar cell line, was found to have relatively low SR-B1 expression. These two cell lines were chosen for subsequent cytotoxicity studies to determine their respective sensitivity to the rHDL/EVR formulation.

3.4. SR-B1 Expression as a Predictor of Sensitivity to rHDL/EVR NPs. Cell viability assays revealed the relative sensitivity of LN229, U87-MG, and astrocytes to rHDL/EVR as 1:3.4:55.9, respectively. These data indicate that the sensitivity of GBM cell lines to the drug containing rHDL NPs may be dependent on their respective SR-B1 expression and that the IC_{50} of EVR was substantially decreased against GBM cells, when delivered in rHDL NPs. The rHDL/EVR NPs also outperformed the free TMZ (the IC_{50} of TMZ was greater than 50 μM against both GBM cell lines {data not shown}). In addition, treatment with empty rHDL NPs had a modest cytotoxic effect against GBM cells, perhaps due to the interaction of Apo A1 with the rHDL receptor [23].

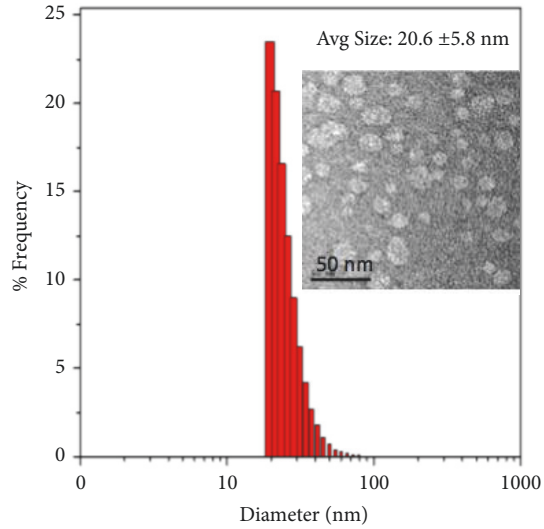

Figure 1: Estimation of rHDL/EVR nanoparticle size via dynamic light scattering (DLS) and Transmission electron microscopy (TEM).

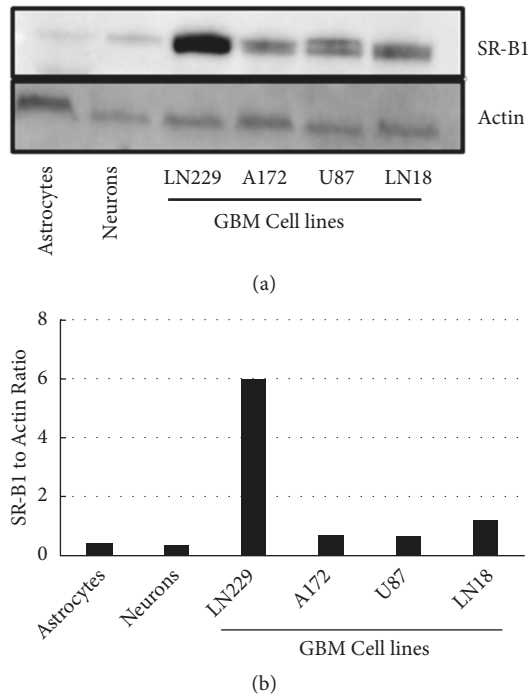

Figure 2: SR-B1 expression in GBM and nonmalignant cell lines via (a) Western blot and (b) densitometry.

As shown in Table 3, the rHDL/EVR nanoparticles markedly potentiated the cytotoxic effect of EVR. Subsequently, a combination of EVR and TMZ, against the highest SR-B1-expressing GBM line (LN229), was also assessed. As seen in Figure 3, free TMZ further enhanced the impact of rHDL/EVR on the GMB (LN229) cells.

3.5. Estimation of Migration/ Invasion Tendencies of GBM Cells. The GBM cell lines, U87-MG (low SR-B1 expressor) and LN229 (a high SR-B1 expressor), were subjected to a

Table 1: Chemical composition of rHDL/EVR nanoparticles.

Component	mg/mL ± SD	Component % of total ± SD
EVR	0.57 ± 0.09	9.3 ± 1.4
Protein	1.23 ± 0.04	20.1 ± 0.7
Phospholipid	3.72 ± 0.19	60.7 ± 3.2
Cholesterol	0.61 ± 0.04	10.0 ± 0.6

Table 2: Storage stability of the rHDL/EVR nanoparticles at different storage conditions.

STORAGE	STORAGE duration (days)			
Temperature	0	1	15	30
%EE∗at 4°C	100±4	99±5	96±7	91±3
% EE at -20°C	100±6	99±3	95±6	96±5

Note: ∗EE is percent encapsulation efficiency.

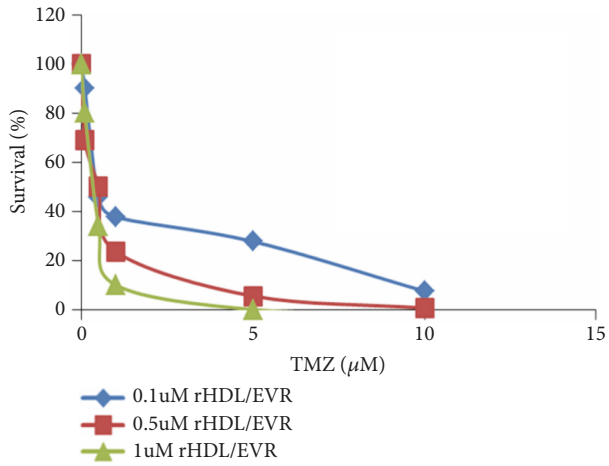

Figure 3: Survival of the LN229 cell line against rHDL EVR+TMZ combination treatment.

matrigel invasion assay in the presence of either free EVR or rHDL/EVR. During rHDL/EVR treatment, invasion was almost completely eliminated in the high SR-B1 expressing cell line (LN229, Figure 4). In addition, the suppression of the migration/invasion tendencies by rHDL/EVR between the low expressor GBM cell lines (U87) and the high expressor cell line (LN229) was significantly different ($*p<0.05$). The tendencies for migration/invasion of the LN229 cells were 13.87 times lower when treated with rHDL/EVR compared to 2.22 times lower tendencies when treated with free EVR (Figure 4) and as such indicate lower propensity for metastatic growth.

3.6. Cell Cycle Analysis of GBM Cells in Response to rHDL/EVR NPs via Flow Cytometry. Next we performed cell cycle analyses to assess the response of GBM cells to EVR and rHDL/EVR with regard to their tendencies to become apoptotic. As shown in Figure 5, treatment with 0.27 uM dose equivalent EVR in rHDL formulation resulted in a marked increase in apoptosis (not expected for a cytostatic agent) while the cell cycle was observed to be arrested at S phase, with less than 1% of the population reaching the G2/M phase, following treatment. Treatment with rHDL/EVR resulted in a 57.7% increase in the apoptotic population of LN229 cells (5.8 times higher than apoptotic population in LN 229 cells treated with EVR). rHDL/EVR also induced 4.3 times more apoptosis in LN229 cells than in U87-MG cells (data not shown). These apoptotic tendencies also correlate well with their respective SR-B1 expression (4.88:1 in favor of the LN229 cells vs. U87-MG cells). To control for the possibility of rHDL being cytotoxic itself, LN229 cells were subjected to empty rHDL treatment. These studies resulted in only 9% of the cell population being apoptotic following treatment (Figure 5).

4. Discussion

Traditional chemotherapy approaches generally produce off-target effects, including toxicity to normal tissues. The rHDL NPs are ideal candidates to protect against the off-target toxicity of drugs, as their hydrophobic core shields the therapeutic agent from release to nonmalignant tissues [6, 24].

Cholesterol transport is a highly conserved and regulated process in the CNS. While only a fraction of the lipoproteins found in the CNS is synthesized *in situ* by astrocytes and oligodendrocytes, most cranial lipoproteins and their components, including Apo A-I, originate from the blood and subsequently cross into the BBB [39]. The SR-B1 receptor is expressed in both astrocytes and neurons, perhaps facilitating the receptor-mediated transport of cholesterol. The SR-B1 expression, however, is far lower than the expression of low density lipoprotein receptor (LDL-R), the predominant receptor for Apolipoprotein E (ApoE) containing lipoproteins [40, 41]. Due to its limited expression in normal compared to much higher levels of expression seen in GBM cells (Figure 2) the SR-B1 receptor is thus a potential novel

Table 3: IC_{50} of everolimus (EVR) formulations against glioblastoma cells (LN 229 and U87) and astrocytes.

Cell line	Free-EVR (μM)	rHDL-EVR (μM)
LN229	>50	0.27±0.05
U87	2.91±0.3	0.92±0.17
Astrocytes	4.27±0.82	15.1±1.24

Note: a range of concentration of 10 nM to 50 μM of each formulation was used for the cytotoxicity studies.

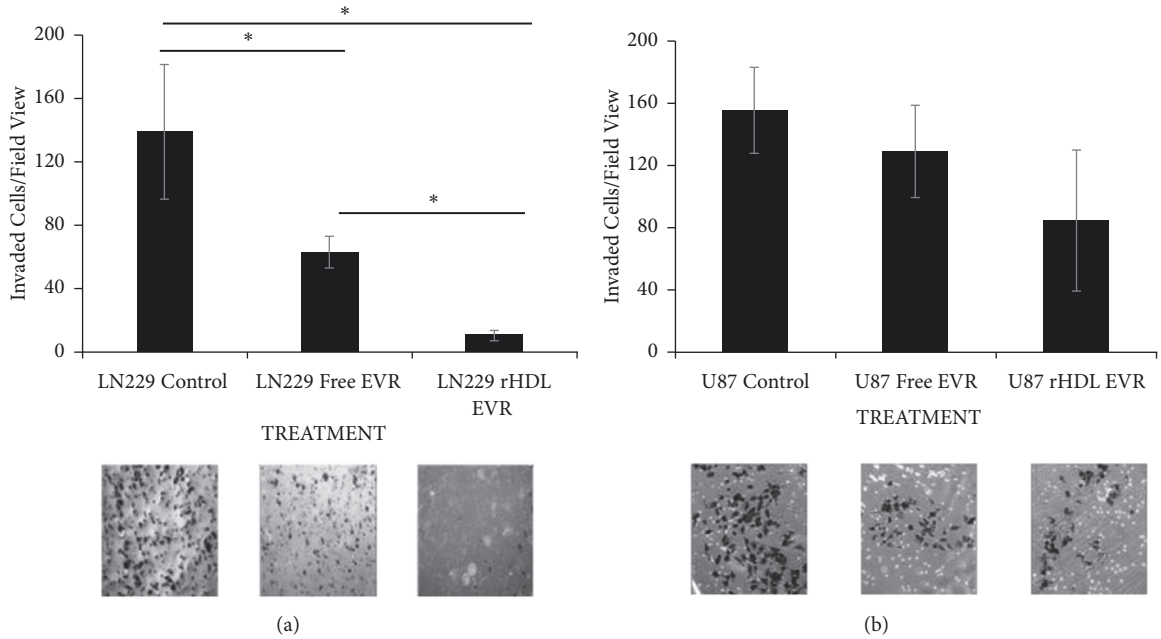

Figure 4: Comparison of the tendency for migration/invasion between GBM cell lines LN229 (a) and U87 (b) with differing SR-B1 expression. ∗Statistically significant ($p<0.05$). No significant difference was found among different groups for U87 cell line.

target for rHDL facilitated therapeutics that could mitigate the off-target cytotoxicity seen in traditional approaches to treat GBM.

We have also evaluated the SR-B1 expression in GBM and survival of patients from an existing TCGA dataset. Kaplan-Meier survival curves for SCARB1 were generated by using R2 genomics and visualization platform. Database (Tumor Glioblastoma-TCGA-540) with survival information was chosen for analysis. The "Kaplan scan" of R2 genomics generates a Kaplan-Meier Plot based on the most optimal mRNA cut-off expression levels to discriminate between a good and bad prognosis cohort. Five-year survival was analyzed and plotted with event-free and overall survival based on survivin expression. It is evident that high SCARB1 expression in GBM correlates well with worse outcome (Figure 6).

The physicochemical characterization of the rHDL/EVR NPs reveal that these particles had similar properties to those rHDL formulations reported earlier in the literature [38, 42]. The EVR NPs examined in this study, contained 9.3% of the drug with the incorporation efficiency (EE) of about 60%. The small size of these NPs (~20 nm in diameter; Figure 1) should allow them to penetrate the interfibrillar domains of tumors, resulting in greater therapeutic efficacy and accumulation of drugs in the tumor mass [43]. The long circulation time of 3-5 days and small size [15, 35, 43] are anticipated to provide advantages for the rHDL "Trojan Horse" drug delivery system [34] over liposomal and other nanocarriers [44].

The cytotoxicity studies (Table 3) indicated that rHDL/EVR formulation was 185 times more potent than free EVR against LN 229 cells, whereas the free EVR was 3.2 times more effective against U87 cells. This discrepancy is likely to be due to the difference in the expression if the SR-B1 receptors (much higher in LN 229 cells compared to U87 cells).

This study highlights the capability of the rHDL NPs to deliver a targeted payload with multimodal mechanisms of action against GBM. It also provides proof of concept regarding the efficacy of delivering a hydrophobic; FDA approved mTOR inhibitor by utilizing transport system targeted to the SR-B1 receptor that is upregulated in most cancers, including GBM.

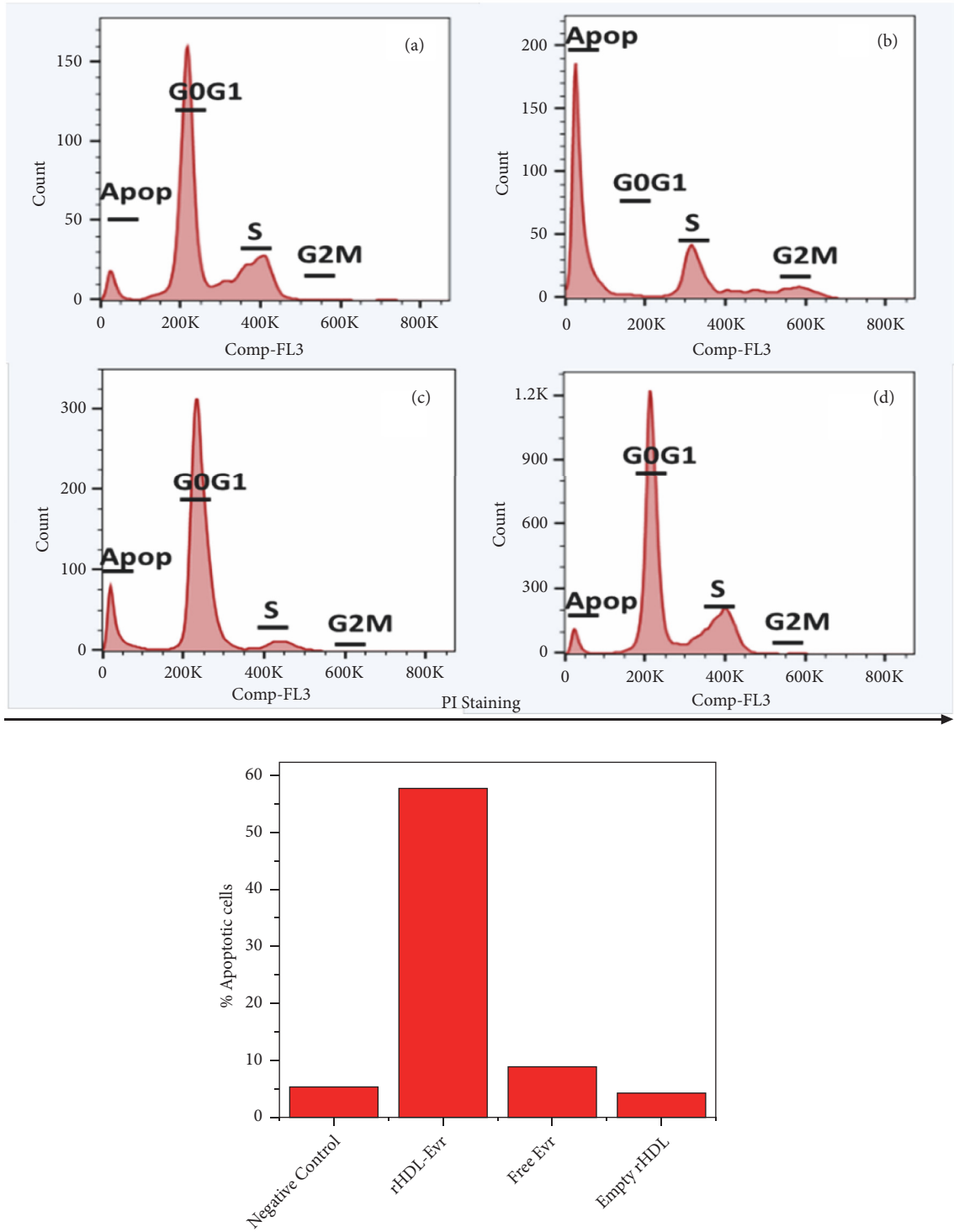

Figure 5: Cell cycle analysis of (a) LN229, negative control, (b) LN229 treated with rHDL/EVR, (c) LN229 treated with Free EVR, and (d) LN229 treated with empty rHDL.

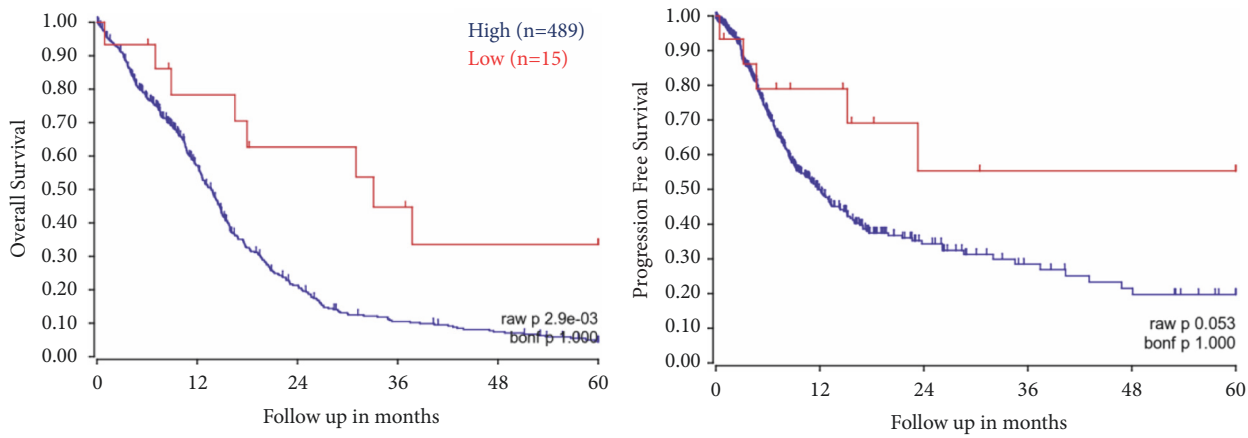

Figure 6: Overall and progression free survival of GBM patients as function of SCARB1 mRNA expression. Curves generated using R2 Genomics Platform and TCGA datasets (acquired from: https://hgserver1.amc.nl/cgi-bin/r2/main.cgi).

Abbreviations

CNS: Central nervous system
EYPC: Egg yolk phosphatidylcholine
EVR: Everolimus
GBM: Glioblastoma
HDL: High density lipoprotein
mTOR: Mammalian Target of Rapamycin
NP: Nanoparticle
SR-B1: Scavenger receptor B type 1
TMZ: Temozolomide
BBB: Blood brain barrier
CNS: Central nervous system
EE: Entrapment efficiency
PDI: Polydispersity index
HIF-1a: Hypoxia inducible factor alpha.

Data Availability

The data presented in this paper is available and open for all readers and interested parties upon request from the corresponding author.

Disclosure

The studies reported in this article do not involve any work with human participants or animals.

Conflicts of Interest

The authors declare that no conflicts of interest exist and none of them received financial remuneration or have financial interests related to the studies reported in this communication.

Acknowledgments

This study was funded by a grant from the Peggy Dickerman Brain Cancer Research Fund (UNTHSC *#77527*), OSTEOMED, Addison TX, and Wheels for Wellness Fort Worth TX. We thank Dr. Meharvan Singh, UNTHSC, for providing the U87-MG astrocytes and also Dr Xiangle Sun, UNTHSC, for assistance with flow cytometry studies.

References

[1] A. Omuro and L. M. DeAngelis, "Glioblastoma and other malignant gliomas: A clinical review," *Journal of the American Medical Association*, vol. 310, no. 17, pp. 1842–1850, 2013.

[2] A. Olar and K. D. Aldape, "Using the molecular classification of glioblastoma to inform personalized treatment," *The Journal of Pathology*, vol. 232, no. 2, pp. 165–177, 2014.

[3] E. W. Larson, H. E. Peterson, W. T. Lamoreaux et al., "Clinical outcomes following salvage gamma knife radiosurgery for recurrent glioblastoma," *World Journal of Clinical Oncology*, vol. 5, no. 2, p. 142, 2014.

[4] O. Lavi, "Redundancy: a critical obstacle to improving cancer therapy," *Cancer Research*, vol. 75, no. 5, pp. 808–812, 2015.

[5] S. A. Rosenberg, "Finding suitable targets is the major obstacle to cancer gene therapy," *Cancer Gene Therapy*, vol. 21, no. 2, pp. 45–47, 2014.

[6] S. Agnihotri and G. Zadeh, "Metabolic reprogramming in glioblastoma: the influence of cancer metabolism on epigenetics and unanswered questions," *Neuro-Oncology*, vol. 18, no. 2, pp. 160–172, 2016.

[7] S. Bette, M. Barz, T. Huber et al., "Retrospective analysis of radiological recurrence patterns in glioblastoma, their prognostic value and association to postoperative infarct volume," *Scientific Reports*, vol. 8, no. 1, 2018.

[8] J. A. Menard, H. C. Christianson, P. Kucharzewska et al., "Metastasis stimulation by hypoxia and acidosis-induced extracellular lipid uptake is mediated by proteoglycan-dependent endocytosis," *Cancer Research*, vol. 76, no. 16, pp. 4828–4840, 2016.

[9] M. Panchoo and A. Lacko, "Scavenger receptor class B type 1 regulates neuroblastoma cell proliferation, migration and invasion," *Biochemical and Biophysical Research Communications*, vol. 495, no. 1, pp. 614–620, 2018.

[10] S. Wilhelm, A. J. Tavares, Q. Dai et al., "Analysis of nanoparticle delivery to tumours," *Nature Reviews Materials*, vol. 1, no. 5, Article ID 16014, 2016.

[11] F. A. Fisusi, A. G. Schätzlein, and I. F. Uchegbu, "Nanomedicines in the treatment of brain tumors," *Nanomedicine*, vol. 13, no. 6, pp. 579–583, 2018.

[12] J. S. Michael, B. Lee, M. Zhang, and J. S. Yu, "Nanotechnology for treatment of glioblastoma multiforme," *Journal of Translational Internal Medicine*, vol. 6, no. 3, pp. 128–133, 2018.

[13] A. Grillone, M. Battaglini, S. Moscato et al., "Nutlin-loaded magnetic solid lipid nanoparticles for targeted glioblastoma treatment," *Nanomedicine*, vol. 14, no. 6, pp. 727–752, 2019.

[14] M. Grabowska, B. F. Grześkowiak, K. Szutkowski et al., "Nano-mediated delivery of double-stranded RNA for gene therapy of glioblastoma multiforme," *PLoS ONE*, vol. 14, no. 3, p. e0213852, 2019.

[15] A. G. Lacko, N. A. Sabnis, B. Nagarajan, and W. J. McConathy, "HDL as a drug and nucleic acid delivery vehicle," *Frontiers in Pharmacology*, vol. 6, no. 247, 2015.

[16] M. Yang, J. Chen, W. Cao et al., "Attenuation of nontargeted cell-kill using a high-density lipoprotein-mimicking peptide–phospholipid nanoscaffold," *Nanomedicine*, vol. 6, no. 4, pp. 631–641, 2011.

[17] S. Yang, M. G. Damiano, H. Zhang et al., "Biomimetic, synthetic HDL nanostructures for lymphoma," *Proceedings of the National Acadamy of Sciences of the United States of America*, vol. 110, no. 7, pp. 2511–2516, 2013.

[18] E. E. Morin, X. Li, and A. Schwendeman, "HDL in Endocrine carcinomas: biomarker, drug carrier, and potential therapeutic," *Frontiers in Endocrinology*, vol. 9, no. 715, 2018.

[19] M. A. Rajora and G. Zheng, "Targeting SR-BI for cancer diagnostics, imaging and therapy," *Frontiers in Pharmacology*, vol. 7, no. 326, 2016.

[20] L. K. Mooberry, M. Nair, S. Paranjape, W. J. McConathy, and A. G. Lacko, "Receptor mediated uptake of paclitaxel from a synthetic high density lipoprotein nanocarrier," *Journal of Drug Targeting*, vol. 18, no. 1, pp. 53–58, 2010.

[21] H. Huang, W. Cruz, J. Chen, and G. Zheng, "Learning from biology: synthetic lipoproteins for drug delivery," *Wiley Interdisciplinary Reviews: Nanomedicine and Nanobiotechnology*, vol. 7, no. 3, pp. 298–314, 2015.

[22] G. Xu, N. Lou, H. Shi et al., "Up-regulation of SR-BI promotes progression and serves as a prognostic biomarker in clear cell renal cell carcinoma," *BMC Cancer*, vol. 18, no. 1, 2018.

[23] D. Schörghofer, K. Kinslechner, A. Preitschopf et al., "The HDL receptor SR-BI is associated with human prostate cancer progression and plays a possible role in establishing androgen independence," *Reproductive Biology and Endocrinology*, vol. 13, no. 1, 2015.

[24] B. Yuan, C. Wu, X. Wang et al., "High scavenger receptor class B type I expression is related to tumor aggressiveness and poor prognosis in breast cancer," *Tumor Biology*, vol. 37, no. 3, pp. 3581–3588, 2016.

[25] D. Goti, A. Hrzenjak, S. Levak-Frank et al., "Scavenger receptor class B, type I is expressed in porcine brain capillary endothelial cells and contributes to selective uptake of HDL-associated vitamin E," *Journal of Neurochemistry*, vol. 76, no. 2, pp. 498–508, 2001.

[26] K. Y. Fung, C. Wang, S. Nyegaard, B. Heit, G. D. Fairn, and W. L. Lee, "SR-BI mediated transcytosis of HDL in brain microvascular endothelial cells is independent of caveolin, clathrin, and pDZK1," *Frontiers in Physiology*, vol. 8, 2017.

[27] I. Kratzer, K. Wernig, U. Panzenboeck et al., "Apolipoprotein A-I coating of protamine–oligonucleotide nanoparticles increases particle uptake and transcytosis in an in vitro model of the blood–brain barrier," *Journal of Controlled Release*, vol. 117, no. 3, pp. 301–311, 2007.

[28] J. Fioravanti, J. Medina-Echeverz, N. Ardaiz et al., "The fusion protein of IFN-α and apolipoprotein A-I crosses the blood-brain barrier by a saturable transport mechanism," *The Journal of Immunology*, vol. 188, no. 8, pp. 3988–3992, 2012.

[29] A. L. Zhou, S. K. Swaminathan, G. L. Curran et al., "Apolipoprotein A-I crosses the blood-brain barrier through clathrin independent and cholesterol-mediated endocytosis," *The Journal of Pharmacology and Experimental Therapeutics*, vol. 369, no. 3, pp. 481–488, 2019.

[30] P. Kadiyala, D. Li, F. M. Nuñez et al., "High density lipoprotein-mimicking nanodiscs for chemo-immunotherapy against glioblastoma multiforme," *ACS Nano*, vol. 26, no. 13(2), Article ID 8b06842, pp. 1365–1384, 2019.

[31] A. G. Lacko, M. Nair, S. Paranjape, S. Johnson, and W. J. McConathy, "High density lipoprotein complexes as delivery vehicles for anticancer drugs," *Anticancer Reseach*, vol. 22, no. 4, pp. 2045–2049, 2002.

[32] T. M. Wise-Draper, G. Moorthy, M. A. Salkeni et al., "A phase Ib study of the dual PI3K/mTOR inhibitor dactolisib (BEZ235) combined with everolimus in patients with advanced solid malignancies," *Targeted Oncology*, vol. 12, no. 3, pp. 323–332, 2017.

[33] D. J. Ma, E. Galanis, S. K. Anderson et al., "A phase II trial of everolimus, temozolomide, and radiotherapy in patients with newly diagnosed glioblastoma: NCCTG N057K," *Neuro-Oncology*, vol. 17, no. 9, pp. 1261–1269, 2015.

[34] A. G. Lacko, M. Nair, S. Paranjape, L. Mooberry, and W. J. McConathy, "Trojan horse meets magic bullet to spawn a novel, highly effective drug delivery model," *Chemotherapy*, vol. 52, no. 4, pp. 171–173, 2006.

[35] A. G. Lacko, M. Nair, L. Prokai, and W. J. McConarthy, "Prospects and challenges of the development of lipoprotein-based drug formulations for anti-cancer drugs," *Expert Opinion on Drug Delivery*, vol. 4, no. 6, pp. 665–675, 2007.

[36] M. M. K. Shahzad, L. S. Mangala, H. D. Han et al., "Targeted delivery of small interfering RNA using rHDL nanoparticles," *Neoplasia*, vol. 13, no. 4, pp. 309–319, 2011.

[37] L. K. Mooberry, N. A. Sabnis, M. Panchoo, B. Nagarajan, and A. G. Lacko, "Targeting the SR-B1 receptor as a gateway for cancer therapy and imaging," *Frontiers in Pharmacology*, vol. 7, 2016.

[38] W. J. McConathy, M. P. Nair, S. Paranjape, L. Mooberry, and A. G. Lacko, "Evaluation of synthetic/reconstituted high-density lipoproteins as delivery vehicles for paclitaxel," *Anti-Cancer Drugs*, vol. 19, no. 2, pp. 183–188, 2008.

[39] R. W. Mahley, "Central nervous system lipoproteins: apoe and regulation of cholesterol metabolism," *Arteriosclerosis, Thrombosis, and Vascular Biology*, vol. 36, no. 7, pp. 1305–1315, 2016.

[40] A. Rigotti, H. E. Miettinen, and M. Krieger, "The role of the high-density lipoprotein receptor SR-BI in the lipid metabolism of endocrine and other tissues," *Endocrine Reviews*, vol. 24, no. 3, pp. 357–387, 2003.

[41] J. Husemann and S. C. Silverstein, "Expression of scavenger receptor class B, Type I, by astrocytes and vascular smooth muscle cells in normal adult mouse and human brain and in alzheimer's disease brain," *The American Journal of Pathology*, vol. 158, no. 3, pp. 825–832, 2001.

[42] N. Sabnis, M. Nair, M. Israel, and W. J. McConathy, "Enhanced solubility and functionality of valrubicin (AD-32) against cancer cells upon encapsulation into biocompatible nanoparticles," *International Journal of Nanomedicine*, vol. 7, pp. 975–983, 2012.

[43] S. Raut, L. Mooberry, L. Sabnis, L. Garud, A. Dossou, and AG. Lacko, "Reconstituted HDL: drug delivery platform for overcoming biological barriers to cancer therapy," *Frontiers in Pharmacology*, vol. 9, no. 1154, 2018.

[44] G. M. Ngandeu Neubi, Y. Opoku-Damoah, X. Gu, Y. Han, J. Zhou, and Y. Ding, "Bio-inspired drug delivery systems: An emerging platform for targeted cancer therapy," *Biomaterials Science*, vol. 6, no. 5, pp. 958–973, 2018.